Decrypting Intestinal Mucosal Repair

by

Natacha Bohin

A dissertation submitted in partial fulfillment
of the requirements for the degree of
Doctor of Philosophy
(Cellular and Molecular Biology)
in the University of Michigan
2019

Doctoral Committee:

Professor Linda C. Samuelson, Chair
Associate Professor Diane Fingar
Professor Ivan Maillard
Associate Professor Jason Spence

Natacha Bohin

nbohin@umich.edu

ORCID iD: 0000-0001-8571-9898

Dedicated to those I love, a sentiment which has the incredible fortune to be preciously requited. / Dédié a ceux que j'aime, un sentiment qui a la précieuse bonne fortune d'être retourné. / Dedicado a todos que eu amo, um sentimento que eu teve a incrível sorte de ter sido devolvido.

Acknowledgements

A few lines of acknowledgements seem inadequate to recognize the incredible mentors, friends and family that have been integral to the completion of this dissertation, but it seems like a good place start.

I would first and foremost like to thank my incredible mentor Dr. Linda Samuelson. What first drew me to Dr. Samuelson as a mentor when I rotated through her laboratory was one of the things that most promoted my development as a scientist: her ability to make discussing data feel like a mutual sharing of ideas between colleagues. Amongst myriad examples, I am especially grateful to her for pushing me to think critically, for emboldening me to connect with the field by attending conferences, presenting my work and applying for funding, for inspiring me to do high quality science, for supporting my pursuit of interests outside of the lab, and for encouraging and supporting me through difficult times.

I would also like to give a heartfelt thanks to my committee members, Dr. Ivan Maillard, Dr. Jason Spence and Dr. Diane Fingar, without whose inquisitiveness, expertise, and invaluable feedback, these projects would never have come to fruition. I am grateful to Dr. Ivan Maillard for his inspired questions and critique, which have led to the conception of the now published project described in Chapter III, to Dr. Diane Fingar for her direction, critical feedback and encouragement of my foray into the study of mTORC1 signaling, and to Dr. Jason

Spence, for his invaluable inquiries and feedback, inviting collaborations, and pushing me to think of alternative interpretations for my data. The advice and guidance of these excellent scientists throughout my training have been critical to my professional development, and to the advancement of my thesis work.

I am so grateful to have been part of the Samuelson lab. It has been such an incredibly supportive environment to work in these past 5 years, thanks to its amazing members past and present, without whose support and friendship I may not have made it through graduate school. A most grateful thanks to Theresa, Elise, Erin, Elizabeth, Yasmine, Kevin, Lindsay, Jasleena and Nobu for always being willing to help, for your invaluable guidance and expertise, and the vital comic relief. I can't imagine a more excellent group of individuals with whom to have spent these past years.

I have received great support from the Cellular and Molecular Biology (CMB) and the Department of Molecular and Integrative Physiology (MIP). Thank you to Dr. Robert Fuller, Dr. Kathy Collins, the CMB administrative staff (Cathy Mitchell, Margarita Bekiares, Jim Musgrave, Pat Ocelnik,, Jessica Kijek and Lauren Perl) and MIP's Michele Boggs and Anne Many for helping me navigate every stage of graduate school.

My past mentors have also been integral to landing me where I am today. Professor Emeritus Dr. Michael Boyle, my undergraduate research advisor, encouraged me to pursue a graduate degree, and provided great advice for picking a good graduate training environment and mentors. I gained instrumental experience in the laboratory of Dr. Qing Li, who stoked my passion for stem cell

research. The guidance of Dr. Li and her husband Dr. Bing Yee in applying to U.S. graduate school as an international student was invaluable.

My deepest gratitude for my amazing friends near and far. I could not ask for a more inspirational, interesting, diverse, ambitious, fun, adventurous, weird, brilliant and just plainly amazing group of people to call friends. I could not have made it through graduate school with my sanity intact, although some of them might argue with me on that last count, without them. From food crawls, trivia, pub hopping and brunch, to Skype dates, weekend getaways, morning workouts, late night drives and ropes courses, I could never thank them enough for them friendship, love and support through the years.

I would not be where I am today without my incredible family.

Thank you Αγγελάκοσ μου for for sharing your scientific brilliance with me, from helping me troubleshoot failing experiments, discussing projects, reviewing drafts of my writing and even sharing materials with me. Most of all, thank you for your endless patience, for always making me laugh, for your love and unwavering belief in me, even when I had my doubts, and for bringing such warmth and happiness to my life. Σε αγαπώ, φλεφερ μου.

I could not be more grateful to the most loving, silly, passionate and encouraging beings in the world, my parents and sister, for being the inspiration behind my choice of career paths, and for their unwavering support my entire life. This support has taken many forms through the years depending on my needs and interests. Counter-intuitively, it has ranged from encouragements to abandon

graduate school in pursuit of a music career as a singing duo with my sister by my side, to pushing me through the most difficult times with utter confidence of my eventual success. Merci Maman, Papa, Titou, Mabelle, et Taquara pour votre amour et encouragements. Vocês são minha inspiração, ma raison d'être, and the sunlight of my life.

Table of Contents

List of Figures

List of Tables

Abstract

Regeneration is a word that has inspired the imagination of artists and scientists alike ever since the word's inception in mid-14th century from Latin meaning "being born again." Today, medical research labs are fascinated with the aim of directing native repair mechanisms to heal damaged tissues.

Amongst the most rapidly renewing tissues in the mammalian body, the lining of the intestine (epithelium) is a particularly pertinent system in which to study regeneration driven by the extraordinary potential of intestinal stem cells (ISC). Prevailing evidence demonstrates the existence of two ISC populations in the intestinal crypts: active stem cells (termed crypt base columnar (CBC) cells), responsible for epithelial cell maintenance during homeostasis, and facultative stem cells (FSC), important to the replenishment of the CBC compartment when damaged (e.g. irradiation, disturbance of the stem cell microenvironment).

In this thesis, I examined the molecular mechanisms regulating the cellular changes mediating the regenerative response stimulated by intestinal damage. The scientific literature describes intestinal regeneration as a complex multiphasic response modulated by a network of signaling factors and cellular compartments (including epithelial Paneth cells and pericryptal subepithelial cells) that aim to restore homeostasis. However, significant knowledge gaps remained with regard

to how the intestine responds to injury, and mobilizes FSC cell populations to remedy the damage.

My studies characterize the intestinal response to irradiation-mediated CBC loss, and propose a mechanism by which damage stimulates the non-epithelial cells in close juxtaposition with the intestinal crypts (termed pericryptal subepithelial cells) to signal to crypt epithelial cells via IGF1 (Chapter II). IGF1 stimulates epithelial cell mTORC1 signaling, which results in mobilization and activation of FSCs to repopulate the vacant CBC compartment.

In my investigations of the intestinal response to irradiation damage, I also demonstrate that commonly employed CreER^{T2} mouse models exhibit inherent toxicity, with CreER^{T2} expressing-CBCs exhibiting impaired function (Chapter III). Activation of CreER^{T2} by tamoxifen treatment leads to DNA damage, which results in delayed intestinal regeneration after irradiation injury. My discoveries inform the GI field in ways to minimize the confounding factor of CreER^{T2} genotoxicity.

In addition to characterizing the mechanisms directing regeneration from known intestinal injury methods (Chapter II), my studies also characterized a novel method of intestinal damage resulting from acute inhibition of a molecular pathway critical to ISC activity: Notch (Chapter IV). While Notch regulation of the ISC niche has been defined in the context of chronic or persistent Notch modulation, no study has yet sought to understand the consequence of short-term Notch inhibition. My data report rapid Paneth cell loss following acute Notch inhibition, which transiently impairs CBC function, and initiates regeneration of the Paneth cell compartment fueled in part by *Dll1*-expressing FSCs, but not by *HopX*-

expressing FSCs. This report is the first indication that certain FSC sub-populations can be selectively activated depending on the nature and/or degree of the intestinal insult, which is critical to understanding the biological nuances of the regenerative response in different damage situations (e.g. developmental abnormalities, disease, irradiation).

My thesis work serves to define key niche cells and pathways regulating ISC function during crypt regeneration after stem cell injury.

Chapter I : Introduction[1]

1.1 Overview of Intestinal Structure and Development

1.1.1 Anatomy and function

The intestine is amongst the largest organs in the mammalian body, a long convoluted tube that is part of the gastrointestinal tract, which extends from mouth to anus. The intestine is categorized into the small and large intestine, the former being connected to the stomach via the duodenum, the most proximal section of the small intestine. From proximal to distal, the small intestine is composed of the duodenum, which is connected to the stomach, the jejunum and the ileum. The large intestine is connected to the ileum via the cecum, which connects with the rest of the organ including the colon, rectum and anal canal. My thesis work focuses primarily on the small intestine, particularly the duodenum, with a few studies pertaining to the ileum. The intestine holds the incredible responsibility of absorbing nutrients to sustain life, and its structural and cellular composition are uniquely tailored to that aim.

[1] Note this chapter is adapted from the following textbook chapter:
Dempsey, P. J., Bohin, N. and Samuelson, L. C. (2018). Notch Pathway Regulation of Intestinal Cell Fate. In: H. M. Said, F. K. Ghishan, J. D. Kaunitz, J. L. Merchant and J. D. Wood, ed., *Physiology of the Gastrointestinal Tract*, 6th ed. Academic Press, pp.141-183.[286]

The intestine is composed of cells originating from each of the three germ layers: the epithelium from endoderm, the mesenchyme (muscle, myofibroblasts) from mesoderm, and the enteric nervous system from ectoderm. The homeobox transcription factor caudal type homeobox 2 (CDX2) is a master regulator of intestinal identity, and *Cdx2* expression is essential for specification of the intestinal epithelium from the primordial gut endoderm, and for establishing normal epithelial-mesenchymal interactions.[1] After morphogenesis of the intestine, stem and transit-amplifying progenitor cells continuously divide and differentiate to maintain the epithelium throughout the lifespan of the organism. At least six distinct epithelial cell types are formed. This includes absorptive enterocytes and three secretory (granulocytic) cell types: mucus-producing goblet cells, antimicrobial peptide-producing Paneth cells, and hormone-releasing endocrine cells. Less frequent intestinal cell types include tuft cells, also called brush cells, which are chemo-sensory cells, which orchestrate intestinal responses to parasite infection,[2–4] and microfold, or M, cells, which transport luminal antigens across the epithelium to mucosa-associated immune cells. The general structures of developing and adult intestine, including epithelial and mesenchymal components, are shown in **Figure 1.1**.

A complex network of signaling pathways and transcription factors work in concert to maintain homeostasis by regulating proliferation and cellular differentiation. Many studies have demonstrated the central importance of Notch signaling for homeostatic control of the intestinal epithelium, regulating both progenitor cell proliferation and cell fate determination. In addition, other

fundamental signaling pathways are critical for intestinal development and homeostasis, including WNT, Hedgehog (HH), and Bone Morphogenetic Protein (BMP).[5] The specific roles of each of these pathways in regulating intestinal stem and progenitor cells to maintain homeostasis has been the topic of extensive research with many breakthroughs emerging primarily from analysis of genetically engineered mouse models.

1.1.2 Intestinal Stem Cells

1.1.2.1 Introduction

The intestinal epithelium is renewed at an extraordinary rate, outpacing almost all other tissues in the mammalian body. A tightly regulated intestinal stem cell (ISC) compartment is therefore required to replenish the various intestinal epithelial cell types to maintain proper tissue function. Substantive evidence suggests that there are two stem cell populations: active stem cells, also termed crypt base columnar (CBC) cells, and facultative stem cells (FSCs), also termed quiescent or reserve stem cells (**Figure 1.2**).[6–14] While the former is responsible for maintenance of intestinal epithelial homeostasis, FSCs respond to damage by contributing to the repopulation of the damaged epithelia (**Figure 1.3**).

A stem cell is a cell that is capable of giving rise to mature cell types. These cells can be functionally identified by various means, although three main techniques have been employed in the intestine: lineage tracing, label retention and intestinal organoid formation. Lineage tracing is a technique that allows permanent labeling of a given cell and all of its progeny via activation of a reporter

gene. If a stem cell is labeled by this method, and intestinal sections are analyzed after some time, a “ribbon” of labeled cells extending from the base of the crypts upwards will be observed. Label retention assays are aimed at identifying slowly cycling cells by labeling their DNA. An injection, or ‘pulse,’ of a DNA label (e.g. bromodeoxyuridine (BrdU)) will mark all cells. The pulse is followed by a ‘chase’ or ‘washout’ period, during which most cells turnover, or divide. In the latter case, mitotically active cells dilute the DNA label with each division, diminishing the labeling intensity. Cells with an adequate labeling intensity are termed ‘label-retaining cells’, and constitute a mitotically dormant or slow cycling cell population believed to represent a subset of the stem cell compartment. Intestinal organoids are three-dimensional intestinal epithelial structures grown *in vitro* whose growth is fueled by stem cells. Establishing organoids from ISCs and assessing intestinal organoid formation, or growth, provides information about ISC activity.

Stem cell activity is regulated by signaling cues from the stem cell microenvironment, also known as the niche. Dysregulated niche signaling can result in unchecked proliferation and tumor formation.[15,16] It is therefore fundamental to our understanding of intestinal homeostasis, regeneration after injury and tumorigenic pathways to uncover the molecular program of ISC regulation.

1.1.3.2 Crypt base columnar stem cell

The discovery of the putative ISC was originally driven by the hypothesis that stem cells would be slowly cycling in order to contribute to intestinal

maintenance throughout life. As such, Potten and colleagues proposed a DNA label-retaining cell type located at the +4 position (4th cell up from the crypt base) to be the putative ISC.[17] On the contrary, the ISC we now know to maintain intestinal homeostasis is rapidly cycling, and known as the CBC, thin cells located at the base of the crypts intercalated between Paneth cells (**Figure 1.2 and 1.3**).[18,19]

The discovery of CBC-specific markers, described in the subsequent section and defined as genes or proteins expressed in a particular cell population that help identify it, facilitated characterization of this cell type. It was demonstrated that these cells were capable of long-term self-renewal, and multipotency.[20] Further, single isolated CBCs were shown to be able to give rise to intestinal organoids that contained all intestinal lineages, and could be passaged virtually indefinitely.[21] Together these data helped cement CBCs as bona fide ISCs. As such, it was most surprising to the field when complete diphtheria toxin-induced ablation of CBCs had little effect on intestinal homeostasis.[22] Fittingly, as with other proliferative cells, CBCs were shown to be highly sensitive to intestinal damage, with dramatic loss of this cell population following administration of DNA damaging agents (e.g. chemotherapeutics, γ-irradiation).[20] Together these reports suggest that another cell type is capable of compensating for the elimination of CBCs and restoring homeostasis following injury, paving the way for the characterization of FSCs described in a subsequent section.

1.1.3.3 Markers of crypt base columnar stem cells

CBC stem cells were first described by Cheng and LeBlond, and the Clevers laboratory subsequently identified the first molecular marker of CBCs, *Lgr5* (**Figure 1.2**).[18] The *Lgr5* gene is regulated by WNT pathway signaling, which is a critical pathway promoting intestinal proliferation and CBC function.[18,23,24] Using a mouse strain with an inducible Cre allele knocked-in to the *Lgr5* locus and the *ROSA26-lacZ* reporter allele for lineage tracing analysis, and 5-bromodeoxyuridine (BrdU)-labeling studies, it was determined that *Lgr5*-positive cells are actively cycling with an average of one round of cell division per day.[23] Importantly, lineage tracing to mark the progeny of *Lgr5*-positive cells, labeled all epithelial cell types, with a time period of ~5 days for a migrating "ribbon" (defined in the previous section) to reach the villus tip, a timing consistent with the known rate of epithelial cell differentiation and migration.[25] The labeling was shown to be long-lived, with labeled ribbons maintained 14 months after induction.[25] Thus demonstrating that *Lgr5*-positive cells were long-lived self-renewing stem cells. *Lgr5* family members (*Lgr4*, *5* and *6*) encode G-protein coupled transmembrane proteins that act as receptors for R-Spondin (RSPO) and potentiate WNT signaling, a developmental pathway whose intestinal activity is described in a subsequent section.[26–29] *Lgr5* is expressed in the proliferative, intervillus zone of the intestine at developmental stages,[30] while it is expressed most highly in CBCs in adulthood with a decreasing gradient of expression moving up the crypt.

Analysis of genes enriched in *Lgr5*-positive cells identified additional markers of the CBC stem cell including achaete scute-like 2 (*Ascl2*; also called

Mash2),[31] olfactomedin4 (*Olfm4*),[32] *Sox9*,[33,34] and others (**Figure 1.2**).[13] Importantly, *Olfm4* is a Notch target gene, suggesting that the CBC stem cell is a direct cellular target of Notch signaling.[35] *Ascl2*, a WNT target gene encoding a transcription factor, was shown to direct the expression of a number of other WNT target genes, including *Lgr5*. Mechanistically, Schuijers et al. recently showed ASCL2 forms a bimodal switch that interprets WNT levels and cooperates transcriptionally with β-catenin/TCF4 to stabilize the stem cell identity of *Lgr5*-positive CBCs.[36]

1.1.3.4 Facultative stem cell

In support of Potten and colleagues' original hypothesis,[17] the field has demonstrated the existence of ISCs distinct from CBCs, known as FSCs, a sub-population of which were described as slowly cycling and label retaining. Current evidence indicates FSCs are a heterogeneous population of intestinal crypt cells with the potential to be mobilized, or activated to stem cell status, during repair or regeneration (**Figure 1.3**). As stem cells, FSCs have the capacity for self-renewal and multipotency, however this capacity is induced by loss of or damage to the actively cycling CBC compartment. Following injury-induced activation, FSCs contribute to repopulation of CBCs, as well as all intestinal epithelial cell lineages.[37] Similarly to CBCs, the characterization of this cell population was facilitated by marker discovery, described in the subsequent section.

1.1.3.5 Historical perspective on facultative stem cells

Decades of research have generated different models regarding the identity of FSCs in the intestinal crypts. Originally termed "+4" cells for their location around the +4 position (**Figure 1.3**) as originally suggested by Potten,[17] early FSC marker discovery and label-retaining studies indicated a population that was mitotically dormant or quiescent and long-lived.[37] However, the evidence now shows that multiple different crypt cell types can function as FSCs, in that they can re-acquire stem cell characteristics and contribute to repair, due to crypt cell plasticity described in the subsequent section. FSC function has been defined using Cre mouse models that mark different types of cells, including mitotically dormant cells, transit-amplifying committed progenitors, and differentiated cells.

Bmi1 and *HopX* were amongst the first FSC markers identified, describing a cell type functionally distinct from *Lgr5*-expressing CBCs originally termed "+4 cells",[6,38] but that we now know labels only a small subset of FSCs originally termed "+4 cells." A member of the Polycomb group gene family that functions in chromatin silencing,[39] BMI1 has been shown to participate in the self-renewal of neuronal, hematopoietic, and leukemic cells.[40–42] In the intestine, BMI1 has been observed to mark cells at the +4 position (as identified by lineage tracing from *Bmi1-CreER*^{T2} mice), a location previously noted to contain long-term label-retaining cells, which were presumed to be stem cells by Potten and others.[18,43–45] Indeed, BMI1 was confirmed to mark a long-lived cell.[43] Lineage tracing for the progeny of *Bmi1*-positive cells using a *Bmi1-CreER*^{T2} mouse crossed to a *ROSA26-lacZ* reporter strain, revealed minimal lineage tracing in the absence of

damage a week after induction of tracing,[46] while many confluent lineage stripes were observed a week following irradiation-mediated CBC loss.[47] Further, single isolated *Bmi1*-positive cells were shown to have organoid forming capacity, giving rise to all intestinal epithelial cell types, including CBCs.[47] This report also suggests that single cell culture of *Bmi1*-positive cells triggers activation of these cells to reconstruct the intestinal epithelium in the form of an organoid. The marker *HopX* shares many similarities with *Bmi1*, and actually, *HopX*-positive cells were shown to co-stain with *Bmi1*-expressing cells.[38] HOPX is an atypical homeodomain-containing protein studied in the heart and neural stem cells.[48–50] Similarly to BMI1, it marks a slow-cycling quiescent label-retaining cells at the +4 position capable of lineage tracing and giving rise to CBCs following irradiation-induced CBC loss.[38,51] Isolated *HopX*-positive cells were also shown to have organoid forming activity.[38] These studies led to the theory that FCSs and CBCs have a hierarchical relationship, with FCSs set aside to replenish the active CBC stem cell pool with injury.

This view has been challenged more recently by many studies that identified additional markers of FSCs by observation of enhanced lineage tracing from cell-specific Cre mouse models following intestinal damage. Among others, they include *mTert*, *Krt19*, *Lrig1*, *Sox9*, *Alpi1*, *Dckl1*, *Neurog3*, and *Lyz* (**Figure 1.2 and 1.4**),[12,38,52–56] markers that describe committed progenitors as well as differentiated cells within the crypts, thus challenging the hierarchical stem cell view first developed from the studies of *Bmi1*- and *HopX*-positive FSCs. This is discussed in more detail in the next section.

1.1.3.6 Crypt cell plasticity

As alluded to above in describing the various cell types encompassed by the term FSC, the intestinal crypt demonstrates incredible plasticity (**Figure 1.3 and 1.4**). In addition to the originally described quiescent FSCs, FSC activity, the ability to mobilize to repopulate the damaged intestinal epithelium, has been reported in committed epithelial progenitor cell types.[12,53] *Alpi*-positive enterocyte progenitors have been shown to have the capacity to dedifferentiate and to become multipotent and self-renewing following targeted ablation of *Lgr5*-positive CBCs.[53] The Notch ligand-expressing, *Dll1*-positive secretory progenitors have also demonstrated the capacity to repopulate all mature intestinal epithelial cell types following damage, and to form organoids,[12] although they have yet to be fully characterized.

These studies reveal that FSCs are a highly heterogeneous population (**Figure 1.3 and 1.4**), encompassing quiescent cells in the lower mid-crypt region (*Bmi1*, *HopX*, *mTert*) as well as fated progenitors in the middle to upper crypt region (*Alpi*, *Dll1*), revealing the incredible plasticity of the intestinal crypt.[6,12,38,43,52,53,57] Further indication of the latter point is the reported ability of mature intestinal epithelial cells residing in the crypt, Paneth and enteroendocrine cells, to de-differentiate and adopt ISC-like characteristics to respond to damage.[58–60] The Paneth cell is described in more detail in the next section.

1.1.3.7 Niche cells

Defining the specific components of the ISC regulatory environment or niche, has been the aim of myriad research laboratories over the years, including describing the signaling pathways involved (including HH, BMP and WNT signaling, described in subsequent sections), as well the specific cellular components (epithelial and mesenchymal). Niche cells support ISC function by stimulating regulatory pathway activity in ISCs via secretion of niche factors or cell-to-cell contact signaling.

For close to a decade, the putative niche cell has been proposed to be the Paneth cell.[61] First identified in 1872 by Dr. Schwalbe and subsequently extensively described by Dr. Paneth,[62,63] Paneth cells are pyramid-shaped cells with basally-situated nuclei and strikingly large apically-situated granules filled with antimicrobial peptides and other immune regulating molecules (including pro-inflammatory cytokines).[64] In the mouse, emergence of these cells occurs 7 to 30 days after birth, together with the formation of crypts.[65–67] Paneth cells are mature intestinal epithelial cells, yet they escape the upward cellular migration concomitant to epithelial cell differentiation, by flowing downward to intercalate between CBCs. In addition to being the only mature intestinal cells known to reside at the base of the crypts, and their close juxtaposition with CBCs, Paneth cells are also unique for being long-lived. While other mature epithelial cells on the villi turnover approximately every 5 days, the lifespan of Paneth cells has been reported to be about 30 days.[64]

The close juxtaposition of Paneth cells to CBCs first hinted at their potential niche-supporting function. The Gordon laboratory, however, rejected this hypothesis when first investigating this question in a Paneth cell ablation mouse model, where a mouse genetic approach expressed attenuated diphtheria toxin A fragment from the Paneth cell-specific cryptdin-2 gene (*CR2*) locus.[68] They came to the conclusion that Paneth cells did not secrete essential niche factors because they did not detect deleterious effects to crypt cell proliferation in their mouse model of Paneth cell ablation.[68] However, significant technological advancements since that time have allowed reassessment of this conclusion, albeit with controversial outcomes. Two mouse genetic studies published in 2012 agreed with the Gordon study. Both studies induced deletion of the transcription factor ATOH1, essential to secretory cell differentiation, which led to complete loss of Paneth cells, as well as other secretory cell types.[69,70] On the other hand, other studies using the Gordon mouse model of Paneth cell ablation, as well as a new model involving deleting the transcription factor SOX9, saw a loss of CBCs concomitant with Paneth cell ablation.[61,71–74] Further, a significant study found that isolated CBCs infrequently form intestinal organoids; however, organoid formation was significantly enhanced when isolated Paneth cells were plated with CBCs.[61] These studies in favor of a Paneth cell niche role are supported by the finding that Paneth cells express several niche factors, such as epidermal growth factor (*Egf*), *Wnt3*, and Notch ligands.[61] The Sabatini lab also suggested that Paneth cells can serve as nutritional sensors to modulate CBC function via the activity of mTOR complex 1 (mTORC1).[75] This compilation of work suggests that Paneth cells serve a niche-

supporting function, but their loss (or their absence in early life) is tolerated by unknown mechanisms. A potential explanation that has yet to be investigated is that in the absence of Paneth cells, CBCs are reprogrammed to function more like immature stem cells, to a state where they rely on niche factors signals coming from non-Paneth sources. This is likely to be a key aspect of cellular plasticity in the intestinal crypt.

In recent years, the existence of a non-epithelial niche cell has been an intriguing avenue of investigation. The controversy of crypts tolerating Paneth cell loss reported by some studies, combined with Paneth cells being absent from the colon and immature postnatal intestine, does hint at other niche-supporting sources. Stromal subepithelial populations have been suggested to be one such source. These cells in the lamina propria are closely apposed to the crypt base and CBCs, and have been believed to support the ISC niche for some time (**Figure 1.1**).[76,77] Stromal subepithelial cells are thought to be direct, paracrine mediators of various niche signals that regulate stem cells, including WNT signaling.[76] A 2011 study found that stromal subepithelial cells could support the growth of organoids from culture of isolated human intestinal crypts without addition of FGF10, WNT3A or even RSPO.[78] These data suggested that stromal subepithelial cells could supply CBCs with the necessary niche factors for intestinal epithelial maintenance.[78]

Within the last few years, several studies have come out seeking to identify the extra-epithelial source of WNT ligand supporting CBCs.[79–81] In 2016, after showing that a subset of mesenchymal cells closely apposed to intestinal crypts

expressed the winged-helix transcription factor *Foxl1*, the Kaestner group employed mouse models expressing diphtheria toxin receptor under the control of a *Foxl1* promoter to ablate the *Foxl1*-positive pericryptal mesenchymal cells.[79] This cell ablation resulted in a dramatic cessation of epithelial cell proliferation, and a loss of epithelial cell WNT signaling.[79] The same year, the Basler group globally deleted Wntless (*Wls*), which is required for WNT secretion.[80] Mice with ablated *Wls* deletion displayed intestinal crypt loss and a dramatic reduction in expression of CBC markers.[80] Systemic delivery of WNT3A was able to partially rescue the loss of crypts and CBCs, and WNT2B administration in culture rescued the inability of Wls organoids to form.[80] This group identified WNT2B-secreting cells to be predominantly *Gli1* or *Acta2* positive.[80] Two years later, the Kaestner group characterized *Foxl1*-positive mesenchymal cells as subepithelial telocytes, thin, sub-epithelial mesenchymal cells with extended cell processes known as telopodes.[81–83] They found that these cells also express *Gli1*, suggesting overlap between the Kaestner group's *Foxl1*-positive telocytes and the Basler's group WNT2b-secreting *Gli1* or *Acta2* positive subepithelial myofibroblasts.[80,81] To test the role of WNT ligand expression in *Foxl1*-positive telocytes, Porcupine (*Porcn*), which is required for WNT secretion, was deleted in *Foxl1-CreER*^{T2} mice. Loss of WNT secretion from these mesenchymal cells led to a radical reduction in stem and progenitor cell proliferation and epithelial WNT pathway signaling.[81] These studies suggest that *Foxl1*-positive subepithelial telocytes induce WNT signaling in CBCs via secretion of key WNT ligands such as WNT2B.

Future research is likely to uncover more niche-supporting cells in the intestine, as work from the Shivdasani group suggests.[84] They found that conditional ablation of WNT ligand secretion, using a *Porcn*-null mouse strain in the intestinal epithelium (using *Villin-CreER*^{T2} mice) and from smooth muscle cells, including stromal subepithelial cells, (using *Myh11-CreER*^{T2} mice) did not disrupt intestinal homeostasis.[84] The authors suggested another source of WNT ligand is at play in the intestinal milieu. This source could include the Kaestner laboratories' *Foxl1*-positive mesenchymal cells, since the Kaestner group's characterization suggests *Foxl1*-positive cells are negative for α smooth muscle actin (αSMA; encoded by *Acta2*) and thus would not have been targeted by the Shivdasani laboratory's mouse model. Given these gaps in our understanding, significant advances remain to be made to understand the incredible signal transduction network that exists in the intestinal stem cell niche, including epithelial cells, stromal cells, smooth muscle cells, vasculature, neurons and components of the extracellular matrix. Of particular interest to the field is the question of how communication between epithelial and mesenchymal cells induces crypt repair responses. In the next sections, developmental signaling pathways whose inter- and intra-compartmental communication is critical to intestinal regulation, will be described.

1.1.4 Developmental signaling pathways

1.1.4.1 Hedgehog Signaling Restricts the Proliferative Zone

In the intestine, HH signaling is exclusively paracrine. The pathway ligands Sonic HH (SHH) and Indian HH (IHH) are secreted from epithelial cells and activate downstream signaling through their receptors Patched1 and 2 and effectors GLI1, 2, and 3 in the mesenchyme.[85–87] GLI2 appears to be the main effector of HH signaling in the developing intestine.[88] At embryonic day 8.5 of mouse development (E8.5), *Ihh* and *Shh* are expressed in the gut endoderm in overlapping patterns,[89,90] and by late fetal development, this expression pattern is restricted toward the proliferating epithelium of the intervillus zone.[91] Mesenchymal cell clusters that form just beneath the epithelium at these zones are HH ligand responsive and drive villus formation starting at E14.5.[92] Mice deficient in SHH or IHH die perinatally and exhibit many gastrointestinal defects, including changes in enteric nervous system development, loss of smooth muscle, and altered epithelial proliferation.[93] Similar phenotypes were observed in studies that examined the consequences of blocking signaling by treating neonatal mice with a HH neutralizing antibody or a pharmacological inhibitor, or by using a genetic mouse model that expressed a secreted form of the pan-HH inhibitor HH interacting protein (HHIP) from the intestinal epithelium via the *Villin* promoter (*Villin-Hhip* mice).[86,92,94] Phenotypes of loss of HH signaling include increased epithelial proliferation and formation of ectopic crypt-like structures, and reduced smooth muscle.[86,92,94] HH signaling is also important for maintaining intestinal homeostasis in the adult. Mice with Cre-activated *Hhip* expression, or a conditional deletion of

Ihh in the intestinal epithelium showed expansion of the proliferative zone and progressive loss of smooth muscle.[95–97] Thus, HH signaling is critical to intestinal development and homeostasis, controlling proliferative capacity and smooth muscle differentiation.

In addition to its role in restricting epithelial cell proliferation and maintaining stromal cell differentiation, HH signaling has also been implicated in the inhibition of ISC self-renewal and differentiation, likely through suppressing WNT signaling.[95–100] Thus, the combined effect of HH signaling is important for villus formation, smooth muscle proliferation and differentiation, and restriction of the epithelial proliferative compartment in perinatal and adult intestine. Furthermore, since HH signaling mutants display epithelial phenotypes, a feedback mechanism that can signal from the mesenchyme back to the epithelium in response to HH signaling must exist. Pertinently, the *Foxl1*-positive putative mesenchymal niche cell described in the previous section has been shown to be HH-responsive to affect WNT and BMP signaling, pathways described in the two subsequent sections.[81] If HH signaling regulates *Foxl1*-positive telocyte control of the intestinal niche, and how, remains to be uncovered, and will be critical to understand niche regulation.

1.1.4.2 BMP Signaling Restricts Crypt Number

Active BMP signaling is transduced through the cytoplasm to the nucleus by the SMAD transcription factors following BMP ligand-mediated receptor activation. BMP signaling in the intestine is bidirectional with genes encoding multiple BMP

ligands, receptors, and SMAD transcription factors, and BMP inhibitors being expressed in both the epithelium and mesenchyme.[101,102] Mesenchymal cells at intervillus and intercryptal regions have been shown to secrete BMP2 and BMP4 ligands.[89,103,104] In the epithelium, it appears that the most active BMP signaling, as determined by the presence of nuclear phospho-SMAD1, 5, and 8 transcription factors, occurs in the villus rather than the crypts.[95,103] This is likely due to inhibition of BMP signaling in the crypt region resulting from enriched expression of BMP inhibitors, including *Noggin* and *Gremlin1* expressed in subcryptal mesenchymal cells.[101,105,106] The pattern of BMP ligand and inhibitor expression leads to the formation of an increasing BMP activity gradient along the crypt-villus axis.[105,106] Pericryptal Foxl1-expressing cells in the mesenchyme, proposed to signal to the intestinal crypts, have been shown to express multiple BMP signaling components (e.g. *Bmp4*-7, *Gremlin1*, *Bmpr1a*), indicating this pathway is likely to be critical in the niche supporting role of these cells and deserving of additional investigation.[81]

A study employed a transgenic mouse in which the villin promoter was used to drive intestinal epithelial expression of the BMP inhibitor *Xenopus* noggin (*X-noggin*). These mice presented with ectopic crypt structures in 3-month-old mice and adenomatous foci development in older mice.[107] This suggested that BMP signaling normally functions to limit crypt number. These types of epithelial changes are reminiscent of a rare, autosomal-dominant gastrointestinal syndrome called familial juvenile polyposis (FJP), which is characterized by development of hamartomatous polyps throughout the gut. Accordingly, mutations in *SMAD4* and

BMPR1A have been identified in FJP patients,[108–110] consistent with BMP signaling alterations in the pathogenesis of this syndrome. Indeed, a second mouse model in which the *Bmpr1a* receptor was conditionally deleted using the interferon-inducible *Mx1-Cre* (induces expression in all interferon-responsive cells resulting in varied recombination in different tissues) also exhibited polyp formation.[105] In contrast, loss of *Bmpr1a* in the epithelium only showed increased proliferation and a defect in secretory cell differentiation, but not formation of ectopic crypts or polyps,[111,112] suggesting that epithelial BMP signaling is not sufficient for driving FJP. Potential candidates that have also been implicated in FJP include WNT signaling, described in the next section, and PTEN, a tumor suppressor antagonistic to mTORC1 signaling, a pathway described in a later section whose role in the intestine has yet to be fully characterized.[113]

In agreement with BMP signaling not being the sole driver of FJP hyperproliferation, depleting BMP signaling exclusively in pericryptal fibroblasts resulted in increased mesenchymal proliferation, development of a reactive stroma, and increased polyposis formation at 1 year.[112] These reports suggest that mesenchymal BMP signaling is primarily responsible for suppressing epithelial hyperproliferation. It is thought that epithelial BMP signaling limits epithelial stem cell proliferation via restriction of ISC self-renewal.[105,111,114–117] There is some evidence that BMP represses ISC self-renewal via WNT pathway suppression;[105] however, this is uncertain as some studies showed no change in WNT signaling after repression of epithelial BMP signaling,[111] or observed that BMP regulation was WNT-independent.[116]

It is likely that BMP signaling is a key factor mediating HH effects on epithelial proliferation and villus morphogenesis. BMP4 and BMP7 are positively regulated by HH signaling,[96] and the ectopic crypt phenotypes in the HH loss-of-function *Villin-Hhip*, and the BMP loss-of-function *X-noggin* mice are similar.[86,107,118,119] During development, HH-responsive mesenchymal clusters (closely apposed collection of mesenchymal cells that drive villus emergence) express BMP ligands in addition to other yet uncharacterized signaling proteins.[120] Manipulating BMP signaling via BMP antagonist or exogenous BMP ligand administration, and conditional *Bmpr1a* receptor deletion in HH-responsive mesenchymal cells resulted in altered formation of mesenchymal clusters, and hence, diminished villus size and emergence.[121] Together these studies demonstrate an important role for BMP in regulating intestinal development and ISC homeostasis, likely via regulation of the niche.

1.1.4.3 WNT Signaling Promotes Proliferation

In opposition to the anti-proliferative effects of the HH and BMP signaling pathways, canonical WNT signaling is a key pathway promoting proliferation in the intestinal crypts. Overactive WNT signaling, such as that seen in the APC^{min} mouse model, leads to enlarged crypts with enhanced proliferation and progression to adenocarcinoma.[122,123] Conversely, blocking WNT signaling by forced expression of the secreted WNT inhibitor Dickopff (*Dkk1*), or inactivation of the critical WNT pathway components T-cell-specific transcription factor 4 (TCF4), the signaling effector β-catenin, the TCF4 target gene *Myc*, or deletion of *Rspo*/*Lgr* complex components, leads to decreased proliferation and crypt loss.[124–129] There

is also evidence that non-canonical WNT signaling through WNT5A is important for aspects of gastrointestinal development and regeneration and inflammation;[130–135] however, canonical WNT signaling through β-catenin and TCF4 appears to be the most important for maintaining survival and promoting proliferation of ISCs.[124,125] Accordingly, downstream targets of TCF4-mediated WNT signaling include pro-proliferation genes such as *c-Myc*,[24,136] and *Ccnd1*,[137,138] as well as stem cell markers *Lgr5* and *Ascl2*.[18,23,24,31]

Numerous WNT ligands, receptors, and co-receptors are expressed in the intestine, with ligands produced in different epithelial cell populations as well as in pericryptal mesenchymal cells.[139] The key cellular source and identification of specific WNTs functioning as ISC niche factors have been an area of active investigation. Global ablation of WNT ligand secretion by pharmacologic inhibition of PORCN led to reduced ISC numbers and blocked proliferation and regeneration.[84,140] Surprisingly, ablation of WNT ligand secretion in the epithelium via genetic deletion of *Porcn* did not disrupt intestinal homeostasis and regeneration, [84,140] demonstrating, as suggested in a previous section, that epithelial cells, such as Paneth cells, are not the key niche cell source of WNTs. Moreover, *Porcn* deletion in *Myh11*-positive subepithelial myofibroblasts did not affect intestinal homeostasis and regeneration.[84] However, pericryptal *Myh11*-negative *Foxl1*-positive telocytes have been shown to be a critical source of WNT signaling by their secretion of WNT ligands, including WNT2b, WNT5a, and RSPO3 among others.[81] Conditional genetic ablation of *Porcn* in these cells ablated WNT signaling in intestinal crypts, depleted stem and progenitor cell

proliferation and impaired intestinal epithelial regeneration.[81] This data suggests Foxl1-positive telocytes may be the most important providers of WNT ligand for CBC WNT signaling.

In addition to regulating stem and progenitor cells, WNT plays a role in cell fate determination in the intestine, with WNT target genes *Sox9* and *EphB2/ EphB3* mediating the differentiation of Paneth cells as well as their retention in the crypt base.[73,74,127,128,141–143]

1.2 Notch Signaling in the Intestine

1.2.1 Introduction to Notch signaling in the intestine

The Notch pathway is an evolutionarily conserved signaling pathway present in all metazoans that influences a wide range of developmental and physiological processes, including the maintenance of self-renewing adult cells and tissues. Since Notch is a critical regulator of proliferation and differentiation in both development and tissue homeostasis (**Figure 1.5**), it is not surprising that dysregulation of Notch activity or mutations within the Notch signaling pathway have been linked with inherited human disorders, as well as cancer.[144–148] First named after a *Drosophila* partial loss-of-function mutation that resulted in “irregular notches” in the wing margin,[149,150] the Notch pathway has been the focus of numerous studies in worms, flies, and mammals.[151–153] Canonical Notch signaling mediates direct cell-to-cell communication to establish differential cell processes in neighboring cells (**Figure 1.6**). Activation of the Notch pathway involves direct physical contact between cells expressing membrane-bound ligands (signal

sending) and cells expressing Notch receptors (signal receiving). Ligand-binding activates sequential proteolytic processing of the Notch receptor to release the Notch receptor intracellular domain (NICD), which subsequently travels to the nucleus to activate the transcription of specific target genes (e.g. *Hes1*). Thus, Notch signaling induces differential gene expression programs in neighboring cells. Signaling events are normally transient, with rapid degradation of NICD limiting the duration of the response. Responses are determined by the cellular context of the signaling, with NICD-targeting specific effector genes to transduce tissue-specific biological responses.

The Notch pathway therefore represents a unique mechanism for short-range cellular communication between juxtaposed cells. Developmental studies, particularly in invertebrates, have shown that this short-range signaling can function in distinct ways to regulate varied and often divergent responses through effects on cell specification, proliferation, apoptosis, differentiation, and tissue patterning.[153–155] For example, Notch signaling is involved in the process of lateral inhibition in which subtle differences in Notch signaling between two equivalent progenitor cells are transcriptionally amplified such that a bias in productive Notch signaling occurs between each cell. This unequal priming of Notch signaling leads to the establishment of neighboring cells as either signal-sending or signal-receiving to pattern the developing tissue. Notch signaling can also occur between two distinct cell populations to establish boundary or inductive cell fate interactions associated with tissue patterning. Moreover, Notch signaling can control binary cell fate decisions between two daughter cells that are dependent on asymmetrical

inheritance of Notch regulatory components. Lastly, Notch signaling has been implicated in stem cell maintenance and self-renewal through cellular interactions between stem cells and juxtaposed niche cells. In many cases of complex tissue and organ formation, these different modes of Notch signaling are used iteratively or in a combinatorial manner to generate complicated differentiation programs and outcomes (**Figure 1.5**).[151–153] Importantly, Notch signaling does not act alone in these events, and invariably the Notch pathway interacts or cross-talks with other key signaling pathways, including the HH, BMP and WNT signaling pathways detailed in the previous sections (and also JAK/STAT, RTK, TGFβ) to establish functional and complex signaling networks required for development and tissue homeostasis.[156–158] Several excellent reviews on canonical Notch signaling have been published and should be consulted for additional detail beyond the scope of my thesis work.[151–153,156,158–161] Not surprisingly, Notch signaling has been shown to play a critical role in gastrointestinal tissues. This section summarizes the current understanding of canonical Notch signaling mechanisms, and highlights the important role that Notch plays in the intestinal epithelium to regulate stem cell self-renewal, progenitor cell proliferation, and cell fate determination.

1.2.2 Features of Notch signaling in the intestine

All of the Notch ligands (*Dll1, Dll3, Dll4, Jag1,* and *Jag2*) and receptors (*Notch1, 2, 3, 4*) are expressed in the mouse gut during early development (E13.5) through adulthood with the exception of *Dll3*, whose expression recedes after early development.[162,163] Based on mRNA expression patterns, the Notch ligands *Dll1*,

Dll4, and/or *Jag1* and receptors *Notch1* and *Notch2* were thought to be the most likely mediators of epithelial Notch signaling in the adult intestine.[163] It has not been fully determined which intestinal cell populations express specific ligands and receptors. It is likely that different cellular targets are involved with distinct aspects of Notch regulation, including stem cell maintenance, progenitor cell proliferation, cell fate specification, and possibly cell maturation. Identification of signal-receiving cells by immunostaining for NICD or HES1 shows positive labeling in several epithelial cells in the crypts, suggesting that Notch signaling is primarily active in both stem and progenitor cells.[164–166] However, other than CBC stem cells, the cellular identity of NICD- and HES1-positive cells have not yet been definitively established. Although *Hes1* mRNA appears to be predominantly localized to the crypts,[165] two reports have also shown nuclear HES1 protein expression in villus enterocytes of the developing intestine.[164,167] Finally, NICD was also observed in scattered goblet cells in one report.[168] Thus, Notch signaling may also be active in mature cells in the villus as well as progenitor cells. Further, although the focus of this chapter is on epithelial Notch signaling, it is worthwhile to note that Notch signaling components are also expressed in the intestinal mesenchyme,[163] where they are important for the development of the enteric nervous, vasculature, and lymphatic systems,[169–172] and likely play a role in inflammatory cell function in the gut.[173,174]

1.2.3 Intestinal Phenotypes of Notch Mutants

Experimental disruption or activation of Notch signaling in mouse has a profound effect on the intestinal epithelium, resulting in changes in proliferation, cellular differentiation, and cell fate specification (**Table 1.1**). Collectively, these studies have demonstrated that Notch signaling is essential for intestinal epithelial cell proliferation, with a pronounced reduction in dividing cells observed upon Notch inhibition. Conversely, experimental models with constitutive activation of Notch signaling exhibit increased proliferation, although, compared to Notch inhibition, fewer studies have explored the effects of Notch activation. In addition to its important role in maintaining progenitor cell proliferation, Notch appears to be the key pathway regulating a binary cell fate decision directing epithelial cell differentiation, with Notch signaling inhibiting secretory cell fate through regulation of the critical transcriptional factors HES1 (and perhaps other HES family members) and ATOH1 (see **Figure 1.5**) to allow absorptive enterocyte differentiation. In most instances, complete disruption of Notch signaling in the intestine results in morbidity due to the extreme cellular remodeling that affects intestinal function, including barrier function. Thus, many of the mutant mice with Notch pathway alterations have been studied at perinatal stages. Analysis in adults is limited to short time periods following multiple days of Notch inhibition (~5 days) due to the rapidity of cellular remodeling in the intestine, with significant morbidity, including death, commonly observed with Notch pathway inhibition. In some instances, adult viability can be maintained in genetic mouse studies through the use of mosaic Cre recombinase drivers to effect genetic changes in only a

fraction of the crypts. Intestinal effects over time following acute Notch inhibition have yet to be characterized.

1.2.4 Mutations in Essential Notch Signaling Components

Complete disruption of Notch signaling in the mouse intestinal epithelium by conditional knockout of the essential DNA-binding protein *RBP-Jκ* resulted in loss of proliferating cells and increased goblet cell number.[175] This was also observed with intestine-specific activation of a dominant-negative form of the Notch transcriptional coactivator MAML.[176] Conversely, constitutive activation of the Notch pathway using NICD transgenic mice, resulted in expansion of the proliferative zone and loss of secretory cells.[177,178] Together, these genetic mouse models demonstrated that Notch signaling normally acts to promote proliferation and inhibit secretory cell differentiation in the intestinal epithelium (**Table 1.1**). Moreover, Notch signaling has been determined to be essential for maintenance of CBCs, with rapid stem cell loss observed after global Notch inhibition with γ-secretase inhibitor treatment.[35]

The Notch receptors *Notch1* and *Notch2* are both expressed in the crypt epithelium and were confirmed to be the key signaling receptors using mice genetically engineered with dual receptor deletion in the intestinal epithelium.[163,165,179] Deletion of both receptors induced a phenotype similar to the intestine-specific *RBP-Jκ* knock-out mouse, suggesting that these receptors function redundantly, and together they likely transmit all of the epithelial Notch signal.[165,179] Similarly, a study that used neutralizing antibodies specific for

NOTCH1 or NOTCH2 receptors showed that simultaneous treatment with both receptor antibodies induced intestinal epithelial cell phenotypes similar to the double receptor-deficient genetic model and to global Notch inhibition with γ-secretase inhibitor.[35,165] Individual *Notch1* receptor deletion or blockade showed moderate goblet cell hyperplasia, but normal goblet cell numbers with *Notch2* loss or blockade, suggesting that NOTCH1 is predominant for cell fate determination.[179] Lineage tracing studies confirmed active NOTCH1 receptor signaling in CBC stem cells,[168] and *Notch1* deletion resulted in reduced stem cell number and decreased expression of the stem cell marker *Olfm4*.[179] Thus, NOTCH1 appears to be the primary receptor regulating ISC function, and NOTCH1 and NOTCH2 receptors together regulate epithelial cell proliferation, cell fate determination, and post-injury regeneration.

In situ hybridization studies demonstrated that the Notch ligands *Dll1, Dll4*, and *Jag1* are expressed in the crypt epithelium of the mouse intestine.[163] *In vivo* function was assessed in mice with inducible, intestinal epithelial-specific deletion of *Dll1*, *Dll4*, and/or *Jag1*.[180] Deletion of *Jag1* or *Dll4* had no apparent effect, while deletion of *Dll1* resulted in a moderate increase in goblet cells, without affecting progenitor cell proliferation.[180] Combined deletion of *Dll1* and *Dll4* showed marked goblet cell hyperplasia with reduced cell proliferation, and loss of stem cells, a phenotype consistent with complete Notch loss-of-function.[180] These data demonstrate that DLL1 and DLL4 are the key ligands regulating intestinal epithelial cell homeostasis. Interestingly, gene expression profiling studies showed that Paneth cells contain *Dll1* and *Dll4* transcripts, suggesting a key signaling

relationship between Paneth cells and stem cells, with Paneth cells presenting Notch ligands DLL1 and DLL4 to adjacent stem cells expressing NOTCH1.[61,181] However, analysis of genetic mouse models with Paneth cell ablation showed that these cells are not required for stem cell maintenance, suggesting alternate or additional cellular sources of Notch ligand are possible.[68,182,183] Indeed, *Dll1* is also expressed in secretory progenitor cells, which could be positioned next to stem cells when Paneth cells are lost.[12,184] The identity of Notch presenting cells and their roles in supporting the niche are still outstanding questions in the field.

The ADAM proteases perform the first essential cleavage of the Notch receptor to activate signaling (**Figure 1.6**). Both ADAM10 and ADAM17 have been shown to cleave the Notch receptors *in vitro*;[185–187] however, studies with genetic mouse models have determined that ADAM10 is the key protease performing this function *in vivo*. Mice with deletion of *Adam10* in the intestinal epithelium exhibited a Notch inhibition phenotype, with loss of proliferation and increased secretory cell differentiation.[176] In contrast, mice with intestine-specific deletion of *Adam17* had apparently normal intestines.[188]

The γ-secretase complex has the ability to cleave more than 60 types of transmembrane proteins, including the Notch receptor, Notch ligands DLL1 and JAG2, ERBB4, CD44, and E-cadherin.[189–193] There does not appear to be a specific consensus sequence to determine whether a protein is cleaved by γ-secretase; instead, the main prerequisite for a potential substrate appears to be prior removal of the ectodomain by sheddases, such as removal of the Notch receptor ectodomain by ADAM10.[189] Rodents treated with the γ-secretase inhibitor

benzodiazepine, dibenzazepine (DBZ) or LY-411,575 exhibited intestinal goblet cell hyperplasia and epithelial degeneration reminiscent of the phenotype observed in Notch disruption models.[35,175,194,195] The similarity of the phenotypes induced by γ-secretase treatment and by complete Notch disruption through genetic models demonstrates that Notch is the dominant γ-secretase substrate in the intestine.

The *Hes* genes are classic transcriptional targets of canonical Notch signaling. The HES proteins are basic helix-loop-helix transcription factors that primarily function as transcriptional repressors.[196] Multiple *Hes* genes are expressed in the intestine, including *Hes1, Hes3, Hes5, Hes6*, and *Hes7*.[163,164,175] HES1-deficient embryos exhibited intestinal phenotypes similar to complete Notch disruption models; however, the phenotype of HES1-deficient mice was not as severe as complete Notch loss-of-function mutants, and an effect on proliferation was not observed.[164,197] A more complete loss-of-function phenotype was observed after combined inactivation of HES1, HES3, and HES5, with reduced cell proliferation and increased secretory cell formation, suggesting that these three Notch effectors cooperatively regulate intestinal homeostasis.[197] A separate study of HES1-deficient embryos reported precocious differentiation of Paneth cells and increased expression of Paneth cell genes.[198] Therefore, Notch signaling through HES1 may also play an important regulatory role in cellular maturation as well as differentiation.

1.2.5 Notch Signaling and Intestinal Stem and Progenitor Cells

Notch signaling regulates several distinct processes in the intestine, including stem cell maintenance, progenitor cell proliferation, cell fate specification, and possibly cell maturation. Since mutations affecting Notch signaling result in altered proliferation, it is reasonable to hypothesize that stem or progenitor cells directly respond to Notch signals. Advances in stem cell research have brought renewed vigor into identification and characterization of ISC populations. Many new intestinal ISC markers have been identified, and methods for *in vitro* culture of ISCs have been developed, allowing for more detailed and mechanistic studies of these cells.[116,199] Currently, there is continued debate about the identity of ISCs with evidence supporting the presence of both facultative and active stem cell populations, as described in previous sections (**Figure 1.2 and 1.3**). Notch signaling in active ISCs was first demonstrated by a lineage tracing experiment that marked a long-lived stem cell capable of undergoing sequential Notch processing and NICD production (**Figure 1.5**).[168] Combined with the discovery that expression of the CBC stem cell marker *Olfm4* is affected by Notch signaling,[35] and the numerous studies characterizing Notch gain-of-function and loss-of-function, these reports demonstrate an essential role of Notch signaling in maintaining the ISC pool.[200,201] They also show that Notch acts iteratively within TA cells to regulate cell fate specification.[200,201] Further studies in this area are necessary to tease out which intestinal progenitor cells carry out distinct Notch-regulated functions.

1.3. Intestinal Regeneration

1.3.1 Methods of intestinal injury

With the intestinal epithelium turning over approximately every 5 days, the intestine is amongst the most regenerative tissues in the human body. As such, a wealth of research has been aimed at understanding the remarkable regenerative capacity of this organ with the hope of using this knowledge to mitigate debilitating intestinal afflictions. Mice are the main animal model employed to study the intestinal regenerative response due to the wealth of genetic and technological tools available. Many methods of inducing a regenerative response in murine models have been employed, including: small bowel resection (SBR), chemotherapeutic drug administration, ionizing radiation and genetic ablation of CBCs. All three of these injury models stimulate a significant regenerative response.

SBR is a well-established surgical procedure in which part, or the entirety of the small bowel, or intestine, is removed.[202,203] Dynamic intestinal adaption subsequently ensues, manifesting as crypt cell hyperproliferation, and longer crypts and villi, resulting in a expanded mucosal surface area.[204] How the post-SBR environment in the remaining intestine and/or surrounding tissue adapts is an interesting avenue of study, especially given the model's therapeutic relevance. Albeit the method of choice to study intestinal adaptation, SBR may not be the ideal model for studying the process of intestinal regeneration. The insult does not target stem cells, instead rousing a body-wide compensatory response to stimulate

mucosal growth in the undisturbed intestine. On the other hand, chemotherapy drugs (including 5-flurouracil, or 5-FU, and doxorubicin, among others) and ionizing radiation are DNA damage agents that target the proliferative stem/progenitor cell compartment.[205] These models are more commonly used to study mechanisms of crypt regeneration.

ISCs are quite sensitive to DNA damage. Ionizing, or γ-irradiation doses as low as 1 Gy can induce ISC apoptosis (**Figure 1.3 and 1.7**).[205] While it is usually believed that a cell's sensitivity to ionizing radiation is correlated with its proliferative status,[206] in the intestinal crypt there has been some debate regarding this topic.[205] Recently, the current dogma is that Lgr5-expressing CBCs are sensitive to irradiation, especially at high doses, and that FSCs (encompassing *HopX*-, *Bmi1*-, *Dll1*-, and *Alpi*-expressing cells) are more radioresistant.[37] These nuances in crypt cell radiosensitivity are controversial. Nonetheless, the ablation of CBCs with high doses of γ-irradiation (>10 Gy) has been well documented, and is the most common method of inducing damage to investigate intestinal epithelial regeneration. Administration of 12 Gy γ-irradiation for example, has been shown to lead to an 86-99% depletion of CBCs.[207]

Another method of ablating CBCs directly is to do so using a genetic mouse model containing a CBC-specific diphtheria toxin receptor (e.g. *Lgr5-GFP-DTR*).[54,208] Administration of diphtheria toxin will specifically target CBCs expressing the receptor, inducing rapid CBC death. CBC loss is associated with FSC activation to replenish the CBC stem cell population and return to homeostasis.[54,208] Thus, γ-irradiation and targeted CBC ablation allow analysis of

mechanisms of crypt cell reprogramming to replace lost CBCs, mechanisms that have yet to be fully elucidated.

1.3.2 The intestinal regenerative response post-irradiation

The damage from high dose γ-irradiation occurs rapidly, with apoptotic cells observed at the crypt base as early as 3-6 hours post-irradiation (HPI) (**Figure 1.7**).[52,208] By 2 days post-irradiation (DPI), studies have demonstrated that *Lgr5*- and *Olfm4*-expressing CBCs have been lost through apoptosis, and FSCs are activating.[6,51,52] 2 DPI, ~18% of *Bmi1*-positive FSCs are in S-phase, compared to ~2% in unirradiated mice,[6] a 9-fold increase. Additionally, HOPX-marked FSCs are increased 2.5-fold with a 3-fold increase in HOPX-positive cells in S-phase.[51] FSC mobilization results in expanded lineage tracing by 4 DPI with a 5-fold increase in *Bmi1* lineage traced cells, and a 9-fold increase in *mTert* lineage-traced crypts.[526] By 7 DPI, confluent Bmi1 lineage stripes can be seen, *Lgr5*-positive CBCs are returning, and intestinal homeostasis is being re-established.[6] FSC generation of CBCs is critical to the regenerative response, as demonstrated by the impaired regenerative capacity in mice in which *Lgr5*-positive cells were genetically ablated.[208] **Figure 1.7** provides an illustrative summary of the regenerative response post-irradiation based on data compiled from previous studies. This response, which can vary slightly based on damage conditions employed, has yet to be fully characterized by a single study.

1.4 IGF/mTOR Signaling in the Intestine

1.4.1 Growth factors in the intestine

The intestine is home to myriad growth factors, polypeptides that bind to receptors on the cell surface to direct tissue growth, cellular proliferation and/or differentiation. They are produced from different cellular sources with different targets, which informs the mode of signaling, including exocrine, autocrine, juxtacrine, paracrine and endocrine (**Figure 1.8**).[209] There are five primary intestinal growth factor families: epidermal growth factor (EGF), transforming growth factor beta (TGF-β), hepatocyte growth factor (HGF), fibroblast growth factor (FGF), and insulin-like growth factor (IGF). A summary of these growth factor families, and their main ligands and receptors, and intestinal expression pattern is found in **Table 1.3**.[209] While all critical to intestinal development, homeostasis and repair, these growth factor families have varying importance in each of these different processes. The predominant role of TGF-β signaling is during intestinal development and in maintaining homeostasis.[209] HGF is best understood to regulate development and liver regeneration, and FGF signaling is most commonly implicated in intestinal homeostasis.[209] The most pertinent growth factor families to ISC regulation and intestinal regeneration are detailed in the following sections, and include EGF and IGF signaling.

1.4.2 EGF in the intestine

EGF family ligands are integral membrane proteins that signal via binding to ErbB receptor tyrosine kinases (RTKs). Receptors to these ligands include EGFR, ERBB3 and ERBB4, with ERBB2 capable of transducing signal without ligand binding.[209] Different ligands bind receptors preferentially and induce homodimerization or heterodimerization in different combinations to elicit distinct cellular effects, including activation of ERK, MAPK, p38 MAPK, JNK and PI3K pathways, among others.[209]

EGF has been reported to be important during development,[209] and in mediating cellular proliferation, intestinal cell shedding, and nutrient and ion transport.[209] Interestingly, genetic ablation of *Egf* does not perturb intestinal homeostasis,[210,211] suggesting ligand family redundancy. However, an important role has been reported for this growth factor in regulating ISCs *in vivo,*[55,212] and intestinal organoids, whose growth and formation are ISC-driven, require EGF.[213,214] The role of EGF in ISC regulation could contribute to its predominant role in the intestine: mediating repair.

One theory suggests that barrier breaches resulting from mucosal injury would allow luminal EGF to access basolaterally-located EGFR,[209] as well as EGFR on the surface of infiltrated immune cells, hence promoting such epithelial wound repair mechanisms.[215,216] This suggests EGF serves as a 'first responder' to injury. There is also data suggesting significant remodeling in the localization of EGF/EGFR production following injury that would allow EGF access to EGFR

without barrier dysfunction. It has been reported that Paneth cells[61,217] and subepithelial myofibroblasts secrete EGF,[218] and that intestinal injury results in elevated EGF levels, as well as EGFR redistribution to the apical surface of enterocytes.[219] This evidence suggests there are other mechanisms by which EGF can access EGFR to promote signaling in response to intestinal injury.

These studies were the foundation for the investigations into the functional role of EGF in repair. Research has shown that intraperitoneal (IP) EGF injections (resulting in EGF accessing basolateral EGFR) are protective to the intestinal mucosa following methotrexate injury in rats.[220] EGF administration is also protective and/or healing in animals subjected to different damage methods (ranging from hydrochloric acid exposure in rabbits, and asphyxia and cold stress-induced necrotizing enterocolitis in rats).[221–223] Further, enhanced or depleted EGF signaling via employment of gain-of-function or loss-of-function EGFR mouse models have reported a protective or sensitizing effect to injury, respectively.[224–226] This *in vivo* work provides compelling evidence for the functional role of EGF in protecting against intestinal injury and/or enhancing repair..

1.4.3 IGF in the intestine

1.4.3.1 IGF signaling

IGF is synthesized by many cell types in the body. The main source of IGF ligands in the GI tract of infants is from breast milk,[227–229] while in adults, intestinal mesenchymal cells are known to secrete IGF1, which signals to epithelial cells.[209] IGF1 binds IGF receptor 1 (IGFR1) and IGF receptor 2 (IGFR2), which mediates

the majority of intestinal effects.[230] Ligand binding leads to IGFR1 auto-phosphorylation, activation of insulin receptor substrate-1 (IRS-1), among other substrates (e.g. GI2 which activates ERK/MAPK signaling[231]), and downstream activation of RAS/ERK/MAPK and phosphoinositide 3-kinase (PI3K).[232] **Figure 1.9** illustrates this mechanism.

IGF signaling is tightly regulated. IGF-binding proteins (IGFBP) 1 through 6 can modulate IGF function, via transport through the body.[233] In the intestine, IGFBPs 3 through 6 are expressed in stromal subepithelial populations and the lamina propria.[234–236]

1.4.3.2 IGF functionality in the intestine

IGF signaling affects cell survival, metabolism and growth, directing intestinal epithelial proliferation and inhibiting apoptosis.[209] The function of this growth factor has been mostly parsed out from pathway stimulation studies (e.g. via exogenous IGF1 administration), although a few studies have reported on the effects of depleting IGF1 signaling. Two studies showed that mice with constitutive deficiencies in IGFR1 and IGF1 are significantly smaller postnatally than controls, remain small throughout life and are designated as "failing to thrive into adulthood."[237,238] Interestingly, intestinal-specific deletion of *Igf1r* in uninjured mice led to no overt phenotype, suggesting another receptor (e.g. IGFR2, insulin receptor) can compensate for loss of IGF1 signaling through IGF1R.[239–241]

In support of a developmental role for IGF signaling, a study in which pig neonates were fed IGF1 found that their small intestine weight was significantly

increased, with longer villi.[242] In rats, 3 and 14-day daily IGF1 administration increased epithelial cell numbers across the crypt-villus axis,[243] and led to significant growth of the GI tract respectively.[244] In agreement, a mouse strain engineered to overexpress *Igf1* under the control of the widely expressed *metallothionein I* promoter, showed larger small intestines (by length and weight) and increased villus height and crypt depth.[245] These mice also demonstrated increased proliferation and reduced apoptosis at baseline and following irradiation, supporting a role of this signaling axis in inhibiting apoptosis and promoting cellular proliferation.[245]

Demonstrating a pro-proliferative and anti-apoptotic role for IGF suggests that IGF signaling would also be critical for preventing intestinal injury or enhancing repair. A 1998 study showed that damage ensuing from DSS-induced colitis in rats was partially attenuated by exogenous administration of IGF1.[246] Additional studies in rats have demonstrated that IGF enhances the adaptive response to SBR,[247–251] and improves recovery from small intestinal transplant.[252] IGF1 administration also improved adaptation in zebrafish that had undergone SBR, and stimulated ISC regeneration.[253] IGF1 was also able to blunt the small intestinal atrophy concomitant with chronic liver disease and sepsis.[254,255] Despite all of this evidence, little is known about the mechanism by which IGF1 promotes intestinal regeneration following damage.

A few studies have attempted to understand this mechanism, employing a rodent irradiation model of intestinal injury. Studies show that exogenous IGF1 administration promotes crypt regeneration and reduces irradiation-induced

apoptosis,[245,256,257] suggesting that IGF1 might function to both reduce injury and promote repair. A potential mechanism via IGF1 inhibition of pro-apoptotic p53 target PUMA through the PI3K/AKT pathway has been proposed.[256] This is thought to occur in CBCs at the crypt base.[256] However, another study has suggested IGF1 may have differential effects on CBC and FSC populations.[257] In this report, they found that IGF1 administration to uninjured mice increased intestinal epithelial growth, and activated different gene expression signatures in CBCs (Sox9-EGFP^{low}) and FSCs (Sox9-EGFP^{high}). Further, IGF1 administration led to increased Sox9-EGFP^{low} CBC cycling and numbers, and Sox9-EGFP^{high} FSC cycling, but did not yield changes to Sox9-EGFP^{high} FSC numbers. Further, *in vitro* IGF1 treatment led to enhanced organoid formation of sorted Sox9-EGFP^{low} CBCs but not Sox9-EGFP^{high} FSCs.[257] Differential IGF1 regulation of CBCs and FSCs warrants further study. These data point to a protective and/or pro-regenerative role for IGF signaling in the intestinal mucosa via epithelial-mesenchymal interactions that have yet to be defined.

1.4.3.3 Pathways engaged by IGF signaling

Ras/ERK/MAPK and PI3K/AKT are the two main pathways downstream of IGF signaling mediating its effects on cellular regulation (**Figure 1.9**).[231] The IGF-induced PI3K/AKT signaling axis upstream of mTORC1 signaling will be the focus of this section.

PI3K/AKT signaling is initiated by IGFR1-phosphorylation of IRS-1, which activates PI3K,[258] thereby producing phosphatidylinositol (3,4,5) trisphosphate

(PIP_3) by phosphorylation of phosphatidylinositol (4,5) biphosphate ($PI4,5P_2$) (**Figure 1.9**). These PI3K lipid products serve as docking sites on the plasma membrane for proteins that have pleckstrin-homology (PH) domains (e.g. AKT). The tumor suppressor protein PTEN is a PIP_3 phosphatase, converting PIP_3 back to $PI4,5P_2$, thus inhibiting downstream PI3K signaling. PIP_3 binds the PH domain of the best characterized PI3K effector, AKT, thereby recruiting it to the plasma membrane and releasing its kinase domain, where it can be phosphorylated at T308 and S473 by PDK1 and mTOR complex 2 (mTORC2), respectively. Maximal activation of AKT is achieved when both residues are phosphorylated. Many additional sites of post-translational modifications have been mapped on AKT, and associated with enhanced or attenuated functionality. Kinase inactivation of AKT occurs via dephosphorylation of T308 by protein phosphatase 2A, and PH domain leucine-rich repeat protein phosphatases (PHLPP) is responsible for S473 dephosphorylation.[259]

Active AKT phosphorylates a range of protein targets, leading to myriad downstream effects, including promoting cell survival, proliferation, growth, and altering metabolism.[258] The three most studied AKT targets include: glycogen synthase kinase 3 (GSK3; includes isoforms GSK3α and GSK3β), Forkhead Box O (FoxO) transcription factors, and tuberous sclerosis complex 2 (TSC2), a negative regulator of mTOR complex 1 (mTORC1) (**Figure 1.9**).[259]

The primary anabolic effect of PI3K/AKT signaling downstream of IGF1, is mediated through mTORC1.[259] The mTOR protein is a highly conserved serine/threonine kinase that nucleates two functionally distinct protein complexes:

mTORC1 and mTORC2. The latter was discussed earlier in this section in the context of its phosphorylation of AKT to augment its AKT activation. mTORC1 is responsible for stimulating processes responsible for cell, tissue and organismal growth. AKT is responsible for the inhibitory phosphorylation of TSC2, which is part of an inhibitory complex to mTORC1.[260] AKT also regulates mTORC1 activity through its phosphorylation of proline-rich AKT substrate of 40 kDa (PRAS40), a non-essential protein component of mTORC1. AKT phosphorylation of PRAS40 at T246, relieves its inhibitory activity towards the complex.[260] The exact mechanism by which this occurs is unclear, and the role of PRAS40 in this regard warrants further study. It remains that TSC inactivation is the dominant method by which AKT regulates mTORC1 activity.[259]

1.4.3.4 The mTOR signaling network

The discovery of mTOR signaling was a result of a cascade of discoveries originating from the collection of soil samples at Rapa Nui island (also known as Easter Island) in 1964, which contained the compound henceforth known as rapamycin (clinically known as sirolimus). Much of the mTOR signaling axis has been elucidated as a result of pioneering studies investigating the mechanism of action of rapamycin.[260]

The protein complex mTORC1 is a master regulator of cellular homeostasis, controlling the balance between anabolism and catabolism (**Figure 1.10**). The complex is made up of three core components: the catalytic subunit mTOR, the regulatory protein associated with mTOR (Raptor), and the mammalian

lethal with Sec13 protein 8 (mLST8). The function of Raptor is two-fold. It is required for the correct subcellular recruitment of mTORC1 to the lysosome for subsequent activation, and it binds the TOR signaling (TOS) motif on mTORC1 substrates to facilitate substrate recruitment to the complex. Meanwhile mLST8 binds to the mTOR kinase domain to stabilize the kinase activation loop of the complex. mTORC1 also contains two inhibitory components, the aforementioned, AKT substrate PRAS40, and DEP domain containing mTOR interacting protein (DEPTOR). To serve as contrast, mTORC2 contains mTOR and mLST8 similarly to mTORC1, however this complex contains rapamycin insensitive companion of mTOR (Rictor) in lieu of Raptor (**Figure 1.11**).[260]

Rapamycin functions via formation of a gain-of-function complex with the petidyl-prolyl-isomerase FKBP12.[261] The rapamycin-FKBP12 complex binds mTOR, thereby sterically hindering the catalytic cleft and blocking substrates from accessing the catalytic site of mTORC1.[262] In contrast, mTORC2 is insensitive to acute rapamycin treatment. Interestingly, prolonged treatment can deplete mTORC2 signaling, which is suggested to result from rapamycin-bound mTOR being unable to incorporate into newly forming mTORC2 complexes.[263,264]

Growth factors (e.g. IGF1), amino acids (e.g. leucine), oxygen, stress, and energy can all modulate mTORC1 activity, mediating changes to mRNA translation, metabolism and protein turnover (**Figure 1. 9**). To illustrate the upstream regulation of mTORC1 warrants describing the convergence of several growth factor-stimulated signaling pathways on TSC2 (**Figure 1.11 and 1.12**).[260] TSC2 is a GAP protein that is part of an inhibitory complex with TSC1 and

TBC1D7, known as the TSC complex. It is responsible for converting Rheb-GTP to Rheb-GDP.[260] Rheb-GTP is essential to mTORC1 activation. Thus the TSC complex serves to maintain Rheb in its GDP-bound form, preventing mTORC1 activation. In addition to growth factor stimulation, amino acid availability also controls complex localization via Rag/Ragulator/v-ATPase interaction at the lysosomal surface (**Figure 1.12**). Without growth factors, the TSC complex maintains Rheb in a GDP-bound form so that it cannot activate mTORC1.[259] In the presence of growth factors, growth factor-stimulated kinases (e.g. AKT, ERK) inactivate the TSC complex by phosphorylating TSC2, allowing GTP-loaded Rheb to activate mTORC1 on the lysosomal surface.[260] As mentioned with the case of PRAS40, mTORC1 can also be regulated independently of the TSC complex. An additional example is that of AMP-activated protein kinase (AMPK), which is capable of inhibitive phosphorylation of Raptor, blocking mTORC1 signaling.[265]

mTORC1 targets include p70S6 Kinase 1 (S6K1) and eIF4E Binding Protein (4EBP), which are involved in regulating protein synthesis (**Figure 1.13**). mTORC1 phosphorylates S6K1 at Thr389, which then allows PDK1 to phosphorylate and activate S6K1.[260] Activated S6K1 then phosphorylates and activates eIF4B, which promotes initiation of mRNA translation.[266] It also phosphorylates PDCD4, an inhibitor of eIF4B, however rather than being activating, phosphorylation targets the substrate for degradation to enhance eIF4B activity.[267] S6K1 also interacts with SKAR, which deposits S6K1 at the exon junction complex during mRNA splicing to enhance translation efficiency of spliced mRNAs.[268] As for 4EBP, mTORC1 phosphorylation of 4EBP triggers

phosphorylated 4EBP dissociation from eIF4E. Unphosphorylated 4EBP normally functions to sequester eIF4E to prevent eIF4F complex assembly. eIF4E dissociation from the complex allows 5' cap-dependent mRNA translation to proceed. Phosphorylation of these common mTORC1 downstream targets is a common method of assessing the status of mTORC1 activity. However, it is worth noting that it has been reported that mTORC1 inhibition can lead to inhibition of some of its downstream signaling elements and not others, by a mechanism that has yet to be characterized.[260] The downstream effectors of mTORC1 involved in nucleotide and lipid synthesis, glucose metabolism and protein turnover (e.g. autophagy) are illustrated in **Figure 1.13** and reviewed expertly by Saxton and Sabatini.[260]

1.4.3.5 mTOR in intestinal pathogenesis

Although critical to the regulation of many tissues throughout the body, the role of mTOR in the intestine has not been fully delineated. The pathway was first implicated in intestinal hyperplasia. A 2015 study demonstrated that mTORC1 activity, specifically 4EBP1-mediated translational elongation, is essential for the proliferation of APC-deficient intestinal epithelial cells, a hallmark of early stage intestinal cancer.[269] A 2007 study found that conditional widespread deletion of PTEN, a key node of the PI3K/AKT/mTORC1 inhibitory network, results in intestinal polyposis, a precancerous neoplasia that results from increased crypt fission stemming from increased ISC and progenitor proliferation.[113] Additional studies support a role for mTORC1 in intestinal polyp formation,[270] and the therapeutic potential of inhibiting the pathway to mitigate tumorigenesis of

colorectal cancer (e.g. rapamycin).[271] These studies suggest mTORC1 plays a critical role in tumorigenic proliferation.

Long-term pharmacologic mTORC1 inhibition via administration of rapamycin is well-tolerated by human patients and animal models alike, although it has been shown to lead to diarrhea in mice, rats and humans due to Na+/H+ exchanger 3 reduction.[272] These gross observations suggest that elevated mTORC1 activity (above the activity that might remain following rapamycin administration) may be dispensable for homeostasis, although studies discussed in the subsequent section point to the contrary. Amidst some controversy potentially attributable to varying methods of manipulating mTORC1 activity, reports agree to a critical role for mTORC1 in regulating ISC function and differentiation during homeostasis.

1.4.3.6 mTOR in intestinal homeostasis

Although there is some debate on the mechanism of action, several studies support a role for mTORC1 in regulation of ISC function. A 2012 study out of the Sabatini lab controversially demonstrated via immunostaining for downstream mTORC1 target phosphorylated ribosomal protein S6 (p-S6) at S235/236, that mTORC1 is active in Paneth cells, but not neighboring CBCs.[273] It is worth noting that unlike the S240/244 sites, phosphorylation of S6 at the S235/236 sites is not specific to mTORC1 signaling.[274] mTORC1 activity was suppressed in mice by calorie restriction, which increased numbers of CBCs and Paneth cells, increased CBC proliferation, reduced transit amplifying progenitor cell proliferation, and

increased organoid forming efficiency. The increased CBC and Paneth cell numbers were also observed following rapamycin administration. The study posited that this effect was due to mTORC1 inhibition in Paneth cells resulting in increased bone stromal antigen 1 (Bst1) secretion of the paracrine product cyclic ADP ribose (cADPR), which results in increased CBC self-renewal over CBC differentiation.[75] While some claims from this study were supported by subsequent reports, multiple labs have since challenged the claim that mTORC1 activity is absent from ISCs.[275–277] These multiple labs have however agreed in a role for mTORC1 in the intestine.

In seemingly direct response to the Sabatini lab report,[273] Igarashi and Guarente showed that indeed, Paneth cells augment CBC function and number via cADPR secretion in response to calorie restriction in a mTORC1-dependent manner.[276] This report did not wholly agree with the Sabatini report however, as it demonstrated that mTORC1 was active in CBCs as well as in Paneth cells. They however resolved this disagreement with the Sabatini report by showing that CBCs were shielded from sensing calorie restriction, observing increased mTORC1 activity in these cells following reduced calorie intake. They proposed that Paneth cell signaling to CBCs mediated the increased mTORC1 activity and increased CBC number.[276]

In 2013, a study that came out shortly after the Sabatini report that employed a *Drosophila melanogaster* model also supported a role for mTORC1 in ISC regulation.[278] This study demonstrated that genetic deletion of *TSC1* or *TSC2*, or overexpression of Rheb, which all lead to mTORC1 hyperactivity, led to rapid

ISC loss, and altered differentiation. Similarly to the Igarashi and Guarente report, this group also found that the role of mTORC1 in ISC maintenance is nutritional status-independent.[278] In further agreement with the importance of mTOR in regulating ISC function, albeit disagreeing with previous reports regarding the nature of this role,[273,279] a group from Cincinnati in 2015 found impaired organoid formation from crypts of mice in which they disrupted several of the genes that code for the components of mTORC1 and 2 using a *Villin-Cre* genetic mouse model to contain the depletion of mTOR signaling to the intestinal epithelium.[280]

In this same 2015 report, the Cincinnati group also reported altered differentiation in their mouse models of mTOR depletion, observing reduced mature enterocyte marker alkaline phosphatase, reduced goblet cell number and size, fewer Paneth cells, and increased enteroendocrine cell numbers in responses to mTOR deletion.[280] The Evers lab also proposed a role for mTORC1 in intestinal differentiation, however their conclusions opposed those of the Cincinnati lab. The Evers lab employed a genetic mouse model constitutively expressing a dominant negative TSC2, resulting in increased mTORC1 activity.[281] They demonstrated that mTORC1 positively regulated Notch signaling to alter cell fate specification, observing decreased goblet and Paneth cell differentiation in their mTORC1 hyperactivation model.[281]

Hence, although the literature agrees to an important role for mTORC1 in ISC regulation, also highlighted in the next section pertaining to mTORC1 activity in FSCs, further research is necessary to clarify the nature of this role, and to

understand how mTORC1 merges its signaling axis with other niche pathways, and the role of the pathway in regulating cellular differentiation in the intestine.

1.4.3.7 mTOR in intestinal regeneration

The literature proposes a pro-regenerative role for mTORC1 activity, involving the pathway in the transition of FSCs to a state capable of contributing to intestinal regeneration. The 2015 report from Cincinnati mentioned in the previous section, employed mouse models of mTOR depletion in the intestinal epithelium to demonstrate impaired organoid formation and cell differentiation at baseline, also investigated the role of the pathway post-injury.[280] They administered 10 Gy irradiation and found mTOR to be critical to intestinal crypt recovery.[280] In agreement with a pro-regenerative role of mTORC1, a 2017 study found rapamycin-treated mice had impaired intestinal adaptation following SBR.[204] The report also found that TSC1-null mice, with hyperactive mTORC1 signaling, demonstrated enhanced adaptation.[204]

A few studies have suggested a mechanism of action for the pro-regenerative effect of mTORC1. The Breault lab at Harvard University published a study in 2015 that proposed that mTORC1 signaling could contribute to the intestinal regenerative/adaptive response via FSC activation.[282] Following extreme nutrient deprivation (48h fast), they observed transient PTEN inhibitory phosphorylation in mTert-positive “dormant” FSCs, which they showed led to cell autonomous activation of mTORC1, and an increase in FSC number.[282] They subsequently compared fasted FSC activity to the activity of FSCs in mice that had

been re-fed following fasting, and observed an enhanced propensity of re-fed FSCs to contribute to CBC lineage tracing.[282] They also found that FSCs lacking PTEN had impaired contribution to intestinal regeneration following irradiation damage, and that this effect was PI3K signaling-dependent.[282] The authors proposed a role for PTEN as a gatekeeper of the fasting/feeding transition in the intestine, which is reminiscent of a similar role for the phosphatase in adipose tissue.[283] They propose that transient PTEN inactivation during fasting, results in an mTORC1-mediated change in FSC status from a dormant to a "poised" state capable of responding to injury by repopulating the CBC niche, or returning to a dormant FSC state.

This proposed response is similar to that observed in muscle stem cells (satellite cells), which are normally mitotically dormant. Rodgers et al. described a mTORC1-dependent "G_{alert}" transition state between G_0 and G_1 stages of the satellite cell cycle, in which satellite cells are functionally poised to respond to injury, or return to a dormant state.[284] Additional research is needed to determine the existence of a parallel G_{alert} state in FSCs, however, the Breault lab does suggest an FSC PTEN/PI3K/AKT/mTORC1-dependent transition state from dormancy in response to injury.

In agreement, the Lengner lab published a study recently demonstrating the cell-autonomous regulation of FSCs by mTORC1 signaling during the regenerative response.[277] In agreement with the Breault lab, the Lengner study first showed that calorie restriction increased FSC number and enhanced regenerative capacity. Subsequent data attributed this effect to mTORC1 activity, which was significantly

enhanced post-irradiation, and even further enhanced when combined with calorie restriction rather than ad libitum feeding. The lab also found that, in the absence of injury, mTORC1 inhibition via rapamycin administration reduced FSC lineage contribution and organoid formation, while mTORC1 activation, via amino acid (leucine) administration, enhanced both. This effect was found to be cell-autonomous. Interestingly, the lab showed that activation of mTORC1 sensitized FSCs to irradiation injury, leading to failed regenerative capacity. These combined results were striking, suggesting two FSC states of mTORC1 activity: cycling, injury sensitive FSCs with high mTORC1 activity ($FSC^{mTORC1high}$), and non-cycling, injury resistant FSCs with low mTORC1 activity ($FSC^{mTORC1low}$). Combined data from the Breault and Lengner labs suggest that $FSC^{mTORC1high}$ and $FSC^{mTORC1low}$ differ in their response to different feeding/fasting conditions, resulting in different outcomes on regenerative capacity. Supplementary work is indispensable to enhancing our understanding of this mechanism.

1.5 Dissertation Summary

Among the largest and most regenerative organs in the body, the intestine has been a source of fascination to scientists for centuries. Incredible leaps have been made to understand intestinal cellular composition and homeostasis thanks to the advent of genetic mouse models, three-dimensional culture systems and cutting edge molecular tools. It is only in the last two decades or so, however, that the scientific community has turned its attention to understanding how the cellular and molecular components of the intestine's intricate environmental milieu direct

ISC-driven mucosal repair.[285] My thesis work aims to advance our understanding of the intestinal regenerative response by exposing the roles of key niche factors IGF1/mTORC1 and Notch signaling in directing repair.

In Chapter II, I characterize the intestinal regenerative response following administration of a CBC-ablating dose of γ-irradiation into three phases: damage, regeneration and recovery. I go on to demonstrate increased secretion of growth factor IGF1, which signals via PI3K/Akt signaling to activate mTORC1. I show IGF1/mTORC1 signaling is crucial to the repair of the intestinal epithelium, and that mTORC1 activity directs FSC activation to contribute to crypt regeneration. I go on to suggest that IGF1 signaling from non-epithelial sources, such as pericryptal myofibroblasts or telocytes, stimulates mTORC1 signaling in FSCs, mobilizing them for regeneration.

In Chapter III, I present a discovery made while characterizing the intestinal response of genetic mouse models to damage, going on to advise proper control parameters in the scientific community's usage of intestinal epithelial-specific genetic mouse strains in research. I find that mouse strains that express the Cre fusion protein $CreER^{T2}$ in the intestinal epithelial (*Villin-CreER*^{T2}) and CBC (*Olfm4-CreER*^{T2} and *Lgr5-CreER*^{T2}) compartments suffer from impaired regenerative capacity, and/or depleted organoid forming capacity. I also find that *Villin-CreER*^{T2} mice demonstrate genotoxicity and increased DNA cleavage at cryptic *lox*P sites. Finally, I present experimental designs to minimize $CreER^{T2}$ toxicity.

In my final data chapter, Chapter IV, I introduce a new method of inducing intestinal damage: acute pharmacological blockage of Notch signaling. My studies

find that administration of one dose of the Notch inhibitor DBZ induces dramatic Paneth cell loss, and significantly impairs CBC activity. The ensuing response is reminiscent of the regenerative response to irradiation damage, with a hyperproliferative surge and rapid return of the Paneth cell compartment. Interestingly, we found that Paneth cell regeneration is at least in part fuelled by Notch ligand *Dll1*-expressing cells, whose numbers are dramatically expanded following Paneth cell loss, and whom are imparted enhanced organoid forming capacity following acute Notch inhibition. HopX-positive FSCs are not found to contribute to this rapid return in Paneth cells, indicative of an interesting selectivity in the regenerative capacity of FSCs and further pointing to the heterogeneity of this population and the remarkable plasticity of the intestinal crypts.

1.6 Figures

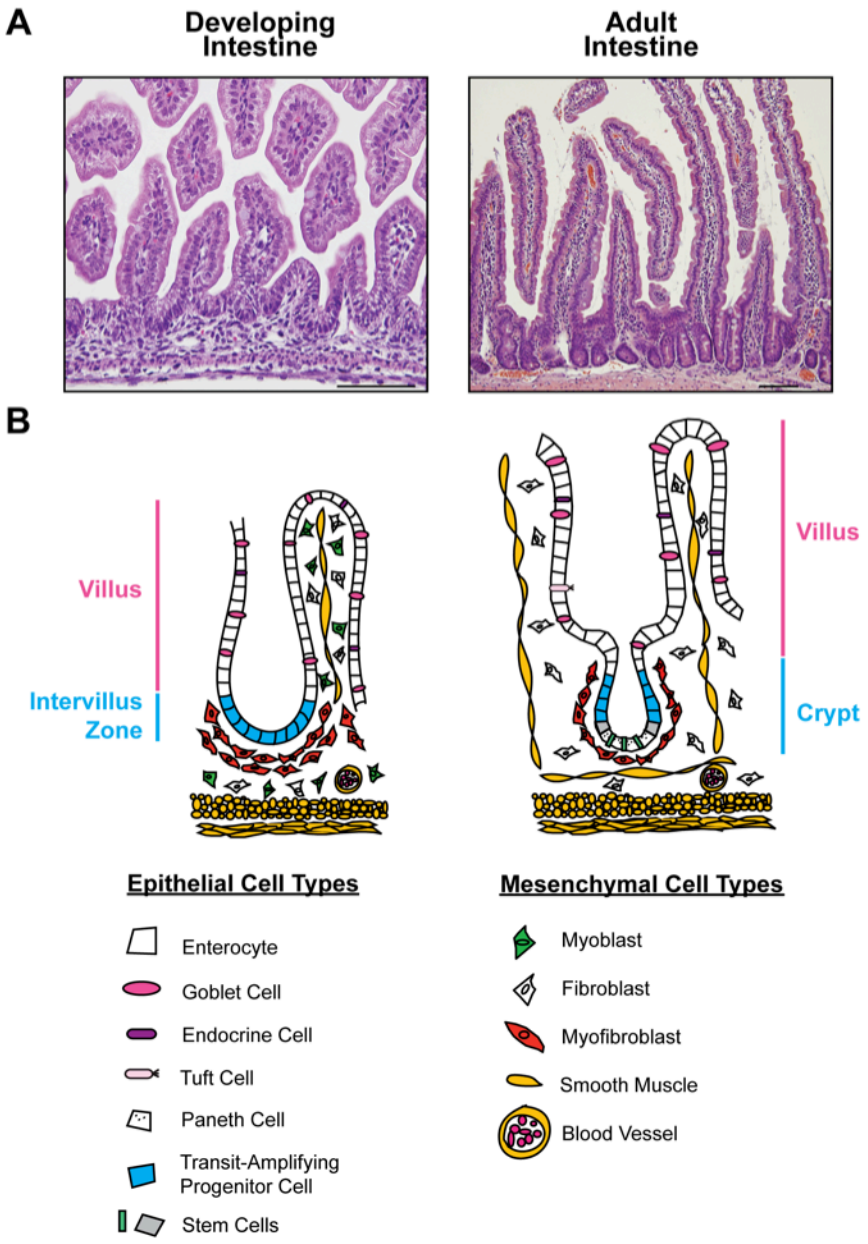

Figure 1.1 Cellular composition of developing and adult mouse intestine.

(A) Hematoxylin and eosin stained paraffin sections of developing (embryonic day 18.5) and adult duodenum. Scale bars, 100 μm. (B) The major cell populations of the epithelium and mesenchyme are depicted schematically. In the adult intestine, stem cells, progenitor cells, and Paneth cells are anchored in the crypts, whereas mature enterocytes, goblet cells, endocrine cells, and tuft cells are primarily located on the villi. Stem cells give rise to the rapidly proliferating transit-amplifying progenitors located on the lateral sides of the crypts. Several crypts surround the base of each villus and provide the mature cell types that migrate onto the villi in organized columns where they eventually reach the villus tip in 3–5 days. In contrast to the other mature cell types, Paneth cells migrate to the base of the crypts where they reside for approximately 20 days. Crypts and Paneth cells do not arise until 2–3 weeks after birth. Proliferating cells in the developing intestine are clustered

together in the so-called “intervillus zone.” Cell types not shown include cells of the enteric nervous system and hematopoietic cells that are resident and likely regulated by Notch signaling. Follicle-associated epithelium, microfold M cells and pericryptal telocytes are also not depicted.[286]

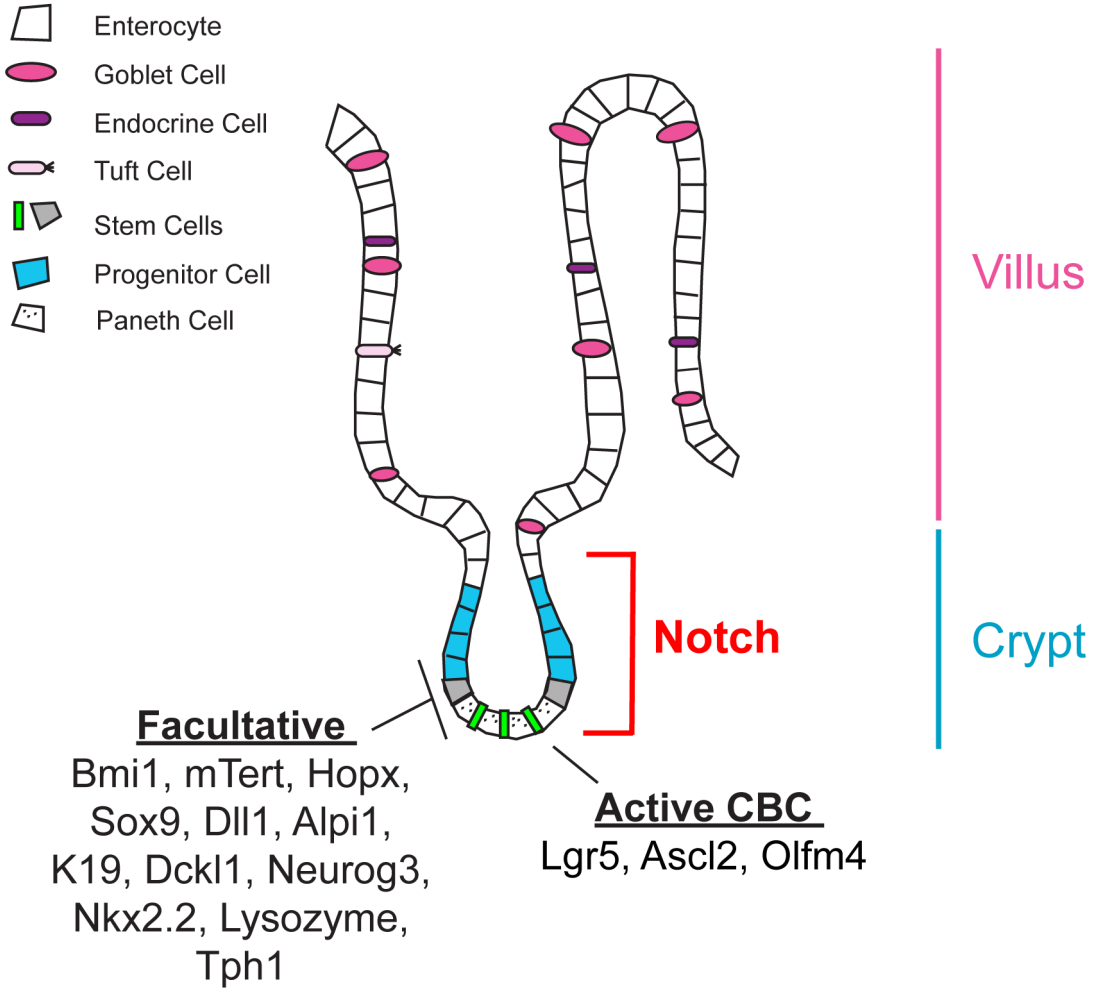

Figure 1.2 Stem cells in the adult small intestine.

Notch signaling is concentrated in the crypts where there are numerous distinct progenitor cell types, including facultative and active stem cells, and transit-amplifying (TA) progenitor cells. The facultative, long-term label-retaining stem cells are located at the “+4 position,” just above the Paneth cell compartment, and the active crypt base columnar (CBC) stem cells reside between the Paneth cells. These two stem cell populations and their possible relationship to each other are under extensive investigation. The current molecular markers for the active stem cell population include Lgr5, Ascl2, and Olfm4. Numerous progenitor cell populations, including secretory and enterocyte progenitors, can act as facultative stem cells, reflecting the considerable plasticity observed within the intestinal stem cell/progenitor compartment. The current molecular markers for facultative stem populations include Bmi1, mTert, Hopx, Sox9, Dll1, alkaline phosphatase (Api1), keratin 19 (K19), doublecortin-like kinase 1 (Dclk1), Neurogenin 3 (Neurog3), NK2 homeobox 2 (Nkx2.2), and Tryptophan hydroxylase 1 (Tph1).[286]

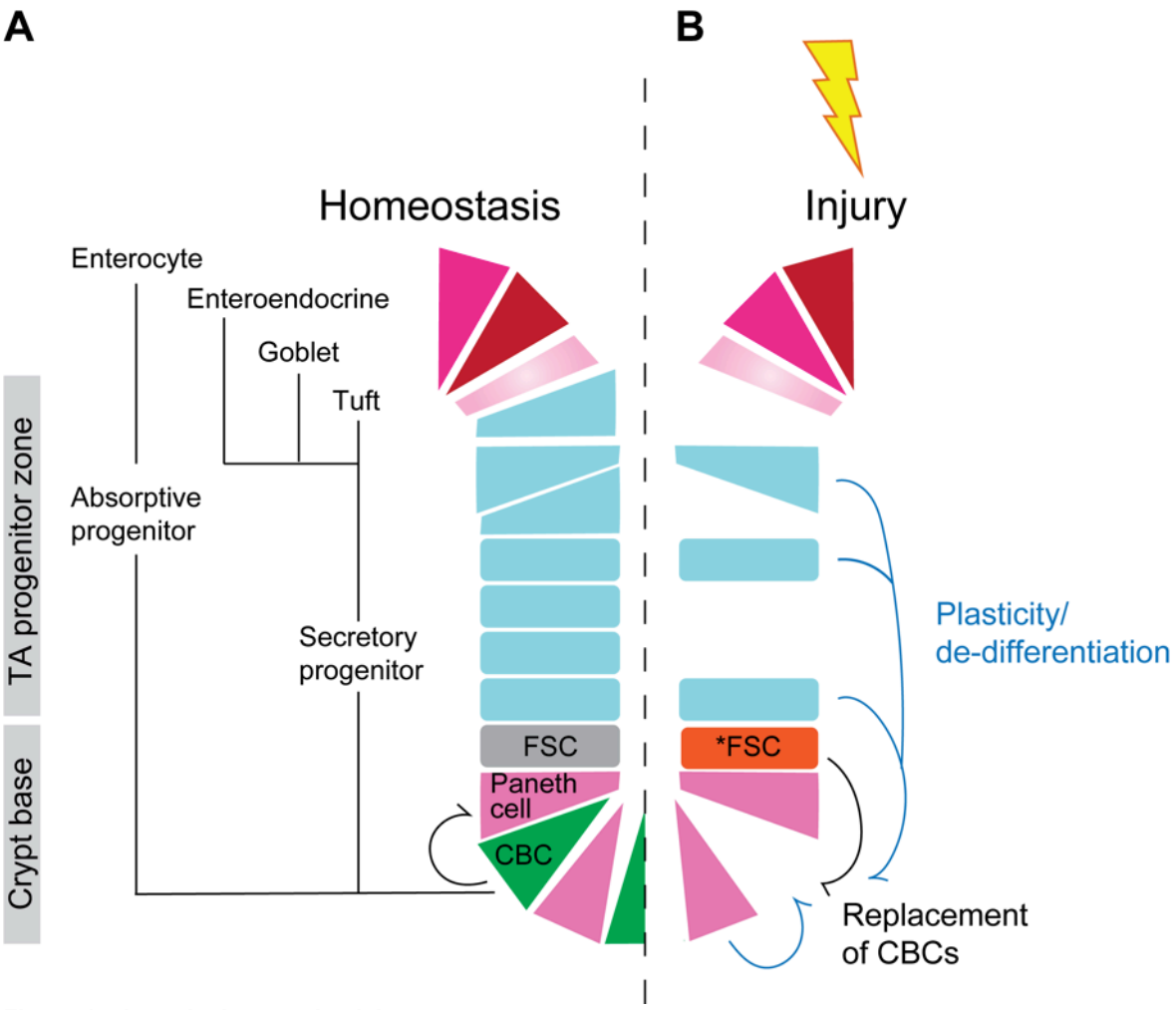

Figure 1.3 Intestinal crypt plasticity.

(A) During homeostasis, CBCs give rise to all differentiated intestinal epithelial cell types, via absorptive and secretory progenitors that go on to mature to enterocytes, goblet, enteroendocrine and tuft cells. FSCs make minimal contribution to homeostatic maintenance. (B) Following irradiation-induced CBC loss however, FSCs mediate regeneration. FSCs considered mitotically dormant during homeostasis at the '+4' crypt position activate, secretory and absorptive progenitors in the mid-crypt region mobilize and Paneth cells de-differentiate, all to the aim of regenerating CBCs, and returning to homeostasis. Note that CBC and FSC self-renewal is excluded from this diagram, as are absorptive M cells, and the de-differentiation potential of enteroendocrine cells. Adapted from Figure 1.[37]

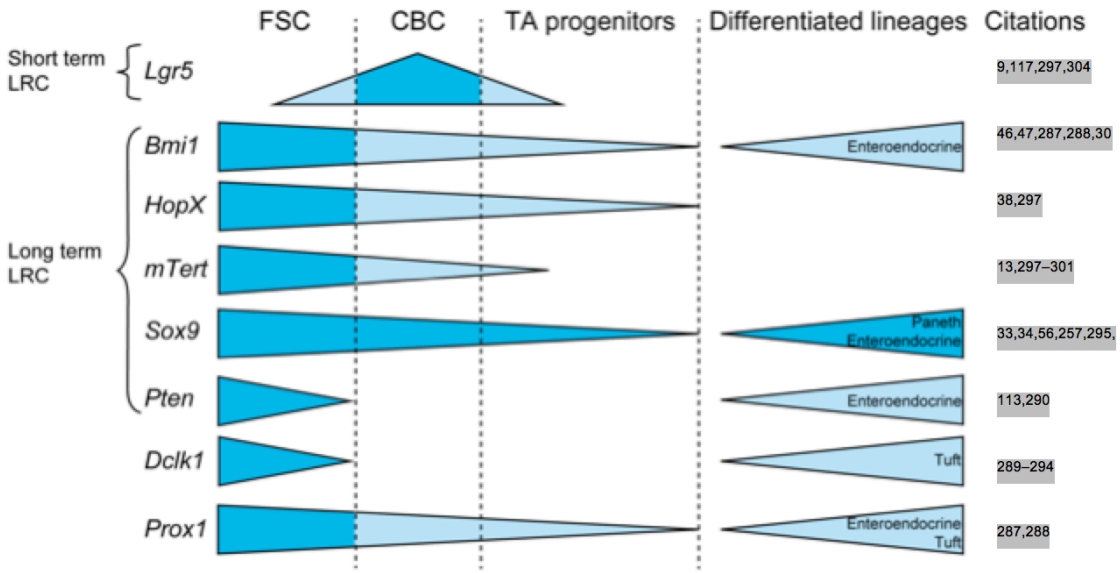

Figure 1.4 Facultative intestinal stem cell heterogeneity by marker expression.

Expression patterns of some of the biomarkers mapped to FSCs, with original marker specificity (dark blue) and expression patterns reported by follow-up studies (light blue). Expression reported by follow-up studies (light blue) also corresponds with lower expression than the expression originally reported (dark blue). LRC: label-retaining cell, see text for definition. Adapted from Figure 3.[37]

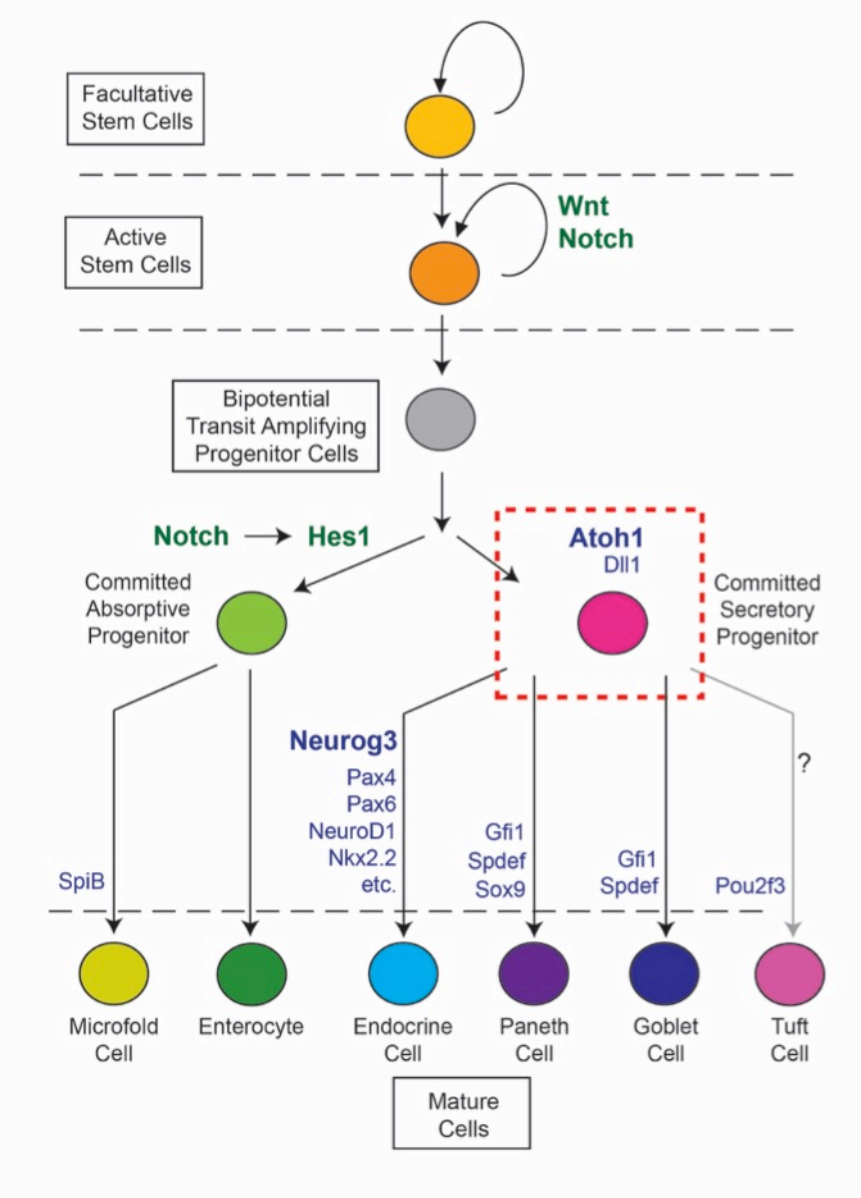

Figure 1.5 Model of intestinal epithelial cell differentiation.

Notch acts iteratively in stem cell renewal and cell fate specification. Stem cell renewal is regulated by WNT and Notch signaling. Upon exiting the stem cell niche, daughter cells are converted into bipotential transit-amplifying progenitor cells, which then undergo Notch-dependent cell fate specification. Notch signaling drives the absorptive cell fate over the default secretory cell fate. Notch signaling activates HES family transcription factors, including HES1, that function to inhibit expression of Atoh1 and thus promote enterocyte cell fate. RANKL-dependent induction of the transcription factor SpiB within the enterocyte lineage promotes the formation of M cells. In contrast, Atoh1 expression induces secretory cell differentiation. Atoh1 is expressed in all secretory pro- genitors and is essential for differentiation into goblet, endocrine, and Paneth cells. Atoh1 is also expressed in mature cells of these three secretory cell types. The involvement of Atoh1 in tuft cell specification is less clear. The identity of the secretory progenitor cell (red dashed box) is not well understood. Some studies suggest that there may not be a common secretory progenitor, and instead each secretory lineage may have its own committed progenitor cell. Critical transcription factors for lineage differentiation are listed in blue. See text for more details.[286]

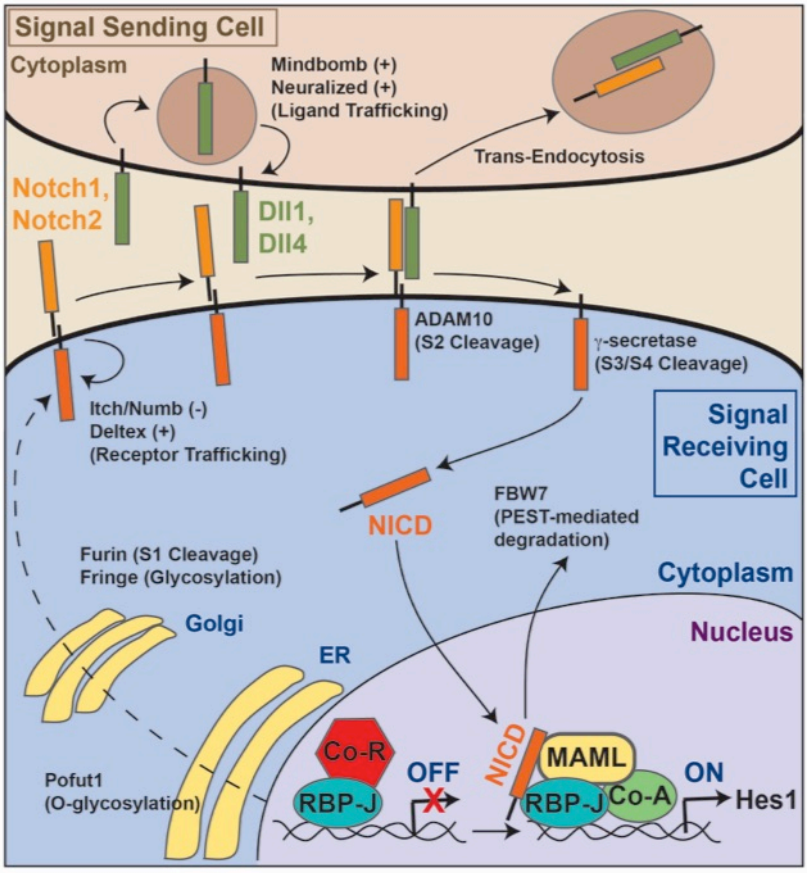

Figure 1.6 The Notch signaling pathway

Notch signaling is involved in short-range communication between juxtaposed cells with the signal-sending cell expressing ligand (Dll1 and Dll4 in intestinal crypts) and the signal-receiving cell expressing Notch receptor (Notch1 and Notch2 in intestinal crypts). Receptor activation is mediated by proteolytic cleavage events, but optimal Notch activity is dependent on posttranslational modifications and membrane trafficking of Notch receptors and ligands (see Table 1.2). In the signal-receiving cell, newly synthesized Notch receptor is O-fucosylated by Pofut1 within the endoplasmic reticulum (ER), which is essential for Notch activity. O-glucosylation, which is required for efficient Notch proteolysis, also occurs at this time. Upon transit through the Golgi, fucose moities are further modified through the addition of N-acetylglucosamine by Fringe O-glycosyltransferases, which can alter ligand-binding specificity. In the Golgi compartment, the Notch receptor is also cleaved within its ectodomain by furin-like proteases (S1 cleavage) to generate a heterodimer held together by noncovalent interactions. Mature Notch receptor is then delivered to the plasma membrane. At the cell surface, steady-state receptor levels needed for productive Notch signaling are regulated by protein interactions (e.g., Numb) and several distinct E3 ubiquitin ligases (e.g., Deltex, Itch/Nedd4), which control receptor trafficking, lysosomal degradation, and recycling. In the signal-sending cell, Notch ligand activity is enhanced through endocytic trafficking, which is also controlled by E3 ubiquitin ligases (e.g., Neuralized, Mindbomb). Upon ligand engagement, the Notch receptor is cleaved by the disintegrin-metalloproteinase ADAM10 (S2 cleavage), which releases the Notch receptor ectodomain and produces a membrane-anchored NEXT fragment. The released receptor ectodomain is trans-endocytosed into the signal-sending cell. Subsequent γ-secretase-dependent cleavage of NEXT (S3/S4 cleavage) releases the bioactive form of the Notch receptor, the Notch intracellular domain (NICD). In the absence of signaling, the DNA-binding protein RBP-Jκ interacts with corepressors (Co-R) to suppress transcription of Notch target genes. However, upon Notch activation, NICD is produced, and it translocates to the nucleus where it interacts with RBP-Jκ, mastermind (MAML) and other coactivators (Co-A) to activate transcription of target genes, including hairy and enhancer of split 1 (Hes1). NICD signaling is terminated by rapid phosphorylation of its C-terminal PEST domain and targeting for proteosomal degradation by E3 ubiquitin ligases such as F-box and WD-40 domain-containing protein 7 (FBW7). Endocytic trafficking components that either reduce (−) or increase (+) the activity of ligands and receptors are noted.[286]

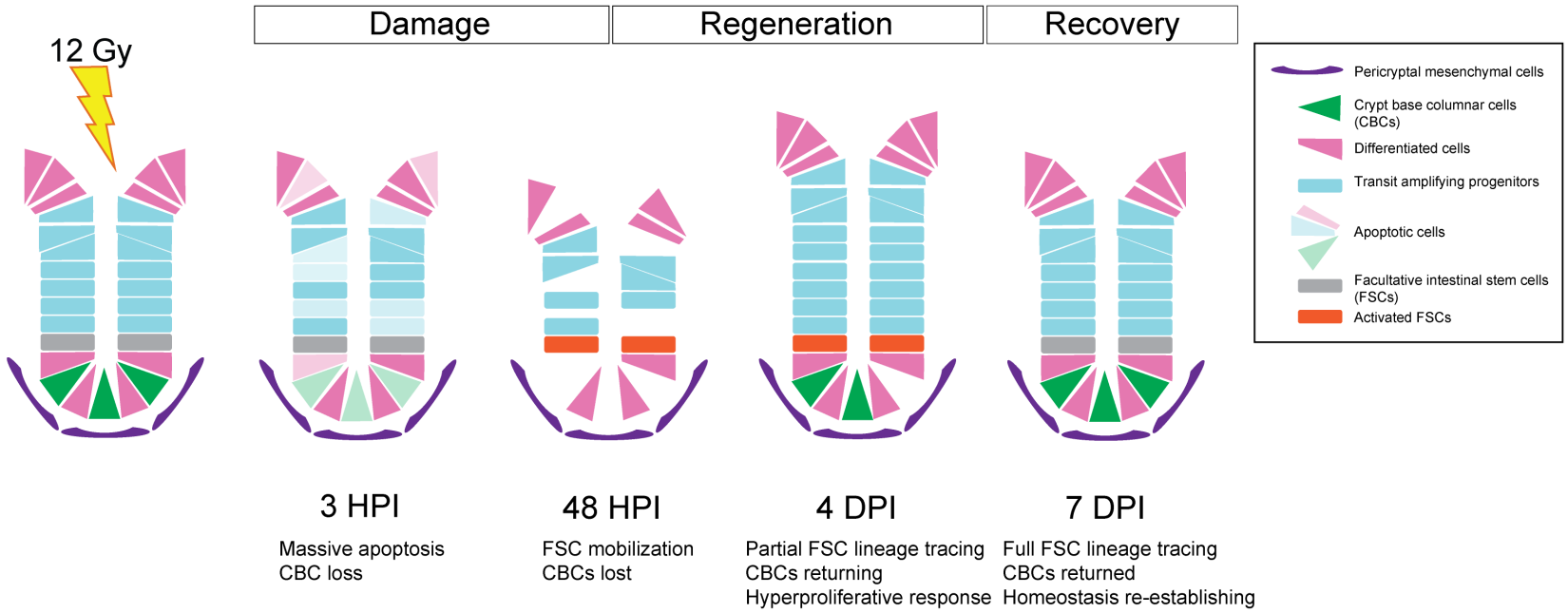

Figure 1.7 The prototypical intestinal regenerative response to high dose irradiation injury

Administration of a high γ-irradiation dose (>10 Gy) is a demonstrated method of injuring the intestinal epithelium that results in a repair response that can be categorized into 3 phases: damage, regeneration and recovery. Within 3-6 hours post-irradiation (HPI), crypt cells undergo massive apoptosis (denoted as faded cells), with crypt base columnar cells (CBCs; green at crypt base) being lost. By 48HPI, CBC loss, perhaps through signaling from pericryptal mesenchymal cells (purple flat cells underlying the crypt) and/or Paneth cells (pink cells intercalated between CBCs) stimulates activation of facultative stem cells (FSCs; from gray inactive to orange active around +4 crypt position) to contribute to crypt repair. Around 4 days post-irradiation (DPI), a hyperpoliferative surge is noted (expansion of mid-crypt progenitors in blue), with expanded crypts, CBCs beginning to re-emerge and some FSC lineage traces. A few days later, 6-7 DPI, homeostasis is on its way to being re-established, with CBCs having mostly returned, and proliferation returning to baseline levels.

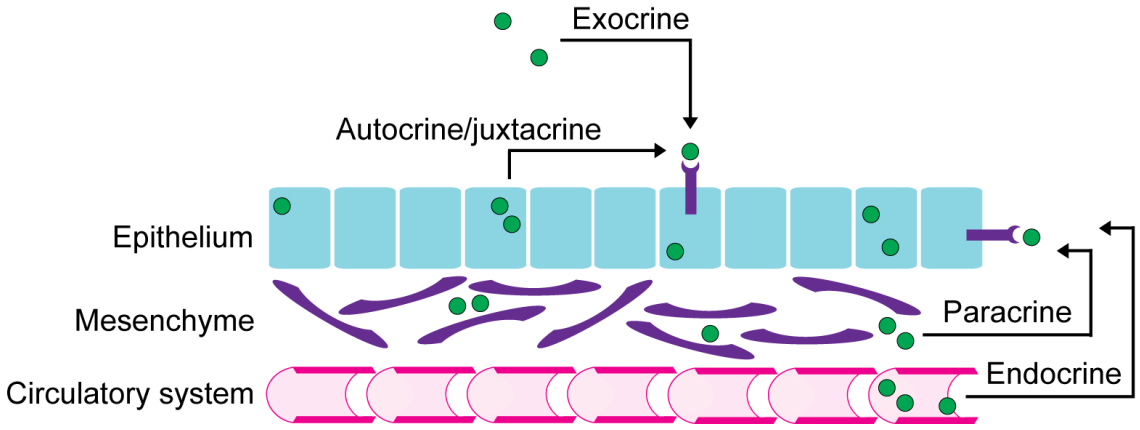

Figure 1.8 Growth factor signaling routes

Growth factors are synthesized from numerous different cellular sources, and have myriad targets throughout the intestine. There are three main modes by which growth factors signal to surrounding tissues: exocrine, autocrine/juxtacrine, paracrine and endocrine signaling. Exogenously derived growth factors, such as those produced in breast milk, employ an exocrine signaling route to affect change to target cells. Signaling from secreted growth factors acting on their own cell's receptors, or on a same cell type locally, is referred to as autocrine and juxtacrine signaling respectively. Paracrine signaling is employed by growth factors secreted from one cell type and acting on another, such as that observed in epithelial to mesenchymal interactions. Growth factors produced in one area or organ, and acting on a distant target cell, often travelling via the circulatory system, are known as signaling via an endocrine route. Adapted from Figure 3.1 of the Sixth Edition of the Physiology of the Gastrointestinal Tract.[209]

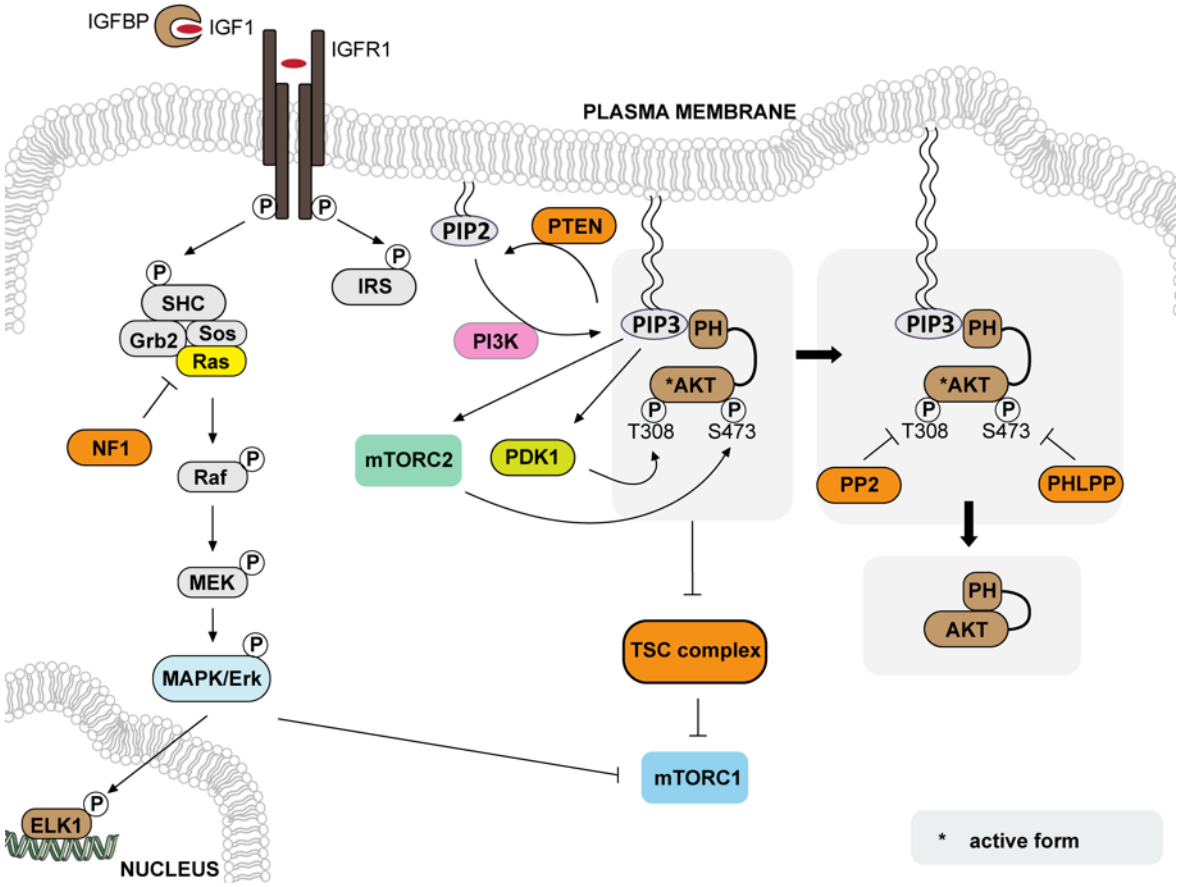

Figure 1.9 Insulin-like growth factor 1 (IGF1) signaling

IGF1 signals via two main signaling axis, the PI3K/AKT and the Ras/ERK/MAPK signaling pathways. In the former pathway, upon IGF1 binding, IGFR1 is activated via autophosphorylation, and proceeds to phosphorylate and activate IRS. IRS promotes PI3K-mediated PIP_3 production, leading to AKT phosphorylation by PDK1 at T308 and mTORC2 at S473. In this phosphorylated active form, AKT proceeds to inhibit the repressive function of the TSC complex on mTORC1. Activated IGFR1 also phosphorylates SHC, which stimulates Raf through the Ras GTPase. Raf triggers a kinase cascade including activation of MAPK/ERK. ERK goes on to inhibit TSC complex activity on mTORC1, and phosphorylate and activate transcription factor ELK1, promoting expression of target genes.

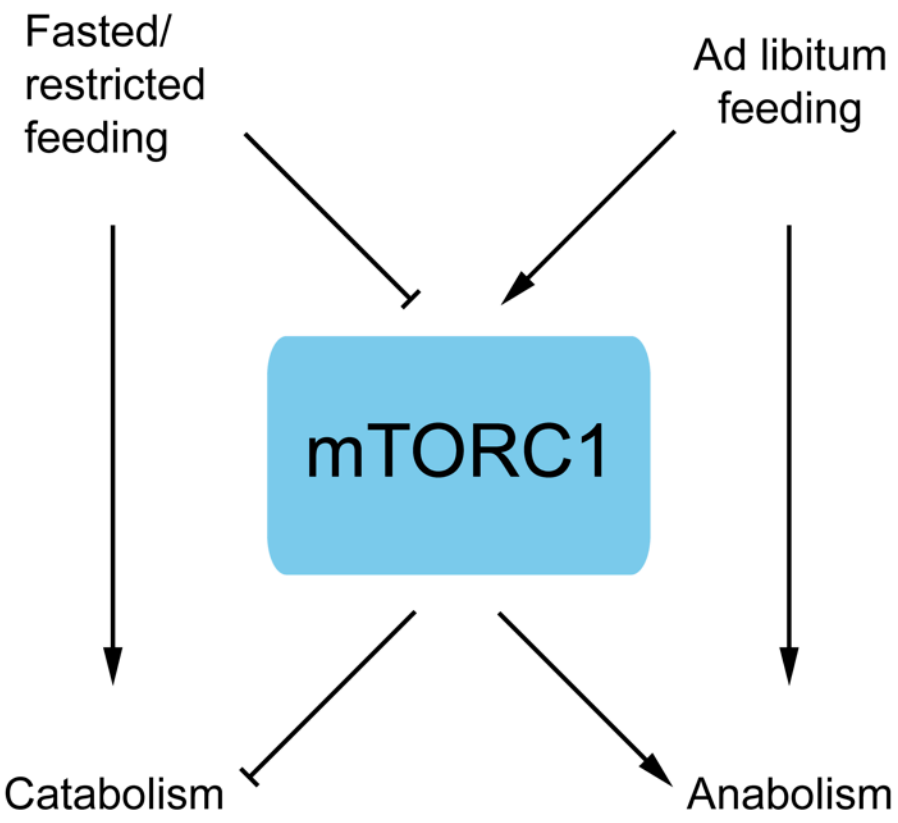

Figure 1.10 mTORC1-dependent catabolic/anabolic balance

In response to nutrient availability (e.g. amino acids, growth factors, energy), mTORC1 maintains tight control over the precarious balance between catabolism and anabolism. Adapted from Figure 4A of Saxton and Sabatini review.[260]

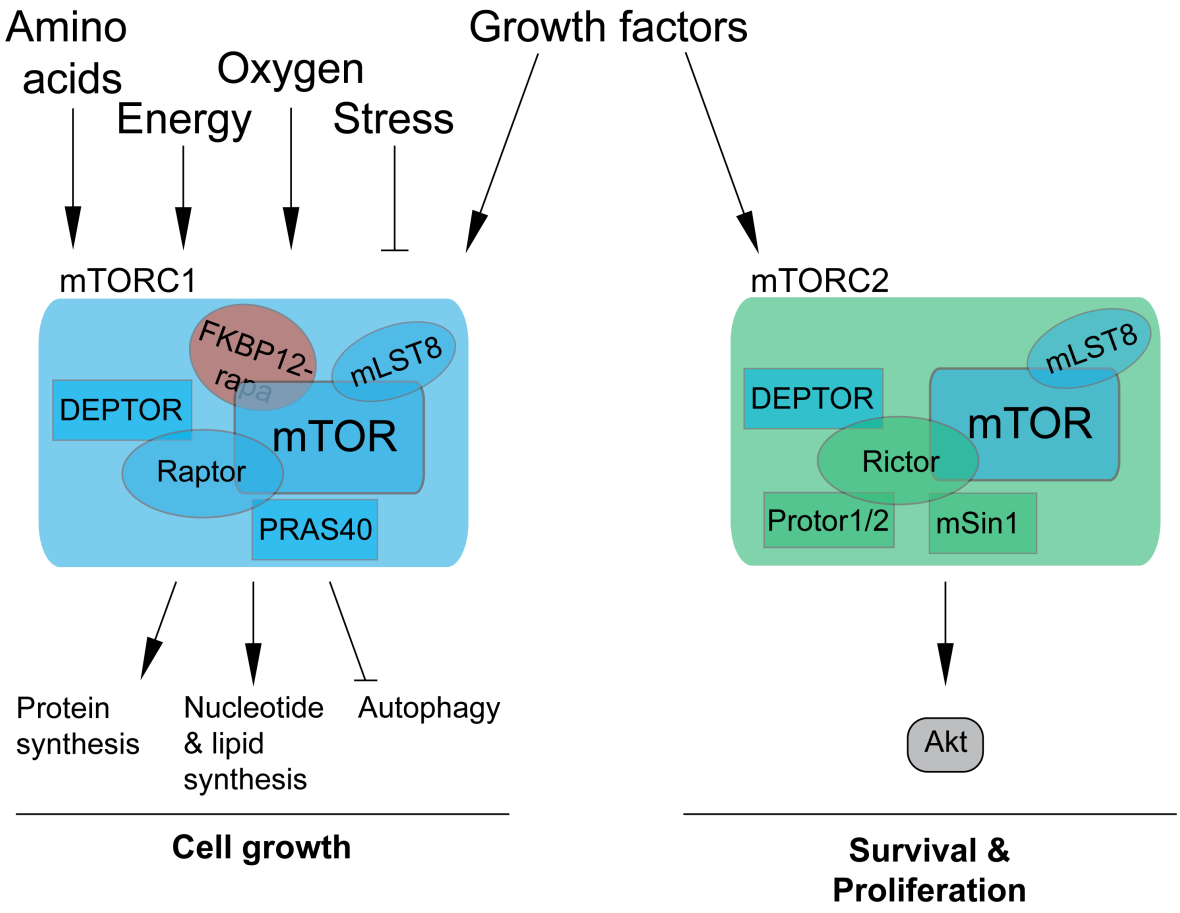

Figure 1.11 mTORC1 versus mTORC2

The mTOR protein is the catalytic subunit of two functionally distinct protein complexes: mTOR complex 1 (mTORC1) and mTOR complex 2 (mTORC2). In mTORC1, Raptor binds mTOR through its HEAT repeats. In mTORC2, Raptor is replaced by Rictor. The subunit DEPTOR binds both Raptor and Rictor to inhibit complex activity. mTORC1 has an additional Raptor-bound inhibitory subunit: PRAS40. On the other hand, Rictor in mTORC2 is bound by regulatory subunits mSin1, and Protor1/2. Both complexes are also comprised of mLST8, which is thought to stabilize complex activity. mTORC1 is rapamycin-sensitive, while mTORC2 is not*. Rapamycin binds FKBP12, and together the complex binds the FRB domain of mTOR, leading to narrowing of the catalytic cleft and substrate occlusion from the active site. These subunit differences result in functional differences between the two complexes. While growth factors promote the activity of both complexes, mTORC1 activity is also controlled by amino acid availability, energy, oxygen and stress. mTORC1 is involved in anabolic pathways (i.e. protein synthesis, lipid and nucleotide synthesis, glucose metabolism and autophagy), and mTORC1 in pro-survival mechanisms via modulation of Akt signaling.
*Extended rapamycin treatment does affect mTORC2 activity. See text for additional detail. Adapted from Figure 1 of Saxton and Sabatini review.[260]

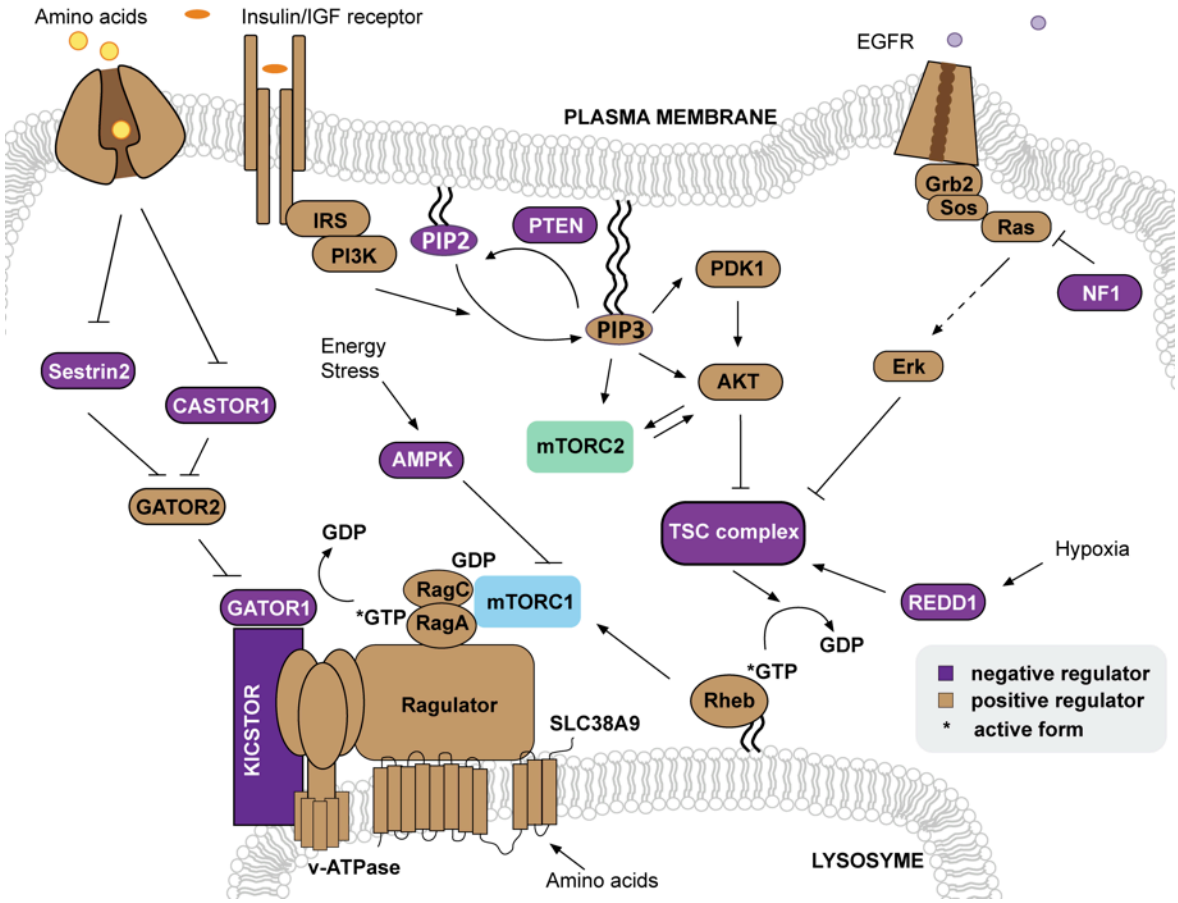

Figure 1.12 Upstream mTORC1 signaling pathways

mTORC1 is regulated by myriad environmental cues including amino acids, growth factors, energy, stress and oxygen. Some of these regulatory axes are illustrated and described here. [AMINO ACIDS] The subcellular localization of mTORC1, critical to its activity, is regulated by cytosolic and lysosomal amino acid availability. The active RagAGTP/RagCGDP heterodimers tether mTORC1 to the lysosome where it can interact with stores of lysosomal membrane-bound Rheb. Active, GTP-bound Rheb activates mTORC1. Lysosomal amino acid content works in part through lysosomal v-ATPase interacting with the Ragulator-Rag heterodimers complex, serving to enhance to the GEF activity of Ragulator to RagA, and in part through the lysosomal amino acid sensor SLC38A9 and its interaction with the Rag-Ragulator-v-ATPase complex. Cytosolic amino acid content on the other hand works through the GATOR1 and GATOR2 complexes. GATOR1 serves as a GAP to RagA, maintaining it in its inactive GDP-bound form. GATOR1 is tethered to the lysosomal membrane surface, in close proximity to the active RagA/C heterodimers, via interaction with KICSTOR. The activity of this negative mTORC1 regulator is inhibited by GATOR2. Cytosolic amino acids work to enhance mTORC1 activity by inhibiting the activity of two negative regulators of GATOR2 and mTORC1 activity, Sestrin2 and CASTOR1. [GROWTH FACTORS] Insulin/IGF signal to mTORC1 via PI3K/AKT signaling. PI3K produces PIP3, which subsequently activates AKT. AKT, whose activity can be enhanced by mTORC2, is a negative regulator of the TSC complex. When active, the TSC complex works as a GAP to GTP-bound Rheb, thereby inactivating it. TSC complex activity is also inhibited by Erk, part of the Ras/Erk signaling cascade stimulated by EGF activity on its receptor EGFR. [OTHERS] mTORC1 activity can also be suppressed via energy and stress-responsive AMPK, a negative regulator of mTORC1, and hypoxia-responsive REDD1, which promotes TSC complex activity. Adapted from Figure 2A of Saxton and Sabatini review.[260]

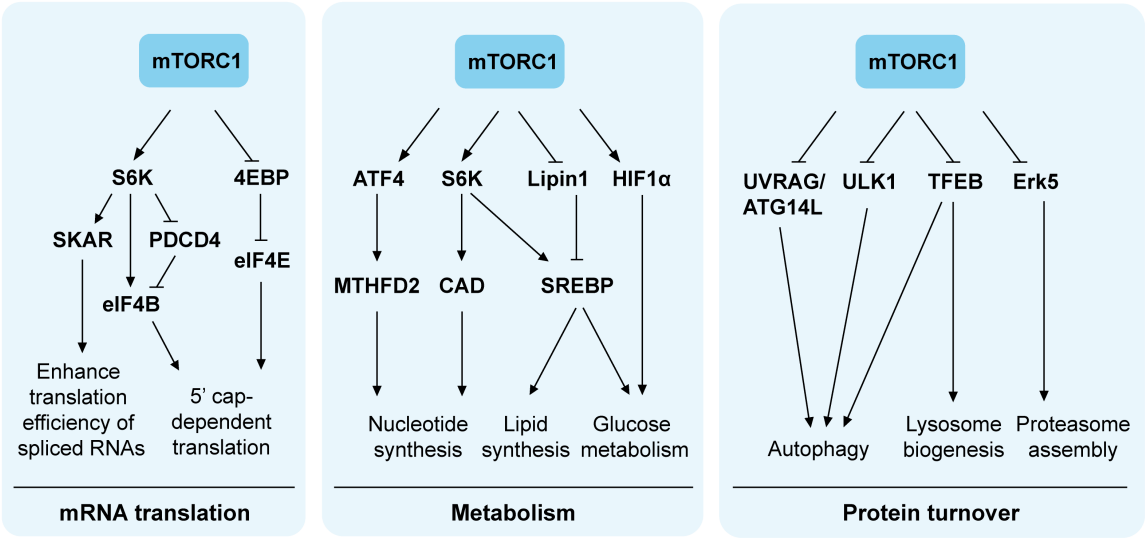

Figure 1.13 Downstream mTORC1 signaling pathways

mTORC1 is involved in promoting mRNA translation, lipid and nucleotide synthesis, glucose metabolism, autophagy and other protein turnover mechanisms. See text for detailed explanation of the downstream mTORC1 pathways involved in mRNA translation. mTORC1 activity leads to enhanced ATF4-dependent expression of the key component to the mitochondrial tetrahydrofolate cycle involved in purine nucleotide synthesis: MTHFD2. Through its phosphorylation and activation of S6K1, mTORC1 also activates carbamoyl-phosphate synthetase (CAD), taking part in pyrimidine synthesis. mTORC1 signaling leads to increased expression of HIF1α (also hypoxia driven), which drives glycolysis over oxidative phosphorylation. mTORC1 activates SREBP (via releasing its inhibition by Lipin1) to promote lipid synthesis and glucose metabolism. mTORC1 also controls autophagy by suppressing protein catabolism. ULK1 activation via AMPK phosphorylation is a key part of autophagy, as it leads to the formation of a complex that drives autophagosome formation. mTORC1 phosphorylates ULK1 in lieu of AMPK to inhibit this process. mTORC1 also phosphorylates the nuclear translocation factor EB (TFEB), thereby inactivating it and preventing its driving lysosome biogenesis and autophagy machinery gene expression. Some studies have also reported a role for mTORC1 in the repression of protein ubiquitylation, and some have found the complex inhibits Erk5, which normally increases the abundance of proteasomal chaperones. Adapted from Figure 2B of Saxton and Sabatini review.[260]

1.7 Tables

Table 1.1 Intestinal Phenotypes of Core Notch Pathway Rodent Models.[286]

Component	Gene/ Complex	Age[a]	Animal Model[b]	Intestinal Phenotype		
				Proliferation	Apoptosis	Cell Specification
Receptor	Notch1	4 wks	LOF; Vil-CreERT2 x floxed Notch1; 12 days after Cre induction	Normal		Normal
	Notch1	2-4 mo	LOF; Vil-CreERT2 x floxed Notch1; 6-60 days after Cre induction	Normal		Moderate yet transient secretory cell hyperplasia; stem cell loss
	Notch1	8 wks	LOF; Vil-Cre x floxed Notch1			Moderate goblet cell hyperplasia; increased number and clustering of M cells
	Notch1	12 wks	LOF; Notch1 inhibiting antibody; 12 days after first injection			Moderate goblet cell hyperplasia
	Notch2	4 wks	LOF; Vil-CreERT2 x floxed Notch2; 6 or12 days after Cre induction	Normal		Normal
	Notch2	12 wks	LOF; Notch2 inhibiting antibody; 12 days after first injection	Normal		Normal
	Notch1 and Notch2	4-8 wks	LOF; Vil-CreERT2 x floxed Notch1/2; 6 or12 days after Cre induction	Decreased		Secretory cell hyperplasia; stem cell loss

	Notch1 and Notch2	12 wks	LOF; Inhibiting antibodies specific for Notch1 and Notch2; 12 days after first injection	Decreased		↓Hes1, ↑Atoh1; secretory cell hyperplasia; stem cell loss
Ligand	Dll1	4 wks	LOF; Vil-CreERT2 x floxed Dll1; 14 days after Cre induction	Normal		Moderate goblet cell hyperplasia
	Dll1	Adult	LOF; Ah-Cre x floxed Dll1; 5-28 days after induction			↑Atoh1, moderate secretory cell hyperplasia
	Dll4	4 wks	LOF; Vil-CreERT2 x floxed Dll4; 14 days after Cre induction	Normal		Normal
	Jag1	4 wks	LOF; Vil-CreERT2 x floxed Jag1; 14 days after Cre induction	Normal		Normal
	Dll1 and Dll4	4 wks	LOF; Vil-CreERT2 x floxed Dll1/Dll4; 3-5 days after Cre induction	Decreased		↓Hes1; goblet cell hyperplasia; stem cell loss
Nuclear Effector	RBP-Jκ	36 wks	LOF; P450-Cre x floxed RBP-J; 4-5 days after Cre induction	Decreased	Normal	↓Hes1, ↑Atoh1; goblet cell hyperplasia but no change in other secretory cell types
	RBP-Jκ	4-5 wks	LOF; Vil-CreERT2 x floxed RBP-J; 6 and 12 days after Cre induction	Decreased		↓Hes1, ↑Atoh1; secretory cell hyperplasia; stem cell loss
	MAML	P0	LOF; 9kbVil-Cre x floxed "STOP" dnMAML	Decreased		Secretory cell hyperplasia

	NICD	P0	GOF; 9kbVil-Cre x ROSA26-floxed "STOP" NICD	Increased	Increased	↑Hes1, ↓Atoh1; decreased goblet and endocrine cells
	NICD	Adult	GOF; Fabpl-Cre x ROSA26-floxed "STOP" NICD x Z/AP reporter mouse	Increased	Normal	Decreased goblet and endocrine cells
Receptor Proteolysis	Adam10	P0, Adult	LOF; 9kbVil-Cre (or Vil-CreERT2) x floxed ADAM10	Decreased		↑Atoh1; secretory cell hyperplasia; stem cell loss
	Adam17	P0, Adult	LOF; 9kbVil-Cre x floxed ADAM17	Normal		Normal
	Adam17	Adult	LOF; hypomorphic allele	Normal when unchallenged		Normal when unchallenged
	γ-secretase	7-8 wks	LOF; pharmacological inhibitors (DBZ, BZ); 1-5 day treatment in rats			↓Hes1, ↑Atoh1; increased goblet and endocrine cells
	γ-secretase	6 wks	LOF; pharmacological inhibitor (LY-411,575); 5 or 15 day treatment in TgCRND8 mice			Goblet cell hyperplasia
	γ-secretase	Adult	LOF; pharmacological inhibitor (DBZ); 5 day treatment in mice	Decreased	Stem cell apoptosis	↑Atoh1; secretory cell hyperplasia; stem cell loss
Glycosyl-transferase Modifier	Pofut1	4 wks, 36 wks	LOF; 12.4kbVil-Cre x floxed Pofut-1	Decreased with dispacement towards top of crypt		↓Hes1 and Hes5, ↑Atoh1; secretory cell hyperplasia (restricted to crypts)
Membrane and Endosomal Trafficking Modifer	Mib1	2-4 wks	LOF; 12.4kbVil-Cre x floxed Mib1	Decreased		Increased secretory cells, mislocated Paneth cells on villi, only 20% of mutants are viable past 4 weeks of age

	Fbxw7	Adult	GOF; 9kbVil-Cre x floxed Fbxw7	Increased	Increased	↑NICD1, ↑Hes1, ↑Hes5, ↓Atoh1; decreased secretory cells
Canonical bHLH Effector	Hes1	E14-E19	LOF; Hes1 knock-out	Normal	Increased in intervillus zone	↑Hes5, ↑Atoh1, increased goblet and endocrine cells
	Hes1	P0	LOF; Hes1 knock-out	Altered distribution along the crypt-villus axis		Precocious differentiation of Paneth cells
	Hes1	P2.5	LOF; Vil-Cre x floxed Hes1	Normal	Increased	Moderate goblet and endocrine cell hyperplasia;
	Hes1	Adult	LOF; Vil-Cre x floxed Hes1	Normal	Normal	Normal
	Hes1, Hes3, Hes5	P2.5, 2 mo, 1 yr	LOF; Vil-Cre x Hes1$^{f/-}$, Hes3$^{-/-}$ and Hes5$^{-/-}$	Decreased	Increased	Secretory cell hyperplasia; Paneth cells mislocalized; expanded colonic crypts
	Hes5	Adult	LOF; Hes5 knock-out			↑Dll1, ↑Fbxw7, moderate goblet cell hyperplasia

LOF, loss-of-function; GOF, gain-of-function.
[a]*Age of Analysis.*
[b]*See references for detailed description of each model.*

Table 1.2 Mammalian Notch Pathway: Core Components and Modulators.[286]

Component/Activity	Gene(s)[a]	Protein type/Activity	Modulatory function
Receptor	Notch1, Notch2, Notch3 and Notch4	Type 1 transmembrane protein	
Ligand	Dll1, Jag1 and Jag2	DSL and DOS domain-containing	
	Dll3 and Dll4	DSL only	
Proteolysis	Furin-like convertase	Proprotein convertase (receptor S1 cleavage)	Heterodimer formation
	Adam10	Metalloproteinase (receptor S2 cleavage)	Initiates receptor signaling[b]
	TspanC8s[c]	Metalloproteinase trafficking/substrate presentation (receptor S2 cleavage)	Positive and negative regulators
	Psen(1 or 2), Ncstn, Psenen, Aph1(a, b or c)	g-Secretase complex: 1:1:1:1 stoichiometry (receptor S3/4 cleavage)	NICD generation
	Adam9, Adam10, Adam12, Adam17	Metalloproteinase (ligand)	Ectodomain shedding
Glycosyltransferase	Pofut1	O-fucosyltransferase (receptor)	Essential for Notch activity
	Fringe family: Lfng, Mfng, Rfng	b1,3-GlnNActransferase (receptor)	Optimal Notch activity/ligand specificity
	Poglut1	O-glucosyltransferase (receptor)	Essential for Notch activity Promotes extracellular cleavage
	Gxylt1, Gxylt12 and Xxylt1	O-xylosyltransferase (receptor)	Negative regulator
	Eogt1	O-GlcNAc transferase (receptor)	Impaired Notch signaling Reduced DLL1/DLL4 binding
Membrane/endosomal trafficking	Mib1	Ring finger E3 ubiquitin ligase (ligand endocytosis)	Optimal ligand activity
	Itch/Nedd4 family	HECT domain E3 ubiquitin ligase (receptor endocytosis)	Reduces Notch activity; lysosomal trafficking/degradation
	Deltex1, 2, 3 and 4	Ring finger E3 ubiquitin ligase (receptor endocytosis)	Optimal receptor activity

	Numb	Receptor binding partner (asymmetric partitioning during cell division)	Negative regulator
	Fbxw7	F-Box ubiquitin ligase (NICD degradation)	Reduces Notch activity; proteosomal trafficking/degradation
	Crumbs	Receptor binding partner (inhibits ligand-independent Notch endocytosis/activation)	Negative regulator
	Commd99	Regulator of endosomal trafficking and Notch recylcling to the cell surface	Positive regulator
Ubiquitin-specific proteases	Usp28 and Usp12	Counteracts Fbxw7	

Productive Notch signaling is dependent on the cell surface presentation and activity of membrane bound ligands and receptors, processes that are controlled by a number of different structural and modifying components.

[a]*Mouse gene symbols are listed; see text for gene definitions and protein activity.*

[b]*Rate-limiting step for initiation of a Notch signaling event.*

[c]*Tspan5, 10 and 14 (positive regulators) and Tspan15 and 33 (negative regulators).*

Table 1.3 Overview of Major Growth Factors, Receptors, and Targets.

Growth Factor Family	Receptors	Ligands	Target Cell Types
Epidermal growth factor	EGFR/ErbB1 ErbB2 ErbB3 ErbB4	EGF, TGFα, NRG-1-4, HB-EGF, amphiregulin, betcellulin, epiregulin, epigen	Epithelium Endothelium Immune ?
Transforming growth factor-β	TβR-I TβR-II	TGFβ, BMP2-7, Activin, inhibin, nodal	Epithelium Endothelium Immune
Insulin-like growth factor	IGFR1 IGFR2	IGF1 IGF2	Epithelium Endothelium
Hepatocyte growth factor	c-Met Co-receptors (CD44)	HGF	Epithelium Endothelium Mesenchyme Immune
Fibroblast growth factor	FGFR1-4 Co-receptors (α/β-klotho)	FGF1, 2, 4, 7, 9, 10, 15/19, 18, 21, 20 (in cancer), 23	Epithelium Mesenchyme
Trefoil factor	CXCR4 Unidentified others	TFF1, TFF2, TFF3	Epithelium Immune
Hedgehog	Ptch1-2	Shh, Ihh, Dhh	Epithelium Immune

Adapted from Table 3.1 of the Sixth Edition of the Physiology of the Gastrointestinal Tract.[209]

1.8 References

1. Gao, N., White, P. & Kaestner, K. H. Establishment of Intestinal Identity and Epithelial-Mesenchymal Signaling by Cdx2. *Dev. Cell* **16,** 588–599 (2009).

2. Howitt, M. R. *et al.* Tuft cells, taste-chemosensory cells, orchestrate parasite type 2 immunity in the gut. *Science (80-.).* **351,** 1329–1333 (2016).

3. Gerbe, F. *et al.* Intestinal epithelial tuft cells initiate type 2 mucosal immunity to helminth parasites. *Nature* **529,** 226–230 (2016).

4. von Moltke, J., Ji, M., Liang, H.-E. & Locksley, R. M. Tuft-cell-derived IL-25 regulates an intestinal ILC2–epithelial response circuit. *Nature* **529,** 221–225 (2016).

5. Crosnier, C., Stamataki, D. & Lewis, J. Organizing cell renewal in the intestine: stem cells, signals and combinatorial control. *Nat. Rev. Genet.* **7,** 349–59 (2006).

6. Yan, K. S. *et al.* The intestinal stem cell markers Bmi1 and Lgr5 identify two functionally distinct populations. *Proc. Natl. Acad. Sci. U. S. A.* **109,** 466–71 (2012).

7. Potten, C. S., Gandara, R., Mahida, Y. R., Loeffler, M. & Wright, N. A. The stem cells of small intestinal crypts: where are they? *Cell Prolif.* **42,** 731–50 (2009).

8. Lund, P. K. Fixing the breaks in intestinal stem cells after radiation: a matter of DNA damage and death or DNA repair and regeneration.

Gastroenterology **143,** 1144–1147 (2012).

9. Buczacki, S. J. A. *et al.* Intestinal label-retaining cells are secretory precursors expressing Lgr5. *Nature* **495,** 65–9 (2013).

10. Barriga, F. M. *et al.* Mex3a Marks a Slowly Dividing Subpopulation of Lgr5+ Intestinal Stem Cells. *Cell Stem Cell* **20,** 801–816.e7 (2017).

11. Itzkovitz, S. *et al.* Single-molecule transcript counting of stem-cell markers in the mouse intestine. *Nat. Publ. Gr.* **14,** (2011).

12. van Es, J. H. *et al.* Dll1+ secretory progenitor cells revert to stem cells upon crypt damage. *Nat. Cell Biol.* **14,** 1099–104 (2012).

13. Muñoz, J. *et al.* The Lgr5 intestinal stem cell signature: robust expression of proposed quiescent '+4' cell markers. *EMBO J.* **31,** 3079–3091 (2012).

14. Richmond, C. A., Shah, M. S., Carlone, D. L. & Breault, D. T. An Enduring Role for Quiescent Stem Cells. *Dev. Dyn.* (2016). doi:10.1002/dvdy.24416

15. Barker, N. *et al.* Crypt stem cells as the cells-of-origin of intestinal cancer. *Nature* **457,** 608–11 (2009).

16. Visvader, J. E. Cells of origin in cancer. *Nature* **469,** 314–322 (2011).

17. Potten, C. S., Kovacs, L. & Hamilton, E. Continuous labelling studies on mouse skin and intestine. *Cell Tissue Kinet.* **7,** 271–83 (1974).

18. Cheng, H. & Leblond, C. P. Origin, differentiation and renewal of the four main epithelial cell types in the mouse small intestine. V. Unitarian Theory of the origin of the four epithelial cell types. *Am. J. Anat.* **141,** 537–61 (1974).

19. Bjerknes, M. & Cheng, H. The stem-cell zone of the small intestinal epithelium. II. Evidence from paneth cells in the newborn mouse. *Am. J. Anat.* **160,** 65–75 (1981).

20. Barker, N. *et al.* Identification of stem cells in small intestine and colon by marker gene Lgr5. *Nature* **449,** 1003–7 (2007).

21. Sato, T. *et al.* Single Lgr5 stem cells build crypt-villus structures in vitro without a mesenchymal niche. *Nature* **459,** 262–265 (2009).

22. Tian, H. *et al.* A reserve stem cell population in small intestine renders Lgr5-positive cells dispensable. *Nature* **478,** 255–9 (2011).

23. Barker, N. *et al.* Identification of stem cells in small intestine and colon by marker gene Lgr5. *Nature* **449,** 1003–7 (2007).

24. van de Wetering, M. *et al.* The beta-catenin/TCF-4 complex imposes a crypt progenitor phenotype on colorectal cancer cells. *Cell* **111,** 241–50 (2002).

25. Barker, N. *et al.* Very Long-term Self-renewal of Small Intestine, Colon, and Hair Follicles from Cycling Lgr5+ve Stem Cells. *Cold Spring Harb. Symp. Quant. Biol.* **73,** 351–356 (2008).

26. de Lau, W. *et al.* Lgr5 homologues associate with Wnt receptors and mediate R-spondin signalling. *Nature* **476,** 293–7 (2011).

27. Ruffner, H. *et al.* R-Spondin Potentiates Wnt/β-Catenin Signaling through Orphan Receptors LGR4 and LGR5. *PLoS One* **7,** e40976 (2012).

28. Carmon, K. S., Gong, X., Lin, Q., Thomas, A. & Liu, Q. R-spondins function

as ligands of the orphan receptors LGR4 and LGR5 to regulate Wnt/beta-catenin signaling. *Proc. Natl. Acad. Sci. U. S. A.* **108,** 11452–7 (2011).

29. Glinka, A. *et al.* LGR4 and LGR5 are R-spondin receptors mediating Wnt/β-catenin and Wnt/PCP signalling. *EMBO Rep.* **12,** 1055–61 (2011).

30. Garcia, M. I. *et al.* LGR5 deficiency deregulates Wnt signaling and leads to precocious Paneth cell differentiation in the fetal intestine. *Dev. Biol.* **331,** 58–67 (2009).

31. van der Flier, L. G. *et al.* Transcription Factor Achaete Scute-Like 2 Controls Intestinal Stem Cell Fate. *Cell* **136,** 903–912 (2009).

32. van der Flier, L. G., Haegebarth, A., Stange, D. E., van de Wetering, M. & Clevers, H. OLFM4 Is a Robust Marker for Stem Cells in Human Intestine and Marks a Subset of Colorectal Cancer Cells. *Gastroenterology* **137,** 15–17 (2009).

33. Formeister, E. J. *et al.* Distinct SOX9 levels differentially mark stem/progenitor populations and enteroendocrine cells of the small intestine epithelium. *Am. J. Physiol. Liver Physiol.* **296,** G1108–G1118 (2009).

34. Furuyama, K. *et al.* Continuous cell supply from a Sox9-expressing progenitor zone in adult liver, exocrine pancreas and intestine. *Nat. Genet.* **43,** 34–41 (2011).

35. VanDussen, K. L. *et al.* Notch signaling modulates proliferation and differentiation of intestinal crypt base columnar stem cells. *Development*

139, 488–97 (2012).

36. Schuijers, J. *et al.* Ascl2 Acts as an R-spondin/Wnt-Responsive Switch to Control Stemness in Intestinal Crypts. *Cell Stem Cell* **16,** 158–170 (2015).

37. Bankaitis, E. D., Ha, A., Kuo, C. J. & Magness, S. T. Reserve Stem Cells in Intestinal Homeostasis and Injury. *Gastroenterology* (2018). doi:10.1053/J.GASTRO.2018.08.016

38. Takeda, N. *et al.* Interconversion between intestinal stem cell populations in distinct niches. *Science* **334,** 1420–4 (2011).

39. Valk-Lingbeek, M. E., Bruggeman, S. W. M. & van Lohuizen, M. Stem Cells and Cancer. *Cell* **118,** 409–418 (2004).

40. Lessard, J. & Sauvageau, G. Bmi-1 determines the proliferative capacity of normal and leukaemic stem cells. *Nature* **423,** 255–260 (2003).

41. Leung, C. *et al.* Bmi1 is essential for cerebellar development and is overexpressed in human medulloblastomas. *Nature* **428,** 337–341 (2004).

42. Molofsky, A. V. *et al.* Bmi-1 dependence distinguishes neural stem cell self-renewal from progenitor proliferation. *Nature* **425,** 962–967 (2003).

43. Sangiorgi, E. & Capecchi, M. R. Bmi1 is expressed in vivo in intestinal stem cells. *Nat. Genet.* **40,** 915–920 (2008).

44. POTTEN, C. S. Extreme sensitivity of some intestinal crypt cells to X and γ irradiation. *Nature* **269,** 518–521 (1977).

45. Potten, C. S. & Grant, H. K. The relationship between ionizing radiation-

induced apoptosis and stem cells in the small and large intestine. *Br. J. Cancer* **78,** 993–1003 (1998).

46. Sangiorgi, E. & Capecchi, M. R. Bmi1 is expressed in vivo in intestinal stem cells. *Nat. Genet.* **40,** 915–920 (2008).

47. Yan, K. S. *et al.* The intestinal stem cell markers Bmi1 and Lgr5 identify two functionally distinct populations. *Proc. Natl. Acad. Sci. U. S. A.* **109,** 466–71 (2012).

48. Chen, F. *et al.* Hop is an unusual homeobox gene that modulates cardiac development. *Cell* **110,** 713–23 (2002).

49. Shin, C. H. *et al.* Modulation of cardiac growth and development by HOP, an unusual homeodomain protein. *Cell* **110,** 725–35 (2002).

50. De Toni, A. *et al.* Regulation of survival in adult hippocampal and glioblastoma stem cell lineages by the homeodomain-only protein HOP. *Neural Dev.* **3,** 13 (2008).

51. Li, N. *et al.* Single-cell analysis of proxy reporter allele-marked epithelial cells establishes intestinal stem cell hierarchy. *Stem cell reports* **3,** 876–91 (2014).

52. Montgomery, R. K. *et al.* Mouse telomerase reverse transcriptase (mTert) expression marks slowly cycling intestinal stem cells. *Proc. Natl. Acad. Sci. U. S. A.* **108,** 179–84 (2011).

53. Tetteh, P. W. *et al.* Replacement of Lost Lgr5-Positive Stem Cells through

Plasticity of Their Enterocyte-Lineage Daughters. *Cell Stem Cell* **18,** 203–213 (2016).

54. Asfaha, S. *et al.* Krt19(+)/Lgr5(-) Cells Are Radioresistant Cancer-Initiating Stem Cells in the Colon and Intestine. *Cell Stem Cell* **16,** 627–38 (2015).

55. Powell, A. E. *et al.* The pan-ErbB negative regulator Lrig1 is an intestinal stem cell marker that functions as a tumor suppressor. *Cell* **149,** 146–58 (2012).

56. Roche, K. C. *et al.* SOX9 Maintains Reserve Stem Cells and Preserves Radioresistance in Mouse Small Intestine. *Gastroenterology* **149,** 1553–1563.e10 (2015).

57. Yousefi, M., Li, L. & Lengner, C. J. Hierarchy and Plasticity in the Intestinal Stem Cell Compartment. *Trends Cell Biol.* **27,** 753–764 (2017).

58. Schmitt, M. *et al.* Paneth Cells Respond to Inflammation and Contribute to Tissue Regeneration by Acquiring Stem-like Features through SCF/c-Kit Signaling. *Cell Rep.* **24,** 2312–2328.e7 (2018).

59. Roth, S. *et al.* Paneth cells in intestinal homeostasis and tissue injury. *PLoS One* **7,** e38965 (2012).

60. Sei, Y. *et al.* Mature enteroendocrine cells contribute to basal and pathological stem cell dynamics in the small intestine. *Am. J. Physiol. Liver Physiol.* **315,** G495–G510 (2018).

61. Sato, T. *et al.* Paneth cells constitute the niche for Lgr5 stem cells in

intestinal crypts. *Nature* **469,** 415–8 (2011).

62. Schwalbe, G. Beiträge zur Kenntniss der Drüsen in den Darmwandungen, in's Besondere der Brunner'schen Drüsen. *Arch. für Mikroskopische Anat.* **8,** 92–140 (1872).

63. Paneth, J. Ueber die secernirenden Zellen des Dünndarm-Epithels. *Arch. für Mikroskopische Anat.* **31,** 113–191 (1887).

64. Clevers, H. C. & Bevins, C. L. Paneth Cells: Maestros of the Small Intestinal Crypts. *Annu. Rev. Physiol.* **75,** 289–311 (2013).

65. Bry, L. *et al.* Paneth cell differentiation in the developing intestine of normal and transgenic mice. *Cell Biol.* **91,** 10335–10339 (1994).

66. Darmoul, D., Brown, D., Selsted, M. E. & Ouellette, A. J. Cryptdin gene expression in developing mouse small intestine. *Am. J. Physiol. Liver Physiol.* **272,** G197–G206 (1997).

67. Inoue, R. *et al.* Postnatal changes in the expression of genes for cryptdins 1â€“6 and the role of luminal bacteria in cryptdin gene expression in mouse small intestine. *FEMS Immunol. Med. Microbiol.* **52,** 407–416 (2008).

68. Garabedian, E. M., Roberts, L. J., McNevin, M. S. & Gordon, J. I. Examining the role of Paneth cells in the small intestine by lineage ablation in transgenic mice. *J. Biol. Chem.* **272,** 23729–40 (1997).

69. Durand, A. *et al.* Functional intestinal stem cells after Paneth cell ablation induced by the loss of transcription factor Math1 (Atoh1). *Proc. Natl. Acad.*

Sci. U. S. A. **109,** 8965–70 (2012).

70. Kim, T.-H., Escudero, S. & Shivdasani, R. A. Intact function of Lgr5 receptor-expressing intestinal stem cells in the absence of Paneth cells. *Proc. Natl. Acad. Sci. U. S. A.* **109,** 3932–7 (2012).

71. Shroyer, N. F., Wallis, D., Venken, K. J. T., Bellen, H. J. & Zoghbi, H. Y. Gfi1 functions downstream of Math1 to control intestinal secretory cell subtype allocation and differentiation. *Genes Dev.* **19,** 2412–2417 (2005).

72. Geiser, J., Venken, K. J. T., De Lisle, R. C. & Andrews, G. K. A Mouse Model of Acrodermatitis Enteropathica: Loss of Intestine Zinc Transporter ZIP4 (Slc39a4) Disrupts the Stem Cell Niche and Intestine Integrity. *PLoS Genet.* **8,** e1002766 (2012).

73. Bastide, P. *et al.* Sox9 regulates cell proliferation and is required for Paneth cell differentiation in the intestinal epithelium. *J. Cell Biol.* **178,** 635–648 (2007).

74. Mori–Akiyama, Y. *et al.* SOX9 Is Required for the Differentiation of Paneth Cells in the Intestinal Epithelium. *Gastroenterology* **133,** 539–546 (2007).

75. Yilmaz, Ö. H. *et al.* mTORC1 in the Paneth cell niche couples intestinal stem-cell function to calorie intake. *Nature* **486,** 490–5 (2012).

76. Powell, D. W., Pinchuk, I. V, Saada, J. I., Chen, X. & Mifflin, R. C. Mesenchymal cells of the intestinal lamina propria. *Annu. Rev. Physiol.* **73,** 213–37 (2011).

77. Yen, T. H. & Wright, N. A. The gastrointestinal tract stem cell niche. *Stem Cell Rev.* **2,** 203–212 (2006).

78. Lahar, N. *et al.* Intestinal subepithelial myofibroblasts support in vitro and in vivo growth of human small intestinal epithelium. *PLoS One* **6,** e26898 (2011).

79. Aoki, R. *et al.* Foxl1-expressing mesenchymal cells constitute the intestinal stem cell niche. *Cell. Mol. Gastroenterol. Hepatol.* **2,** 175–188 (2016).

80. Valenta, T. *et al.* Wnt Ligands Secreted by Subepithelial Mesenchymal Cells Are Essential for the Survival of Intestinal Stem Cells and Gut Homeostasis. *Cell Rep.* **15,** 911–918 (2016).

81. Shoshkes-Carmel, M. *et al.* Subepithelial telocytes are an important source of Wnts that supports intestinal crypts. *Nature* **557,** 242–246 (2018).

82. Cretoiu, D., Cretoiu, S. M., Simionescu, A. A. & Popescu, L. M. Telocytes, a distinct type of cell among the stromal cells present in the lamina propria of jejunum. *Histol. Histopathol.* **27,** 1067–78 (2012).

83. Carmona, I. C., Bartolomé, M. J. L. & Escribano, C. J. Identification of telocytes in the lamina propria of rat duodenum: transmission electron microscopy. *J. Cell. Mol. Med.* **15,** 26–30 (2011).

84. San Roman, A. K., Jayewickreme, C. D., Murtaugh, L. C. & Shivdasani, R. A. Wnt secretion from epithelial cells and subepithelial myofibroblasts is not required in the mouse intestinal stem cell niche in vivo. *Stem cell reports* **2,**

127–34 (2014).

85. Kolterud, Å. *et al.* Paracrine Hedgehog Signaling in Stomach and Intestine: New Roles for Hedgehog in Gastrointestinal Patterning. *Gastroenterology* **137,** 618–628 (2009).

86. Madison, B. B. *et al.* Epithelial hedgehog signals pattern the intestinal crypt-villus axis. *Development* **132,** 279–289 (2005).

87. Büller, N. V. J. A., Rosekrans, S. L., Westerlund, J. & van den Brink, G. R. Hedgehog Signaling and Maintenance of Homeostasis in the Intestinal Epithelium. *Physiology* **27,** 148–155 (2012).

88. Huang, H. *et al.* Specific Requirement of Gli Transcription Factors in Hedgehog-mediated Intestinal Development. *J. Biol. Chem.* **288,** 17589–17596 (2013).

89. Bitgood, M. J. & McMahon, A. P. HedgehogandBmpGenes Are Coexpressed at Many Diverse Sites of Cell–Cell Interaction in the Mouse Embryo. *Dev. Biol.* **172,** 126–138 (1995).

90. Echelard, Y. *et al.* Sonic hedgehog, a member of a family of putative signaling molecules, is implicated in the regulation of CNS polarity. *Cell* **75,** 1417–30 (1993).

91. Ramalho-Santos, M., Melton, D. A. & McMahon, A. P. Hedgehog signals regulate multiple aspects of gastrointestinal development. *Development* **127,** 2763–72 (2000).

92. Walton, K. D. *et al.* Hedgehog-responsive mesenchymal clusters direct patterning and emergence of intestinal villi. *Proc. Natl. Acad. Sci.* **109,** 15817–15822 (2012).

93. Smith, E. *et al.* Generation and Characterization of a Notch1 Signaling-Specific Reporter Mouse Line. doi:10.1002/dvg.22030

94. Wang, L. C. *et al.* Disruption of hedgehog signaling reveals a novel role in intestinal morphogenesis and intestinal-specific lipid metabolism in mice. *Gastroenterology* **122,** 469–82 (2002).

95. Kosinski, C. *et al.* Indian Hedgehog Regulates Intestinal Stem Cell Fate Through Epithelial−Mesenchymal Interactions During Development. *Gastroenterology* **139,** 893–903 (2010).

96. van Dop, W. A. *et al.* Loss of Indian Hedgehog Activates Multiple Aspects of a Wound Healing Response in the Mouse Intestine. *Gastroenterology* **139,** 1665–1676.e10 (2010).

97. Zacharias, W. J. *et al.* Hedgehog Is an Anti-Inflammatory Epithelial Signal for the Intestinal Lamina Propria. *Gastroenterology* **138,** 2368–2377.e4 (2010).

98. Gagné-Sansfaçon, J., Allaire, J. M., Jones, C., Boudreau, F. & Perreault, N. Loss of Sonic Hedgehog Leads to Alterations in Intestinal Secretory Cell Maturation and Autophagy. *PLoS One* **9,** e98751 (2014).

99. Liang, R. *et al.* Hedgehog signaling displays a biphasic expression pattern during intestinal injury and repair. *J. Pediatr. Surg.* **47,** 2251–2263 (2012).

100. Varnat, F. *et al.* PPARβ/δ Regulates Paneth Cell Differentiation Via Controlling the Hedgehog Signaling Pathway. *Gastroenterology* **131,** 538–553 (2006).

101. Li, X. *et al.* Deconvoluting the intestine: molecular evidence for a major role of the mesenchyme in the modulation of signaling cross talk. *Physiol. Genomics* **29,** 290–301 (2007).

102. Yeung, T. M., Chia, L. A., Kosinski, C. M. & Kuo, C. J. Regulation of self-renewal and differentiation by the intestinal stem cell niche. *Cell. Mol. Life Sci.* **68,** 2513–2523 (2011).

103. Haramis, A.-P. G. *et al.* De Novo Crypt Formation and Juvenile Polyposis on BMP Inhibition in Mouse Intestine. *Science (80-.).* **303,** 1684–1686 (2004).

104. Hardwick, J. C. H. *et al.* Bone morphogenetic protein 2 is expressed by, and acts upon, mature epithelial cells in the colon. *Gastroenterology* **126,** 111–21 (2004).

105. He, X. C. *et al.* BMP signaling inhibits intestinal stem cell self-renewal through suppression of Wnt–β-catenin signaling. *Nat. Genet.* **36,** 1117–1121 (2004).

106. Kosinski, C. *et al.* Gene expression patterns of human colon tops and basal crypts and BMP antagonists as intestinal stem cell niche factors. *Proc. Natl. Acad. Sci.* **104,** 15418–15423 (2007).

107. Haramis, A.-P. G. *et al.* De novo crypt formation and juvenile polyposis on

BMP inhibition in mouse intestine. *Science* **303,** 1684–6 (2004).

108. Houlston, R. *et al.* Mutations in DPC4 (SMAD4) cause juvenile polyposis syndrome, but only account for a minority of cases. *Hum. Mol. Genet.* **7,** 1907–12 (1998).

109. Howe, J. R. *et al.* Germline mutations of the gene encoding bone morphogenetic protein receptor 1A in juvenile polyposis. *Nat. Genet.* **28,** 184–187 (2001).

110. Howe, J. R. *et al.* Mutations in the SMAD4/DPC4 gene in juvenile polyposis. *Science* **280,** 1086–8 (1998).

111. Auclair, B. A., Benoit, Y. D., Rivard, N., Mishina, Y. & Perreault, N. Bone Morphogenetic Protein Signaling Is Essential for Terminal Differentiation of the Intestinal Secretory Cell Lineage. *Gastroenterology* **133,** 887–896 (2007).

112. Allaire, J. M. *et al.* Bmp signaling in colonic mesenchyme regulates stromal microenvironment and protects from polyposis initiation. *Int. J. Cancer* **138,** 2700–2712 (2016).

113. He, X. C. *et al.* PTEN-deficient intestinal stem cells initiate intestinal polyposis. *Nat. Genet.* **39,** 189–98 (2007).

114. Reynolds, A. *et al.* Canonical Wnt signals combined with suppressed TGFβ/BMP pathways promote renewal of the native human colonic epithelium. *Gut* **63,** 610–621 (2014).

115. Whissell, G. *et al.* The transcription factor GATA6 enables self-renewal of colon adenoma stem cells by repressing BMP gene expression. *Nat. Cell Biol.* **16,** 695–707 (2014).

116. Qi, Z. *et al.* BMP restricts stemness of intestinal Lgr5+ stem cells by directly suppressing their signature genes. *Nat. Commun.* **8,** 13824 (2017).

117. Sato, T. *et al.* Single Lgr5 stem cells build crypt-villus structures in vitro without a mesenchymal niche. *Nature* **459,** 262–5 (2009).

118. Roberts, D. J. *et al.* Sonic hedgehog is an endodermal signal inducing Bmp-4 and Hox genes during induction and regionalization of the chick hindgut. *Development* **121,** 3163–74 (1995).

119. Shyer, A. E., Huycke, T. R., Lee, C., Mahadevan, L. & Tabin, C. J. Bending Gradients: How the Intestinal Stem Cell Gets Its Home. *Cell* **161,** 569–580 (2015).

120. Walton, K. D., Freddo, A. M., Wang, S. & Gumucio, D. L. Generation of intestinal surface: an absorbing tale. *Development* **143,** 2261–2272 (2016).

121. Walton, K. D. *et al.* Villification in the mouse: Bmp signals control intestinal villus patterning. *Development* **143,** 427–436 (2016).

122. Andreu, P. *et al.* Crypt-restricted proliferation and commitment to the Paneth cell lineage following Apc loss in the mouse intestine. *Development* **132,** 1443–1451 (2005).

123. Sansom, O. J. *et al.* Loss of Apc in vivo immediately perturbs Wnt signaling,

differentiation, and migration. *Genes Dev.* **18,** 1385–1390 (2004).

124. Ireland, H. *et al.* Inducible cre-mediated control of gene expression in the murine gastrointestinal tract: effect of loss of β-catenin. *Gastroenterology* **126,** 1236–1246 (2004).

125. Korinek, V. *et al.* Depletion of epithelial stem-cell compartments in the small intestine of mice lacking Tcf-4. *Nat. Genet.* **19,** 379–383 (1998).

126. Kuhnert, F. *et al.* Essential requirement for Wnt signaling in proliferation of adult small intestine and colon revealed by adenoviral expression of Dickkopf-1. *Proc. Natl. Acad. Sci.* **101,** 266–271 (2004).

127. Pinto, D., Gregorieff, A., Begthel, H. & Clevers, H. Canonical Wnt signals are essential for homeostasis of the intestinal epithelium. *Genes Dev.* **17,** 1709–1713 (2003).

128. de Lau, W. *et al.* Lgr5 homologues associate with Wnt receptors and mediate R-spondin signalling. *Nature* **476,** 293–297 (2011).

129. Muncan, V. *et al.* Rapid loss of intestinal crypts upon conditional deletion of the Wnt/Tcf-4 target gene c-Myc. *Mol. Cell. Biol.* **26,** 8418–26 (2006).

130. Cervantes, S., Yamaguchi, T. P. & Hebrok, M. Wnt5a is essential for intestinal elongation in mice. *Dev. Biol.* **326,** 285–94 (2009).

131. Bakker, E. R. M. *et al.* Induced Wnt5a expression perturbs embryonic outgrowth and intestinal elongation, but is well-tolerated in adult mice. *Dev. Biol.* **369,** 91–100 (2012).

132. Miyoshi, H., Ajima, R., Luo, C. T., Yamaguchi, T. P. & Stappenbeck, T. S. Wnt5a Potentiates TGF- Signaling to Promote Colonic Crypt Regeneration After Tissue Injury. *Science (80-.).* **338,** 108–113 (2012).

133. Sato, A. *et al.* The Wnt5a-Ror2 axis promotes the signaling circuit between interleukin-12 and interferon-γ in colitis. *Sci. Rep.* **5,** 10536 (2015).

134. Yamada, M. *et al.* Ror2 is Required for Midgut Elongation During Mouse Development. doi:10.1002/dvdy.22212

135. Zhao, D. *et al.* WNT5A transforms intestinal CD8αα^{+} IELs into an unconventional phenotype with pro-inflammatory features. *BMC Gastroenterol.* **15,** 173 (2015).

136. He, T. C. *et al.* Identification of c-MYC as a target of the APC pathway. *Science* **281,** 1509–12 (1998).

137. Shtutman, M. *et al.* The cyclin D1 gene is a target of the beta-catenin/LEF-1 pathway. *Proc. Natl. Acad. Sci. U. S. A.* **96,** 5522–7 (1999).

138. Tetsu, O. & McCormick, F. β-Catenin regulates expression of cyclin D1 in colon carcinoma cells. *Nature* **398,** 422–426 (1999).

139. Gregorieff, A. *et al.* Expression Pattern of Wnt Signaling Components in the Adult Intestine. *Gastroenterology* **129,** 626–638 (2005).

140. Kabiri, Z. *et al.* Stroma provides an intestinal stem cell niche in the absence of epithelial Wnts. *Development* **141,** 2206–15 (2014).

141. Batlle, E. *et al.* Beta-catenin and TCF mediate cell positioning in the

intestinal epithelium by controlling the expression of EphB/ephrinB. *Cell* **111,** 251–63 (2002).

142. Farin, H. F., Van Es, J. H. & Clevers, H. Redundant sources of Wnt regulate intestinal stem cells and promote formation of Paneth cells. *Gastroenterology* **143,** 1518–1529.e7 (2012).

143. Mustata, R. C. *et al.* Lgr4 is required for Paneth cell differentiation and maintenance of intestinal stem cells ex vivo. *EMBO Rep.* **12,** 558–564 (2011).

144. Louvi, A. & Artavanis-Tsakonas, S. Notch and disease: A growing field. *Semin. Cell Dev. Biol.* **23,** 473–480 (2012).

145. Penton, A. L., Leonard, L. D. & Spinner, N. B. Notch signaling in human development and disease. *Semin. Cell Dev. Biol.* **23,** 450–457 (2012).

146. Lobry, C., Oh, P., Mansour, M. R., Look, A. T. & Aifantis, I. Notch signaling: switching an oncogene to a tumor suppressor. *Blood* **123,** 2451–2459 (2014).

147. Aster, J. C., Pear, W. S. & Blacklow, S. C. The Varied Roles of Notch in Cancer. *Annu. Rev. Pathol. Mech. Dis.* **12,** 245–275 (2017).

148. Vinson, K. E., George, D. C., Fender, A. W., Bertrand, F. E. & Sigounas, G. The Notch pathway in colorectal cancer. *Int. J. Cancer* **138,** 1835–1842 (2016).

149. Mohr, O. L. Character Changes Caused by Mutation of an Entire Region of a

Chromosome in Drosophila. *Genetics* **4,** 275–82 (1919).

150. Poulson, D. F. Chromosomal Deficiencies and the Embryonic Development of Drosophila Melanogaster. *Proc. Natl. Acad. Sci. U. S. A.* **23,** 133–7 (1937).

151. Fortini, M. E. Notch Signaling: The Core Pathway and Its Posttranslational Regulation. *Dev. Cell* **16,** 633–647 (2009).

152. Kopan, R. & Ilagan, M. X. G. The Canonical Notch Signaling Pathway: Unfolding the Activation Mechanism. *Cell* **137,** 216–233 (2009).

153. Bray, S. J. Notch signalling in context. *Nat. Rev. Mol. Cell Biol.* **17,** 722–735 (2016).

154. Greenwald, I. & Rubin, G. M. Making a difference: the role of cell-cell interactions in establishing separate identities for equivalent cells. *Cell* **68,** 271–81 (1992).

155. Artavanis-Tsakonas, S., Rand, M. D. & Lake, R. J. Notch signaling: cell fate control and signal integration in development. *Science* **284,** 770–6 (1999).

156. Guruharsha, K. G., Kankel, M. W. & Artavanis-Tsakonas, S. The Notch signalling system: recent insights into the complexity of a conserved pathway. *Nat. Rev. Genet.* **13,** 654–666 (2012).

157. Borggrefe, T. *et al.* The Notch intracellular domain integrates signals from Wnt, Hedgehog, TGFβ/BMP and hypoxia pathways. *Biochim. Biophys. Acta - Mol. Cell Res.* **1863,** 303–313 (2016).

158. LaFoya, B. *et al.* Notch: A multi-functional integrating system of microenvironmental signals. *Dev. Biol.* **418,** 227–241 (2016).

159. D'Souza, B., Meloty-Kapella, L. & Weinmaster, G. in *Current topics in developmental biology* **92,** 73–129 (2010).

160. Guo, B., McMillan, B. J. & Blacklow, S. C. Structure and function of the Mind bomb E3 ligase in the context of Notch signal transduction. *Curr. Opin. Struct. Biol.* **41,** 38–45 (2016).

161. Kovall, R. A. & Blacklow, S. C. in *Current topics in developmental biology* **92,** 31–71 (2010).

162. Sander, G. R. & Powell, B. C. Expression of notch receptors and ligands in the adult gut. *J. Histochem. Cytochem.* **52,** 509–516 (2004).

163. Schroder, N. & Gossler, A. Expression of Notch pathway components in fetal and adult mouse small intestine. *Gene Expr Patterns* **2,** 247–250 (2002).

164. Jensen, J. *et al.* Control of endodermal endocrine development by Hes-1. *Nat. Genet.* **24,** 36–44 (2000).

165. Riccio, O. *et al.* Loss of intestinal crypt progenitor cells owing to inactivation of both Notch1 and Notch2 is accompanied by derepression of CDK inhibitors p27Kip1 and p57Kip2. *EMBO Rep.* **9,** 377–83 (2008).

166. Wu, Y. *et al.* Therapeutic antibody targeting of individual Notch receptors. *Nature* **464,** 1052–1057 (2010).

167. Yang, Q., Bermingham, N. A., Finegold, M. J. & Zoghbi, H. Y. Requirement

of Math1 for secretory cell lineage commitment in the mouse intestine. *Science* **294,** 2155–2158 (2001).

168. Vooijs, M. *et al.* Mapping the consequence of Notch1 proteolysis in vivo with NIP-CRE. *Development* **134,** 535–544 (2006).

169. Bernier-Latmani, J. *et al.* DLL4 promotes continuous adult intestinal lacteal regeneration and dietary fat transport. *J. Clin. Invest.* **125,** 4572–4586 (2015).

170. Choi, D. *et al.* Laminar flow downregulates Notch activity to promote lymphatic sprouting. *J. Clin. Invest.* **127,** 1225–1240 (2017).

171. Okamura, Y. & Saga, Y. Notch signaling is required for the maintenance of enteric neural crest progenitors. *Development* **135,** 3555–3565 (2008).

172. Roca, C. & Adams, R. H. Regulation of vascular morphogenesis by Notch signaling. *Genes Dev.* **21,** 2511–2524 (2007).

173. Obata, Y. *et al.* Epithelial-stromal interaction via Notch signaling is essential for the full maturation of gut-associated lymphoid tissues. *EMBO Rep.* **15,** 1297–304 (2014).

174. Viant, C. *et al.* Transforming growth factor–β and Notch ligands act as opposing environmental cues in regulating the plasticity of type 3 innate lymphoid cells. *Sci. Signal.* **9,** ra46-ra46 (2016).

175. van Es, J. H. *et al.* Notch/gamma-secretase inhibition turns proliferative cells in intestinal crypts and adenomas into goblet cells. *Nature* **435,** 959–63

(2005).

176. Tsai, Y.-H. *et al.* ADAM10 regulates Notch function in intestinal stem cells of mice. *Gastroenterology* **147,** 822–834.e13 (2014).

177. Fre, S. *et al.* Notch signals control the fate of immature progenitor cells in the intestine. *Nature* **435,** 964–8 (2005).

178. Stanger, B. Z., Datar, R., Murtaugh, L. C. & Melton, D. a. Direct regulation of intestinal fate by Notch. *Proc. Natl. Acad. Sci. U. S. A.* **102,** 12443–8 (2005).

179. Carulli, A. J. *et al.* Notch receptor regulation of intestinal stem cell homeostasis and crypt regeneration. *Dev. Biol.* **402,** 98–108 (2015).

180. Pellegrinet, L. *et al.* Dll1- and dll4-mediated notch signaling are required for homeostasis of intestinal stem cells. *Gastroenterology* **140,** 1230-1240.e1–7 (2011).

181. Sasaki, N. *et al.* Reg4+ deep crypt secretory cells function as epithelial niche for Lgr5+ stem cells in colon. *Proc. Natl. Acad. Sci. U. S. A.* **113,** E5399-407 (2016).

182. Durand, A. *et al.* Functional intestinal stem cells after Paneth cell ablation induced by the loss of transcription factor Math1 (Atoh1). *Proc. Natl. Acad. Sci.* **109,** 8965–8970 (2012).

183. Kim, T.-H., Escudero, S. & Shivdasani, R. A. Intact function of Lgr5 receptor-expressing intestinal stem cells in the absence of Paneth cells. *Proc. Natl. Acad. Sci.* **109,** 3932–3937 (2012).

184. Stamataki, D. *et al.* Delta1 Expression, Cell Cycle Exit, and Commitment to a Specific Secretory Fate Coincide within a Few Hours in the Mouse Intestinal Stem Cell System. *PLoS One* **6,** e24484 (2011).

185. van Tetering, G. *et al.* Metalloprotease ADAM10 Is Required for Notch1 Site 2 Cleavage. *J. Biol. Chem.* **284,** 31018–31027 (2009).

186. Bozkulak, E. C. & Weinmaster, G. Selective Use of ADAM10 and ADAM17 in Activation of Notch1 Signaling. *Mol. Cell. Biol.* **29,** 5679–5695 (2009).

187. Brou, C. *et al.* A novel proteolytic cleavage involved in Notch signaling: the role of the disintegrin-metalloprotease TACE. *Mol. Cell* **5,** 207–16 (2000).

188. Feng, Y. *et al.* Loss of ADAM17-Mediated Tumor Necrosis Factor Alpha Signaling in Intestinal Cells Attenuates Mucosal Atrophy in a Mouse Model of Parenteral Nutrition. *Mol. Cell. Biol.* **35,** 3604–21 (2015).

189. Tolia, A. & De Strooper, B. Structure and function of γ-secretase. *Semin. Cell Dev. Biol.* **20,** 211–218 (2009).

190. Ikeuchi, T. & Sisodia, S. S. The Notch ligands, Delta1 and Jagged2, are substrates for presenilin-dependent "gamma-secretase" cleavage. *J. Biol. Chem.* **278,** 7751–4 (2003).

191. Lammich, S. *et al.* Presenilin-dependent Intramembrane Proteolysis of CD44 Leads to the Liberation of Its Intracellular Domain and the Secretion of an Aβ-like Peptide. *J. Biol. Chem.* **277,** 44754–44759 (2002).

192. Ni, C.-Y., Murphy, M. P., Golde, T. E. & Carpenter, G. gamma -Secretase

Cleavage and Nuclear Localization of ErbB-4 Receptor Tyrosine Kinase. *Science (80-.).* **294,** 2179–2181 (2001).

193. Marambaud, P. *et al.* A presenilin-1/gamma-secretase cleavage releases the E-cadherin intracellular domain and regulates disassembly of adherens junctions. *EMBO J.* **21,** 1948–1956 (2002).

194. Milano, J. *et al.* Modulation of Notch Processing by γ-Secretase Inhibitors Causes Intestinal Goblet Cell Metaplasia and Induction of Genes Known to Specify Gut Secretory Lineage Differentiation. *Toxicol. Sci.* **82,** 341–358 (2004).

195. Wong, G. T. *et al.* Chronic Treatment with the γ-Secretase Inhibitor LY-411,575 Inhibits γ-Amyloid Peptide Production and Alters Lymphopoiesis and Intestinal Cell Differentiation. *J. Biol. Chem.* **279,** 12876–12882 (2004).

196. Fischer, A. & Gessler, M. Delta Notch and then? Protein interactions and proposed modes of repression by Hes and Hey bHLH factors. *Nucleic Acids Res.* **35,** 4583–4596 (2007).

197. Ueo, T. *et al.* The role of Hes genes in intestinal development, homeostasis and tumor formation. *Development* **139,** 1071–82 (2012).

198. Suzuki, K. *et al.* Hes1-deficient mice show precocious differentiation of Paneth cells in the small intestine. *Biochem. Biophys. Res. Commun.* **328,** 348–352 (2005).

199. Ootani, A. *et al.* Sustained in vitro intestinal epithelial culture within a Wnt-

dependent stem cell niche. *Nat. Med.* **15,** 701–706 (2009).

200. Demitrack, E. S. & Samuelson, L. C. Notch regulation of gastrointestinal stem cells. *J. Physiol.* **594,** 4791–803 (2016).

201. Noah, T. K. & Shroyer, N. F. Notch in the intestine: regulation of homeostasis and pathogenesis. *Annu. Rev. Physiol.* **75,** 263–88 (2013).

202. Longshore, S. W., Wakeman, D., McMellen, M. & Warner, B. W. Bowel resection induced intestinal adaptation: progress from bench to bedside. *Minerva Pediatr.* **61,** 239–51 (2009).

203. O'Brien, D. P. *et al.* Epithelial Permeability Is Not Increased in Rats Following Small Bowel Resection. *J. Surg. Res.* **97,** 65–70 (2001).

204. Barron, L. *et al.* Intestinal Epithelial-Specific mTORC1 Activation Enhances Intestinal Adaptation After Small Bowel Resection. *Cell. Mol. Gastroenterol. Hepatol.* **3,** 231–244 (2017).

205. Blanpain, C., Mohrin, M., Sotiropoulou, P. A. & Passegué, E. DNA-damage response in tissue-specific and cancer stem cells. *Cell Stem Cell* **8,** 16–29 (2011).

206. Gudkov, A. V. & Komarova, E. A. The role of p53 in determining sensitivity to radiotherapy. *Nat. Rev. Cancer* **3,** 117–129 (2003).

207. Hua, G. *et al.* Crypt base columnar stem cells in small intestines of mice are radioresistant. *Gastroenterology* **143,** 1266–76 (2012).

208. Metcalfe, C., Kljavin, N. M., Ybarra, R. & de Sauvage, F. J. Lgr5+ stem cells

are indispensable for radiation-induced intestinal regeneration. *Cell Stem Cell* **14,** 149–59 (2014).

209. Schumacher, M. A., Danopoulos, S., Al Alam, D. & Frey, M. R. in *Physiology of the Gastrointestinal Tract* (eds. Said, H. M., Ghishan, F. K., Kaunitz, J. D., Merchant, J. L. & Wood, J. D.) 71–101 (Academic Press, 2018).

210. Troyer, K. L. *et al.* Growth retardation, duodenal lesions, and aberrant ileum architecture in triple null mice lacking EGF, amphiregulin, and TGF-alpha. *Gastroenterology* **121,** 68–78 (2001).

211. Luetteke, N. C. *et al.* Targeted inactivation of the EGF and amphiregulin genes reveals distinct roles for EGF receptor ligands in mouse mammary gland development. *Development* **126,** 2739–50 (1999).

212. Scopelliti, A. *et al.* Local Control of Intestinal Stem Cell Homeostasis by Enteroendocrine Cells in the Adult Drosophila Midgut. *Curr. Biol.* **24,** 1199–1211 (2014).

213. Sato, T. & Clevers, H. Growing Self-Organizing Mini-Guts from a Single Intestinal Stem Cell: Mechanism and Applications. *Science (80-.).* **340,** 1190–1194 (2013).

214. Schumacher, M. A. *et al.* The use of murine-derived fundic organoids in studies of gastric physiology. *J. Physiol.* **593,** 1809–1827 (2015).

215. Lu, N. *et al.* Activation of the Epidermal Growth Factor Receptor in Macrophages Regulates Cytokine Production and Experimental Colitis. *J.*

Immunol. **192,** 1013–1023 (2014).

216. Hardbower, D. M. *et al.* EGFR regulates macrophage activation and function in bacterial infection. *J. Clin. Invest.* **126,** 3296–3312 (2016).

217. Damjanov, I., Mildner, B. & Knowles, B. B. Immunohistochemical localization of the epidermal growth factor receptor in normal human tissues. *Lab. Invest.* **55,** 588–92 (1986).

218. Miró, L. *et al.* Aldosterone induces myofibroblast EGF secretion to regulate epithelial colonic permeability. *Am. J. Physiol. Physiol.* **304,** C918–C926 (2013).

219. Avissar, N. E., Wang, H. T., Miller, J. H., Iannoli, P. & Sax, H. C. Epidermal growth factor receptor is increased in rabbit intestinal brush border membrane after small bowel resection. *Dig. Dis. Sci.* **45,** 1145–52 (2000).

220. Hirano, M. *et al.* Epidermal growth factor enhances repair of rat intestinal mucosa damaged by oral administration of methotrexate. *J. Gastroenterol.* **30,** 169–76 (1995).

221. Riegler, M. *et al.* Epidermal growth factor promotes rapid response to epithelial injury in rabbit duodenum in vitro. *Gastroenterology* **111,** 28–36 (1996).

222. Frey, M. R., Dise, R. S., Edelblum, K. L. & Polk, D. B. p38 kinase regulates epidermal growth factor receptor downregulation and cellular migration. *EMBO J.* **25,** 5683–5692 (2006).

223. Dvorak, B. *et al.* Epidermal growth factor reduces the development of necrotizing enterocolitis in a neonatal rat model. *Am. J. Physiol. Liver Physiol.* **282,** G156–G164 (2002).

224. B. Egger, M. W. Büchler, J. Lakshma, M. W. B. J. L. P. M. V. E. E. Mice Harboring a Defective Epidermal Growth Factor Receptor-(Waved-2) Have an Increased Susceptibility to Acute Dextran-Sulfate-induced Colitis. *Scand. J. Gastroenterol.* **35,** 1181–1187 (2000).

225. Dubé, P. E. *et al.* Epidermal growth factor receptor inhibits colitis-associated cancer in mice. *J. Clin. Invest.* **122,** 2780–2792 (2012).

226. Egger, B. *et al.* Reduced susceptibility of mice overexpressing transforming growth factor alpha to dextran sodium sulphate induced colitis. *Gut* **43,** 64–70 (1998).

227. Donovan, S. M., Hintz, R. L. & Rosenfeld, R. G. Insulin-like growth factors I and II and their binding proteins in human milk: effect of heat treatment on IGF and IGF binding protein stability. *J. Pediatr. Gastroenterol. Nutr.* **13,** 242–53 (1991).

228. Eriksson, U., Duc, G., Froesch, E. R. & Zapf, J. Insulin-like growth factors (IGF) I and II and IGF binding proteins (IGFBPs) in human colostrum/transitory milk during the first week postpartum: comparison with neonatal and maternal serum. *Biochem. Biophys. Res. Commun.* **196,** 267–73 (1993).

229. Chaurasia, O. P., Marcuard, S. P. & Seidel, E. R. Insulin-like growth factor I

in human gastrointestinal exocrine secretions. *Regul. Pept.* **50,** 113–9 (1994).

230. Rechler, M. M. & Nissley, S. P. Insulin-like growth factor (IGF)/somatomedin receptor subtypes: structure, function, and relationships to insulin receptors and IGF carrier proteins. *Horm. Res.* **24,** 152–9 (1986).

231. Kuemmerle, J. F. & Murthy, K. S. Coupling of the insulin-like growth factor-I receptor tyrosine kinase to Gi2 in human intestinal smooth muscle: Gbetagamma -dependent mitogen-activated protein kinase activation and growth. *J. Biol. Chem.* **276,** 7187–94 (2001).

232. Izumi, T. *et al.* Insulin-like growth factor I rapidly stimulates tyrosine phosphorylation of a Mr 185,000 protein in intact cells. *J. Biol. Chem.* **262,** 1282–7 (1987).

233. Firth, S. M. & Baxter, R. C. Cellular Actions of the Insulin-Like Growth Factor Binding Proteins. *Endocr. Rev.* **23,** 824–854 (2002).

234. Shoubridge, C. A., Steeb, C.-B. & Read, L. C. IGFBP mRNA expression in small intestine of rat during postnatal development. *Am. J. Physiol. Liver Physiol.* **281,** G1378–G1384 (2001).

235. Winesett, D. E. *et al.* Regulation and localization of the insulin-like growth factor system in small bowel during altered nutrient status. *Am. J. Physiol. Liver Physiol.* **268,** G631–G640 (1995).

236. Kuemmerle, J. F. Insulin-like growth factors in the gastrointestinal tract and

liver. *Endocrinol. Metab. Clin. North Am.* **41,** 409–23, vii (2012).

237. Liu, J. P., Baker, J., Perkins, A. S., Robertson, E. J. & Efstratiadis, A. Mice carrying null mutations of the genes encoding insulin-like growth factor I (Igf-1) and type 1 IGF receptor (Igf1r). *Cell* **75,** 59–72 (1993).

238. Butler, A. A. & LeRoith, D. Minireview: Tissue-Specific *Versus* Generalized Gene Targeting of the *igf1* and *igf1r* Genes and Their Roles in Insulin-Like Growth Factor Physiology. *Endocrinology* **142,** 1685–1688 (2001).

239. Rowland, K. J. *et al.* Loss of Glucagon-Like Peptide-2–Induced Proliferation Following Intestinal Epithelial Insulin-Like Growth Factor-1–Receptor Deletion. *Gastroenterology* **141,** 2166–2175.e7 (2011).

240. Santoro, M. A. *et al.* Obesity and intestinal epithelial deletion of the insulin receptor, but not the IGF 1 receptor, affect radiation-induced apoptosis in colon. *Am. J. Physiol. Gastrointest. Liver Physiol.* **309,** G578-89 (2015).

241. Ussar, S. *et al.* Regulation of Glucose Uptake and Enteroendocrine Function by the Intestinal Epithelial Insulin Receptor. *Diabetes* **66,** 886–896 (2017).

242. Burrin, D. G., Wester, T. J., Davis, T. A., Amick, S. & Heath, J. P. Orally administered IGF-I increases intestinal mucosal growth in formula-fed neonatal pigs. *Am. J. Physiol. Integr. Comp. Physiol.* **270,** R1085–R1091 (1996).

243. Steeb, C. B., Trahair, J. F. & Read, L. C. Administration of insulin-like growth factor-I (IGF-I) peptides for three days stimulates proliferation of the small

intestinal epithelium in rats. *Gut* **37,** 630–8 (1995).

244. Steeb, C. B., Trahair, J. F., Tomas, F. M. & Read, L. C. Prolonged administration of IGF peptides enhances growth of gastrointestinal tissues in normal rats. *Am. J. Physiol. Liver Physiol.* **266,** G1090–G1098 (1994).

245. Wilkins, H. R. *et al.* Reduction of spontaneous and irradiation-induced apoptosis in small intestine of IGF-I transgenic mice. *Am. J. Physiol. Liver Physiol.* **283,** G457–G464 (2002).

246. Howarth, G. S., Xian, C. J. & Read, L. C. Insulin-like growth factor-I partially attenuates colonic damage in rats with experimental colitis induced by oral dextran sulphate sodium. *Scand. J. Gastroenterol.* **33,** 180–90 (1998).

247. Vanderhoof, J. A. *et al.* Truncated and native insulinlike growth factor I enhance mucosal adaptation after jejunoileal resection. *Gastroenterology* **102,** 1949–1956 (1992).

248. Mantell, M. P. *et al.* Resection-induced colonic adaptation is augmented by IGF-I and associated with upregulation of colonic IGF-I mRNA. *Am. J. Physiol. Liver Physiol.* **269,** G974–G980 (1995).

249. Dahly, E. M., Guo, Z. & Ney, D. M. IGF-I augments resection-induced mucosal hyperplasia by altering enterocyte kinetics. *Am. J. Physiol. Integr. Comp. Physiol.* **285,** R800–R808 (2003).

250. Lemmey, A. B. *et al.* Treatment with IGF-I peptides improves function of the remnant gut following small bowel resection in rats. *Growth Factors* **10,** 243–

52 (1994).

251. Gillingham, M. B., Dahly, E. M., Murali, S. G. & Ney, D. M. IGF-I treatment facilitates transition from parenteral to enteral nutrition in rats with short bowel syndrome. *Am. J. Physiol. Integr. Comp. Physiol.* **284,** R363–R371 (2003).

252. Wei Zhang, W. L. F. W. T. A. J. A. R. M. P. M. A. B. T. R. Z. R. J. S. J. L. R. Insulin-like Growth Factor-i Improves Mucosal Structure And Function In Transplanted Rat Small Intestine. *Transplantation* **59,** 755–761 (1995).

253. Schall, K. A. *et al.* Adult zebrafish intestine resection: a novel model of short bowel syndrome, adaptation, and intestinal stem cell regeneration. *Am. J. Physiol. Liver Physiol.* **309,** G135–G145 (2015).

254. Inaba, T. *et al.* Insulin-Like Growth Factor 1 Has Beneficial Effects, Whereas Growth Hormone Has Limited Effects on Postoperative Protein Metabolism, Gut Integrity, and Splenic Weight in Rats With Chronic Mild Liver Injury. *J. Parenter. Enter. Nutr.* **21,** 55–62 (1997).

255. Chen, K. *et al.* Insulin-like Growth Factor-I Prevents Gut Atrophy and Maintains Intestinal Integrity in Septic Rats. *J. Parenter. Enter. Nutr.* **19,** 119–124 (1995).

256. Qiu, W., Leibowitz, B., Zhang, L. & Yu, J. Growth factors protect intestinal stem cells from radiation-induced apoptosis by suppressing PUMA through the PI3K/AKT/p53 axis. *Oncogene* **29,** 1622–1632 (2010).

257. Van Landeghem, L. *et al.* IGF1 stimulates crypt expansion via differential activation of 2 intestinal stem cell populations. *FASEB J.* **29,** 2828–42 (2015).

258. Denduluri, S. K. *et al.* Insulin-like growth factor (IGF) signaling in tumorigenesis and the development of cancer drug resistance. *Genes Dis.* **2,** 13–25 (2015).

259. Manning, B. D. & Toker, A. Leading Edge Review AKT/PKB Signaling: Navigating the Network. *Cell* **169,** 381–405 (2017).

260. Saxton, R. A. & Sabatini, D. M. mTOR Signaling in Growth, Metabolism, and Disease. *Cell* **168,** 960–976 (2017).

261. Chung, J., Kuo, C. J., Crabtree, G. R. & Blenis, J. Rapamycin-FKBP specifically blocks growth-dependent activation of and signaling by the 70 kd S6 protein kinases. *Cell* **69,** 1227–36 (1992).

262. Yang, H. *et al.* mTOR kinase structure, mechanism and regulation. *Nature* **497,** 217–23 (2013).

263. Lamming, D. W. *et al.* Rapamycin-Induced Insulin Resistance Is Mediated by mTORC2 Loss and Uncoupled from Longevity. *Science (80-.).* **335,** 1638–1643 (2012).

264. Sarbassov, D. D. *et al.* Prolonged rapamycin treatment inhibits mTORC2 assembly and Akt/PKB. *Mol. Cell* **22,** 159–68 (2006).

265. Gwinn, D. M. *et al.* AMPK Phosphorylation of Raptor Mediates a Metabolic

Checkpoint. *Mol. Cell* **30,** 214–226 (2008).

266. Holz, M. K., Ballif, B. A., Gygi, S. P. & Blenis, J. mTOR and S6K1 Mediate Assembly of the Translation Preinitiation Complex through Dynamic Protein Interchange and Ordered Phosphorylation Events. *Cell* **123,** 569–580 (2005).

267. Dorrello, N. V. *et al.* S6K1- and TRCP-Mediated Degradation of PDCD4 Promotes Protein Translation and Cell Growth. *Science (80-.).* **314,** 467–471 (2006).

268. Ma, X. M., Yoon, S.-O., Richardson, C. J., Jülich, K. & Blenis, J. SKAR Links Pre-mRNA Splicing to mTOR/S6K1-Mediated Enhanced Translation Efficiency of Spliced mRNAs. *Cell* **133,** 303–313 (2008).

269. Faller, W. J. *et al.* mTORC1-mediated translational elongation limits intestinal tumour initiation and growth. *Nature* **517,** 497–500 (2015).

270. Fujishita, T., Aoki, K., Lane, H. A., Aoki, M. & Taketo, M. M. Inhibition of the mTORC1 pathway suppresses intestinal polyp formation and reduces mortality in Apc 716 mice. *Proc. Natl. Acad. Sci.* **105,** 13544–13549 (2008).

271. Gulhati, P. *et al.* Targeted inhibition of mammalian target of rapamycin signaling inhibits tumorigenesis of colorectal cancer. *Clin. Cancer Res.* **15,** 7207–16 (2009).

272. Yang, J. *et al.* Rapamycin Inhibition of mTOR Reduces Levels of the Na+/H+ Exchanger 3 in Intestines of Mice and Humans, Leading to Diarrhea.

Gastroenterology (2015). doi:10.1053/j.gastro.2015.03.046

273. Yilmaz, Ö. H. *et al.* mTORC1 in the Paneth cell niche couples intestinal stem-cell function to calorie intake. *Nature* **486,** 490–495 (2012).

274. Roux, P. P. *et al.* RAS/ERK signaling promotes site-specific ribosomal protein S6 phosphorylation via RSK and stimulates cap-dependent translation. *J. Biol. Chem.* **282,** 14056–64 (2007).

275. Kapuria, S., Karpac, J., Biteau, B., Hwangbo, D. & Jasper, H. Notch-Mediated Suppression of TSC2 Expression Regulates Cell Differentiation in the Drosophila Intestinal Stem Cell Lineage. *PLoS Genet.* **8,** e1003045 (2012).

276. Igarashi, M. & Guarente, L. mTORC1 and SIRT1 Cooperate to Foster Expansion of Gut Adult Stem Cells during Calorie Restriction. *Cell* **166,** 436–450 (2016).

277. Yousefi, M. *et al.* Calorie Restriction Governs Intestinal Epithelial Regeneration through Cell-Autonomous Regulation of mTORC1 in Reserve Stem Cells. *Stem cell reports* **10,** 703–711 (2018).

278. Quan, Z., Sun, P., Lin, G. & Xi, R. TSC1/2 regulates intestinal stem cell maintenance and lineage differentiation through Rheb-TORC1-S6K but independently of nutritional status or Notch regulation. *J. Cell Sci.* **126,** 3884–3892 (2013).

279. Igarashi, M. & Guarente, L. mTORC1 and SIRT1 Cooperate to Foster

Expansion of Gut Adult Stem Cells during Calorie Restriction. *Cell* **166,** 436–450 (2016).

280. Sampson, Leesa L., Davis, Ashley K., Grogg, Matthew W., Zheng, Y. mTOR disruption causes intestinal epithelial cell defects and intestinal atrophy postinjury in mice. *The FASEB Journal* (2015). doi:10.1096/fj.15-278606

281. Zhou, Y., Rychahou, P., Wang, Q., Weiss, H. L. & Evers, B. M. TSC2/mTORC1 signaling controls Paneth and goblet cell differentiation in the intestinal epithelium. *Cell Death Dis.* **6,** e1631 (2015).

282. Richmond, C. A. *et al.* Dormant Intestinal Stem Cells Are Regulated by PTEN and Nutritional Status. *Cell Rep.* **13,** 2403–11 (2015).

283. Nelson, V. L. B., Jiang, Y.-P., Dickman, K. G., Ballou, L. M. & Lin, R. Z. Adipose tissue insulin resistance due to loss of PI3K p110α leads to decreased energy expenditure and obesity. *Am. J. Physiol. Endocrinol. Metab.* **306,** E1205-16 (2014).

284. Rodgers, J. T. *et al.* mTORC1 controls the adaptive transition of quiescent stem cells from G0 to G(Alert). *Nature* **509,** 393–6 (2014).

285. Kim, C.-K., Yang, V. W. & Bialkowska, A. B. The Role of Intestinal Stem Cells in Epithelial Regeneration Following Radiation-Induced Gut Injury. *Curr. stem cell reports* **3,** 320–332 (2017).

286. Dempsey, P. J., Bohin, N. & Samuelson, L. C. in *Physiology of the Gastrointestinal Tract* (eds. Said, H. M., Ghishan, F. K., Kaunitz, J. D.,

Merchant, J. L. & Wood, J. D.) 141–183 (Academic Press, 2018).

287. Yan, K. S. *et al.* Intestinal Enteroendocrine Lineage Cells Possess Homeostatic and Injury-Inducible Stem Cell Activity. *Cell Stem Cell* **21,** 78–90.e6 (2017).

288. Jadhav, U. *et al.* Dynamic Reorganization of Chromatin Accessibility Signatures during Dedifferentiation of Secretory Precursors into Lgr5+ Intestinal Stem Cells. *Cell Stem Cell* **21,** 65–77.e5 (2017).

289. Barker, N., van Oudenaarden, A. & Clevers, H. Identifying the stem cell of the intestinal crypt: strategies and pitfalls. *Cell Stem Cell* **11,** 452–60 (2012).

290. Bjerknes, M. & Cheng, H. Re-examination of P-PTEN staining patterns in the intestinal crypt. *Nat. Genet.* **37,** 1016–1017 (2005).

291. Giannakis, M. *et al.* Molecular properties of adult mouse gastric and intestinal epithelial progenitors in their niches. *J. Biol. Chem.* **281,** 11292–300 (2006).

292. May, R. *et al.* Identification of a Novel Putative Gastrointestinal Stem Cell and Adenoma Stem Cell Marker, Doublecortin and CaM Kinase-Like-1, Following Radiation Injury and in Adenomatous Polyposis Coli/Multiple Intestinal Neoplasia Mice. *Stem Cells* **26,** 630–637 (2008).

293. May, R. *et al.* Doublecortin and CaM Kinase-like-1 and Leucine-Rich-Repeat-Containing G-Protein-Coupled Receptor Mark Quiescent and Cycling Intestinal Stem Cells, Respectively. *Stem Cells* **27,** 2571–2579

(2009).

294. Nakanishi, Y. *et al.* Dclk1 distinguishes between tumor and normal stem cells in the intestine. *Nat. Genet.* **45,** 98–103 (2013).

295. Shi, Z., Chiang, C.-I., Mistretta, T.-A., Major, A. & Mori-Akiyama, Y. SOX9 directly regulates IGFBP-4 in the intestinal epithelium. *Am. J. Physiol. Gastrointest. Liver Physiol.* **305,** G74-83 (2013).

296. Van Landeghem, L. *et al.* Activation of two distinct Sox9-EGFP-expressing intestinal stem cell populations during crypt regeneration after irradiation. *Am. J. Physiol. Gastrointest. Liver Physiol.* **302,** G1111-32 (2012).

297. Li, N., Nakauka-Ddamba, A., Tobias, J., Jensen, S. T. & Lengner, C. J. Mouse Label-Retaining Cells Are Molecularly and Functionally Distinct From Reserve Intestinal Stem Cells. *Gastroenterology* **151,** 298–310.e7 (2016).

298. Montgomery, R. K. *et al.* Mouse telomerase reverse transcriptase (mTert) expression marks slowly cycling intestinal stem cells. *Proc. Natl. Acad. Sci. U. S. A.* **108,** 179–84 (2011).

299. Zeng, X. & Hou, S. X. Enteroendocrine cells are generated from stem cells through a distinct progenitor in the adult Drosophila posterior midgut. *Development* **142,** 644–53 (2015).

300. Breault, D. T. *et al.* Generation of mTert-GFP mice as a model to identify and study tissue progenitor cells. *Proc. Natl. Acad. Sci. U. S. A.* **105,** 10420–5 (2008).

301. Schepers, A. G., Vries, R., van den Born, M., van de Wetering, M. & Clevers, H. Lgr5 intestinal stem cells have high telomerase activity and randomly segregate their chromosomes. *EMBO J.* **30,** 1104–9 (2011).

302. Tian, H. *et al.* A reserve stem cell population in small intestine renders Lgr5-positive cells dispensable. *Nature* **478,** 255–9 (2011).

303. Grün, D. *et al.* Single-cell messenger RNA sequencing reveals rare intestinal cell types. *Nature* **525,** 251–255 (2015).

304. Date, S. & Sato, T. Mini-Gut Organoids: Reconstitution of the Stem Cell Niche. *Annu. Rev. Cell Dev. Biol.* **31,** 269–289 (2015).

Chapter II: IGF1/mTORC1 Signaling Directs the Intestinal Regenerative Response[2]

2.1 Summary

Background & Aims: Intestinal stem cells responsible for intestinal epithelial maintenance, known as crypt base columnar cells (CBCs), die following 12 Gy γ-irradiation, and facultative stem cells (FSCs) drive the ensuing regenerative response. Our aim was to assess the role and mechanism of the growth factor IGF1 in mediating FSC contribution to the regenerative response.

Methods: IGF1 and mTORC1 signaling were pharmacologically modulated by administering mice BMS-754807 or rapamycin, respectively. Genetic mouse models were also employed, using tamoxifen-inducible deletion of Raptor to inhibit, or TSC1 to increase mTORC1 signaling in the intestinal epithelium. A genetic mouse model to lineage trace from Bmi1-positive FSCs was also employed.

Results: We observed increased growth factor expression, including IGF1, with the onset of the regenerative response 2 days post-irradiation. Inhibition of IGF1 signaling via BMS-754807 treatment impaired crypt regeneration, and

[2] Note this chapter is adapted from the following article in preparation:
Bohin, N., McGowan, K. P., Carlson, E. A., Keeley, T. M., Samuelson, L. C. IGF1/mTORC1 Signaling Directs the Intestinal Regenerative Response. *CMGH*. (2019). [In Preparation].

decreased the activity of downstream mTORC1. Coincident with increased IGF1 expression, mTORC1 activity surged concomitantly with the regenerative phase. Inhibition of mTORC1 mirrored the regenerative impairments observed with BMS-754807 treatment. Pharmacologic mTORC1 inhibition with rapamycin blocked FSC mobilization 1-2 DPI. We confirmed in genetic models using *Villin-CreER^{T2};Raptor$^{F/F}$* mice, that depletion of mTORC1 activity impaired regeneration and activated a feedback mechanism by upregulating IGF1 expression.

Conclusions: Our study shows that IGF1 signaling through mTORC1 drives crypt regeneration. We propose that IGF1 secretion from pericryptal mesenchymal cells stimulates mTORC1 in FSCs, resulting in their activation to regenerate lost CBCs.

2.2 Introduction

The intestinal epithelium is continually renewed throughout life by adult stem cells. Two intestinal stem cell (ISC) populations have been identified by their distinct roles during homeostasis and following intestinal damage. Active stem cells, also termed crypt base columnar (CBC) cells, maintain the epithelial cell population during homeostasis, fueling cell renewal every 5-7 days.[1] Facultative stem cells (FSCs) on the other hand, which are also termed quiescent or reserve stem cells, repopulate the CBC niche following stem cell loss. Many different cells in the crypt are capable of reprogramming to function as FSCs, including quiescent cells,[2–5] progenitor cells,[6–8] as well as differentiated cells.[9–11] Administration of a lethal dose of γ-irradiation (e.g. 12 Gy) is a common way of inducing CBC loss and

FSC mobilization to replenish the intestinal epithelium.[2,3,6,7,12,13] Little is known about the mechanism of FCS activation to regenerate the intestinal epithelium after radiation injury.

Intestinal homeostasis and mucosal repair are tightly regulated by the stem cell niche, the crypt/pericryptal microenvironment that consists of signaling factors and cell-to-cell interactions that direct stem cell function. Previously identified niche factors include developmental factors, such as Wnt, Notch and BMP, and growth factors, including epidermal growth factor (EGF), and insulin-like growth factor 1 (IGF1).[14] While the focus of the literature has predominantly been on characterizing niche factors that control CBC-driven homeostasis, fewer studies have sought to define niche factor control of intestinal mucosal repair.

IGF1 has in recent years been proposed to be a critical niche factor in the intestinal regenerative response. Exogenous administration or transgenic overexpression of IGF1 has been shown to promote intestinal epithelial growth and healing under gut injury conditions.[15–19] In one of these studies, IGF1 enhanced stem cell proliferation and crypt regeneration after injury induced by 14 Gy abdominal irradiation.[19] This study also showed that IGF1 administration enhanced the potential for FSCs to form organoids, suggesting that IGF1 can enhance FSC activation post irradiation to promote crypt repair. The mechanism by which IGF1 functions to regulate crypt cell plasticity during intestinal repair remains a gap in our understanding.

The mammalian Target of Rapamycin Complex 1 (mTORC1) signaling complex is regulated by IGF1 via PI3K/Akt signaling. The active mTORC1 complex

is regulates cellular homeostasis through integration of molecular pathways and environmental cues.[20] However, the role of mTORC1 in regulating ISCs is controversial and not well understood, perhaps due to studies employing varying means to modulate its activity, from nutritional challenges to genetic approaches, which could differentially affect other pathways.[21–26] Some studies suggest that mTORC1 may function in crypt repair.[25,27] Mice with intestinal epithelial deletion of mTOR (which would disrupt both mTORC1 and mTORC2) using *Villin-Cre* mice, were more sensitive to 10 Gy γ-irradiation, with reduced capacity to regenerate crypts and CBCs.[25] Interestingly, this study showed that deletion of the mTORC2 complex gene *Rictor* had no effect on crypt regeneration, suggesting that mTORC1 is the key pathway mediating the mTOR effect, although mTORC1 was not tested directly.[25] Another study examined the function of mTORC1 for intestinal adaptation after small bowel resection, showing that mTORC1 inactivation via treatment with the mTORC1 inhibitor rapamycin diminished adaptation, while pathway activation via deletion of the negative regulator *TSC1* enhanced crypt cell proliferation and adaptation.[27] Interestingly, these studies showed no effects of mTOR gene deletion or rapamycin treatment on crypt proliferation during homeostasis.

Two additional studies have recently proposed a mechanism by which mTORC1 and/or PTEN activity, as regulated by nutrient exposure, in FSCs informs FSC contribution to intestinal epithelial repopulation post-injury.[24,28] Collectively the findings suggest that mTORC1 plays a key role in crypt

regeneration, although, the mechanism by which mTORC1 becomes activated, and the direct role of this pathway in FSC mobilization still requires investigation.

Our study investigated the mechanism of IGF1 induction of regeneration of the intestinal crypts after 12 Gy γ-irradiation. Our findings suggest that mesenchymal IGF1 secretion promotes intestinal crypt repair by stimulating mTORC1 activity in FSCs.

2.3 Experimental Procedures

2.3.1 Mice

Mouse use was approved by the Institutional Animal Care & Use Committee at the University of Michigan. Mice were housed in ventilated and automated watering cages with a 12-hour light/dark cycle under specific pathogen-free conditions. The following mouse strains were employed: *Villin-CreER^{T2}* (gift from Robine lab),[29] *Raptor$^{F/F}$* (JAX 013188),[30,31] *TSC1$^{F/F}$* (JAX 05680),[32] *Bmi1-CreER^{T2}* (JAX 010531),[3] *ROSA26-lacZ* (JAX 003474).[33] Mice were maintained on a C57BL/6 strain background. Mice of both sexes aged 1.5-4 months were used.

To activate CreER^{T2}-mediated recombination, mice were injected intraperitoneally with tamoxifen (Sigma; 100 mg/kg; 10 mg/mL in 5% ethanol and 95% corn oil) or vehicle (5% ethanol, 95% corn oil) once per day for the number of days indicated, and tissue was collected as indicated. To inhibit mTORC1 activity, mice were injected intraperitoneally with rapamycin (LC Laboratories; 4mg/kg; 25mg/mL in 5% Tween80, 5% polyethylene glycol 400 in saline) or vehicle (5%

Tween80 and 5% polyethylene glycol 400 in saline) daily for 5 or 7 days, as indicated, prior to tissue collection. To inhibit IGF1 signaling, mice were injected with BMS-754807 (MedChemExpress; 25mg/kg; 100mM in 80% polyethylene glycol 400 and 20% water) or vehicle (80% polyethylene glycol 400, 20% water) daily for 5 days, as indicated, prior to tissue collection. To induce intestinal injury, mice were exposed to 1 dose of 12 Gy whole-body irradiation from a ^{137}Cs source. Animals were injected intraperitoneally with 5-ethynyl-2'-deoxyuridine (EdU; Life Technologies; 25 mg/kg) 2h prior to tissue collection.

2.3.2 Tissue Collection

Intestinal tissue was harvested following *ad libitum* feeding and fixed in 4% paraformaldehyde in 1X PBS overnight before paraffin processing, or flash frozen for subsequent RNA or protein extraction as previously described,[34] and as illustrated in **Figure 2.1**.

2.3.3 Histological Analysis

Duodenal paraffin sections (5μm) were stained with H&E to assess intestinal morphology. The EdU-Click-it kit (Life Technologies) was used to identify proliferating cells. Regeneration was assessed using the adapted crypt microcolony survival assay method.[35] Regenerating crypts were measured as the number of well-oriented crypts with 4 or more EdU-positive cells divided by the total number of well-oriented crypts. Well-oriented crypts were identified from images of adjacent H&E-stained sections. Immunostaining with rabbit antibodies to

γ-H2AX (1:50, Cell Signaling 9718) and phospho-S6 (S240/244) (1:300, Cell Signaling 5364) was performed as described.[36] A goat anti-rabbit IgG Alexa Fluor 488 polyclonal secondary antibody was used (1:400, Invitrogen A27034). Images were captured on a Nikon E800 microscope with Olympus DP controller software.

2.3.4 Western Blot Analysis

Full thickness duodenal tissue was homogenized and lysed in RIPA buffer (Thermo, 89900) containing protease and phosphatase inhibitor cocktail (Thermo Scientific, 78440). Cell lysates (40 µg protein) were mixed with NuPAGE LDS Sample Buffer (Thermo, NP0007) and separated by sodium dodecyl sulfate polyacrylamide gel electrophoresis using NuPAGE MOPS SDS Running Buffer (Thermo, NP0001) and NuPAGE 4-12% Bis-Tris gels (Thermo, NP0335), following manufacturer recommendations. Protein transfer onto 0.45µm pore size nitrocellulose membrane (GE Healthcare) at 100V for 45 min preceded blocking in Odyssey Blocking Buffer (Li-COR, 927-40000) for 1 hour at room temperature.

Immunoblotting with rabbit antibodies to phospho-S6 (S240/244) (1:500, Cell Signaling 5364) and phospho-4EBP1 (1:200, Cell Signaling 2855), and mouse antibodies to S6 total (1:200, Cell Signaling 2317), 4EBP1 (1:200, Cell Signaling 9644), and GAPDH (1:10,000, Thermo Scientific MA5-15738) was performed on a rocking platform overnight at 4°C. Subsequent to rinsing the membrane in TBST (Tris-buffered saline, 0.1% Tween 20), IRDye 800CW Goat α-rabbit (1:10,000, LI-COR 925-32211) and IRDye 680RD Goat α-mouse (1:10,000, LI-COR 925-68070) secondary antibodies were used to visualize probed proteins. Membrane was

scanned on an Odyssey Imager (LI-COR). Western blot analysis was performed using the free Image Studio Lite software (LI-COR).

2.3.5 Gene Expression Analysis

RNA from full-thickness duodenal tissue segments was isolated as previously described.[37] mRNA abundance was measured by quantitative reverse transcriptase polymerase chain reaction (qPCR) as previously described,[36] using IGF1 primers with sequences: CAACTCCCAGCTGTGCAATT (forward) and GCCGAGGTGAACACAAAACT (reverse), which yielded a 151 bp amplified product. Assays for each sample were run in triplicate and normalized to *Gapdh* or *Hprt* as indicated, as an internal control, with *Gapdh* primer sequences: TCA AGA AGG TGG TGA AGC AGG (forward) and TAT TAT GGG GGT CTG GGA TGG (reverse), which yielded a 350 bp amplified product, and *Hprt* primer sequences: AGG ACC TCT CGA AGT GTT GGA TAC (forward) and AAC TTG CGC TCA TCT TAG GCT TTG (reverse).

For growth factor array analysis, RNAs from unirradiated, 48 hours post irradiation (HPI), 4 days post irradiation (DPI) and 6 DPI were submitted to the University of Michigan DNA Sequencing Core who performed quality control analysis of the samples, ran RT^2 Profiler™ PCR Mouse Growth Factor Arrays (Qiagen; PAMM-041Z) and analyzed the data (**Figure 2.3** and **Appendix Tables 2.1, 2.2. and 2.3**). Three independent biological samples were assessed for each time point.

2.3.6 Statistical Analysis

All experiments were performed with at least 3 biological replicates per group. Quantitative data are presented as mean ± SEM. Comparisons between 2 groups were conducted with unpaired two-tailed Student *t* tests using the Prism software (Graphpad). Significance is reported as *(P<0.05), **(P<0.01), ***(P<0.001), and ***P<0.0001).

2.4 Results

2.4.1 The Intestinal Regenerative Response has Three Phases

We characterized the intestinal response following damage induced by 12 Gy whole body γ-irradiation. Histological analysis revealed gross morphological changes, particularly apparent in the crypt compartment, which allowed categorization of the post-damage response into three distinct phases: damage, regeneration and recovery (**Figure 2.2A**). The damage phase is characterized by rapid cellular injury, followed by crypt collapse. At 3 HPI, DNA double-strand breaks were demonstrated throughout the epithelium by γ-H2AX staining (**Figure 2.2B**). This DNA damage appears largely resolved by 12 HPI (**Figure 2.2B**), but cell proliferation is almost totally lost at this time, as demonstrated by EdU incorporation (**Figure 2.2C).** By 48 HPI, crypt architecture is destroyed, with de-cellularization and crypt loss (**Figure 2.2A**). The regenerative phase, which is apparent at 3 days post-irradiation (DPI), is characterized by crypt recovery

(**Figure 2.2A**). The hallmark of this phase of the post-damage response is the hyperproliferative surge and expanded crypts that occurs 3-5 DPI (**Figure 2.2C-D**). We denote 6 DPI as the beginning of the recovery phase, where the regenerative response is resolving, and crypt structure and the intestinal epithelium are returning to baseline.

2.4.2 Surge of IGF1 Signaling During the Regenerative Phase

We next sought to identify growth factors that might play a role in mediating the response to radiation injury. We assessed growth factor expression signatures using a Qiagen qPCR based array designed to measure 84 mouse growth factor mRNAs. We analyzed time points across the three phases of the regenerative response, and compared to unirradiated (UNIRR) baseline (**Figure 2.2A**). Several growth factors showed a coordinate increase in mRNA abundance with damage (48 HPI) and regeneration (4 DPI), with a return towards baseline during the recovery phase (6 DPI; **Figures 2.2A** and **2.3A**). IGF1 was amongst the growth factors with the most dramatic changes in expression in response to damage. We confirmed the dynamic expression of IGF1 mRNA abundance by qPCR analysis, which revealed a 6-fold increase at 48HPI (**Figure 2.3B**). To identify the cellular source of IGF1 we used the RNAscope *in situ* hybridization method, which demonstrated expression in pericryptal mesenchymal cells (**Figure 2.3C**). In light of a previous study demonstrating intestinal pro-regenerative properties of IGF1 *in vivo*,[19] and an *in vitro* study showing that IGF1 promoted growth of human

intestinal stem cells, we focused the rest of our study on the role of this signaling axis.

2.4.3 Inhibition of IGF1/mTORC1 Signaling Impairs Intestinal Regeneration

We tested the effect of pharmacological inhibition of IGF1 using the reversible IGF1 receptor (IGF1R) inhibitor BMS-754807 (BMS). Mice were administered a 12 Gy dose of γ-irradiation, and treated immediately after, and daily thereafter, with BMS (25mg/kg) or vehicle, with tissue harvest at 5 DPI (**Figure 2.4A**). At baseline, inhibition of this pathway had no discernible effect on intestinal homeostasis; tissue architecture and cellular proliferation did not differ from controls (**Figure 2.5**). Marked differences were however noted at 5 DPI between BMS and vehicle-treated mice challenged with 12 Gy γ-irradiation (**Figure 2.4A-E**). BMS-treated mice had a more pronounced post-irradiation weight loss compared to controls (**Figure 2.4A**) and histological analysis showed more extensive intestinal damage, with blunted villi (**Figure 2.4B**). BMS-treated mice had 20% fewer regenerating crypts, consistent with impaired regeneration (**Figure 2.4C-D**).

IGF1 signaling is known to activate the PI3K/AKT pathway, which releases inhibition of mTORC1 signaling,[38,39] so we next aimed to assess changes to mTORC1 activity. We confirmed inhibition of downstream mTORC1 signaling with BMS treatment by immunostaining for mTORC1 target p-S6(S240/244) (**Figure 2.4E**). Thus, pharmacological inhibition of IGF1 signaling results in impaired intestinal regeneration, and decreased mTORC1 activity.

2.4.4 Elevated mTORC1 Activity in Intestinal Crypts Post Irradiation

We next asked whether the compromised intestinal regenerative capacity in response to IGF1 inhibition is due to depleted mTORC1 activity. We first assessed changes to mTORC1 activity post-irradiation by Western blot analysis, with increased phosphorylation of mTORC1 targets, ribosomal protein S6 and 4EBP1, coincident with the regenerative phase (**Figure 2.6A-C**) and the surge in IGF1 expression (**Figure 2.3A-B**). Immunohistological analysis confirmed changes in S6 phosphorylation status (S240/244), which were most pronounced in the crypts, alluding to a role for increased mTORC1 signaling in the crypts following damage (**Figure 2.6D**).

2.4.5 Inhibition of mTORC1 Signaling Impairs Intestinal Regeneration

We next tested whether mTORC1 inhibition would mirror the impaired intestinal regeneration observed with inhibition of IGF1 signaling. To inhibit mTORC1 activity, we treated mice with rapamycin or vehicle daily, starting immediately following exposure to 12 Gy γ-irradiation (**Figure 2.7A**). Similar to BMS, rapamycin administration to non-irradiated mice did not affect intestinal tissue morphology, cellular proliferation, or mRNA abundance of markers of stem cells (*Lgr5, Olfm4*) or differentiated cells (*Mmp7, Chga, Muc2*) (**Figure 2.8**). In contrast, inhibition of the pathway in irradiated mice impaired intestinal regeneration (**Figure 2.7A-H**), similar to the effect of IGF1 inhibition (**Figure 2.4A-**

D). At 3 DPI, the intestines of vehicle-treated mice began to recover with a typical regenerative response, characterized by expanded crypts and increased proliferation (**Figure 2.7C, E**). In contrast, rapamycin-treated mice had fewer, and smaller crypts (**Figure 2.7C**). We measured a 43.4% decrease in regenerating crypts in rapamycin-treated mice (**Figure 2.7G**). Further, at 5 DPI, the villi of rapamycin-treated mice were blunted, similarly to BMS-treated mice, consistent with impaired regeneration at 3 DPI (**Figure 2.7D**). Crypt regeneration at this time point was still compromised in mTORC1-inhibited intestine, with about 33.2% fewer regenerating crypts (**Figure 2.7F, H).** These results suggest that IGF1 signaling works via mTORC1 to support the intestinal regenerative response.

2.4.6 mTORC1 Inhibition Blocks FSC Contribution to Regeneration

To identify the key timing for mTORC1 function in crypt repair, we varied the inhibitor treatment by delaying rapamycin administration to 24 and 48 HPI (**Figure 2.9A-E**). Mice initiating rapamycin treatment at 24 HPI had a similar effect on regeneration as observed in our previous experiment, in which mice started rapamycin treatment at the time of radiation. Both groups of rapamycin-treated mice exhibited enhanced weight loss and reduced numbers of regenerating crypts (**Figure 2.9A, C-E** compared to **Figure 2.7C, E, G**). In contrast, mice initiating rapamycin treatment at 48 HPI exhibited a normal crypt regeneration response (**Figure 2.9B, C-E**). These findings suggest that the key window for mTORC1 action is 24-48 HPI. Importantly this timing corresponds to the timing for

mobilization of facultative intestinal stem cells (FSCs), suggesting that mTORC1 might play a role in the mobilization and/or proliferation of these cells following radiation injury.[12,40]

To test whether mTORC1 is important to FSC contribution to the regenerative response, we assessed FSC activity post-irradiation in an mTORC1-depleted context. *Bmi1-CreER^{T2};ROSA26-lacZ* mice were irradiated, and immediately treated with tamoxifen, to induce lineage tracing from Bmi1-positive FSCs, along with rapamycin or vehicle. Rapamycin or vehicle treatment was continued daily thereafter. We observed fewer lineage traces from rapamycin-treated FSCs compared to vehicle-treated counterparts (**Figure 2.9F**). This data indicates that mTORC1 is critical to FSC mobilization following intestinal injury.

2.4.7 Genetic Depletion of mTORC1 Results in Impaired Regeneration

Given the potential off-target effects common to pharmacological inhibitors, we used genetic models to validate our finding that mTORC1 activity is crucial to the intestinal regenerative response following injury. *Villin-CreER^{T2};Raptor$^{F/F}$* mice were treated with 100mg/kg tamoxifen daily for 4 days to induce deletion of *Raptor*, which encodes a mTORC1 protein subunit essential to the activity of the complex, and irradiated 24 hours following the last injection of tamoxifen (**Figure 2.10A).** *Villin-CreER^{T2}* mice were used as controls to account for any effects of CreER^{T2} toxicity.[41] We first confirmed depleted mTORC1 activity in *Villin-CreER^{T2};Raptor$^{F/F}$* mice by immunostaining for the downstream mTORC1 target p-

S6(S240/244) (**Figure 2.10B**). Consistent with impaired regeneration, we observed that at 3 DPI, *Villin-CreER^{T2};Raptor$^{F/F}$* mice had lost significantly more weight post-irradiation than *Villin-CreER^{T2}* controls (**Figure 2.10A**). Histological analysis of *Villin-CreER^{T2};Raptor$^{F/F}$* also revealed significant impairment in crypt regeneration (**Figure 2.10C-E** compared to **Figure 2.7C, E, G**). At 3DPI, *Villin-CreER^{T2};Raptor$^{F/F}$* crypts appeared few, small and de-cellularized compared to controls (**Figure 2.10C**). Proliferation was dramatically reduced in the *Raptor*-deleted intestine (**Figure 2.10D**), with a 3-fold decrease in regenerating crypts compared to *Villin-CreER^{T2}* controls (**Figure 2.10E**). Notably, the reduced regenerative capacity was almost twice that observed in rapamycin-treated mice (**Figure 2.10E** compared to **2.7G**). These findings demonstrate that the impaired regeneration observed with rapamycin administration is attributable to the importance of mTORC1 in this response.

Given the reported enhancement in regeneration following *in vivo* IGF1 administration post-irradiation,[19] and our findings suggesting that IGF1 works via mTORC1 to contribute to intestinal regeneration, we sought to determine if increased mTORC1 activity might enhance regeneration. To this aim, we irradiated tamoxifen-treated *Villin-CreER^{T2};Tsc1$^{F/F}$* mice, to activate mTORC1 by deletion of a negative regulator. Interestingly, we did not observe body weight differences, histological changes, or variations in proliferation or regenerative capacity in these animals compared to *Villin-CreER^{T2}* controls (**Figure 2.10A, C-E**). Thus, we find that genetic mTORC1 depletion results in impaired intestinal regeneration, but that activation of the pathway does not lead to an improved regenerative capacity.

We finally sought to understand how genetic modulation of mTORC1 activity might affect IGF1. We assessed IGF1 expression by qPCR in our *Villin-CreER^{T2};Raptor$^{F/F}$* and *Villin-CreER^{T2};Tsc1$^{F/F}$* animals, compared to *Villin-CreER^{T2}* controls at baseline and post-irradiation. At baseline, there were no changes in IGF1 expression between these genetic models of varying mTORC1 activity levels (**Figure 2.10F**). Following irradiation, IGF1 expression was increased in all animal models (**Figure 2.10F**), as expected from our data indicating a surge of IGF1 expression concomitant with the regenerative phase (**Figure 2.3B**). However, surprisingly, the induction in IGF1 expression in *Villin-CreER^{T2};Raptor$^{F/F}$*, mTORC1-depleted mice post-irradiation was almost doubled compared to the surge observed in *Villin-CreER^{T2}* controls (**Figure 2.10F**). This data suggests a potential feedback mechanism is at play in enhancing IGF1 induction in response to mTORC1 depletion following injury.

2.5 Discussion

Our study shows that the intestinal response to crypt damage induced by 12 Gy whole body irradiation is characterized by 3 phases: damage (3-48 HPI), regeneration (3-5 DPI) and recovery (6+ DPI). Cellular injury preferentially targets CBCs, with rapid stem cell depletion and crypt collapse followed by mobilization of FSCs and crypt regeneration.[5,40,42] The irradiation damage stimulates expression of IGF1, which our work suggests promotes mTORC1 activity in the regenerating crypts during the regeneration phase. Inhibition of either IGF1 or mTORC1 signaling results in a severe impairment in crypt regeneration and enhanced body

weight loss, compared to uninhibited controls. Our findings indicate that IGF1/mTORC1 signaling is particularly important 24-48 HPI, coincident with the timing of FSC mobilization, with impaired FSC contribution to regeneration when mTORC1 activity is depleted. Further, in agreement with previous reports,[43–47] we show that IGF1 production is localized to pericryptal mesenchymal cells, which have been reported to serve a stem cell niche-supporting function via paracrine signaling.[48–51] Pericryptal mesenchymal cell to crypt cell IGF1 communication is also supported by evidence showing expression of the IGF receptor 1 (IGFR1) on the basolateral membrane of crypt cells.[44,52] Thus, our studies propose a mechanism by which CBC loss induces mesenchymally-secreted IGF1 signaling to intestinal crypt cells to elevate mTORC1 activity, stimulating FSC contribution to regeneration (**Figure 2.11**).

The study of IGF1 signaling in the intestine has mostly been parsed out from pathway stimulation studies, including a 2015 report employing exogenous IGF1 administration to demonstrate a pro-regenerative role for this growth factor.[19] Based on their data showing IGF1 administration enhanced the organoid forming potential of FSCs, this report suggested that IGF1 administration enhanced FSC potential by an unknown mechanism.[19] Our work aimed to remediate this gap in knowledge, and to contribute to the body of literature seeking to understand the role of IGF1 signaling in the intestine given how few studies have reported on the effects of depleting IGF1 in the intestine.[53–57] In agreement with the aforementioned 2015 study, our data proposes that IGF1 is indeed involved in controlling FSC contribution to the intestinal epithelium, working through mTORC1.

The literature is in agreement with our data implicating mTORC1 in intestinal mucosal repair. A 2015 report from Cincinnati employing mouse models of mTOR depletion in the intestinal epithelium demonstrated that mTOR was critical to intestinal crypt recovery from 10 Gy irradiation.[25] However the group did not specify whether the activity of mTORC1 and mTORC2 combined or mTORC1 alone was implicated. A few studies have however suggested a mechanism of action for the regenerative role of mTORC1.

The Breault lab proposed that transient inactivation of the negative mTORC1 regulator PTEN during extreme nutrient deprivation (48h fast), results in a change in FSC status that is mTORC1-dependent from a “dormant” to a “poised” state capable of repopulating the intestinal epithelium.[26,58] Interestingly, the Lengner lab showed that calorie restriction led to an mTORC1-dependent enhancement in regenerative capacity post-injury.[24] This data was initially counter-intuitive, calorie restriction leads to depleted mTORC1 activity in uninjured intestine,[26,59] and our data demonstrated reduced regeneration following mTORC1 depletion (**Figure 2.7**). However, while the Lengner lab showed that mTORC1 activity was enhanced post-irradiation (in agreement with our data in **Figure 2.6**), they found mTORC1 activity was further enhanced by calorie restriction compared to ad libitum feeding. The Lengner lab also showed that mTORC1 activation via leucine administration sensitized FSCs to irradiation injury, leading to reduced regenerative capacity. These results combined with our data showing reduced *Bmi1*-positive FSC contribution to intestinal repair in rapamycin-treated mice (**Figure 2.9**) and the Breault lab report implicating mTORC1 in mobilizing FSCs to

contribute to repair, suggest that mTORC1 is responsible for transitioning FSCs into a “poised” state that is capable of responding to repair, but is also more sensitive to DNA damage. This is in agreement with the Rodgers group’s observation of a mTORC1-dependent muscle stem cell (satellite cell; normally mitotically dormant) transition state from dormancy to functionally poised in response to muscle injury.[28]

Surprisingly, our genetic study leading to increased mTORC1 activity in *Villin-CreER^{T2};Tsc1$^{F/F}$* mice yielded unexpected outcomes. Because our data intimates mTORC1 as the mechanism through which IGF1 regulates the regenerative response, we expected that increased mTORC1 activity resulting from *Tsc1* deletion would increase crypt regeneration. A previous study found that IGF1 administration to mice enhanced regenerative capacity after irradiation injury.[19] Our observation that increased mTORC1 activity did not enhance regeneration suggests that the regenerative response, including increases in multiple growth factors, has effectively maximally activated mTORC1 to stimulate crypt cell repair. Barron et *al.* reported that tamoxifen-activated *Villin-CreER^{T2};Tsc1$^{F/F}$* mice had enhanced adaptation to small bowel resection, with proliferation and normal weight gain when compared to controls.[27] This finding suggested that increased mTORC1 signaling due to *Tsc1* deletion enhanced crypt regeneration in this injury context. The enhanced adaptation described by Barron et *al.* was small however, and differences between our two studies using *Villin-CreER^{T2};Tsc1$^{F/F}$* mice could be attributed to differences in the nature of intestinal injury. Further, the difference between our data indicating IGF1/mTORC1 signaling

is critical to intestinal regeneration and our findings that *Tsc1*-deleted mice do not have enhanced regenerative capacity may be the result of differences in acute versus long term stem cell and crypt remodeling to achieve homeostasis.

One query arising from our findings is the identity of the cells secreting IGF1. Several studies have emerged in recent years identifying a non-epithelial, pericryptal niche cell that supports CBC function by secreting critical factors to support epithelial cell function, including intestinal stem cells.[48–51] Although the cellular localization of IGF1 had not previously been defined, our studies show IGF1 mRNA localization to pericryptal mesenchymal cells (**Figure 2.3C**). Notably, IGF1 receptors are preferentially expressed in epithelial stem/progenitor cells and one study showed stem cell expansion after IGF1 treatment.[19] Although future studies are warranted, we propose that IGF1 is secreted by pericryptal pericryptal cells after epithelial injury. Further, we propose that IGF1 signals to FSCs by binding surface IGF receptors to promote downstream mTORC1 activity, to activate FSCs to repopulate the damaged crypt compartment (**Figure 2.11**). Future directions should be targeted to further understand the mesenchymal stem cell population expressing IGF1 as a niche cell for ISCs.

2.6 Author Contributions

NB and LCS designed the project. NB, KPM, EAC and TK performed experiments. NB, KPM and LCS interpreted data and wrote the manuscript, and all co-authors provided critical feedback.

2.7 Acknowledgements

We thank Yasmine Abushukur for technical help, Erin Collin and Lindsay Griffin for maintaining the mouse colony, and Dr. Douglas Yee for advice on selecting inhibitors of IGF1 signaling. NB was supported by the Cellular and Molecular Biology program, a Rackham research grant and the Benard L. Maas Fellowship. The research was funded by NIH R01-DK118023 to LCS, and Core support from the Michigan Gastrointestinal Research Center Grant NIH P30-DK34933.

2.8 Figures

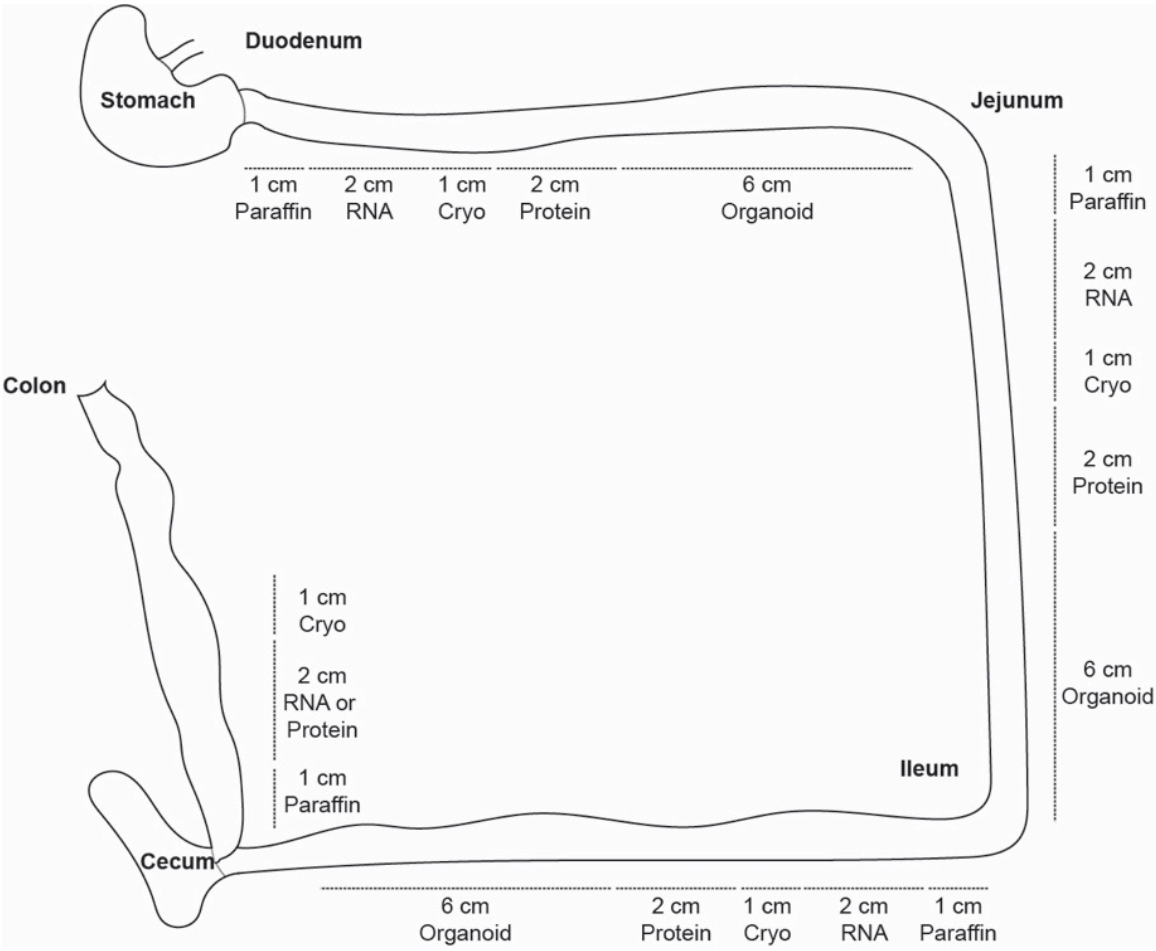

Figure 2.1 Intestinal tissue collection.

Diagram illustrating how the sections of mouse intestine are allocated to different analysis, including paraffin processing, cryogenic (cryo) embedding, RNA and protein extraction, and organoid formation (Chapters III and IV).

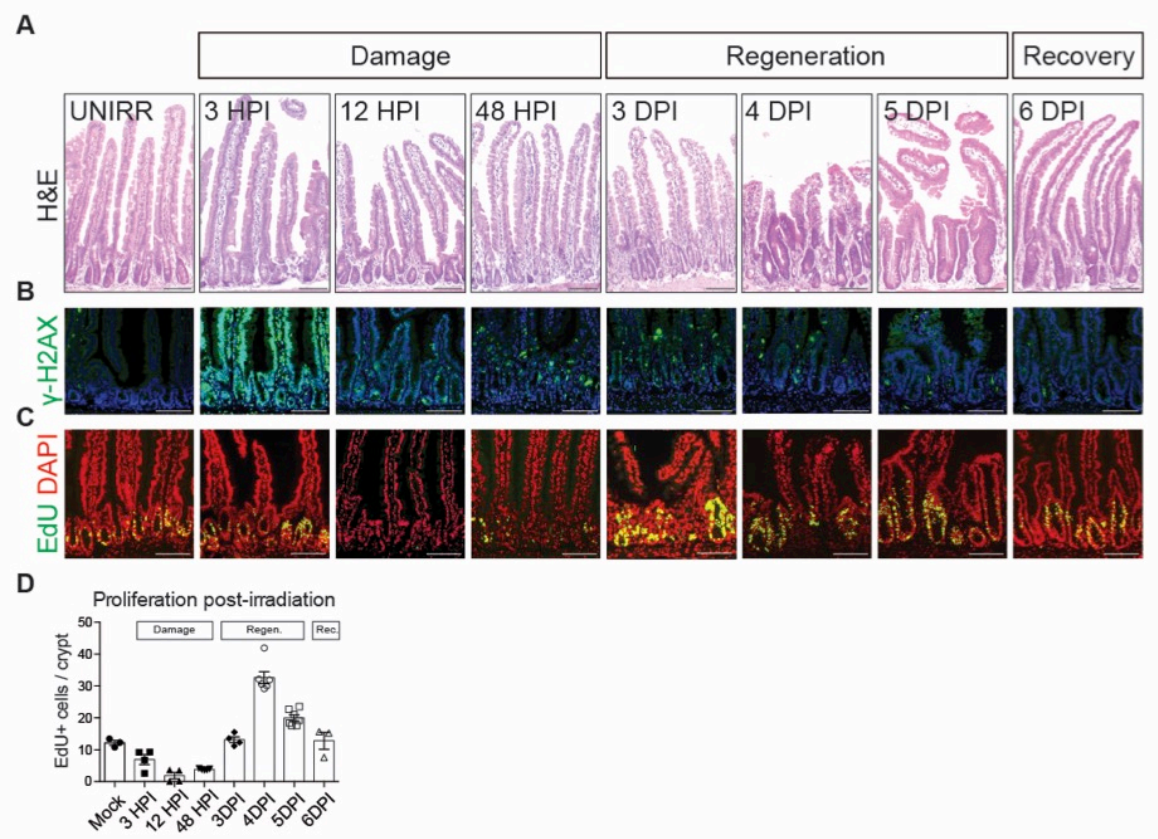

Figure 2.2 Three phases of the intestinal regenerative response post-irradiation.

Mice were unirradiated or administered 12 Gy γ-irradiation, and intestinal tissue was collected at various times points, including 3 hours post-irradiation (HPI), 12 HPI, 48 HPI, 3 days post irradiation (DPI), 4 DPI, 5 DPI, and 6 DPI. (A) Duodenal histology was assessed by H&E staining. (B) DNA damage was assessed by immunostaining for γ-H2AX. (C) Cellular proliferation was assessed by EdU incorporation (green) with nuclear counterstain DAPI (red). (D) The number of Edu+ cells was counted at the various time points post irradiation. Proliferating cell number is presented as EdU-positive cells per crypt (mean +/- SEM, n=3-6 mice/group). Scale bars = 100μm.

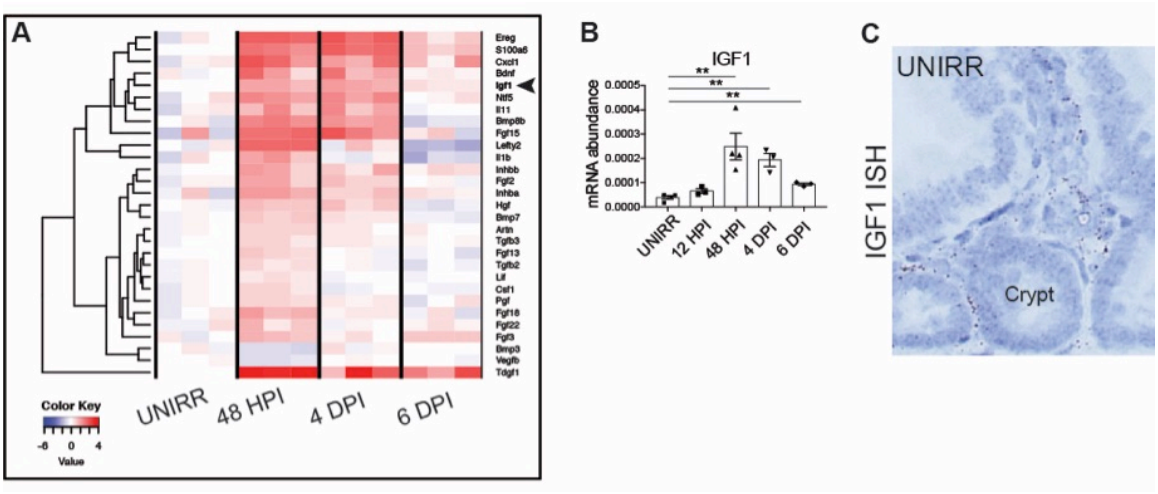

Figure 2.3 IGF1 growth factor expression increases during the regenerative response.

Duodenal tissue from unirradiated (UNIRR) and irradiated mice harvested at 48 hours post-irradiation (HPI), 4 days post-irradiation (DPI) and 6 DPI was analyzed for expression of 84 growth factors by qPCR array analysis. (A) Heatmap of growth factor expression after irradiation injury, with red meaning more and blue meaning less expressed, relative to UNIRR control (n=3 mice/group). (B) qPCR analysis of *Igf1* mRNA abundance normalized to *Gapdh* displayed as mean +/- SEM (n=3-4 mice/group; **p<0.01 by Student's *t*-test). (C) *In situ* hybridization (ISH) for *Igf1* on UNIRR tissue.

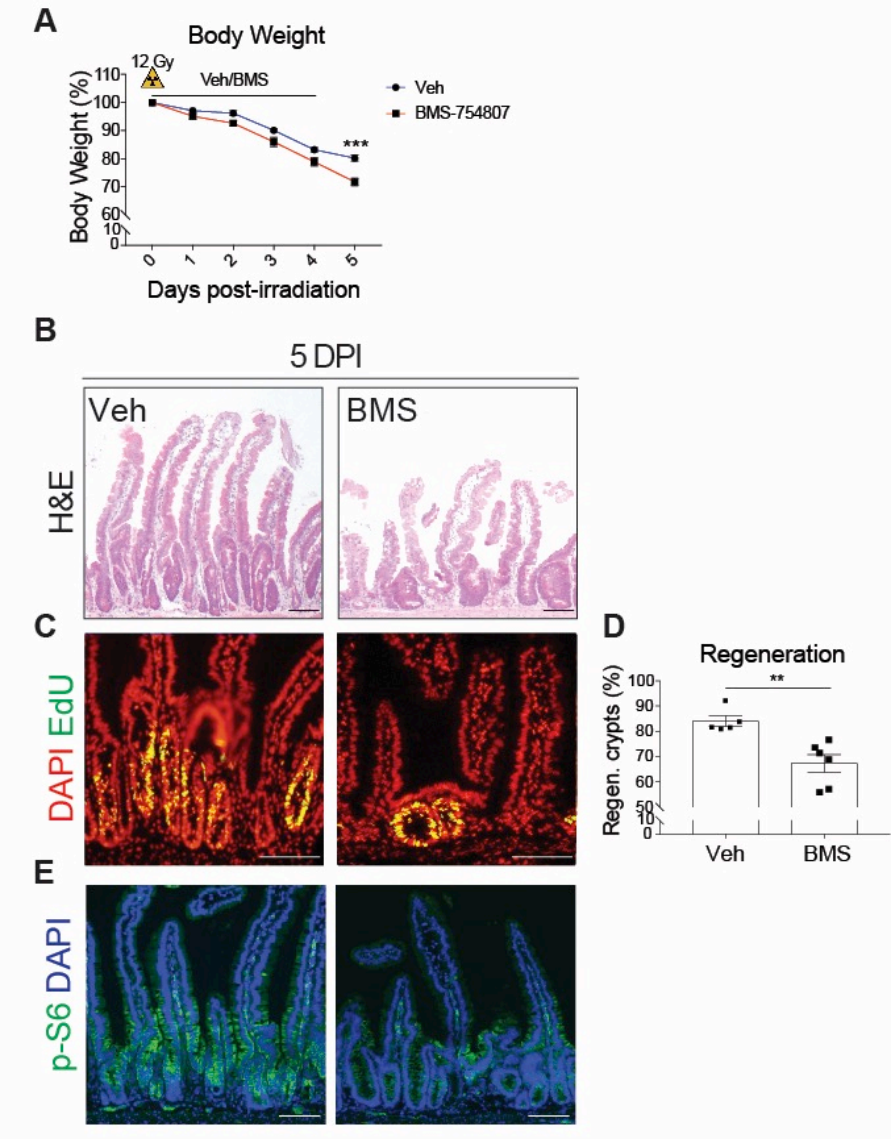

Figure 2.4 IGFR1 inhibition impairs intestinal regeneration.

Mice administered 12 Gy γ-irradiation were treated within an hour of challenge, and daily thereafter, with BMS-754807 (BMS; 25mg/kg) or vehicle (Veh). (A) Mouse body weight relative to weight at the initiation of treatment (n=5-6 mice/group). (B-D) Duodenal crypt regeneration was assessed at 5 DPI by (B) H&E staining, and (C) EdU incorporation. (D) Crypt regeneration was measured (n=5-6 mice/group). (E) Immunofluorescent images of duodenal tissue stained for mTORC1 target p-S6(S240/244). Quantitative data are presented as mean +/- SEM (**P<0.01, ***P<0.001 by Student's *t*- test). Scale bars = 100μm.

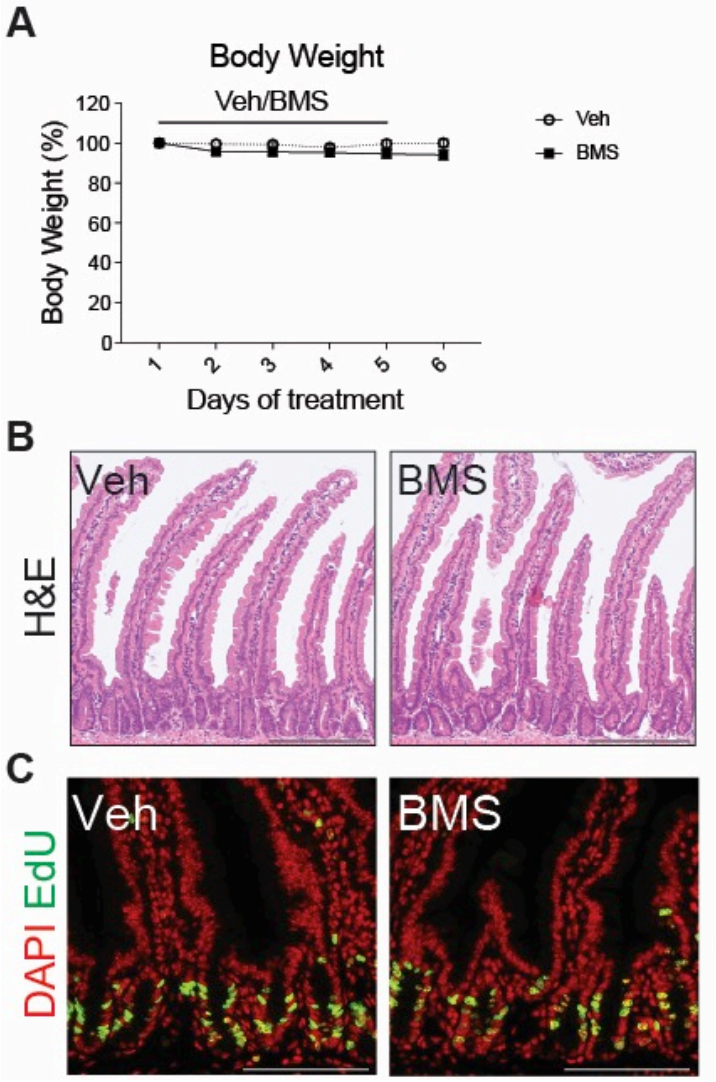

Figure 2.5 IGFR1 inhibition does not perturb intestinal homeostasis.

Duodenal tissue was harvested from mice 24 hours following administration of BMS or Veh daily for five days. (A) Mouse body weight relative to weight at the initiation of treatment (n=5 mice/group). Assessment of disruption of intestinal homeostasis was examined via (B) H&E staining, and (C) EdU incorporation. Quantitative data are presented as mean +/- SEM. Scale bars = 100μm.

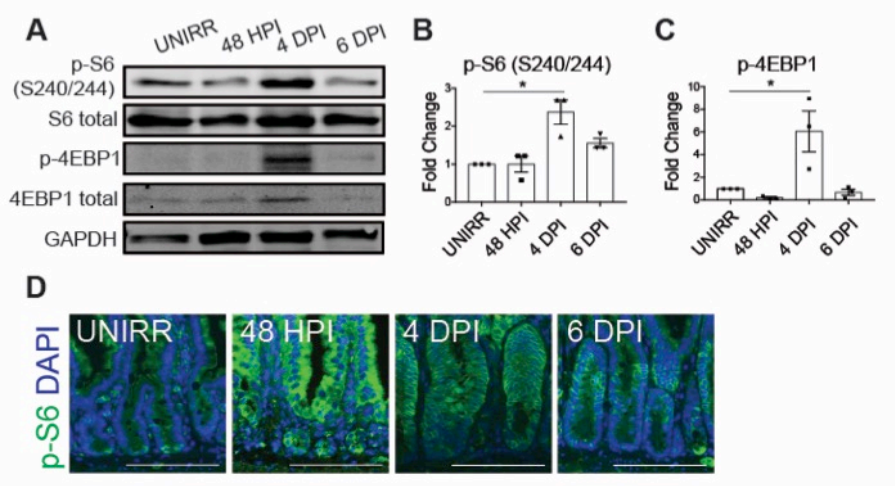

Figure 2.6 mTORC1 activity increases during the regenerative response.

(A-D) Protein levels of mTORC1 signaling components in UNIRR duodenum compared to samples collected 48 HPI, 4 DPI and 6 DPI, as assessed by western blotting and immunostaining. (A) Western blot analysis for p-S6(S240/244), total S6, p-4EBP1, total 4EBP1, and loading control GAPDH. (B) p-S6 and (C) p-4EBP1 band signal was quantified and displayed as mean +/- SEM (n=3 mice/group; **p<0.01 by Student's *t*-test). (D) Immunofluorescent images of p-S6-stained duodenal tissue at various time points post-irradiation compared to unirradiated control. Scale bars = 100μm.

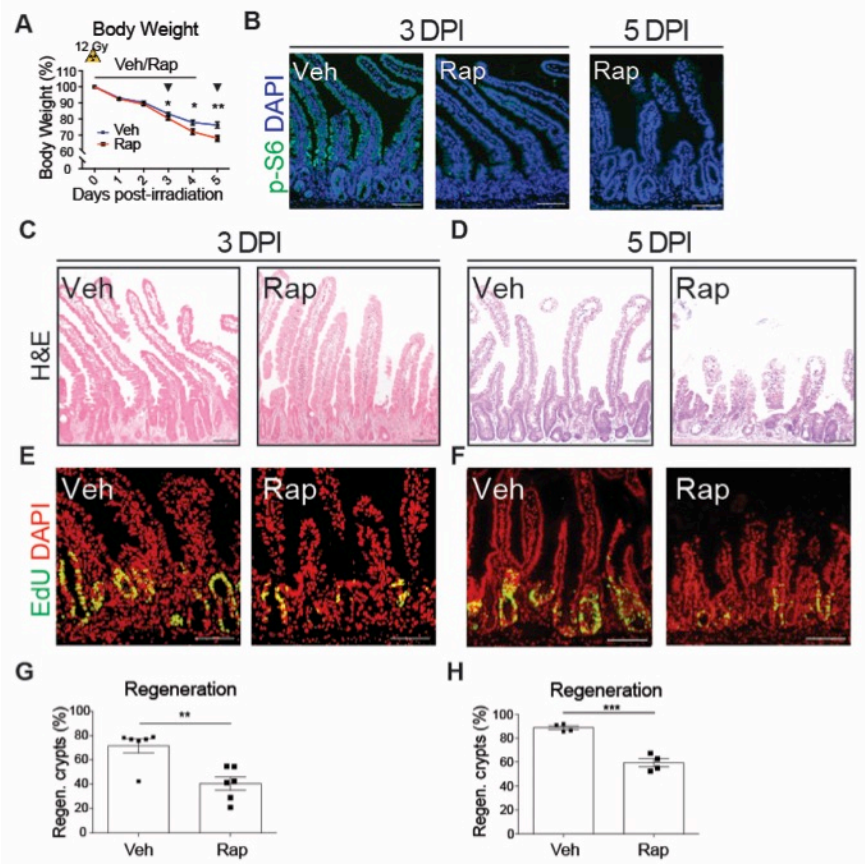

Figure 2.7 mTORC1 inhibition leads to impaired intestinal regeneration.

(A-H) Mice administered 12 Gy γ-irradiation were treated within an hour of challenge, and daily thereafter, with rapamycin (Rap; 4mg/kg) or Veh, and euthanized 3 and 5 DPI, as indicated by arrowheads. (A) Mouse body weight relative to weight at the initiation of treatment (n=16-25 mice/group). (B) Immunofluorescent images of p-S6-stained duodenal tissue harvested 3 and 5 DPI from Veh- and Rap-treated animals. (C-H) Duodenal crypt regeneration was assessed at (C, E, G) 3 DPI and (D, F, H) 5 DPI by (C-D) H&E staining, and (E-F) EdU incorporation. (G-H) Crypt regeneration was measured (n=4-6 mice/group). Quantitative data are presented as mean +/- SEM (*P<0.05, **P<0.01, ***P<0.001 by Student's *t*-test). Scale bars = 100μm.

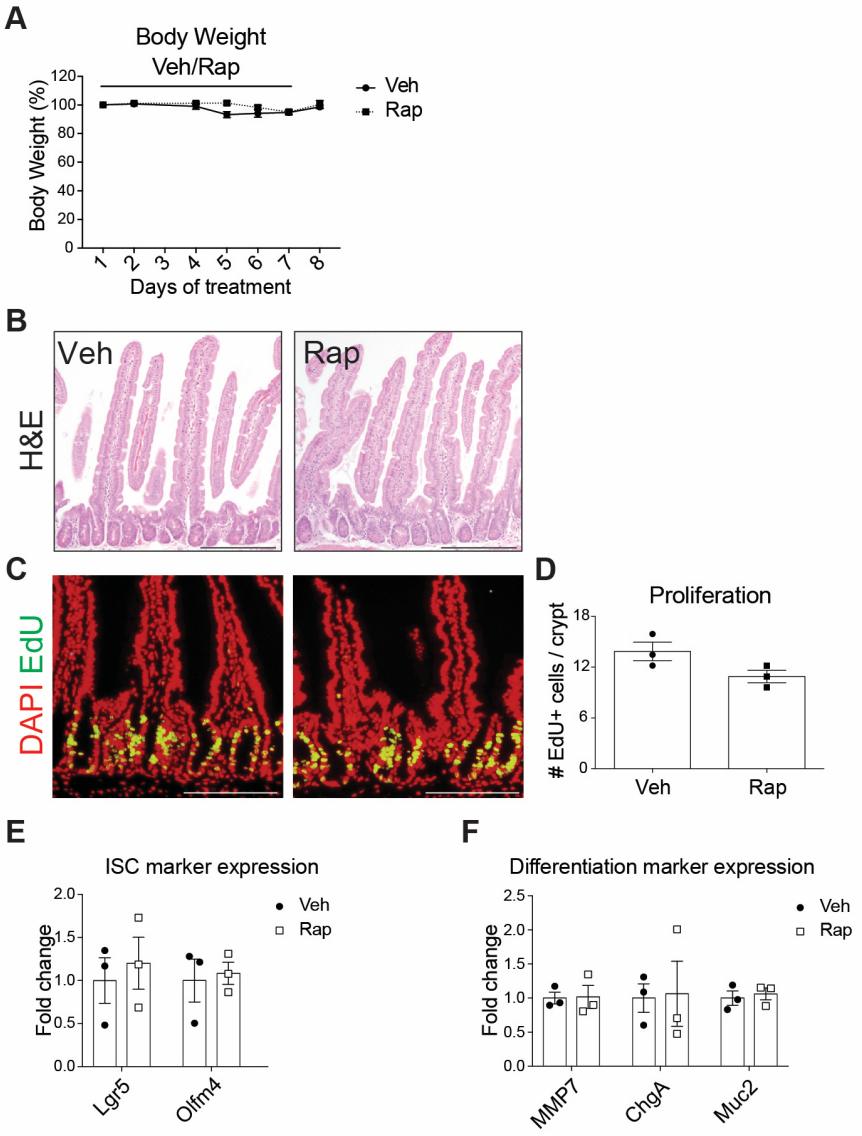

Figure 2.8 mTORC1 inhibition does not perturb intestinal homeostasis.

(A-G) Mice were administered Rap or Veh daily over 7 days and duodenal tissue was harvested 24 hours following the last injection. (A) Mouse body weight relative to weight at the initiation of treatment. Intestinal homeostasis was assessed by (B) H&E staining, (C-D) EdU incorporation, (E-F) and expression of intestinal stem and differentiated cell markers. (E-F) qPCR analysis from full thickness duodenum for markers of intestinal (E) stem (*Lgr5*, *Olfm4*), and (F) differentiated cells (*Mmp7*, *Chga*, *Muc2*) normalized to *Gapdh*. Quantitative data are presented as mean +/- SEM. Scale bars = 100μm.

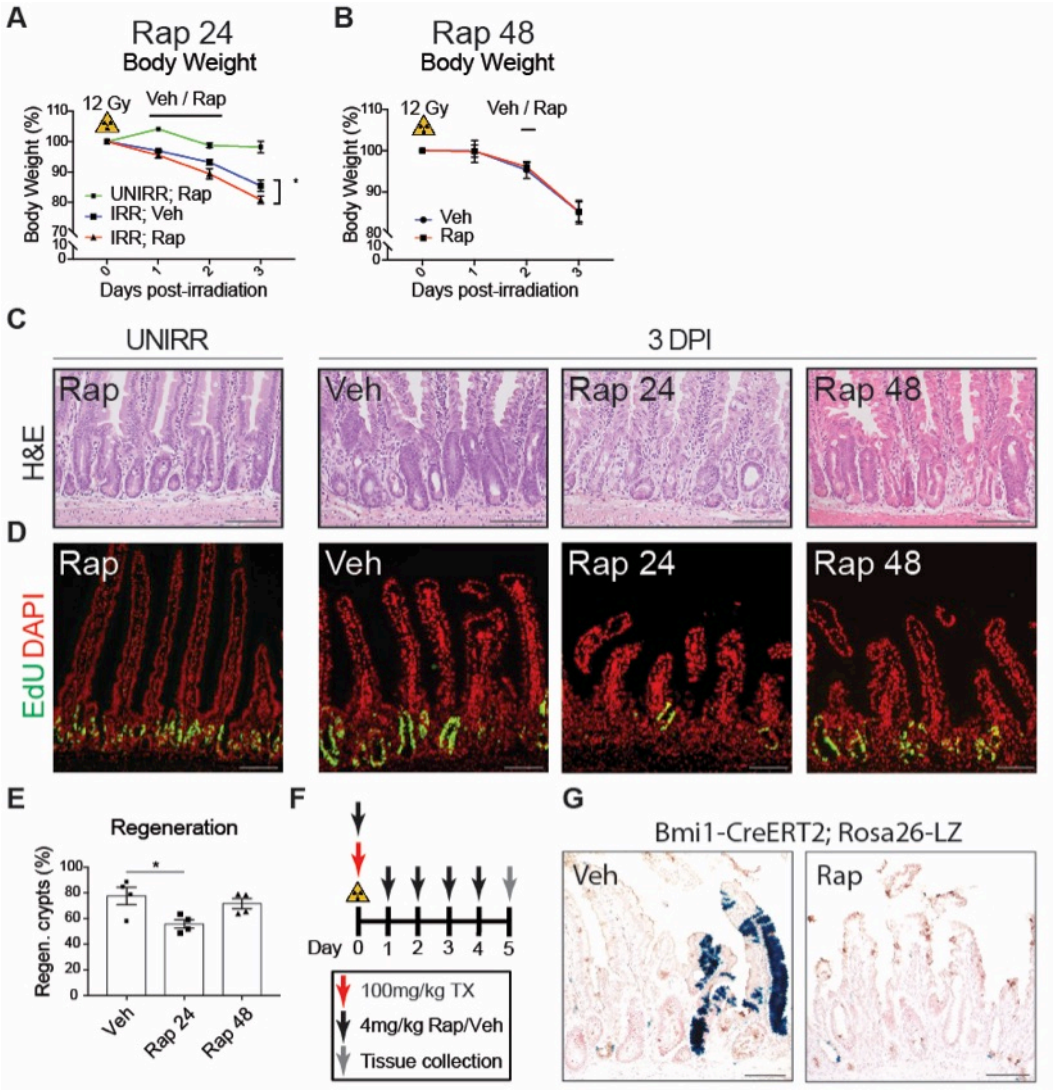

Figure 2.9 Rapamycin impairs facultative stem cell contribution to intestinal regeneration.

(A-E) Mice administered were treated with Rap or Veh starting 24 HPI (Rap 24) or 48 HPI (Rap 48) after 12 Gy γ-irradiation, and analyzed at 3 DPI. (A-B) Mouse body weight relative to weight at the initiation of the experiment (n=4 mice/group). (C-E) Duodenal crypt regeneration was assessed by (C) H&E staining, and (D) EdU incorporation, with (E) crypt regeneration quantitated (n=4 mice/group). (F) *Bmi1-CreER^{T2};ROSA26-lacZ* mice 12 Gy γ-irradiation were injected with a single dose of tamoxifen (TX; 100mg/kg), and daily thereafter, with Rap or Veh for 5 days. (G) 5 DPI duodenal sections were stained for X-gal to visualize lineage traces (n=2-3 mice/group). Quantitative data are presented as mean +/- SEM (**P<0.01, ***P<0.001 by Student's *t*-test). Scale bars = 100μm.

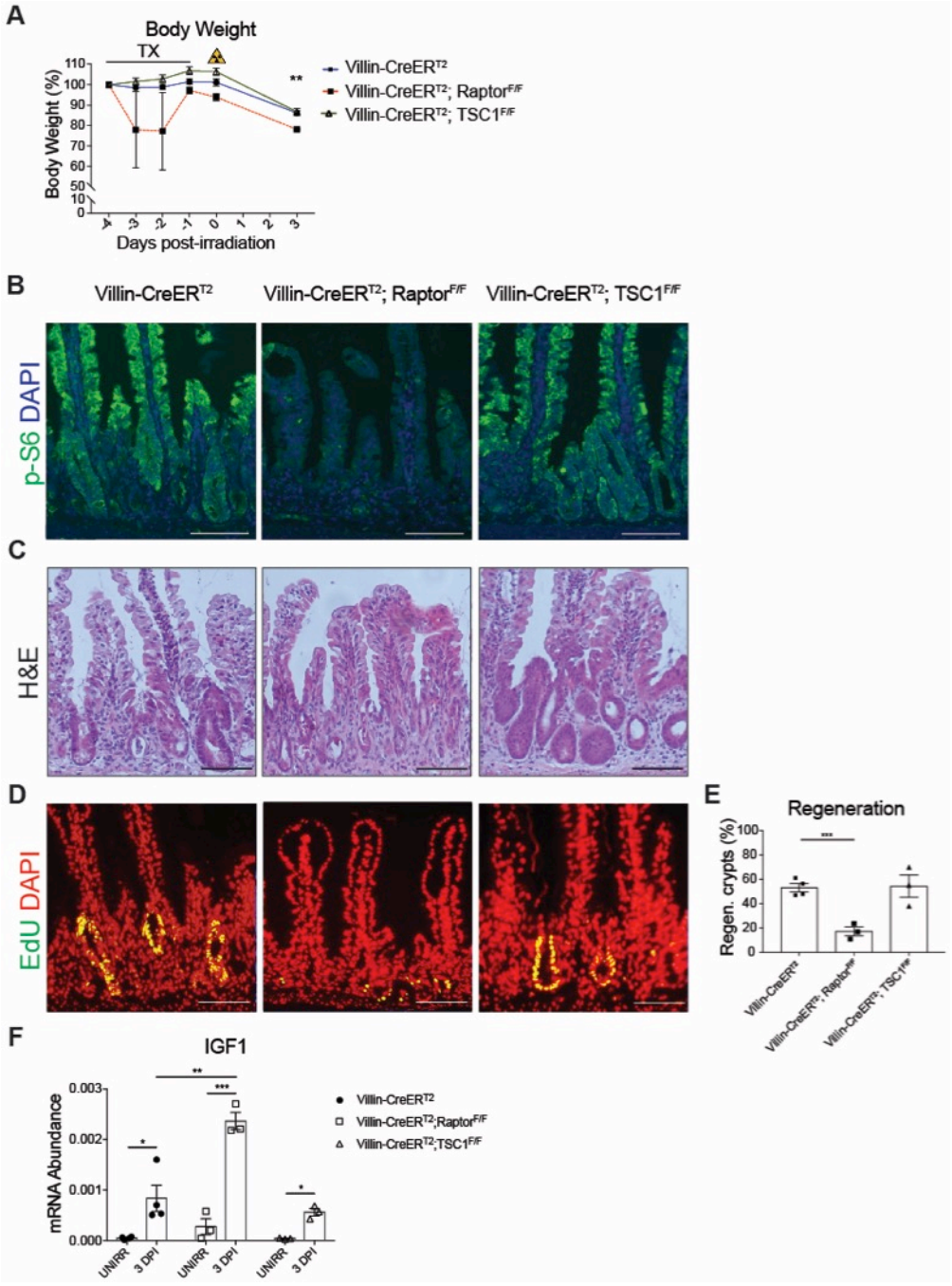

Figure 2.10 Genetic mTORC1 depletion leads to impaired intestinal regeneration.

(A-F) *Villin-CreER^{T2}*, *Villin-CreER^{T2};Raptor$^{F/F}$* and *Villin-CreER^{T2};Tsc1$^{F/F}$* mice were treated daily with TX over 4 days, irradiated 24 hours following the last TX injection and the intestine was analyzed 3 DPI. (A) Mouse body weight relative to weight at the initiation of the experiment (n=3-4 mice/group). (B) Genetic modulation of mTORC1 activity was confirmed by p-S6(S240/244) immunostaining. (C-E) Duodenal crypt regeneration was assessed by (C) H&E staining, and (D) EdU incorporation. (E) Crypt regeneration was measured (n=3-4 mice/group). (F) qPCR analysis of *Igf1* mRNA abundance in unirradiated and 3DPI normalized to *Hprt* (n=3-4 mice/group). Quantitative data are presented as mean +/- SEM (*p<0.05, **p<0.01, ***p<0.001 by Student's *t*-test). Scale bars = 100μm.

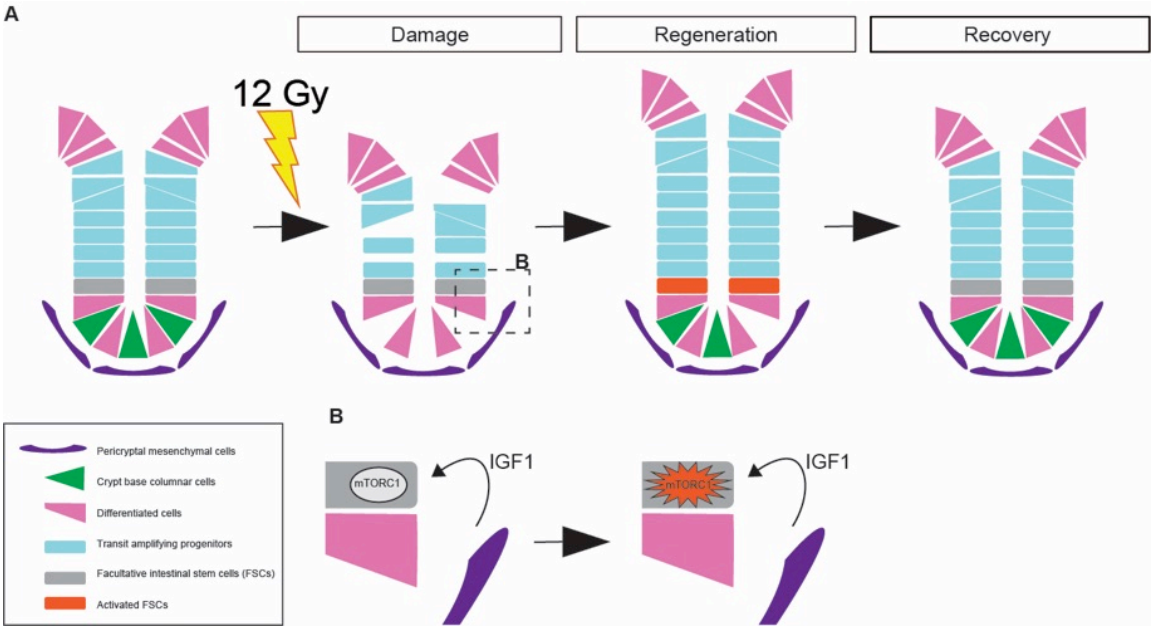

Figure 2.11 Pericryptal IGF1 secretion stimulates mTORC1-mediated FSC mobilization.

(A-B) Our model proposes that increased IGF1 secretion in response to irradiation results in mTORC1 activation in FSCs, and their mobilization to contribute to intestinal regeneration.

2.9 References

1. Barker, N. Adult intestinal stem cells: critical drivers of epithelial homeostasis and regeneration. *Nat. Rev. Mol. Cell Biol.* **15,** 19–33 (2014).

2. Takeda, N. *et al.* Interconversion between intestinal stem cell populations in distinct niches. *Science* **334,** 1420–4 (2011).

3. Sangiorgi, E. & Capecchi, M. R. Bmi1 is expressed in vivo in intestinal stem cells. *Nat. Genet.* **40,** 915–920 (2008).

4. Yan, K. S. *et al.* The intestinal stem cell markers Bmi1 and Lgr5 identify two functionally distinct populations. *Proc. Natl. Acad. Sci. U. S. A.* **109,** 466–71 (2012).

5. Montgomery, R. K. *et al.* Mouse telomerase reverse transcriptase (mTert) expression marks slowly cycling intestinal stem cells. *Proc. Natl. Acad. Sci. U. S. A.* **108,** 179–84 (2011).

6. van Es, J. H. *et al.* Dll1+ secretory progenitor cells revert to stem cells upon crypt damage. *Nat. Cell Biol.* **14,** 1099–104 (2012).

7. Tetteh, P. W. *et al.* Replacement of Lost Lgr5-Positive Stem Cells through Plasticity of Their Enterocyte-Lineage Daughters. *Cell Stem Cell* **18,** 203–213 (2016).

8. Yousefi, M., Li, L. & Lengner, C. J. Hierarchy and Plasticity in the Intestinal Stem Cell Compartment. *Trends Cell Biol.* **27,** 753–764 (2017).

9. Schmitt, M. *et al.* Paneth Cells Respond to Inflammation and Contribute to

Tissue Regeneration by Acquiring Stem-like Features through SCF/c-Kit Signaling. *Cell Rep.* **24,** 2312–2328.e7 (2018).

10. Sei, Y. *et al.* Mature enteroendocrine cells contribute to basal and pathological stem cell dynamics in the small intestine. *Am. J. Physiol. Liver Physiol.* **315,** G495–G510 (2018).

11. Roth, S. *et al.* Paneth Cells in Intestinal Homeostasis and Tissue Injury. *PLoS One* **7,** e38965 (2012).

12. Tian, H. *et al.* A reserve stem cell population in small intestine renders Lgr5-positive cells dispensable. *Nature* **478,** 255–9 (2011).

13. Montgomery, R. K. *et al.* Mouse telomerase reverse transcriptase (mTert) expression marks slowly cycling intestinal stem cells. *Proc. Natl. Acad. Sci. U. S. A.* **108,** 179–84 (2011).

14. Santos, A. J. M., Lo, Y.-H., Mah, A. T. & Kuo, C. J. The Intestinal Stem Cell Niche: Homeostasis and Adaptations. *Trends Cell Biol.* (2018). doi:10.1016/j.tcb.2018.08.001

15. Howarth, G. S., Xian, C. J. & Read, L. C. Insulin-like growth factor-I partially attenuates colonic damage in rats with experimental colitis induced by oral dextran sulphate sodium. *Scand. J. Gastroenterol.* **33,** 180–90 (1998).

16. Lemmey, A. B. *et al.* Treatment with IGF-I peptides improves function of the remnant gut following small bowel resection in rats. *Growth Factors* **10,** 243–52 (1994).

17. Gillingham, M. B., Dahly, E. M., Murali, S. G. & Ney, D. M. IGF-I treatment facilitates transition from parenteral to enteral nutrition in rats with short bowel syndrome. *Am. J. Physiol. Integr. Comp. Physiol.* **284,** R363–R371 (2003).

18. Qiu, W., Leibowitz, B., Zhang, L. & Yu, J. Growth factors protect intestinal stem cells from radiation-induced apoptosis by suppressing PUMA through the PI3K/AKT/p53 axis. *Oncogene* **29,** 1622–1632 (2010).

19. Van Landeghem, L. *et al.* IGF1 stimulates crypt expansion via differential activation of 2 intestinal stem cell populations. *FASEB J.* **29,** 2828–42 (2015).

20. Saxton, R. A. & Sabatini, D. M. mTOR Signaling in Growth, Metabolism, and Disease. *Cell* **168,** 960–976 (2017).

21. Yilmaz, Ö. H. *et al.* mTORC1 in the Paneth cell niche couples intestinal stem-cell function to calorie intake. *Nature* **486,** 490–495 (2012).

22. Kapuria, S., Karpac, J., Biteau, B., Hwangbo, D. & Jasper, H. Notch-Mediated Suppression of TSC2 Expression Regulates Cell Differentiation in the Drosophila Intestinal Stem Cell Lineage. *PLoS Genet.* **8,** e1003045 (2012).

23. Igarashi, M. & Guarente, L. mTORC1 and SIRT1 Cooperate to Foster Expansion of Gut Adult Stem Cells during Calorie Restriction. *Cell* **166,** 436–450 (2016).

24. Yousefi, M. *et al.* Calorie Restriction Governs Intestinal Epithelial Regeneration through Cell-Autonomous Regulation of mTORC1 in Reserve Stem Cells. *Stem cell reports* **10,** 703–711 (2018).

25. Sampson, Leesa L., Davis, Ashley K., Grogg, Matthew W., Zheng, Y. mTOR disruption causes intestinal epithelial cell defects and intestinal atrophy postinjury in mice. *The FASEB Journal* (2015). doi:10.1096/fj.15-278606

26. Richmond, C. A. *et al.* Dormant Intestinal Stem Cells Are Regulated by PTEN and Nutritional Status. *Cell Rep.* **13,** 2403–11 (2015).

27. Barron, L. *et al.* Intestinal Epithelial-Specific mTORC1 Activation Enhances Intestinal Adaptation After Small Bowel Resection. *Cell. Mol. Gastroenterol. Hepatol.* **3,** 231–244 (2017).

28. Rodgers, J. T. *et al.* mTORC1 controls the adaptive transition of quiescent stem cells from G0 to G(Alert). *Nature* **509,** 393–6 (2014).

29. el Marjou, F. *et al.* Tissue-specific and inducible Cre-mediated recombination in the gut epithelium. *Genesis* **39,** 186–93 (2004).

30. Sengupta, S., Peterson, T. R., Laplante, M., Oh, S. & Sabatini, D. M. mTORC1 controls fasting-induced ketogenesis and its modulation by ageing. *Nature* **468,** 1100–1104 (2010).

31. Peterson, T. R. *et al.* mTOR Complex 1 Regulates Lipin 1 Localization to Control the SREBP Pathway. *Cell* **146,** 408–420 (2011).

32. Kwiatkowski, D. J. *et al.* A mouse model of TSC1 reveals sex-dependent

lethality from liver hemangiomas, and up-regulation of p70S6 kinase activity in Tsc1 null cells. *Hum. Mol. Genet.* **11,** 525–34 (2002).

33. Soriano, P. Generalized lacZ expression with the ROSA26 Cre reporter strain. *Nat. Genet.* **21,** 70–71 (1999).

34. VanDussen, K. L. *et al.* Notch signaling modulates proliferation and differentiation of intestinal crypt base columnar stem cells. *Development* **139,** 488–97 (2012).

35. Cohn, S. M., Schloemann, S., Tessner, T., Seibert, K. & Stenson, W. F. *Prostaglandins Mediate Intestinal Crypt Survival after Radiation Crypt Stem Cell Survival in the Mouse Intestinal Epithelium Is Regulated by Prostaglandins Synthesized through Cyclooxygenase-1*. *J. Clin. Invest* **99,** (1997).

36. Lopez-Diaz, L. *et al.* Parietal cell hyperstimulation and autoimmune gastritis in cholera toxin transgenic mice. *Am. J. Physiol. Liver Physiol.* **290,** G970–G979 (2006).

37. Carulli, A. J. *et al.* Notch receptor regulation of intestinal stem cell homeostasis and crypt regeneration. *Dev. Biol.* **402,** 98–108 (2015).

38. Manning, B. D. & Toker, A. Leading Edge Review AKT/PKB Signaling: Navigating the Network. *Cell* **169,** 381–405 (2017).

39. Zhou, W., Rowitz, B. M. & Dailey, M. J. Insulin/IGF-1 enhances intestinal epithelial crypt proliferation through PI3K/Akt, and not ERK signaling in

obese humans. *Exp. Biol. Med.* **243,** 911–916 (2018).

40. Yan, K. S. *et al.* The intestinal stem cell markers Bmi1 and Lgr5 identify two functionally distinct populations. *Proc. Natl. Acad. Sci. U. S. A.* **109,** 466–71 (2012).

41. Bohin, N., Carlson, E. A. & Samuelson, L. C. Genome Toxicity and Impaired Stem Cell Function after Conditional Activation of CreERT2 in the Intestine. *Stem Cell Reports* **0,** (2018).

42. Li, N. *et al.* Single-cell analysis of proxy reporter allele-marked epithelial cells establishes intestinal stem cell hierarchy. *Stem cell reports* **3,** 876–91 (2014).

43. Winesett, D. E. *et al.* Regulation and localization of the insulin-like growth factor system in small bowel during altered nutrient status. *Am. J. Physiol. Liver Physiol.* **268,** G631–G640 (1995).

44. Ney, D. M. *et al.* Investigation of Insulin-Like Growth Factor (IGF)-I and Insulin Receptor Binding and Expression in Jejunum of Parenterally Fed Rats Treated with IGF-I or Growth Hormone [1]. *Endocrinology* **140,** 4850–4860 (1999).

45. Simmons, J. G., Pucilowska, J. B., Keku, T. O. & Lund, P. K. IGF-I and TGF-β1 have distinct effects on phenotype and proliferation of intestinal fibroblasts. *Am. J. Physiol. Liver Physiol.* **283,** G809–G818 (2002).

46. Simmons, J. G., Pucilowska, J. B. & Lund, P. K. Autocrine and paracrine

actions of intestinal fibroblast-derived insulin-like growth factors. *Am. J. Physiol. Liver Physiol.* **276,** G817–G827 (1999).

47. Pucilowska, J. B. *et al.* IGF-I and procollagen alpha1(I) are coexpressed in a subset of mesenchymal cells in active Crohn's disease. *Am. J. Physiol. Gastrointest. Liver Physiol.* **279,** G1307-22 (2000).

48. Lahar, N. *et al.* Intestinal subepithelial myofibroblasts support in vitro and in vivo growth of human small intestinal epithelium. *PLoS One* **6,** e26898 (2011).

49. Aoki, R. *et al.* Foxl1-expressing mesenchymal cells constitute the intestinal stem cell niche. *Cell. Mol. Gastroenterol. Hepatol.* **2,** 175–188 (2016).

50. Valenta, T. *et al.* Wnt Ligands Secreted by Subepithelial Mesenchymal Cells Are Essential for the Survival of Intestinal Stem Cells and Gut Homeostasis. *Cell Rep.* **15,** 911–918 (2016).

51. Shoshkes-Carmel, M. *et al.* Subepithelial telocytes are an important source of Wnts that supports intestinal crypts. *Nature* **557,** 242–246 (2018).

52. Fruchtman, S. *et al.* Suppressor of cytokine signaling-2 modulates the fibrogenic actions of GH and IGF-I in intestinal mesenchymal cells. *Am J Physiol Gastrointest Liver Physiol* **289,** 342–350 (2005).

53. Liu, J. P., Baker, J., Perkins, A. S., Robertson, E. J. & Efstratiadis, A. Mice carrying null mutations of the genes encoding insulin-like growth factor I (Igf-1) and type 1 IGF receptor (Igf1r). *Cell* **75,** 59–72 (1993).

54. Butler, A. A. & LeRoith, D. Minireview: Tissue-Specific *Versus* Generalized Gene Targeting of the *igf1* and *igf1r* Genes and Their Roles in Insulin-Like Growth Factor Physiology. *Endocrinology* **142,** 1685–1688 (2001).

55. Rowland, K. J. *et al.* Loss of Glucagon-Like Peptide-2–Induced Proliferation Following Intestinal Epithelial Insulin-Like Growth Factor-1–Receptor Deletion. *Gastroenterology* **141,** 2166–2175.e7 (2011).

56. Santoro, M. A. *et al.* Obesity and intestinal epithelial deletion of the insulin receptor, but not the IGF 1 receptor, affect radiation-induced apoptosis in colon. *Am. J. Physiol. Gastrointest. Liver Physiol.* **309,** G578-89 (2015).

57. Ussar, S. *et al.* Regulation of Glucose Uptake and Enteroendocrine Function by the Intestinal Epithelial Insulin Receptor. *Diabetes* **66,** 886–896 (2017).

58. Nelson, V. L. B., Jiang, Y.-P., Dickman, K. G., Ballou, L. M. & Lin, R. Z. Adipose tissue insulin resistance due to loss of PI3K p110α leads to decreased energy expenditure and obesity. *Am. J. Physiol. Endocrinol. Metab.* **306,** E1205-16 (2014).

59. Yilmaz, Ö. H. *et al.* mTORC1 in the Paneth cell niche couples intestinal stem-cell function to calorie intake. *Nature* **486,** 490–5 (2012).

2.10 Appendix

Appendix Table 2.1 Table showing the comparison between the normalized cycle threshold (Ct) values of 84 growth factor genes from UNIRR and 48 HPI samples.

								Mock Irradiated			48 Hours			4 Days			6 Days		
Gene Bank	Symbol	Description	logFC	AveExpr	t	P.Value	adj.P.Val	PAM M041 Plate 1	PAM M041 Plate 2	PAM M041 Plate 3	PAM M041 Plate 1	PAM M041 Plate 2	PAM M041 Plate 3	PAM M041 Plate 1	PAM M041 Plate 2	PAM M041 Plate 3	PAM M041 Plate 1	PAM M041 Plate 2	PAM M041 Plate 3
NM_011313	S100a6	S100 calcium binding protein A6 (calcyclin)	-2.856300133	1.0706658667	-12.06377148	2.15E-07	1.68E-05	3.0630376	2.9841846	3.0664342	-0.148 8696	-0.111 2968	0.582 3288	-0.799 4798	-0.300 2294	-0.469 2444	1.4843786	1.8758174	1.3983356
NM_007950	Ereg	Epiregulin	-3.654474133	4.9852258667	-9.524896492	2.02E-06	7.89E-05	7.8766046	6.4867596	6.9011292	3.3549354	3.2953638	3.650 7718	3.0734792	3.842 0966	3.250 8386	5.6249286	6.6077654	5.858 0376
NM_007559	Bmp8b	Bone morphogenetic protein 8b	-2.797479133	9.7595873667	-8.582421077	5.29E-06	0.000137505	10.624374 6	10.326599 6	11.562270 2	8.137 6504	7.746 0718	8.237 0848	8.392 4532	8.693 6286	8.501 2586	12.073758 6	11.364284 4	11.455613 6
NM_010512	Igf1	Insulin-like growth factor 1	-1.916 0684	5.1695125267	-7.359306956	3.65E-05	0.000712242	NA	6.2589006	6.6587702	4.344 6264	4.411 2368	4.872 4378	4.162 8152	4.365 7296	4.649 2636	5.5104536	5.8429084	5.787 4956

NM_19819	Ntf5	Neurotrophin 5	-2.492264467	12.3053502	-6.35908881	7.32E-05	0.00114669	14.414845	13.794240	12.839537	10.930827	11.116682	11.524319	10.876162	11.573232	10.957042	13.603085	13.213799	12.820426
NM_007557	Bmp7	Bone morphogenetic protein 7	-1.182783133	7.30466886	-6.04066053	0.00011969	0.00145595	7.9223216	7.3297156	7.7227622	6.4271424	6.5605168	6.4387908	6.7999652	7.0713926	7.1307686	8.0647806	8.0267554	8.1611146
NM_008176	Cxcl1	Chemokine (C-X-C motif) ligand 1	-3.248444133	10.7493843	-5.05745479	0.00045433	0.00506255	13.394085	12.151445	12.047755	8.5398404	8.9788668	10.329146	10.209771	10.783438	9.2860736	11.046809	12.118943	10.106335
NM_008006	Fgf2	Fibroblast growth factor 2	-1.705751133	8.78776095	-4.87003498	0.00060270	0.00587640	10.188341	9.2035826	9.1711342	7.4714824	7.5737088	8.4006138	8.0597152	8.4067146	8.3737276	9.6422596	9.1029214	9.8589296
NM_010427	Hgf	Hepatocyte growth factor	-1.410369067	7.52304334	-4.85745 69255	0.00082490	0.00714921	NA	7.6953736	8.4841492	6.5159764	6.7879898	6.7342108	6.6155292	7.1318486	6.6846086	8.7107716	8.9223204	8.4706986
NM_008380	Inhba	Inhibin beta-A	-2.147391133	9.12383295	-4.40265 0467	0.00124628	0.00883732	10.521185	8.7307816	11.066744	7.7877774	7.8551908	8.2335698	9.0241422	9.0577156	8.6557806	9.2995316	9.4440984	9.8094776
NM_008381	Inhbb	Inhibin beta-B	-1.731224133	9.22074761 7	-4.43974 0637	0.00117515 6	0.00883732 3	10.565219 6	9.9916646	9.9804662	8.0176224	8.2352518	9.0908038	8.8402092	9.5694896	8.1889186	9.7358436	9.1278434	9.3056386
NM_011156	Tdgf1	Teratocarcinoma-derived growth factor 1	-5.63812781 4	16.7127814	-4.93195 1327	0.00111916	0.00920.30 8368	19.861007	NA	14.523699	14.887753	13.928123	18.461207	14.443518	NA	NA	18.105168	15.896185	

2			62433	4	42123	1	6	6	6		4	8	8	2	6			4	6
NM_009368	Tgfb3	Transforming growth factor, beta 3	-0.872834837233	8.32737178	-4.278272874	0.00151986	0.00911916	9.0148256	8.5242746	8.6612152	7.7236964	7.6856888	8.1724258	8.1634182	8.2405996	8.4221386	8.3942066	8.4942254	8.4317466
NM_009711	Artn	Artemin	-1.079756828395	9.52028395	-4.208182905	0.00170125	0.00947844	10.263923	9.609026	9.921242	8.874214	8.840558	8.842028	9.405852	9.403476	9.864976	9.274256	9.912904	10.025630
NM_008005	Fgf18	Fibroblast growth factor 18	-1.841283467	12.1976591	-4.094907674	0.0020441	0.01062931	13.340165	12.853940	12.093350	10.553797	11.321438	10.888369	12.331584	12.088024	12.271924	13.192995	11.846158	13.590159
NM_010200	Fgf13	Fibroblast growth factor 13	-1.023777467	8.5928140333	-3.897998002	0.00282353	0.01295504	8.8751626	8.5336686	8.8122092	7.5250804	7.6431268	7.9815008	8.7823912	8.3745446	9.1205086	9.0395006	8.8529884	9.5730866
NM_011697	Vegfb	Vascular endothelial growth factor B	0.776485533	7.4733892	3.904508557	0.00279332	0.01295504	7.3712026	7.5055296	6.9793652	8.1422794	8.0513108	7.9919638	7.1758832	6.9581246	7.1210306	7.2507166	7.4441144	7.6891496
NM_007540	Bdnf	Brain derived neurotrophic factor	-2.250070467	11.8826039	-3.811830928	0.00325709	0.01337121	12.615310	13.582813	13.131354	9.6960704	10.722559	12.160636	9.9437452	11.644499	11.057780	12.686931	12.584298	12.765246
NM_008361	Il1b	Interleukin 1 beta	-1.928392133	8.0152477	-3.837996236	0.00311854	0.01337121	9.1403526	7.2444306	7.9650722	6.1277164	5.7024638	6.7344988	8.3937792	8.7329756	7.8666436	10.152923 6	8.9653674	9.1567486
NM_0	Fgf	Fibroblast growth factor	-	15.90	-	0.004	0.017	18.83	15.20	18.76	14.30	14.29	14.00	13.52	14.63	15.30	16.94	16.35	18.66

08003	15	15	3.399312133	42221 2	3.635582164	37388 8	05816 2	2725 6	8133 6	8366 2	7159 4	5983 8	8145 8	7632 2	9672 6	2190 6	0478 6	7240 4	2936 6
NM_008350	Il11	Interleukin 11	-1.924293 8	11.42749745	-3.541601097	0.00512542 1	0.01903727 8	13.481435 6	12.046293 6	11.697871 2	10.845372 4	9.6356288	10.971717 8	9.6982872	11.174472 6	10.347640 6	12.819888 6	12.229299 4	12.182061 6
NM_023304	Fgf22	Fibroblast growth factor 22	-1.203174467	11.97653078	-3.366450296	0.00690315 3	0.02438897 1	12.724231 6	12.812637 6	11.682204 2	10.706513 4	11.784683 8	11.118352 8	12.681243 2	12.166174 6	12.471473 6	12.063241 6	11.578338 4	11.929274 6
NM_008007	Fgf3	Fibroblast growth factor 3	-1.535728 8	13.8697248	-3.695777515	0.00719162	0.02438897 1	14.093090 6	15.339836 6	14.458742 2	12.767975 4	13.107983 8	13.408523 8	NA	13.672322 6	14.702512 6	13.276535 6	NA	NA
NM_007778	Csf1	Colony stimulating factor 1 (macrophage)	-0.896353467	7.64004686 7	-3.095373286	0.01099718 6	0.03574085 3	8.3771456	7.2941266	7.5068442	6.5301614	6.7558028	7.2030918	8.2594312	7.9860486	7.9055856	7.9031236	7.9736514	7.9855496
NM_173404	Bmp3	Bone morphogenetic protein 3	0.990808942	6.96581628 3	3.026773739	0.01238140 8	0.03576851 1	6.9570366	6.1405106	7.2540622	7.6435534	7.6990748	7.9816638	6.0328112	7.0516706	6.4044526	6.8522316	6.6132294	6.9594986
NM_177099	Lefty2	Left-right determination factor 2	-3.443298 6	17.96781106	-3.759399992	0.01193627 1	0.03576851 1	NA	18.645538 6	17.570948 2	NA	14.664944 8	NA	18.597327 2	16.636292 6	NA	NA	19.582135 4	20.077490 6
NM_009367	Tgfb2	Transforming growth factor, beta 2	-0.847642133	8.8581462	-3.066900057	0.01155154 3	0.03576851 1	9.2531686	8.7206876	8.9670022	7.9029814	8.3318368	8.1631138	8.9693952	8.7022676	9.2912276	9.8198056	8.8824324	9.2938356

NM_008501	Lif	Leukemia inhibitory factor	-0.647560867	8.660766617	-2.856112886	0.016642419	0.046361025	9.0229606	8.3931566	8.8827652	8.2510534	7.8959628	8.2091838	9.0407282	8.5653426	8.9763926	9.0072956	8.9438284	8.7405296
NM_008827	Pgf	Placental growth factor	-1.024631467	9.671740617	-2.798181457	0.018403127	0.049806495	10.576232	9.6847136	9.9495492	9.0016854	8.9742118	9.1607038	9.4115592	9.6886466	9.5648726	10.832275 6	9.9708834	9.2455536
NM_013609	Ngf	Nerve growth factor	-1.077093567	12.25852698	-2.604529305	0.027860182	0.072436474	NA	12.817756 6	13.081069 2	11.482352 4	11.593008 8	12.541596 8	12.388837 2	11.832556 6	12.061114 6	12.101785 6	11.916675 4	13.027043 6
NM_007554	Bmp4	Bone morphogenetic protein 4	-0.502244133	5.530883367	-2.434641924	0.034571663	0.086986765	5.6185626	5.2013416	5.4223182	4.8169994	4.8395038	5.0789868	6.2359032	5.6678986	5.7241876	5.8868996	5.9036954	5.9743036
NM_008008	Fgf7	Fibroblast growth factor 7	-0.755276467	8.584481283	-2.406915063	0.036267728	0.088402587	9.0568086	7.9820726	8.3035972	7.9832504	7.6949148	7.3984838	9.0743702	9.2070506	9.2121256	9.1073166	8.5546434	9.4391416
NM_010216	Figf	C-fos induced growth factor	-0.702217467	8.766616455	-2.309266491	0.042912965	0.101430645	9.4802056	8.4658226	9.1185672	8.2767854	8.2786518	8.4025058	8.1823392	8.2000076	8.9347606	8.9482096	9.5535864	9.3579556
NM_007556	Bmp6	Bone morphogenetic protein 6	-0.666260133	8.844636783	-2.197131107	0.052004475	0.119304384	9.3180386	8.3203026	8.9154822	8.2285124	8.0995148	8.2270158	9.0245412	9.1163086	8.9521426	8.8897776	9.1374064	9.9065986
NM_008001	Fgf10	Fibroblast growth factor 10	-1.044568278	9.978	-2.160039920	0.055	0.123	11.257404	9.5859006	9.8687822	8.8999644	9.0210428	9.6575158	8.8978812	10.246737	9.8544136	10.725312	10.434852	11.294385

2			21467	3	53796	6	8	6							6		6	4	6
NM_0 0975 5	Bm p1	Bone morphogenetic protein 1	-0.5712648	6.876 9237	-2.1344 69369	0.057 86428 7	0.125 37262 3	7.060 3256	6.323 6306	7.082 9282	6.412 8564	6.467 7518	5.872 4818	7.225 9722	7.202 3166	7.544 9766	7.309 6286	6.844 6454	7.175 5706
NM_0 5300 9	Zfp 91	Zinc finger protein 91	0.3820 752	2.985 7062	2.0696 06434	0.064 59112	0.136 16506 4	3.198 2956	2.673 8356	2.985 2802	3.425 2724	3.391 9728	3.186 3918	2.692 4792	2.718 2496	2.690 5246	2.879 3976	3.085 9634	2.900 8116
NM_0 1011 3	Egf	Epidermal growth factor	-0.7274 21467	10.77 79316 2	-2.0070 3274	0.071 77805 9	0.137 08297 7	11.14 4220 6	10.81 3688 6	11.22 5007 2	10.24 6808 4	9.751 2268	11.00 2616 8	11.15 3788 2	10.18 7605 6	11.12 5705 6	11.15 7771 6	10.53 9523 4	10.98 7216 6
NM_0 1051 4	Igf2	Insulin-like growth factor 2	-0.4219 33233	10.18 49579 8	-2.0519 64277	0.069 47420 5	0.137 08297 7	NA	9.774 4106	9.880 0972	9.398 3774	9.548 4328	9.269 1518	10.35 6511 2	10.79 3238 6	10.64 3441 6	10.77 9822 6	10.77 4430 4	10.81 6623 6
NM_0 1055 4	Il1a	Interleukin 1 alpha	-1.0938 37467	8.893 55736 7	-2.0047 29826	0.072 05643 6	0.137 08297 7	9.356 3216	9.169 7366	9.061 6982	9.334 4714	6.911 8398	8.059 9328	8.108 0942	8.930 2776	8.933 6586	9.206 1936	9.290 5634	10.35 9900 6
NM_0 3116 8	Il6	Interleukin 6	-1.4175 554	11.67 69715 3	-2.0501 39571	0.069 68167 3	0.137 08297 7	NA	12.26 0450 6	12.07 2194 2	11.47 1913 4	10.15 2138 8	10.62 2248 8	10.80 8245 2	11.52 5604 6	10.57 9854 6	13.68 4095 6	13.83 0885 4	11.43 9055 6
NM_0 0926 3	Sp p1	Secreted phosphoprotein 1	-1.8386 458	7.855 4667	-1.9863 54432	0.074 31431	0.138 01229	9.968 0006	8.465 7956	9.125 8262	6.427 4564	6.627 1578	8.989 0708	5.630 2102	6.973 1796	7.335 0926	7.671 9986	6.855 0944	10.19 6717 6
NM_0	Tgf	Transforming growth	-	5.655	-	0.079	0.144	6.135	5.232	5.302	4.926	5.068	5.249	5.580	5.768	5.679	6.401	6.218	6.298

11577	b1	factor, beta 1	0.4749818	222283	1.945493249	57516	345639	3986	2026	0142	7414	0148	9138	5612	7156	9486	9866	2094	9606
NM_008360	Il18	Interleukin 18	0.4745 45533	1.433 462283	1.7266 12455	0.114 132454	0.202 325714	1.335 0986	0.584 1806	1.094 0462	1.545 8234	1.834 9368	1.056 2018	2.493 8802	1.925 7836	2.154 3916	0.931 5356	0.971 1224	1.274 5466
NM_009971	Csf3	Colony stimulating factor 3 (granulocyte)	-2.4318 558	13.82 481198	-1.7103 32265	0.120 376205	0.208 652089	16.37 0785 6	14.79 6825 6	13.59 5820 2	12.01 0582 4	12.19 5435 8	13.26 1845 8	12.50 7876 2	15.59 3798 6	12.86 7518 6	NA	17.37 8545 4	11.49 3897 6
NM_010094	Lefty1	Left right determination factor 1	0.3869 38867	8.523 2862	1.5535 10902	0.150 542284	0.255 267351	8.541 8916	8.126 2766	7.889 6622	8.748 9894	8.589 8948	8.379 7628	8.409 0092	8.223 7096	8.386 7696	9.456 6356	8.730 0824	8.796 7506
NM_007553	Bmp2	Bone morphogenetic protein 2	-0.4586 37133	6.189 48745	-1.5010 63428	0.163 433135	0.271 229458	5.553 8156	5.597 1856	6.564 0362	5.344 1494	5.345 6048	5.649 3718	6.209 6512	6.439 8186	6.167 9706	7.524 7016	6.687 4354	7.190 1086
NM_008808	Pdgfa	Platelet derived growth factor, alpha	-0.4179 13133	6.653 06195	-1.4318 1896	0.181 909254	0.295 602538	7.191 1226	6.319 0366	6.352 4622	6.171 4654	6.297 3168	6.140 0998	7.136 6162	7.061 6176	7.472 6136	6.852 3856	6.057 3784	6.784 6286
NM_009362	Tff1	Trefoil factor 1	-1.7639 448	10.93 600145	-1.3779 80704	0.197 481016	0.302 029786	11.30 6482 6	12.32 4024 6	15.40 7466 2	11.08 4423 4	11.52 2701 8	11.13 9013 8	7.250 5392	9.023 0736	8.136 3506	9.215 1176	14.32 3055 4	10.49 9768 6
NM_031199	Tgfa	Transforming growth factor alpha	-0.2318 69133	7.220 880617	-1.3834 01853	0.195 863676	0.302 029786	7.494 1846	7.369 7266	7.451 1782	7.063 2814	7.362 4548	7.193 7458	7.175 2852	7.081 2556	7.031 7686	7.200 1316	6.975 8984	7.251 6566

NM_009505	Vegfa	Vascular endothelial growth factor A	-0.313914467	3.8389461137	-1.392913708	0.19305291	0.30202978	3.9847886	3.3746376	3.7957642	3.2017734	3.3136438	3.6980298	4.8134282	4.4538636	4.5479126	3.5178586	3.5448954	3.8207576
NM_010272	Gdf11	Growth differentiation factor 11	0.386884933	9.0779865287	1.270368584	0.23489428	0.35234914 2	NA	8.6629276	8.5397232	8.7409024	9.0295648	9.1941638	8.8979592	8.8209826	9.1372376	9.0185216	9.8332594	9.9826096
NM_007555	Bmp5	Bone morphogenetic protein 5	-0.281315467	5.8139917	-1.184451902	0.26291307	0.37285853 6	5.8051126	5.0782476	5.6098372	5.3557534	5.2910168	5.0024808	6.2793652	6.2776876	6.2675416	6.5349666	5.9312304	6.3346606
NM_010197	Fgf1	Fibroblast growth factor 1	-0.387265133	8.0648961177	-1.190776959	0.26052786 9	0.37285853 6	8.6988466	7.4211386	8.2531592	7.3763644	7.8953218	7.9396628	7.9792952	7.9601316	8.3113806	8.0887406	8.1909234	8.6637886
NM_010275	Gdnf	Glial cell line derived neurotrophic factor	-0.560932133	9.8568922	-1.198075	0.25780371 6	0.37285853 6	10.999585 6	9.0196806	9.3310132	9.1154124	9.5006268	9.0514438	10.2032612	9.6690566	9.5915506	10.796632 6	10.062335 4	10.942107 6
NM_021704	Cxcl12	Chemokine (C-X-C motif) ligand 12	-0.245858019	5.6548679822	-1.142644924	0.28182870 2	0.39254712	NA	5.4173466	5.9094592	5.4118524	5.4238348	5.4171158	5.4864912	5.7919026	5.5578886	5.8385386	5.9292004	6.0199176
NM_008109	Gdf5	Growth differentiation factor 5	-0.706492 8	14.506962555	-1.318606439	0.30442791 9	0.41658557 4	NA	14.343345 6	NA	NA	13.636852 8	NA	14.541388 2	NA	NA	NA	NA	15.506263 6
NM_001020	Fgf4	Fibroblast growth factor 4	-0.992284667	13.15	-1.066613225	0.31310889	0.42115	15.758705	12.083528	11.984543	12.245068	12.525683	12.079238	14.699778	13.134535	12.923776	13.167399	14.140875	NA

2			62133	1	01688	1		6	6	2	4	8	8	2	6	6	6	4	
NM_0 1078 4	Md k	Midkine	-0.2771 218	7.141 73445	-1.0396 85235	0.322 33680 3	0.426 14018	7.299 3646	6.712 1356	7.391 8062	7.120 8794	6.791 8078	6.659 2538	7.093 7162	7.206 5206	7.312 4536	7.461 8416	6.908 7254	7.742 3086
NM_0 1020 5	Fgf 8	Fibroblast growth factor 8	-0.6770 95133	15.13 67816 2	-1.0116 53614	0.334 93724 2	0.435 41841 4	14.45 1362 6	14.02 7545 6	16.56 2304 2	14.11 7229 4	14.14 5816 8	14.74 6880 8	14.59 3020 2	16.22 5336 6	15.96 2815 6	14.88 2685 6	16.36 4455 4	15.56 1926 6
NM_0 1361 1	No dal	Nodal	-0.4304 644	13.95 67268 9	-0.7703 77969	0.465 35872 3	0.595 04885 9	NA	15.02 3296 6	13.49 1870 2	14.42 1261 4	13.56 5079 8	13.49 5015 8	NA	13.23 2527 6	14.37 2158 6	13.85 4991 6	14.15 4340 4	NA
NM_0 0996 9	Csf 2	Colony stimulating factor 2	-0.3278 36133	11.28 33725 3	-0.7208 69648	0.487 06967 3	0.603 69287 4	11.09 4751 6	9.892 2346	11.62 1909 2	10.75 9304 4	10.47 1894 8	10.39 4187 8	11.85 8039 2	12.26 3796 6	13.14 4311 6	11.77 4685 6	10.98 4679 4	11.14 0675 6
NM_0 1020 3	Fgf 5	Fibroblast growth factor 5	-0.9662 417	15.40 04133 8	-0.7310 99527	0.487 59809 1	0.603 69287 4	15.43 1327 6	18.85 0864 6	13.64 1592 2	14.42 1067 4	15.59 5638 8	NA	15.56 3651 2	15.53 7779 6	NA	15.11 0808 6	14.45 0990 4	NA
NM_0 0755 8	Bm p8a	Bone morphogenetic protein 8a	-0.1614 51467	7.019 42028 3	-0.6486 77419	0.530 77926 8	0.643 98441	6.450 8076	6.082 5956	6.875 0462	6.258 9254	6.407 2528	6.257 9168	8.027 2492	7.541 7696	8.073 5886	7.679 8226	7.180 2404	7.397 8286
NM_0 0874 2	Ntf 3	Neurotrophin 3	-0.2027 40467	8.184 05636 7	-0.6392 48794	0.536 65367 5	0.643 98441	8.067 5716	7.157 3656	7.933 6382	7.563 3794	7.402 4378	7.584 5368	9.578 1922	8.574 8416	8.870 6166	8.644 2026	8.137 9654	8.693 9286

NM_0 0837 1	Il7	Interleukin 7	0.1403 27433	8.091 0868	0.5760 41435	0.578 29773 6	0.683 44277 8	NA	8.338 8656	7.909 4442	8.224 3494	8.364 1568	8.204 9408	8.052 8512	7.979 8646	7.962 9436	8.230 8096	7.608 0954	8.125 6336
NM_0 1940 0	Ra bep 1	Rabaptin, RAB GTPase binding effector protein 1	0.0930 39533	5.600 5022	0.4830 77241	0.639 17068 6	0.744 10915 6	5.496 0156	5.174 1256	5.767 8192	5.433 5124	5.731 4028	5.552 1638	5.573 2922	5.624 3156	5.656 3066	5.809 8056	5.618 8614	5.768 4056
NM_0 0744 5	Am h	Anti-Mullerian hormone	- 0.4063 938	17.11 16113 7	- 0.4417 37054	0.667 83286	0.750 73156 5	15.58 1298 6	18.21 6710 6	19.06 4509 2	18.55 2323 4	17.19 2196 8	15.89 8816 8	15.39 0675 2	17.37 7356 6	16.17 2028 6	17.43 8071 6	16.69 7015 4	17.75 8333 6
NM_0 0800 4	Fgf 17	Fibroblast growth factor 17	- 0.3828 441	16.06 20087 7	- 0.4652 88617	0.664 45520 7	0.750 73156 5	NA	NA	16.00 6792 2	14.88 3252 4	16.36 4643 8	NA	16.77 6855 2	NA	NA	15.66 7678 6	16.67 2830 4	NA
NM_0 0835 1	Il12 a	Interleukin 12A	0.4620 65533	13.99 84703 7	0.4333 28814	0.673 73345 6	0.750 73156 5	14.10 1105 6	11.82 1930 6	12.28 0215 2	13.17 4141 4	12.34 5932 8	14.06 9373 8	13.92 3728 2	18.35 9099 6	14.11 5188 6	14.77 3385 6	14.20 6609 4	14.81 0933 6
NM_0 1019 8	Fgf 11	Fibroblast growth factor 11	0.1015 44867	8.684 42853 3	0.3097 55191	0.762 93918 7	0.838 15854 3	8.357 8896	7.928 1556	8.022 5572	7.834 9984	8.297 2308	8.481 0078	10.05 9811 2	9.247 6296	9.308 9466	8.816 7476	8.386 5424	9.471 6256
NM_0 0950 6	Ve gfc	Vascular endothelial growth factor C	- 0.0512 79467	9.746 12311 7	- 0.2357 66265	0.818 24783 4	0.886 43515 4	9.703 5556	9.396 3526	9.564 7672	9.397 1664	9.530 4628	9.583 2078	10.33 5368 2	9.648 1926	9.965 3606	9.840 7256	9.788 3484	10.19 9969 6
NM_0 2128	Il4	Interleukin 4	- 0.1704	12.05 33028	- 0.2176	0.832 44792	0.889 4649	NA	11.40 4266	11.43 5452	11.41 5841	12.12 3139	10.20 9253	12.24 3512	11.55 6168	13.34 1214	12.49 0359	14.34 2415	12.02 4706

3			47733		0744				6	2	4	8	8	2	6	6	6	4	6
NM_01056 4	Inha	Inhibin alpha	-0.0570694	11.0714258 9	-0.1391 70392	0.892 29121	0.934 919022	NA	10.72 8912 6	10.41 5612 2	9.818 5994	10.51 5616 8	11.21 1362 8	11.49 9491 2	11.21 0779 6	11.48 6402 6	12.18 8725 6	11.42 4018 4	11.28 6163 6
NM_01359 8	Kitl	Kit ligand	0.0586592	3.753 494867	0.1301 50508	0.898 960598	0.934 919022	3.791 1376	3.288 3876	3.680 8272	3.478 8894	3.608 1468	3.849 2938	2.493 1232	4.188 8146	4.310 4306	4.284 0666	3.540 5324	4.528 2886
NM_01351 8	Fgf9	Fibroblast growth factor 9	0.0268 22867	11.11 44902	0.0982 84028	0.923 598046	0.935 592826	10.43 3576 6	10.52 1978 6	10.48 3697 2	10.72 4554 4	10.70 3882 8	10.09 1283 8	12.81 3437 2	12.20 5771 6	12.46 4879 6	11.05 4656 6	10.51 1710 4	11.36 4453 6
NM_14574 1	Gdf10	Growth differentiation factor 10	0.0848 592	12.08 812053	0.1054 27995	0.918 066384	0.935 592826	13.09 3639 6	10.62 5335 6	10.82 0174 2	11.41 5884 4	12.19 0293 8	11.18 7548 8	11.46 6424 2	13.27 1632 6	14.58 4130 6	11.70 1453 6	12.63 0769 4	12.07 0159 6
NM_01020 1	Fgf14	Fibroblast growth factor 14	-0.0185 60467	9.910 584867	-0.0662 2786	0.948 467583	0.948 467583	10.61 7950 6	10.17 1701 6	10.41 4168 2	10.09 9863 4	11.05 4268 8	9.994 0068	8.972 3922	9.302 1976	9.202 8116	9.527 7386	9.765 4754	9.804 4436
NM_00975 6	Bmp10	Bone morphogenetic protein 10	NA	14.33 55976	NA	NA	NA	NA	NA	NA	NA	NA	14.21 54598	NA	NA	NA	NA	14.45 57354	NA
NM_01020 4	Fgf6	Fibroblast growth factor 6	NA	17.35 00847	NA	NA	NA	NA	NA	NA	NA	NA	19.97 00298	NA	NA	NA	NA	NA	14.73 01396

NM_008366	Il2	Interleukin 2	NA	14.6125653	NA	NA	NA	NA	NA	14.433942	NA	13.597968	13.724148	14.910197	15.773966	15.235246	NA	NA	NA
NM_010556	Il3	Interleukin 3	NA	14.3433715 2	NA	NA	NA	NA	NA	14.523127 2	15.194874 4	14.702956 8	14.536383 8	NA	NA	NA	NA	12.759515 4	NA
NM_008493	Lep	Leptin	NA	19.7642197	NA	NA	NA	NA	NA	NA	NA	19.096516 8	NA	NA	20.431922 6	NA	NA	NA	NA
NM_010834	Mstn	Myostatin	NA	15.6276996	NA	NA	NA	NA	16.311700 6	NA	NA	NA	NA	NA	NA	NA	NA	NA	14.943698 6

Appendix Table 2.2 Table showing the comparison between the normalized cycle threshold (Ct) values of 84 growth factor genes from UNIRR and 4 DPI samples.

								Mock Irradiated			48 Hours			4 Days			6 Days		
Gene Bank	Symbol	Description	logFC	AveExpr	t	P.Value	adj.P.Val	PAM M041 Plate 1	PAM M041 Plate 2	PAM M041 Plate 3	PAM M041 Plate 1	PAM M041 Plate 2	PAM M041 Plate 3	PAM M041 Plate 1	PAM M041 Plate 2	PAM M041 Plate 3	PAM M041 Plate 1	PAM M041 Plate 2	PAM M041 Plate 3
NM_011313	S100a6	S100 calcium binding protein A6 (calcyclin)	-3.560877	1.070665867	-15.03956865	2.50E-08	1.95E-06	3.063 0376	2.984 1846	3.066 4342	-0.148 8696	0.111 2968	0.582 3288	-0.799 4798	-0.300 2294	-0.469 2444	1.484 3786	1.875 8174	1.398 3356
NM_007950	Ereg	Epiregulin	-3.699359667	4.985225867	-9.641852653	1.81E-06	7.05E-05	7.876 6046	6.486 7596	6.901 1292	3.354 9354	3.295 3638	3.650 7718	3.073 4792	3.842 0966	3.250 8386	5.624 9286	6.607 7654	5.858 0376
NM_013518	Fgf9	Fibroblast growth factor 9	2.014945333	11.11044902	7.3831 38667	2.03E-05	0.000396755	10.43 3576 6	10.52 1978 6	10.48 3697 2	10.72 4554 4	10.70 3882 8	10.09 1283 8	12.81 3437 2	12.20 5771 6	12.46 4879 6	11.05 4656 6	10.51 1710 4	11.36 4453 6
NM_010512	Igf1	Insulin-like growth factor 1	-2.066232651	5.1697	-7.936063215	1.98E-05	0.000396755	NA	6.258 9006	6.658 7702	4.344 6264	4.411 2368	4.872 4378	4.162 8152	4.365 7296	4.649 2636	5.510 4536	5.842 9084	5.787 4956
NM_007559	Bmp8b	Bone morphogenetic protein 8b	-2.308634667	9.759587367	-7.082689049	2.92E-05	0.000455986	10.62 4374 6	10.32 6599 6	11.56 2270 2	8.137 6504	7.746 0718	8.237 0848	8.392 4532	8.693 6286	8.501 2586	12.07 3758 6	11.36 4284 4	11.45 5613 6

NM_19819	Ntf5	Neurotrophin 5	-2.547395333	12.3053502	-6.4997 56898	6.09E-05	0.000791702	14.414845 6	13.794240 6	12.839537 2	10.930827 4	11.116682 8	11.524319 8	10.876162 2	11.573232 6	10.957042 6	13.603085 6	13.213799 4	12.820426 6
NM_007558	Bmp8a	Bone morphogenetic protein 8a	1.411386	7.0194202833	5.6706 46706	0.000186652	0.002079834	6.4508076	6.0825956	6.8750462	6.2589254	6.4072528	6.2579168	8.0272492	7.5417696	8.0735886	7.6798226	7.1802404	7.3978286
NM_010198	Fgf11	Fibroblast growth factor 11	1.435928333	8.6842853 3	4.3801 94393	0.001291551	0.011115048	8.3578896	7.9281556	8.0225572	7.8349984	8.2972308	8.4810078	10.059811 2	9.2476296	9.3089466	8.8167476	8.3865424	9.4716256
NM_010201	Fgf14	Fibroblast growth factor 14	-1.242139667	9.9105848667	-4.4322 29742	0.001189207	0.011115048	10.617950 6	10.171701 6	10.414168 2	10.099863 4	11.054268 8	9.9940068	8.9723922	9.3021976	9.2028116	9.5277386	9.7654754	9.8044436
NM_008360	Il18	Interleukin 18	1.186911	1.4334622833	4.3185 18341	0.001425006	0.011115048	1.3350986	0.5841806	1.0940462	1.5458234	1.8349368	1.0562018	2.4938802	1.9257836	2.1543916	0.9315356	0.9711224	1.2745466
NM_010427	Hgf	Hepatocyte growth factor	-1.279099267	7.5230433455	-4.4053 6134	0.001587992	0.011260308	NA	7.6953736	8.4841492	6.5159764	6.7879898	6.7342108	6.6155292	7.1318486	6.6846086	8.7107716	8.9223204	8.4706986
NM_008742	Ntf3	Neurotrophin 3	1.288358333	8.1840563667	4.0622 45317	0.002155889	0.014013281	8.0675716	7.1573656	7.9336382	7.5633794	7.4024378	7.5845368	9.5781922	8.5748416	8.8706166	8.6442026	8.1379654	8.6939286
NM_00950	Vegfa	Vascular endothelial growth factor A	0.886671333	3.8389461 1	3.9343 73168	0.002659 01	0.015954 06	3.9847886	3.3746376	3.7957642	3.2017734	3.3136438	3.6980298	4.8134282	4.4538636	4.5479126	3.5178586	3.5448954	3.8207576

5				7		1	4												
NM_0 0754 0	Bd nf	Brain derived neurotrophic factor	-2.2278 17667	11.88 26039 5	-3.7741 32593	0.003 46808 4	0.016 90691	12.61 5310 6	13.58 2813 6	13.13 1354 2	9.696 0704	10.72 2559 8	12.16 0636 8	9.943 7452	11.64 4499 6	11.05 7780 6	12.68 6931 6	12.58 4298 4	12.76 5246 6
NM_0 0817 6	Cxc l1	Chemokine (C-X-C motif) ligand 1	-2.4380 01	10.74 93843 7	-3.7956 87826	0.003 34575 7	0.016 90691	13.39 4085 6	12.15 1445 6	12.04 7755 2	8.539 9404	8.978 8668	10.32 9146 8	10.20 9771 2	10.78 3438 6	9.286 0736	11.04 6809 6	12.11 8943 4	10.10 6335 6
NM_0 0936 2	Tff1	Trefoil factor 1	-4.8760 03333	10.93 60014 5	-3.8090 97941	0.003 27192 8	0.016 90691	11.30 6482 6	12.32 4024 6	15.40 7466 2	11.08 4423 4	11.52 2701 8	11.13 9013 8	7.250 5392	9.023 0736	8.136 3506	9.215 1176	14.32 3055 4	10.49 9768 6
NM_0 0835 0	Il11	Interleukin 11	-2.0017 33333	11.42 74974 5	-3.6841 26077	0.004 03138 7	0.018 49695 4	13.48 1435 6	12.04 6293 6	11.69 7871 2	10.84 5372 4	9.635 6288	10.97 1717 8	9.698 2872	11.17 4472 6	10.34 7640 6	12.81 9888 6	12.22 9299 4	12.18 2061 6
NM_0 1051 4	Igf2	Insulin-like growth factor 2	0.7704 76567	10.18 49579 8	3.7470 15561	0.004 33991 8	0.018 80630 9	NA	9.774 4106	9.880 0972	9.398 3774	9.548 4328	9.269 1518	10.35 6511 2	10.79 3238 6	10.64 3441 6	10.77 9822 6	10.77 4430 4	10.81 6623 6
NM_0 0800 6	Fgf 2	Fibroblast growth factor 2	-1.2409 67	8.787 76095	-3.5430 44459	0.005 11292 1	0.020 98988 5	10.18 8341 6	9.203 5826	9.171 1342	7.471 4824	7.573 7088	8.400 6138	8.059 7152	8.406 7146	8.373 7276	9.642 2596	9.102 9214	9.858 9296
NM_0 0755 7	Bm p7	Bone morphogenetic protein 7	-0.6575 57667	7.304 66886 7	-3.3581 42884	0.007 00180 8	0.024 82459 3	7.922 3216	7.329 7156	7.722 7622	6.427 1424	6.560 5168	6.438 7908	6.799 9652	7.071 3926	7.130 7686	8.064 7806	8.026 7554	8.161 1146
NM_0	Csf	Colony stimulating factor 2	1.5524	11.28	3.4135	0.006	0.024	11.09	9.892	11.62	10.75	10.47	10.39	11.85	12.26	13.14	11.77	10.98	11.14

09969	2	(granulocyte-macrophage)	17333	337253	6679	370047	824593	47516	2346	19092	93044	18948	41878	80392	37966	43116	46856	46794	06756
NM_008381	Inhbb	Inhibin beta-B	-1.312911	9.220747617	-3.366972657	0.006896997	0.024824593	10.565219	9.9916646	9.9804662	8.0176224	8.2352518	9.0908038	8.8402092	9.5694896	8.1889186	9.7358436	9.1278434	9.3056386
NM_008003	Fgf15	Fibroblast growth factor 15	-3.113243333	15.902422212	-3.329630081	0.007351579	0.024931441	18.832725	15.208133	18.768366	14.307159	14.295983	14.008145	13.527632	14.639672	15.302190	16.940478	16.357240	18.662936
NM_007555	Bmp5	Bone morphogenetic protein 5	0.777132333	5.8139917	3.27204146	0.008113797	0.026369841	5.8051126	5.0782476	5.6098372	5.3557534	5.2910168	5.0024808	6.2793652	6.2776876	6.2675416	6.5349666	5.9312304	6.3346606
NM_009263	Spp1	Secreted phosphoprotein 1	-2.54038	7.8554667	-2.74446283 8	0.020202488	0.063031763	9.9680006	8.4657956	9.1258262	6.4274564	6.6271578	8.9890708	5.6302102	6.9731796	7.3350926	7.6719986	6.8550944	10.196717 6
NM_011562	Tdgf1	Teratocarcinoma-derived growth factor 1	-3.6323252	16.712781444	-2.90051081 1	0.022023535	0.066070604	20.308368 6	19.861007 6	NA	14.523699 4	14.887753 8	13.928123 8	18.461207 2	14.443518 6	NA	NA	18.105168 4	15.896185 6
NM_008351	Il12a	Interleukin 12A	2.731588333	13.998470377	2.561705749	0.027744613	0.080151105	14.101105 6	11.821930 6	12.280215 2	13.174141 4	12.345932 8	14.069373 8	13.923728 2	18.359099 6	14.115188 6	14.773385 6	14.206609 4	14.810933 6
NM_008380	Inhba	Inhibin beta-A	-1.193691	9.12383295	-2.44743736	0.033820885	0.094215322	10.521185 6	8.7307816	11.066744 2	7.7877774	7.8551908	8.2335698	9.0241422	9.0577156	8.6557806	9.2995316	9.4440984	9.8094776

NM_008008	Fgf7	Fibroblast growth factor 7	0.717022667	8.58448128 3	2.285007853	0.044739046	0.120332606	9.056 8086	7.982 0726	8.303 5972	7.983 2504	7.694 9148	7.398 4838	9.074 3702	9.207 0506	9.212 1256	9.107 3166	8.554 6434	9.439 1416
NM_007554	Bmp4	Bone morphogenetic protein 4	0.461922333	5.53088336 7	2.239180912	0.048 39627	0.121771259	5.618 5626	5.201 3416	5.422 3182	4.816 9994	4.839 5038	5.078 9868	6.235 9032	5.667 8986	5.724 1876	5.886 8996	5.903 6954	5.974 3036
NM_009368	Tgfb3	Transforming growth factor, beta 3	-0.458053	8.32737178 3	-2.245185143	0.047 90116	0.121771259	9.014 8256	8.524 2746	8.661 2152	7.723 6964	7.685 6888	8.172 4258	8.163 4182	8.240 5996	8.422 1386	8.394 2066	8.494 2254	8.431 7466
NM_013609	Ngf	Nerve growth factor	-0.855243433	12.2585269 8	-2.068071571	0.067668282	0.155244389	NA	12.81 7756 6	13.08 1069 2	11.48 2352 4	11.59 3008 8	12.54 1596 8	12.38 8837 2	11.83 2556 6	12.06 1114 6	12.10 1785 6	11.91 6675 4	13.02 7043 6
NM_008808	Pdgfa	Platelet derived growth factor, alpha	0.602742	6.65306195	2.065064136	0.065089021	0.155244389	7.191 1226	6.319 0366	6.352 4622	6.171 4654	6.297 3168	6.140 0998	7.136 6162	7.061 6176	7.472 6136	6.852 3856	6.057 3784	6.784 6286
NM_031199	Tgfa	Transforming growth factor alpha	-0.34226	7.22088061 7	-2.042027377	0.067670631	0.155244389	7.494 1846	7.369 7266	7.451 1782	7.063 2814	7.362 4548	7.193 7458	7.175 2852	7.081 2556	7.031 7686	7.200 1316	6.975 8984	7.251 6566
NM_145741	Gdf10	Growth differentiation factor 10	1.594346	12.0881205 3	1.980795275	0.075010377	0.161507455	13.09 3639 6	10.62 5335 6	10.82 0174 2	11.41 5884 4	12.19 0293 8	11.18 7548 8	11.46 6424 2	13.27 1632 6	14.58 4130 6	11.70 1453 6	12.63 0769 4	12.07 0159 6
NM_001056	Inha	Inhibin alpha	0.826628733	11.0714258	2.01583063	0.073 69454	0.161 50745	NA	10.72 8912	10.41 5612	9.818 5994	10.51 5616	11.21 1362	11.49 9491	11.21 0779	11.48 6402	12.18 8725	11.42 4018	11.28 6163

4				9		3	5		6	2		8	8	2	6	6	6	4	6
NM_009506	Vegfc	Vascular endothelial growth factor C	0.428082	9.74612317	1.968181432	0.07661251	0.16150745	9.7035556	9.3963526	9.5647672	9.3971664	9.5304628	9.5832078	10.335368	9.6481926	9.9653606	9.8407256	9.7883484	10.199969
NM_010216	Figf	C-fos induced growth factor	-0.582496	8.76661645	-1.915556985	0.08364813	0.17169879	9.4802056	8.4658226	9.1185672	8.2767854	8.2786518	8.4025058	8.1823392	8.2000076	8.9347606	8.9482096	9.5535864	9.3579556
NM_009755	Bmp1	Bone morphogenetic protein 1	0.502127	6.8769237	1.876143429	0.08930651	0.17861302	7.0603256	6.3236306	7.0829282	6.4128564	6.4677518	5.8724818	7.2259722	7.2023166	7.5449766	7.3096286	6.8446454	7.1755706
NM_031168	Il6	Interleukin 6	-1.195087673	11.6769715	-1.728395504	0.11698960	0.22812973	NA	12.260450 6	12.072194 2	11.471913 4	10.152138 8	10.622248 8	10.808245 2	11.525604 6	10.579854 6	13.684095 6	13.830885 4	11.439055 6
NM_009711	Artn	Artemin	-0.373506667	9.52028395	-1.455683696	0.17534874 7	0.3335903	10.263923 6	9.6049026	9.9281242	8.8764214	8.8420558	8.8392028	9.4075852	9.4063476	9.8624976	9.2714256	9.9152904	10.025630 6
NM_007445	Amh	Anti-Mullerian hormone	-1.307486	17.1116113 7	-1.421195435	0.18489645 4	0.34285634 5	15.581298 6	18.216710 6	19.064509 2	18.552323 4	17.192196 8	15.898816 8	15.390675 2	17.377356 6	16.172028 6	17.438071 6	16.697015 4	17.758333 6
NM_008827	Pgf	Placental growth factor	-0.515139	9.67174061 7	-1.406800083	0.18901054 9	0.34285634 5	10.576232 6	9.6847136	9.9495492	9.0016854	8.9742118	9.1607038	9.4115592	9.6886466	9.5648726	10.832275 6	9.9708834	9.2455536

NM_053009	Zfp91	Zinc finger protein 91	-0.252052667	2.9857062	-1.365306674	0.20130604	0.35686072	3.1982956	2.6738356	2.9852802	3.4252724	3.3919728	3.1863918	2.6924792	2.7182496	2.6905246	2.8793976	3.0859634	2.9008116
NM_007553	Bmp2	Bone morphogenetic protein 2	0.367467667	6.18948745	1.202676877	0.25608710	0.42944930	5.5538156	5.5971856	6.5640362	5.3441494	5.3456048	5.6493718	6.2096512	6.4398186	6.1679706	7.5247016	6.6874354	7.1901086
NM_008002	Fgf10	Fibroblast growth factor 10	-0.571018333	9.9786278 3	-1.18085684	0.26427649 5	0.42944930 4	11.257404 6	9.5859006	9.8687822	8.8999644	9.0210428	9.6575158	8.8978812	10.246737 6	9.8544136	10.725312 6	10.434852 4	11.294385 6
NM_008005	Fgf18	Fibroblast growth factor 18	-0.531974333	12.1976591 2	-1.18380074	0.26343267 4	0.42944930 4	13.340165 6	12.853940 6	12.093350 2	10.553797 4	11.321438 8	10.888369 8	12.331584 2	12.088024 6	12.271924 6	13.192995 6	11.846158 4	13.590159 6
NM_021283	Il4	Interleukin 4	0.960439067	12.0533028	1.22617463	0.25035757 1	0.42944930 4	NA	11.404266 6	11.435452 2	11.415841 4	12.123139 8	10.209253 8	12.243512 2	11.556168 6	13.341214 6	12.490359 6	14.342415 4	12.024706 6
NM_010272	Gdf11	Growth differentiation factor 11	0.3507344	9.07798652 7	1.151665327	0.27828507 5	0.44298440 5	NA	8.6629276	8.5397232	8.7409024	9.0295648	9.1941638	8.8979592	8.8209826	9.1372376	9.0185216	9.8332594	9.9826096
NM_007778	Csf1	Colony stimulating factor 1 (macrophage)	0.324316333	7.64004686 7	1.119960096	0.28823069 3	0.44963988 2	8.3771456	7.2941266	7.5068442	6.5301614	6.7558028	7.2030918	8.2594312	7.9860486	7.9055856	7.9031236	7.9736514	7.9855496
NM_011697	Vegfb	Vascular endothelial growth factor B	-0.2003	7.4733892	-1.0074	0.33685224	0.51518578	7.3712026	7.5055296	6.9793652	8.1422794	8.0513108	7.9919638	7.1758832	6.9581246	7.1210306	7.2507166	7.4441144	7.6891496

7			53		62431	2	2												
NM_01055 4	Il1a	Interleukin 1 alpha	-0.538575333	8.8935736 7	-0.987073552	0.346283707	0.519425561	9.3563216	9.1697366	9.0616982	9.3344714	6.9118398	8.0599328	8.1080942	8.9302776	8.9336586	9.2061936	9.2905634	10.359900 6
NM_00800 7	Fgf 3	Fibroblast growth factor 3	-0.443138867	13.8697248	-0.953841308	0.370782401	0.545679761	14.093090 6	15.339836 6	14.458742 2	12.767975 4	13.107983 8	13.408523 8	NA	13.672322 6	14.702512 6	13.276535 6	NA	NA
NM_17340 4	Bm p3	Bone morphogenetic protein 3	-0.287558333	6.9658162833	-0.878372341	0.399819076	0.565452207	6.9570366	6.1405106	7.2540622	7.6435534	7.6990748	7.9816638	6.0328112	7.0516706	6.4044526	6.8522316	6.6132294	6.9594986
NM_00997 1	Csf 3	Colony stimulating factor 3 (granulocyte)	-1.264746	13.824811988	-0.889500064	0.396222867	0.565452207	16.370785 6	14.796825 6	13.595820 2	12.010582 4	12.195435 8	13.261845 8	12.507876 2	15.593798 6	12.867518 6	NA	17.378545 4	11.493897 6
NM_01020 5	Fgf 8	Fibroblast growth factor 8	0.579986667	15.1367816 2	0.866563026	0.405965687	0.565452207	14.451362 6	14.027545 6	16.562304 2	14.117229 4	14.145816 8	14.746880 8	14.593020 2	16.225336 6	15.962815 6	14.882685 6	16.364455 4	15.561926 6
NM_00800 4	Fgf 17	Fibroblast growth factor 17	0.770063	16.0620087 7	0.810508097	0.460378977	0.629992284	NA	NA	16.006792 2	14.883252 4	16.364643 8	NA	16.776855 2	NA	NA	15.667678 6	16.672830 4	NA
NM_01361 1	No dal	Nodal	-0.455240 3	13.9567268 9	-0.743732384	0.480369938	0.644677566	NA	15.023296 6	13.491870 2	14.421261 4	13.565079 8	13.495015 8	NA	13.232527 6	14.372158 6	13.854991 6	14.154340 4	NA
NM_0	Ra	Rabaptin, RAB GTPase	0.1386	5.600	0.7199	0.487	0.644	5.496	5.174	5.767	5.433	5.731	5.552	5.573	5.624	5.656	5.809	5.618	5.768

1940 0	bep 1	binding effector protein 1	51333	5022	01542	64072 3	67756 6	0156	1256	8192	5124	4028	1638	2922	3156	3066	8056	8614	4056
NM_0 1011 3	Egf	Epidermal growth factor	- 0.2386 05667	10.77 79316 2	- 0.6583 38263	0.524 79934	0.682 23914 2	11.14 4220 6	10.81 3688 6	11.22 5007 2	10.24 6808 4	9.751 2268	11.00 2616 8	11.15 3788 2	10.18 7605 6	11.12 5705 6	11.15 7771 6	10.53 9523 4	10.98 7216 6
NM_1 7709 9	Left y2	Left-right determination factor 2	- 0.4914 335	17.96 78110 6	- 0.6571 34453	0.538 69299 1	0.688 82054 6	NA	18.64 5538 6	17.57 0948 2	NA	14.66 4944 8	NA	18.59 7327 2	16.63 6292 6	NA	NA	19.58 2135 4	20.07 7490 6
NM_0 1009 4	Left y1	Left right determination factor 1	0.1538 86	8.523 2862	0.6178 32943	0.550 13542 8	0.692 10586 1	8.541 8916	8.126 2766	7.889 6622	8.748 9894	8.589 8948	8.379 7628	8.409 0092	8.223 7096	8.386 7696	9.456 6356	8.730 0824	8.796 7506
NM_0 0755 6	Bm p6	Bone morphogenetic protein 6	0.1797 23	8.844 63678 3	0.5926 73904	0.566 21611 8	0.701 02947 9	9.318 0386	8.320 3026	8.915 4822	8.228 5124	8.099 5148	8.227 0158	9.024 5412	9.116 3086	8.952 1426	8.889 7776	9.137 4064	9.906 5986
NM_0 0837 1	Il7	Interleukin 7	- 0.1256 01767	8.091 0868	- 0.5155 92854	0.618 20534 8	0.753 43776 8	NA	8.338 8656	7.909 4442	8.224 3494	8.364 1568	8.204 9408	8.052 8512	7.979 8646	7.962 9436	8.230 8096	7.608 0954	8.125 6336
NM_0 1157 7	Tgf b1	Transforming growth factor, beta 1	0.1198 7	5.655 22228 3	0.4909 79393	0.633 75996 7	0.760 51196 1	6.135 3986	5.232 2026	5.302 0142	4.926 7414	5.068 0148	5.249 9138	5.580 5612	5.768 7156	5.679 9486	6.401 9866	6.218 2094	6.298 9606
NM_0 0836 1	Il1b	Interleukin 1 beta	0.2145 14333	8.015 2477	0.4269 38686	0.678 23335 8	0.797 83113 4	9.140 3526	7.244 4306	7.965 0722	6.127 7164	5.702 4638	6.734 4988	8.393 7792	8.732 9756	7.866 6436	10.15 2923 6	8.965 3674	9.156 7486

NM_00851	Lif	Leukemia inhibitory factor	0.094527	8.660766617	0.4169 18045	0.685316487	0.797831134	9.022 9606	8.393 1566	8.882 7652	8.251 0534	7.895 9628	8.209 1838	9.040 7282	8.565 3426	8.976 3926	9.007 2956	8.943 8284	8.740 5296
NM_01020 2	Fgf 4	Fibroblast growth factor 4	0.3104 37667	13.15 846671	0.3336 9543	0.746 031573	0.843 340039	15.75 8705 6	12.08 3528 6	11.98 4543 2	12.24 5068 4	12.52 5683 8	12.07 9238 8	14.69 9778 2	13.13 4535 6	12.92 3776 6	13.16 7399 6	14.14 0875 4	NA
NM_00810 9	Gdf 5	Growth differentiation factor 5	0.1980 426	14.50 696255	0.3696 29029	0.743 298899	0.843 340039	NA	14.34 3345 6	NA	NA	13.63 6852 8	NA	14.54 1388 2	NA	NA	NA	NA	15.50 6263 6
NM_01020 3	Fgf 5	Fibroblast growth factor 5	-0.4238 794	15.40 041338	-0.3207 25165	0.757 437972	0.844 002311	15.43 1327 6	18.85 0864 6	13.64 1592 2	14.42 1067 4	15.59 5638 8	NA	15.56 3651 2	15.53 7779 6	NA	15.11 0808 6	14.45 0990 4	NA
NM_01078 4	Mdk	Midkine	0.0697 94667	7.141 73445	0.2618 50509	0.798 612104	0.877 348509	7.299 3646	6.712 1356	7.391 8062	7.120 8794	6.791 8078	6.659 2538	7.093 7162	7.206 5206	7.312 4536	7.461 8416	6.908 7254	7.742 3086
NM_02170 4	Cxcl12	Chemokine (C-X-C motif) ligand 12	-0.0513 08767	5.654 867982	-0.2385 16064	0.816 668381	0.884 72408	NA	5.417 3466	5.909 4592	5.411 8524	5.423 8348	5.417 1158	5.486 4912	5.791 9026	5.557 8886	5.838 5386	5.929 2004	6.019 9176
NM_01359 8	Kitl	Kit ligand	0.0773 38667	3.753 494867	0.1715 95704	0.867 088461	0.926 478081	3.791 1376	3.288 3876	3.680 8272	3.478 8894	3.608 1468	3.849 2938	2.493 1232	4.188 8146	4.310 4306	4.284 0666	3.540 5324	4.528 2886
NM_01019	Fgf 1	Fibroblast growth factor 1	-0.0407	8.064 89611	-0.1253	0.902 63568	0.951 4268	8.698 8466	7.421 1386	8.253 1592	7.376 3644	7.895 3218	7.939 6628	7.979 2952	7.960 1316	8.311 3806	8.088 7406	8.190 9234	8.663 7886

7			79	7	88757	2													
NM_01020 0	Fgf 13	Fibroblast growth factor 13	0.018801333	8.592814033	0.071585439	0.944306322	0.956570041	8.8751626	8.5336686	8.8122092	7.5250804	7.6431268	7.9815008	8.7823912	8.3745446	9.1205086	9.0395006	8.8529884	9.5730866
NM_02330 4	Fgf 22	Fibroblast growth factor 22	0.033272667	11.976530778	0.09309604	0.927617856	0.956570041	12.724231626	12.812637686	11.682204092	10.706513804	11.784683268	11.118352008	12.681243912	12.166174446	12.471473086	12.063241006	11.578338884	11.929274706
NM_01027 5	Gdnf	Glial cell line derived neurotrophic factor	0.037863	9.8568922	0.080869054	0.937099907	0.956570041	10.999585616	9.0196806	9.3310132	9.1154124	9.5006268	9.0514438	10.203261 2	9.6690566	9.5915506	10.796632 6	10.062335 4	10.942107 6
NM_00936 7	Tgfb2	Transforming growth factor, beta 2	0.007344	8.8581462	0.026577173	0.979310415	0.979310415	9.2531686	8.7206876	8.9670022	7.9029814	8.3318368	8.1631138	8.9693952	8.7022676	9.2912276	9.8198056	8.8824324	9.2938356
NM_00975 6	Bmp10	Bone morphogenetic protein 10	NA	14.3355976	NA	NA	NA	NA	NA	NA	NA	NA	14.215459 8	NA	NA	NA	NA	14.455735 4	NA
NM_01020 4	Fgf 6	Fibroblast growth factor 6	NA	17.3500847	NA	NA	NA	NA	NA	NA	NA	NA	19.970029 8	NA	NA	NA	NA	NA	14.730139 6
NM_00836 6	Il2	Interleukin 2	NA	14.6125765 3	NA	NA	NA	NA	NA	14.433940 2	NA	13.597962 8	13.724143 8	14.910197 2	15.773966 6	15.235248 6	NA	NA	NA

NM_01055	Il3	Interleukin 3	NA	14.3433715	NA	NA	NA	NA	NA	14.523127	15.194874	14.702956	14.536383	NA	NA	NA	NA	12.759515	NA
NM_008493	Lep	Leptin	NA	19.7642197	NA	NA	NA	NA	NA	NA	NA	19.096516	NA	NA	20.431922	NA	NA	NA	NA
NM_010834	Mstn	Myostatin	NA	15.6276996	NA	NA	NA	NA	16.311706	NA	NA	NA	NA	NA	NA	NA	NA	NA	14.943986

Appendix Table 2.3 Table showing the comparison between the normalized cycle threshold (Ct) values of 84 growth factor genes from UNIRR and 6 DPI samples.

								Mock Irradiated			48 Hours			4 Days			6 Days		
Gene Bank	Symbol	Description	logFC	AveExpr	t	P.Value	adj.P.Val	PAM M041 Plate 1	PAM M041 Plate 2	PAM M041 Plate 3	PAM M041 Plate 1	PAM M041 Plate 2	PAM M041 Plate 3	PAM M041 Plate 1	PAM M041 Plate 2	PAM M041 Plate 3	PAM M041 Plate 1	PAM M041 Plate 2	PAM M041 Plate 3
NM_011313	S100a6	S100 calcium binding protein A6 (calcyclin)	-1.451708267	1.0706658677	-6.13385346	9.90E-05	0.00772451	3.0630376	2.9841846	3.0664342	-0.1488696	0.1112968	0.5823288	-0.7994798	-0.3002294	-0.4692444	1.4843786	1.8758174	1.3983356
NM_010514	Igf2	Insulin-like growth factor 2	0.9630383	10.1849579	4.68349026	0.00105765	0.04124849	NA	9.7744106	9.8800972	9.3983774	9.5484328	9.2691518	10.356511	10.793238	10.643441	10.779822	10.774430	10.816623
NM_007553	Bmp2	Bone morphogenetic protein 2	1.2290694	6.1894874	4.02259431	0.00230026	0.05980690	5.5538156	5.5971856	6.5640362	5.3441494	5.3456048	5.6493718	6.2096512	6.4398186	6.1679706	7.5247016	6.6874354	7.1901086
NM_007558	Bmp8a	Bone morphogenetic protein 8a	0.9498014067	7.0194202833	3.81614952	0.00323378	0.06305889	6.4508076	6.0825956	6.8750462	6.2589254	6.4072528	6.2579168	8.0272492	7.5417696	8.0735886	7.6798226	7.1802404	7.3978286
NM_007555	Bmp5	Bone morphogenetic protein 5	0.7692020067	5.8139917	3.23872761	0.00859126	0.09609800	5.8051126	5.0782476	5.6098372	5.3557534	5.2910168	5.0024808	6.2793652	6.2776876	6.2675416	6.5349666	5.9312304	6.3346606

NM_010272	Gdf11	Growth differentiation factor 11	1.010138133	9.07798652	3.316871865	0.008062418	0.09809800	NA	8.6629276	8.5397232	8.7409024	9.0295648	9.1941638	8.8979592	8.8209826	9.1372376	9.0185216	9.8332594	9.9826096
NM_010094	Lefty1	Left right determination factor 1	0.808546067	8.5232862	3.246210803	0.008481567	0.09809800	8.5418916	8.1262766	7.8896622	8.7489894	8.5898948	8.3797628	8.4090092	8.2237096	8.3867696	9.4566356	8.7300824	8.7967506
NM_011577	Tgfb1	Transforming growth factor, beta 1	0.749847067	5.65522228 3	3.071322745	0.011463614	0.11177023 9	6.1353986	5.2322026	5.3020142	4.9267414	5.0680148	5.2499138	5.5805612	5.7687156	5.6799486	6.4019866	6.2182094	6.2989606
NM_007950	Ereg	Epiregulin	-1.0579206	4.98522586 7	-2.757318959	0.019756433	0.15410015 7	7.8766046	6.4867596	6.9011292	3.3549354	3.2953638	3.6507718	3.0734792	3.8420966	3.2508386	5.6249286	6.6077654	5.8580376
NM_010512	Igf1	Insulin-like growth factor 1	-0.7452162	5.16951252 7	-2.862254168	0.018168152	0.15410015 7	NA	6.2589006	6.6587702	4.3446264	4.4112368	4.8724378	4.1628152	4.3657296	4.6492636	5.5104536	5.8429084	5.7874956
NM_007554	Bmp4	Bone morphogenetic protein 4	0.507558733	5.53088336 7	2.460404586	0.033065571	0.16664251 2	5.6185626	5.2013416	5.4223182	4.8169994	4.8395038	5.0789868	6.2359032	5.6678986	5.7241876	5.8868996	5.9036954	5.9743036
NM_007559	Bmp8b	Bone morphogenetic protein 8b	0.793470733	9.75958736 7	2.434298746	0.034592172	0.16664251 2	10.624374 6	10.326599 6	11.562270 2	8.1376504	7.7460718	8.2370848	8.3924532	8.6936286	8.5012586	12.073758 6	11.364284 4	11.455613 6
NM_001019	Fgf11	Fibroblast growth factor 11	0.788771067	8.68442853	2.406088468	0.036031952	0.16664251	8.3578896	7.9281556	8.0225572	7.8349984	8.2972308	8.4810078	10.059811	9.2476296	9.3089466	8.8167476	8.3865424	9.4716256

8				3		2	2							2					
NM_01020 1	Fgf 14	Fibroblast growth factor 14	-0.702054267	9.9105848667	-2.505085285	0.03060493 4	0.16664251 2	10.617950 6	10.171701 6	10.414168 2	10.099863 4	11.054268 8	9.9940068	8.9723922	9.3021976	9.2028116	9.5277386	9.7654754	9.8044436
NM_00836 1	Il1b	Interleukin 1 beta	1.308394733	8.0152477	2.604041976	0.02578018 4	0.16664251 2	9.1403526	7.2444306	7.9650722	6.1277164	5.7024638	6.7344988	8.3937792	8.7329756	7.8666436	10.152923 6	8.9653674	9.1567486
NM_01056 4	Inh a	Inhibin alpha	1.0607068	11.0714258 9	2.5866 57311	0.02870001 8	0.16664251 2	NA	10.728912 6	10.415612 2	9.8185994	10.515616 8	11.211362 8	11.499491 2	11.210779 6	11.486402 6	12.188725 6	11.424018 4	11.286163 6
NM_00874 2	Ntf 3	Neurotrophin 3	0.7725 07067	8.1840563667	2.4357 45656	0.034 50578	0.16664251 2	8.0675716	7.1573656	7.9336382	7.5633794	7.4024378	7.5845368	9.5781922	8.5748416	8.8706166	8.6442026	8.1379654	8.6939286
NM_01156 2	Tdgf1	Teratocarcinoma-derived growth factor 1	-3.0840111	16.7127814 4	-2.462667037	0.04204205 7	0.18218224 7	20.308368 6	19.861007 6	NA	14.523699 4	14.887753 8	13.928123 8	18.461207 2	14.443518 6	NA	NA	18.105168 4	15.896185 6
NM_00817 6	Cxcl1	Chemokine (C-X-C motif) ligand 1	-1.440399267	10.7493843 7	-2.24253639	0.04811897 1	0.19754103 8	13.394085 6	12.151445 6	12.047755 2	8.5399404	8.9788668	10.329146 8	10.209771 2	10.783438 6	9.2860736	11.046809 6	12.118943 4	10.106335 6
NM_00755 7	Bmp7	Bone morphogenetic protein 7	0.4259504	7.3046688667	2.1753 26024	0.05397594 3	0.20048207 3	7.9223216	7.3297156	7.7227622	6.4271424	6.5605168	6.4387908	6.7999652	7.0713926	7.1307686	8.0647806	8.0267554	8.1611146

NM_00807	Fgf3	Fibroblast growth factor 3	-1.354020867	13.8697248	-2.3041 01728	0.05329757 3	0.20048207 3	14.093090 6	15.339836 6	14.458742 2	12.767975 4	13.107983 8	13.408523 8	NA	13.672322 6	14.702512 6	13.276535 6	NA	NA
NM_01042 7	Hgf	Hepatocyte growth factor	0.611502133	7.52304334 5	2.1060 81934	0.06358337 1	0.22543195 1	NA	7.6953736	8.4841492	6.5159764	6.7879898	6.7342108	6.6155292	7.1318486	6.6846086	8.7107716	8.9223204	8.4706986
NM_00838 1	Inhbb	Inhibin beta-B	-0.7893416	9.22074761 7	-2.0242 73987	0.06972587 4	0.22660908 9	10.565219 6	9.9916646	9.9804662	8.0176224	8.2352518	9.0908038	8.8402092	9.5694896	8.1889186	9.7358436	9.1278434	9.3056386
NM_17709 9	Lefty2	Left-right determination factor 2	1.7215696	17.9678110 6	2.3020 46357	0.06688795 4	0.22660908 9	NA	18.645538 6	17.570948 2	NA	14.664944 8	NA	18.597327 2	16.636292 6	NA	NA	19.582135 4	20.077490 6
NM_02128 3	Il4	Interleukin 4	1.5326 34467	12.0533028	1.9566 85817	0.08113367 1	0.25313705 3	NA	11.404266 6	11.435452 2	11.415841 4	12.123139 8	10.209253 8	12.243512 2	11.556168 6	13.341214 6	12.490359 6	14.342415 4	12.024706 6
NM_00808	Fgf7	Fibroblast growth factor 7	0.5862 07733	8.58448128 3	1.8681 2682	0.09049997 3	0.27149991 8	9.0568086	7.9820726	8.3035972	7.9832504	7.6949148	7.3984838	9.0743702	9.2070506	9.2121256	9.1073166	8.5546434	9.4391416
NM_01351 8	Fgf9	Fibroblast growth factor 9	0.4971 894	11.1144902	1.8217 95472	0.09769076	0.27879463 6	10.433576 6	10.521978 6	10.483697 2	10.724554 4	10.703882 8	10.091283 8	12.813437 2	12.205771 6	12.464879 6	11.054656 6	10.511710 4	11.364453 6
NM_01027	Gdnf	Glial cell line derived neurotrophic factor	0.8169 32067	9.8568922	1.7448 30669	0.11080299	0.27879463	10.999585	9.0196806	9.3310132	9.1154124	9.5006268	9.0514438	10.203261	9.6690566	9.5915506	10.796632	10.062335	10.942107

5						6	6	6						2			6	4	6
NM_008351	Il12a	Interleukin 12A	1.862559067	13.99847037	1.746723037	0.11046225 8	0.27879463 6	14.101105 6	11.821930 6	12.280215 2	13.174141 4	12.345932 8	14.069373 8	13.923728 2	18.359099 6	14.115188 6	14.773385 6	14.206609 4	14.810933 6
NM_031199	Tgfa	Transforming growth factor alpha	-0.295800933	7.220880617	-1.764838439	0.10724826 1	0.27879463 6	7.494 1846	7.369 7266	7.451 1782	7.063 2814	7.362 4548	7.193 7458	7.175 2852	7.081 2556	7.031 7686	7.200 1316	6.975 8984	7.251 6566
NM_009506	Vegfc	Vascular endothelial growth factor C	0.388122733	9.74612311 7	1.784461755	0.10386299 9	0.27879463 6	9.703 5556	9.396 3526	9.564 7672	9.397 1664	9.530 4628	9.583 2078	10.335368 2	9.648 1926	9.965 3606	9.840 7256	9.788 3484	10.199969 6
NM_010200	Fgf13	Fibroblast growth factor 13	0.414845067	8.592814033	1.579508529	0.14448900 1	0.34669808 8	8.875 1626	8.533 6686	8.812 2092	7.525 0804	7.643 1268	7.981 5008	8.782 3912	8.374 5446	9.120 5086	9.039 5006	8.852 9884	9.573 0866
NM_008109	Gdf5	Growth differentiation factor 5	1.16291 8	14.506962 5	2.170483779	0.14667996	0.34669808 8	NA	14.343345 6	NA	NA	13.636852 8	NA	14.541388 2	NA	NA	NA	NA	15.506263 6
NM_023304	Fgf22	Fibroblast growth factor 22	-0.549406267	11.976530 78	-1.537224185	0.15444680 3	0.35431913 7	12.724231 6	12.812637 6	11.682204 2	10.706513 4	11.784683 8	11.118352 8	12.681243 2	12.166174 6	12.471473 6	12.063241 6	11.578338 4	11.929274 6
NM_007556	Bmp6	Bone morphogenetic protein 6	0.4599 864	8.844636783	1.516900649	0.15944294 3	0.35532998 6	9.318 0386	8.320 3026	8.915 4822	8.228 5124	8.099 5148	8.227 0158	9.024 5412	9.116 3086	8.952 1426	8.889 7776	9.137 4064	9.906 5986

NM_01369	Ngf	Nerve growth factor	-0.6009 11367	12.25 852698	-1.4530 68993	0.179 190452	0.379 84801	NA	12.81 77566	13.08 10692	11.48 23524	11.59 30088	12.54 15968	12.38 88372	11.83 25566	12.06 11146	12.10 17856	11.91 66754	13.02 70436
NM_009368	Tgfb3	Transforming growth factor, beta 3	-0.2933 78933	8.327 371783	-1.4380 21413	0.180 184313	0.379 84801	9.014 8256	8.524 2746	8.661 2152	7.723 6964	7.685 6888	8.172 4258	8.163 4182	8.240 5996	8.422 1386	8.394 2066	8.494 2254	8.431 7466
NM_019400	Rabep1	Rabaptin, RAB GTPase binding effector protein 1	0.2530 374	5.600 5022	1.3138 13651	0.217 490272	0.442 705963	5.496 0156	5.174 1256	5.767 8192	5.433 5124	5.731 4028	5.552 1638	5.573 2922	5.624 3156	5.656 3066	5.809 8056	5.618 8614	5.768 4056
NM_009362	Tff1	Trefoil factor 1	-1.6666 77267	10.93 600145	-1.3019 96022	0.221 352981	0.442 705963	11.30 64826	12.32 40246	15.40 74662	11.08 44234	11.52 27018	11.13 90138	7.250 5392	9.023 0736	8.136 3506	9.215 1176	14.32 30554	10.49 97686
NM_009367	Tgfb2	Transforming growth factor, beta 2	0.3517 384	8.858 1462	1.2726 44029	0.231 191882	0.450 824169	9.253 1686	8.720 6876	8.967 0022	7.902 9814	8.331 8368	8.163 1138	8.969 3952	8.702 2676	9.291 2276	9.819 8056	8.882 4324	9.293 8356
NM_021704	Cxcl12	Chemokine (C-X-C motif) ligand 12	0.2658 15967	5.654 867982	1.2356 83146	0.246 963229	0.451 117279	NA	5.417 3466	5.909 4592	5.411 8524	5.423 8348	5.417 1158	5.486 4912	5.791 9026	5.557 8886	5.838 5386	5.929 2004	6.019 9176
NM_008002	Fgf10	Fibroblast growth factor 10	0.5808 21067	9.978 682783	1.2011 28737	0.256 661392	0.451 117279	11.25 74046	9.585 9006	9.868 7822	8.899 9644	9.021 0428	9.657 5158	8.897 8812	10.24 67376	9.854 4136	10.72 53126	10.43 48524	11.29 43856
NM_031168	Il6	Interleukin 6	0.8183 56467	11.67 697153	1.1835 48083	0.266 043524	0.451 117279	NA	12.26 0450	12.07 2194	11.47 1913	10.15 2138	10.62 2248	10.80 8245	11.52 5604	10.57 9854	13.68 4095	13.83 0885	11.43 9055

8				3		3	9		6	2	4	8	8	2	6	6	6	4	6
NM_0			-		-	0.254	0.451	10.52		11.06									
0838	Inh		0.5885	9.123	1.2066	62439	11727	1185	8.730	6744	7.787	7.855	8.233	9.024	9.057	8.655	9.299	9.444	9.809
0	ba	Inhibin beta-A	346	83295	32593	4	9	6	7816	2	7774	1908	5698	1422	7156	7806	5316	0984	4776
NM_0				3.753		0.265	0.451												
1359			0.5308	49486	1.1778	43403	11727	3.791	3.288	3.680	3.478	3.608	3.849	2.493	4.188	4.310	4.284	3.540	4.528
8	Kitl	Kit ligand	45067	7	16181	6	9	1376	3876	8272	8894	1468	2938	1232	8146	4306	0666	5324	2886
NM_1			-		-	0.256	0.451	14.41	13.79	12.83	10.93	11.11	11.52	10.87	11.57	10.95	13.60	13.21	12.82
9819	Ntf		0.4704	12.30	1.2003	95621	11727	4845	4240	9537	0827	6682	4319	6162	3232	7042	3085	3799	0426
0	5	Neurotrophin 5	37267	53502	35036	5	9	6	6	2	4	8	8	2	6	6	6	4	6
NM_0						0.307													
0975	Bm	Bone morphogenetic	0.2876	6.876	1.0747	06515	0.509	7.060	6.323	7.082	6.412	6.467	5.872	7.225	7.202	7.544	7.309	6.844	7.175
5	p1	protein 1	534	9237	85933	4	59749	3256	6306	9282	8564	7518	4818	9722	3166	9766	6286	6454	5706
NM_0			-		-	0.330	0.537												10.19
0926	Sp	Secreted phosphoprotein	0.9452	7.855	1.0212	60129	22710	9.968	8.465	9.125	6.427	6.627	8.989	5.630	6.973	7.335	7.671	6.855	6717
3	p1	1	706	4667	09439	8	9	0006	7956	8262	4564	1578	0708	2102	1796	0926	9986	0944	6
NM_0				11.28		0.365	0.582	11.09		11.62	10.75	10.47	10.39	11.85	12.26	13.14	11.77	10.98	11.14
0996	Csf	Colony stimulating factor 2	0.4303	33725	0.9463	69521	12708	4751	9.892	1909	9304	1894	4187	8039	3796	4311	4685	4679	0675
9	2	(granulocyte-macrophage)	81733	3	54283	9	4	6	2346	2	4	8	8	2	6	6	6	4	6
NM_0			-	15.40	-	0.395	0.582	15.43	18.85	13.64	14.42	15.59		15.56	15.53		15.11	14.45	
1020	Fgf		1.1936	04133	0.9032	34723	57225	1327	0864	1592	1067	5638		3651	7779		0808	0990	
3	5	Fibroblast growth factor 5	953	8	00586	1	7	6	6	2	4	8	NA	2	6	NA	6	4	NA

NM_010205	Fgf8	Fibroblast growth factor 8	0.589285067	15.1367816 2	0.880455845	0.398741352	0.582572257	14.451362	14.027545 6	16.562304 2	14.117229 4	14.145816 8	14.746880 8	14.593020 2	16.225336 6	15.962815 6	14.882685 6	16.364455 4	15.561926 6
NM_010216	Figf	C-fos induced growth factor	0.265052067	8.76661645	0.871632316	0.403319255	0.582572257	9.4802056	8.4658226	9.1185672	8.2767854	8.2786518	8.4025058	8.1823392	8.2000076	8.9347606	8.9482096	9.5535864	9.3579556
NM_010784	Mdk	Midkine	0.236523067	7.14173445	0.887369887	0.395179403	0.582572257	7.2993646	6.7121356	7.3918062	7.1208794	6.7918078	6.6592538	7.0937162	7.2065206	7.3124536	7.4618416	6.9087254	7.7423086
NM_011697	Vegfb	Vascular endothelial growth factor B	0.175961067	7.4733892	0.884809132	0.396496055	0.582572257	7.3712026	7.5055296	6.9793652	8.1422794	8.0513108	7.9919638	7.1758832	6.9581246	7.1210306	7.2507166	7.4441144	7.6891496
NM_009711	Artn	Artemin	-0.194867933	9.52028395	-0.75946723	0.464643417	0.624865285	10.263923 6	9.6049026	9.9281242	8.8764214	8.8420558	8.8392028	9.4075852	9.4063476	9.8624976	9.2714256	9.9152904	10.025630 6
NM_007778	Csf1	Colony stimulating factor 1 (macrophage)	0.2280694	7.64004686 7	0.787591006	0.448725787	0.624865285	8.3771456	7.2941266	7.5068442	6.5301614	6.7558028	7.2030918	8.2594312	7.9860486	7.9055856	7.9031236	7.9736514	7.9855496
NM_145741	Gdf10	Growth differentiation factor 10	0.621077733	12.0881205 3	0.771619109	0.457721593	0.624865285	13.093639 6	10.625335 6	10.820174 2	11.415884 4	12.190293 8	11.187548 8	11.466424 2	13.271632 6	14.584130 6	11.701453 6	12.630769 4	12.070159 6
NM_001055	Il1a	Interleukin 1 alpha	0.422967067	8.89355736	0.775192585	0.455769884	0.624865286	9.3563216	9.1697366	9.0616982	9.3344714	6.9118398	8.0599328	8.1080942	8.9302776	8.9336586	9.2061936	9.2905634	10.359900

4				7		1	5												6
NM_00754 0	Bdnf	Brain derived neurotrophic factor	-0.431000 6	11.8826039 5	-0.730155 54	0.48161343 7	0.63670929	12.615310 6	13.582813 6	13.131354 2	9.6960704	10.722559 8	12.160636 8	9.9437452	11.644499 6	11.057780 6	12.686931 6	12.584298 4	12.765246 6
NM_01019 7	Fgf1	Fibroblast growth factor 1	0.1901 02733	8.064 896117	0.5845 34819	0.571 4735	0.73661742 4	8.698 8466	7.421 1386	8.253 1592	7.376 3644	7.895 3218	7.939 6628	7.979 2952	7.960 1316	8.311 3806	8.088 7406	8.190 9234	8.663 7886
NM_00850 1	Lif	Leukemia inhibitory factor	0.1309 23733	8.660 766617	0.5774 48422	0.57607260 1	0.73661742 4	9.022 9606	8.393 1566	8.882 7652	8.251 0534	7.895 9628	8.209 1838	9.040 7282	8.565 3426	8.976 3926	9.007 2956	8.943 8284	8.740 5296
NM_00837 1	Il7	Interleukin 7	-0.135975 367	8.091 0868	-0.558176 284	0.58994436 8	0.74218807 6	NA	8.338 8656	7.909 4442	8.224 3494	8.364 1568	8.204 9408	8.052 8512	7.979 8646	7.962 9436	8.230 8096	7.608 0954	8.125 6336
NM_01011 3	Egf	Epidermal growth factor	-0.166134 933	10.7779316 2	-0.458383 847	0.65622054 8	0.81246353 5	11.144220 6	10.813688 6	11.225007 2	10.246808 4	9.7512268	11.002616 8	11.153788 2	10.187605 6	11.125705 6	11.157771 6	10.539523 4	10.987216 6
NM_01361 1	Nodal	Nodal	-0.252917 4	13.9567268 9	-0.413194 66	0.69137483 7	0.83524607 6	NA	15.023296 6	13.491870 2	14.421261 4	13.565079 8	13.495015 8	NA	13.232527 6	14.372158 6	13.854991 6	14.154340 4	NA
NM_00950 5	Vegfa	Vascular endothelial growth factor A	-0.090559 6	3.838 946117	-0.401834 645	0.69603839 7	0.83524607 6	3.984 7886	3.374 6376	3.795 7642	3.201 7734	3.313 6438	3.698 0298	4.813 4282	4.453 8636	4.547 9126	3.517 8586	3.544 8954	3.820 7576

NM_00744	Amh	Anti-Mullerian hormone	-0.3230326	17.11161137	-0.3511 26097	0.732 58819 4	0.852 86386 7	15.58 1298 6	18.21 6710 6	19.06 4509 2	18.55 2323 4	17.19 2196 8	15.89 8816 8	15.39 0675 2	17.37 7356 6	16.17 2028 6	17.43 8071 6	16.69 7015 4	17.75 8333 6
NM_01020 2	Fgf4	Fibroblast growth factor 4	0.3785 45033	13.15 846671	0.3639 4721	0.724 05755 9	0.852 86386 7	15.75 8705 6	12.08 3528 6	11.98 4543 2	12.24 5068 4	12.52 5683 8	12.07 9238 8	14.69 9778 2	13.13 4535 6	12.92 3776 6	13.16 7399 6	14.14 0875 4	NA
NM_00997 1	Csf3	Colony stimulating factor 3 (granulocyte)	-0.4849223	13.82 481198	-0.3050 42126	0.767 06994 5	0.868 50717	16.37 0785 6	14.79 6825 6	13.59 5820 2	12.01 0582 4	12.19 5435 8	13.26 1845 8	12.50 7876 2	15.59 3798 6	12.86 7518 6	NA	17.37 8545 4	11.49 3897 6
NM_00800 3	Fgf15	Fibroblast growth factor 15	-0.2828566	15.90 422212	-0.3025 16618	0.768 29480 4	0.868 50717	18.83 2725 6	15.20 8133 6	18.76 8366 2	14.30 7159 4	14.29 5983 8	14.00 8145 8	13.52 7632 2	14.63 9672 6	15.30 2190 6	16.94 0478 6	16.35 7240 4	18.66 2936 6
NM_00800 5	Fgf18	Fibroblast growth factor 18	0.1139524	12.19 765912	0.2534 23531	0.804 94049	0.896 93368 9	13.34 0165 6	12.85 3940 6	12.09 3350 2	10.55 3797 4	11.32 1438 8	10.88 8369 8	12.33 1584 2	12.08 8024 6	12.27 1924 6	13.19 2995 6	11.84 6158 4	13.59 0159 6
NM_00800 4	Fgf17	Fibroblast growth factor 17	0.1634623	16.06 200877	0.1986 63496	0.851 62353 7	0.909 95391 6	NA	NA	16.00 6792 2	14.88 3252 4	16.36 4643 8	NA	16.77 6855 2	NA	NA	15.66 7678 6	16.67 2830 4	NA
NM_00836 0	Il18	Interleukin 18	0.0546264	1.433 462283	0.1987 55685	0.846 33233 2	0.909 95391 6	1.335 0986	0.584 1806	1.094 0462	1.545 8234	1.834 9368	1.056 2018	2.493 8802	1.925 7836	2.154 3916	0.931 5356	0.971 1224	1.274 5466
NM_00880	Pdgfa	Platelet derived growth factor, alpha	-0.0560	6.653 06195	-0.1921	0.851 38986	0.909 95391	7.191 1226	6.319 0366	6.352 4622	6.171 4654	6.297 3168	6.140 0998	7.136 6162	7.061 6176	7.472 6136	6.852 3856	6.057 3784	6.784 6286

8			76267		23806	8	6												
NM_0 0882 7	Pgf	Placental growth factor	- 0.0539 276	9.671 74061 7	- 0.1472 71693	0.885 76783 7	0.933 64718	10.57 6232 6	9.684 7136	9.949 5492	9.001 6854	8.974 2118	9.160 7038	9.411 5592	9.688 6466	9.564 8726	10.83 2275 6	9.970 8834	9.245 5536
NM_1 7340 4	Bm p3	Bone morphogenetic protein 3	0.0244 50067	6.965 81628 3	0.0746 84889	0.941 89975 4	0.979 57574 4	6.957 0366	6.140 5106	7.254 0622	7.643 5534	7.699 0748	7.981 6638	6.032 8112	7.051 6706	6.404 4526	6.852 2316	6.613 2294	6.959 4986
NM_0 0800 6	Fgf 2	Fibroblast growth factor 2	0.0136 84067	8.787 76095	0.0390 68933	0.969 58426 3	0.995 09963 8	10.18 8341 6	9.203 5826	9.171 1342	7.471 4824	7.573 7088	8.400 6138	8.059 7152	8.406 7146	8.373 7276	9.642 2596	9.102 9214	9.858 9296
NM_0 0835 0	Il11	Interleukin 11	0.0018 83067	11.42 74974 5	0.0034 65724	0.997 30113 6	0.997 30113 6	13.48 1435 6	12.04 6293 6	11.69 7871 2	10.84 5372 4	9.635 6288	10.97 1717 8	9.698 2872	11.17 4472 6	10.34 7640 6	12.81 9888 6	12.22 9299 4	12.18 2061 6
NM_0 5300 9	Zfp 91	Zinc finger protein 91	0.0029 204	2.985 7062	0.0158 19081	0.987 68173 9	0.997 30113 6	3.198 2956	2.673 8356	2.985 2802	3.425 2724	3.391 9728	3.186 3918	2.692 4792	2.718 2496	2.690 5246	2.879 3976	3.085 9634	2.900 8116
NM_0 0975 6	Bm p10	Bone morphogenetic protein 10	NA	14.33 55976	NA	NA	NA	NA	NA	NA	NA	NA	14.21 5459 8	NA	NA	NA	NA	14.45 5735 4	NA
NM_0 1020 4	Fgf 6	Fibroblast growth factor 6	NA	17.35 00847	NA	NA	NA	NA	NA	NA	NA	NA	19.97 0029 8	NA	NA	NA	NA	NA	14.73 0139 6

NM_008366	Il2	Interleukin 2	NA	14.6125763	NA	NA	NA	NA	NA	14.433942	NA	13.597968	13.724148	14.910197	15.773966	15.235248	NA	NA	NA
NM_010556	Il3	Interleukin 3	NA	14.3433715 2	NA	NA	NA	NA	NA	14.523127 2	15.194874 4	14.702956 8	14.536383 8	NA	NA	NA	NA	12.759515 4	NA
NM_008493	Lep	Leptin	NA	19.7642197	NA	NA	NA	NA	NA	NA	NA	19.096516 8	NA	NA	20.431922 6	NA	NA	NA	NA
NM_010834	Mstn	Myostatin	NA	15.6276996	NA	NA	NA	NA	16.311700 6	NA	NA	NA	NA	NA	NA	NA	NA	NA	14.943698 6

Chapter III: Genome Toxicity and Impaired Stem Cell Function After Conditional Activation of CreER^{T2} in the Intestine[3]

3.1 Summary

With the tamoxifen-inducible CreER^{T2} system, genetic recombination can be temporally controlled in a cell-type-specific manner in intact animals, permitting dissection of the molecular underpinnings of mammalian physiology. Here we present a significant drawback to CreER^{T2} technology for analysis of intestinal stem cells. Using the intestine-specific *Villin-CreER^{T2}* mouse strain, we observed delayed intestinal regeneration post irradiation. *Villin-CreER^{T2}* activation was associated with DNA damage and cryptic *loxP* site cleavage. Analysis of stem cell-specific CreER^{T2} strains showed that the genome toxicity impairs function of crypt base columnar stem cells, resulting in loss of organoid initiating activity. Importantly, the stem cell impairment is short-lived, with return to normal by 7 days post tamoxifen treatment. Our findings demonstrate that mouse genetic experiments that utilize CreER^{T2} should consider the confounding effects of

[3] Note this chapter is adapted from the following published article:
Bohin, N., Carlson, E. A., Samuelson, L. C. Genome Toxicity and Impaired Stem Cell Function After Conditional Activation of CreERT2 in the Intestine. *Stem Cell Reports*. (2018).[354]

enhanced stem cell sensitivity to genome toxicity resulting from CreER^{T2} activation.

3.2 Introduction

The Cre-*lox*P system is a powerful genome editing tool that revolutionized *in vivo* genetic studies. The site-specific Cre recombinase catalyzes recombination between two 34-bp *lox*P DNA recognition sites to induce deletion or activation of target transgenes.[1] The adaptation of this system from its bacteriophage origin requires that Cre and *lox*P be engineered into the mouse genome. Since the mouse genome does not contain *lox*P sites, recombination is designed to be specific to the engineered target construct.

One advance to the Cre-*lox*P system was the development of inducible Cre by fusion with a mutated ligand-binding domain of the estrogen receptor (ER).[2] The CreER recombinases (e.g. CreER^{T2}) are activated by the estrogen receptor antagonist tamoxifen (TX), which allows temporal control of target gene rearrangement. In the absence of TX, CreER is cytoplasmic. TX binding induces CreER transfer into the nucleus to catalyze recombination between *lox*P sites. The recombined allele is a permanent genetic change. Thus, this system has been a powerful tool to study adult stem cell function. In particular, there are numerous CreER mouse strains used to study intestinal stem cells (ISC), including *Villin-CreER^{T2}*,[3] which is expressed throughout the intestinal epithelium, including stem and progenitor cells, and ISC specific *Olfm4-CreER^{T2}* [4] and *Lgr5-CreER^{T2}*.[5]

Off-target recombination has been observed at cryptic *lox*P (*clox*P) sites,

which have DNA sequence similarity to *lox*P.[6] The consequences of illegitimate Cre recombination vary from cellular toxicity to overt developmental and pathological defects. Cre expression in developing spermatids led to male sterility due to genomic rearrangements,[7] and widespread developmental defects occurred after TX activation of CreER^{T2} during embryonic development.[8] CreER^{T2} genotoxicity in proliferating adult tissues has also been described, with TX-activated CreER^{T2} causing epithelial atrophy and metaplasia in stomach,[9] and chromosomal rearrangements in immature hematopoietic cells.[10] These reports suggest that proliferating stem and progenitor cells may be particularly sensitive to Cre-mediated genotoxicity, although this has not been tested in most adult stem cell populations.

One of the most proliferative adult tissues is the intestine, where adult stem cells fuel rapid epithelial cell turnover. Whether off-target DNA cleavage and genotoxicity are an issue for ISC Cre drivers has not been reported. In this study we observed functional ISC defects following TX-induction of CreER^{T2} in the mouse intestine. Whole body γ-irradiation subsequent to *Villin-CreER^{T2}* activation resulted in delayed intestinal regeneration. ISC defects were demonstrated by impaired organoid-forming efficiency. Our findings suggest that the flood of TX-activated CreER^{T2} into the nucleus leads to cleavage at c*lox*P sites and DNA double stranded breaks (DSBs), which impair ISC function. Thus, this study holds significant implications for experiments studying intestinal homeostasis and regeneration in mouse genetic models to mitigate CreER^{T2} toxicity in ISCs.

3.3 Experimental Procedures

3.3.1 Mice

Mouse use was approved by the Institutional Animal Care & Use Committee at the University of Michigan. Mice were housed in ventilated and automated watering cages with a 12-hour light/dark cycle under specific pathogen-free conditions. The following mouse strains were employed: *Villin-CreER^{T2}*,[3] *Villin-Cre*,[11] *Olfm4-ires-EGFP-CreER^{T2}* (gift from Dr. Hans Clevers),[4] *Lgr5-EGFP-ires-CreER^{T2}* (JAX strain 008875),[12] *HopX-CreER^{T2}* (JAX strain 017606).[13] Mice were maintained on a C57BL/6 strain background. Mice of both sexes aged 1.5-4 months were used. To activate CreER^{T2}-mediated recombination, mice were injected intraperitoneally with TX (Sigma; 50 or 100 mg/kg; 10 mg/mL in 5% ethanol and 95% corn oil) or VEH (5% ethanol, 95% corn oil) once per day for 1 or 5 days, and tissue was collected as indicated. To induce intestinal injury, mice were exposed to 1 dose of 12 Gy whole-body irradiation from a ^{137}Cs source. Animals were injected intraperitoneally with 5-ethynyl-2'-deoxyuridine (EdU; 25 mg/kg; Life Technologies) 2h prior to tissue collection.

3.3.2 Tissue Collection

Intestinal tissue was harvested following *ad libitum* feeding and fixed in 4% paraformaldehyde in 1X PBS overnight before paraffin processing, as previously described, or flash frozen for subsequent DNA extraction or protein extraction as

previously described,[14] and as illustrated in **Figure 2.1**. Intestinal crypts were harvested from duodenum, as previously described.[15]

3.3.3 Organoid Culture

Mouse intestinal organoid cultures were established from duodenal crypts and maintained as described,[16] with modifications. Longitudinally opened 6 cm of proximal intestinal tissue was washed in ice cold DPBS (Gibco), with antibiotics penicillin-streptomycin (1X) and gentamycin (1X; Gibco) for 20 min, cut into 1 cm pieces, and incubated in 15 mM EDTA in DPBS with antibiotics for 35 min at 4°C on a rocking platform. Tissue was vortexed for 2 min., and the solution was passed through a 70-µm filter. Crypts were gravity settled for 10min, the supernatant was decanted, the remaining pellet was resuspended in 1X DPBS with antibiotics, and centrifuged at 150x*g* for 10 min. The resulting crypt pellet was resuspended in complete culture media [50% L-WRN-conditioned media,[17] 20% fetal bovine serum (Atlas Biologicals), antibiotics, 2 mM L- glutamine (Gibco), 1X Fungizone (Gibco) and Y- 27632 (10 µM; Tocris) in advanced DMEM/F12 (Gibco)]. To test organoid formation efficiency, 600 crypts (extrapolated by determining crypt number per µL by counting crypts from a 5 µL droplet of crypt suspension) were mixed with 120 µL Matrigel (BD Biosciences), and 40 µL aliquots were plated in pre-warmed 24-well plates. After 30 min at 37°C, 500 µL complete culture media was overlaid. Culture media without Y-27632 was replaced every other day. The efficiency of organoid formation was determined by counting organoids at 3 days following plating, and normalizing to the number of plated crypts.

3.3.4 Western Blot Analysis

Isolated duodenal crypts were lysed in RIPA buffer (Thermo, 89900) containing protease and phosphatase inhibitor cocktail (Thermo, 78440). Cell lysates (40 µg protein) were mixed with NuPAGE LDS Sample Buffer (Thermo, NP0007) and separated by sodium dodecyl sulfate polyacrylamide gel electrophoresis using NuPAGE MOPS SDS Running Buffer (Thermo, NP0001) and NuPAGE 4-12% Bis-Tris gels (Thermo, NP0335), following manufacturer recommendations. Protein transfer onto 0.45µm pore size nitrocellulose membrane (GE Healthcare) at 100V for 45 min preceded blocking in Odyssey Blocking Buffer (Li-COR, 927-40000) for 1 hour at room temperature. Immunoblotting with rabbit α-γ-H2AX (1:50, Cell Signaling), rabbit α-cleaved caspase 3 (1:500, Cell Signaling), and mouse α-GAPDH (1:10,000, Thermo Scientific) was performed on a rocking platform overnight at 4°C. IRDye 800CW Goat α-rabbit (1:10,000, LI-COR 925-32211) and IRDye 680RD Goat α-mouse (1:10,000, LI-COR 925- 68070) secondary antibodies were used to visualize probed proteins. Membrane was scanned on an Odyssey Imager (LI-COR). Western blot analysis was performed using the free Image Studio Lite software (LI-COR).

3.3.5 Immunohistochemistry

Duodenal paraffin sections (5µm) were stained with H&E to analyze intestinal morphology. Villus height was determined by measuring from the tip of intact villi to the top shoulder of adjacent crypts using ImageJ software (1.52a;

Wayne Rasband, National Institutes of Health). Immunostaining with rabbit α-Ki67 (1:200, Thermo), and rabbit α-γ-H2AX (1:50, Cell Signaling) was performed as described.[18] A goat anti-rabbit IgG Alexa Fluor 488 polyclonal secondary antibody was used (1:400, Invitrogen). EdU-Click-it kit (Life Technologies) was used to identify proliferating cells. The number of EdU-positive cells was counted from well-oriented crypts, identified from images obtained from adjacent H&E-stained sections. Regeneration was assessed using the adapted crypt microcolony survival assay method.[19] Regenerating crypts were measured as the number of well-oriented crypts with 4 or more EdU-positive cells divided by the total number of well-oriented crypts. Images were captured on a Nikon E800 microscope with Olympus DP controller software, except for γ-H2AX-immunostained images, which were captured on a Leica SP5 inverted confocal microscope with Leica software.

3.3.6 Gene integrity analysis

For quantification of *clox*P amplification, DNA from duodenal crypts was extracted using the Easy-DNA kit (Invitrogen, K1800-01). Quantitative polymerase chain reaction was performed as previously described,[18] using 40ng DNA and *clox*P primers with sequences: GGT CTG AGC TAT ACT TAC AAA GGT (forward) and GCT ATC ACA ATG GTG GTC CG (reverse), which yielded a 300 bp amplified product size. Assays for each sample were run in triplicate and normalized to *Gapdh* as an internal control, with primer sequences: TCA AGA AGG TGG TGA AGC AGG (forward) and TAT TAT GGG GGT CTG GGA TGG (reverse), which yielded a 350 bp amplified product size.

3.3.7 Statistical analysis

All experiments were performed with at least 3 biological replicates per group. Quantitative data are presented as mean ± SEM. Comparisons between 2 groups were conducted with unpaired two-tailed Student *t* tests using the Prism software (Graphpad). Significance is reported as * (P<0.05), **(P<0.01), ***(P<0.001), and #(P<0.0001).

3.4 Results

3.4.1 Impaired intestinal regeneration in Villin-CreER^{T2} mice

We tested the effect of *Villin-CreER^{T2}* on ISC function after treatment with TX (100 mg/kg) or vehicle (VEH). Histological analysis did not reveal any gross intestinal changes induced by TX treatment; tissue architecture and cellular proliferation did not differ from controls (**Figure 3.1**). However, marked differences were observed between TX- and VEH-treated *Villin-CreER^{T2}* mice after challenge with 12 Gy irradiation (**Figure 3.2**). TX-treated mice had a more pronounced post-irradiation weight loss compared to controls (**Figure 3.2A**) and histological analysis showed more extensive intestinal damage (**Figure 3.2B-O**). 3 days post-irradiation (DPI), the intestines of VEH-treated mice began to recover with a typical regenerative response, characterized by expanded crypts and increased proliferation (**Figure 3.2B,E**). In contrast, TX-treated mice had extensive decellularized crypts and very few, small crypt structures (**Figure 1C**). We also observed decreased proliferation and fewer regenerating crypts in the TX group

(**Figure 3.2G,H**). At 5 DPI, the villi of TX-treated *Villin-CreER^{T2}* mice were blunted, consistent with impaired regeneration at 3 DPI (**Figure 3.2I-K**). However, crypts at this time point were undergoing robust regeneration, similar to control (**Figure 3.2L-O**). Thus, TX-activation of *Villin-CreER^{T2}* results in delayed intestinal regeneration, consistent with enhanced damage following 12 Gy irradiation.

3.4.2 Impaired organoid formation after Villin-CreER^{T2} activation

To understand the basis for the altered response of *Villin-CreER^{T2}* mice to irradiation, we tested if CreER^{T2} activation affects ISC function by measuring organoid forming efficiency in unirradiated, treated mice. Duodenal crypts were isolated from TX- or VEH-treated mice 1 day post-treatment, and cultured under conditions that support ISC growth (**Figure 3.2P**). While crypts isolated from VEH-treated mice grew into typical spheroids by 3 days in culture, crypts isolated from TX-treated *Villin-CreER^{T2}* mice exhibited very poor organoid growth (**Figure 3.2Q-R**). Quantification showed that 25-fold fewer organoids grew in cultures initiated from TX-treated mice than VEH-treated mice (**Figure 3.2S**). The extreme loss of organoid forming activity in TX-activated *Villin-CreER^{T2}* mice suggests impaired ISC function.

3.4.3 Impaired ISC function is not due to tamoxifen toxicity

We tested whether the delayed regenerative response to irradiation and the impaired organoid forming efficiency were due to TX toxicity, which has been

observed in other studies.[20,21] Irradiated, nontransgenic C57BL/6 mice treated with TX or VEH had similar changes to body weight and intestinal histology, including villus height, proliferation rate, and crypt regeneration (**Figure 3.3A-H**). Further, TUNEL staining and organoid forming efficiency did not differ between the two groups (**Figure 3.3I-K**). These data showed that toxicity caused by TX treatment of *Villin-CreER^{T2}* mice was not a direct effect of TX.

Next, we determined whether the TX effect on Cre recombinase was independent of CreER-mediated nuclear translocation. We treated *Villin-Cre* mice, which exhibit constitutive Cre expression in intestinal epithelial cells [11], with TX or VEH, followed by 12 Gy irradiation. In contrast to the response in *Villin-CreER^{T2}* mice, we saw no heightened sensitivity to irradiation in TX-treated *Villin-Cre* mice (**Figure 3.3L-S**). Further, there was no change in TUNEL staining or organoid forming efficiency (**Figure 3.3T-V**). Notably, these transgenic strains express similar amounts of Cre protein, so the toxicity is not due to higher levels of Cre recombinase expression in *Villin-CreER^{T2}* mice (**Figure 3.3W**). Together these results support the conclusion that TX-activation of *Villin-CreER^{T2}* mediates impaired intestinal regeneration and organoid formation, and not TX toxicity, or interactions between TX and constitutively active Cre recombinase.

3.4.4 Impaired organoid formation after CreER^{T2} activation in ISCs

Heightened sensitivity to radiation and impaired organoid forming capacity of *Villin-CreER^{T2}* mice after TX treatment suggested that CreER activation induced

stem cell damage. We tested ISC-specific CreER^{T2} mouse strains that target crypt base columnar (CBC) ISCs, including *Olfm4-CreER^{T2}* and *Lgr5-CreER^{T2}*. Similar to our findings with *Villin-CreER^{T2}* mice, TX-treated *Olfm4-CreER^{T2}* mice had normal intestinal histology and proliferation under basal conditions (**Figure 3.1F-J**). In contrast to the delayed regenerative response in TX-treated *Villin-CreER^{T2}* mice, we observed normal responses to irradiation in TX-treated *Olfm4-CreER^{T2}* and *Lgr5-CreER^{T2}* mice, with cellular proliferation and crypt regeneration at 3 DPI similar to VEH-treated controls (**Figure 3.4A-B, D-E** and **Figure 3.5A-F**). However, organoid forming activity was reduced in both strains after TX treatment, similar to *Villin-CreER^{T2}* (**Figure 3.4G-H, J-K**). TX treatment resulted in 10-fold fewer organoids in *Olfm4-CreER^{T2}* and 2-fold fewer organoids in *Lgr5-CreER^{T2}* (**Figure 3.4M-N**). The results suggest that actively cycling, CBC ISCs are sensitive to CreER^{T2} activation, leading to impaired ISC function.

We also tested one CreER strain that targets a facultative stem cell (FSC) population, *HopX-CreER^{T2}*.[13] The expression of this Cre driver is limited to very few cells in the crypt, which can participate in crypt regeneration after γ-irradiation.[22] In contrast to toxicity observed after TX activation of CreER^{T2} in CBCs, the response to radiation, and organoid forming ability were unchanged in *HopX-CreER^{T2}* mice (**Figure 3.4C,F,I,L,O** and **Figure 3.5G-I**).

3.4.5 CreER^{T2} activates DNA cleavage at cryptic loxP sites

We next considered the mechanism by which CreER^{T2} activation leads to impaired ISC function. We posited that TX-mediated CreER^{T2} nuclear translocation

induces DNA cleavage. To test this, we performed western blotting for γ-H2AX, which marks DNA DSBs [23] and observed a 3-fold increase in the crypts of TX-treated *Villin-CreER^{T2}* mice compared to controls (**Figure 3.6A,B**). Analysis of C57BL/6 mice showed no differences in γ-H2AX levels between TX- and VEH-treated mice, again demonstrating that the effect is due to activation of CreER^{T2} and not to TX toxicity (**Figure 3.6D,E**). We also saw increased γ-H2AX staining in cells at the crypt base (**Figure 3.6G**). In agreement, TUNEL staining mirrored the γ-H2AX results, demonstrating increased DNA damage (**Figure 3.6I**).

To determine whether TX-treated *Villin-CreER^{T2}* mice exhibited DNA damage-induced programmed cell death, we immunoblotted for the apoptotic marker cleaved caspase 3 and found levels to be unchanged in both TX-treated *Villin-CreER^{T2}* and C57BL/6 mice (**Figure 3.6A,C,D,F**). We also confirmed these results by quantifying the number of cleaved caspase 3-positive cells per crypt in tissue sections, showing that induction of DSBs did not induce apoptosis (**Figure 3.6H**). The findings suggest that *Villin-CreER^{T2}* activation results in increased DNA cleavage without inducing apoptosis. This agrees with our results showing no obvious histological changes to the duodenum following TX activation under basal conditions (**Figure 3.1A-E**).

We tested whether activated CreER^{T2} might induce DNA damage by inappropriately targeting regions in the mouse genome with sequence similarity to *lox*P. We designed real-time qPCR primers around the locus of a c*lox*P site (accession number AF033025) previously reported to serve as an active site for Cre recombinase.[6] We assessed the integrity of this genomic region following

CreER^{T2} activation by comparing amplification from crypt cell DNA isolated from TX- and VEH-treated *Villin-CreER^{T2}* mice (**Figure 3.6J**). Real-time qPCR analysis revealed that TX-treated duodenal *Villin-CreER^{T2}* crypt DNA had reduced amplification of this genomic region compared to VEH-treated controls, indicating reduced concentration of this *clox*P site in the genome (**Figure 3.6K**). These results demonstrate that TX-mediated translocation of CreER^{T2} to the nucleus is associated with illegitimate DNA cleavage at a c*lox*P site.

3.4.6 Resolution of CreER^{T2}-induced ISC genotoxicity

Understanding the value of the inducible *Villin-CreER^{T2}* mouse strain for genetic analysis of mammalian ISC function, we investigated 3 methods to minimize ISC toxicity. The first, termed “delayed", involved postponing intestinal challenge for 1 week after the final TX injection (**Figure 3.7A-J**). Analysis of body weight after irradiation showed similar profiles in TX- and VEH-treated mice (**Figure 3.7A**). Analysis of intestinal regeneration at 3 and 5 DPI revealed no changes to intestinal histology, including cellular proliferation, crypt regeneration and villus height (**Figure 3.7B-J**).

Further evidence in support of a delay resolving the *Villin-CreER^{T2}* genotoxicity was shown by normal levels of γ-H2AX and cleaved caspase 3 in the duodenal crypts of *Villin-CreER^{T2}* mice isolated 7 days following the final TX or VEH injection (**Figure 3.7K-M**). Similarly, crypt DNA isolated from TX-treated *Villin-CreER^{T2}* mice 7 days following the final injection had normal c*lox*P amplification (**Figure 3.7N**). Further, TUNEL-labeling was similar between VEH-

and TX-treated *Villin-CreER^{T2}* animals with delay (**Figure 3.7O**). Finally, duodenal crypts isolated 7 days following treatment showed normal organoid forming efficiency (**Figure 3.7P**). Similar findings were observed for the CBC-specific *Olfm4-CreER^{T2}* mouse (**Figure 3.8E-H**; compare **Figure 3.8D** to **Figure 3.4M**).

We investigated 2 additional methods of administering TX: daily administration of a lower TX dose (50mg/kg) over 5 days (5x50; **Figure 3.7Q-R**), and administration of a single 100mg/kg dose of TX (1x100; **Figure 3.7S-T**), with tissue harvest 1d later. The results revealed a modest increase in DSBs, as observed by TUNEL staining, in the 5x50 experimental paradigm (**Figure 3.7Q**) together with a significant decrease in organoid forming efficiency (**Figure 3.7R**). In contrast, we did not observe TX-mediated CreER^{T2} toxicity in the 1x100 experiment (**Figure 3.7S-T**). Thus, we have shown that genotoxicity is dose- and time-dependent, and identified 2 methods that minimize damage by reducing the TX dose (1x100) or building in a delay after TX treatment.

3.5 Discussion

Our study shows that intestine-specific CreER^{T2} drivers promote illegitimate DNA cleavage events at c*lox*P sites and markedly diminish CBC ISC function. TX activation of the widely used *Villin-CreER^{T2}* resulted in delayed crypt regeneration after epithelial cell damage induced by γ-irradiation. The intestine normally has a remarkable regenerative capacity, with ISC replacement and crypt repair completed within a week after almost complete elimination of the proliferating crypt compartment with 12 Gy whole-body γ-irradiation.[24] TX-treated *Villin-CreER^{T2}*

mice exhibited enhanced weight loss and a delay in crypt regeneration after irradiation, in comparison to VEH-treated *Villin-CreER^{T2}* controls. The regenerative defect suggested a mechanism of ISC toxicity, which was confirmed by loss of organoid-forming activity in TX-treated CreER^{T2} mouse strains (**Figure 3.9**). Impaired organoid formation was observed in *Villin-CreER^{T2}* mice, a strain with broad CreER^{T2} expression in all intestinal epithelial cells, as well as 2 strains with expression limited to CBC ISCs, *Olfm4-CreER^{T2}* and *Lgr5-CreER^{T2}*. These CreER^{T2} driver strains have been extensively used for studies of ISC function, including analysis of mechanisms regulating crypt regeneration after irradiation injury, and ISC activity by measurement of organoid forming potential. A review of the literature suggests that this is the first report of CBC stem cell toxicity resulting from Cre-mediated genotoxicity.

While we observed changes to both crypt regeneration and organoid forming efficiency in TX-treated *Villin-CreER^{T2}* mice, we were surprised that TX-treated *Olfm4-CreER^{T2}* and *Lgr5-CreER^{T2}* mice had impaired organoid forming efficiency but normal regenerative responses. Administration of γ-irradiation doses above 10 Gy has been shown to induce loss of CBC ISCs through apoptosis.[25,26] Normal regeneration in *Olfm4-CreER^{T2}* and *Lgr5-CreER^{T2}* mice suggests that the effect observed in *Villin-CreER^{T2}* animals may not be solely caused by CreER^{T2} activation in CBCs. Rather, the delayed regenerative response could be a result of CreER^{T2}-induced damage to FSCs, which are mobilized to repair the crypts following CBC loss.[13,27–29] FSCs are also thought to contribute to organoid formation. This led to our analysis of the *HopX-CreER^{T2}* mouse strain, which

activates CreER^{T2} in a small subset of FSCs.[13] This strain showed no effect on intestinal regeneration or organoid formation following TX administration. This may reflect the small number of crypt cells targeted by *HopX-CreER^{T2}*. A rigorous interrogation of CreER^{T2} mouse strains with different coverage of FSCs may be warranted (e.g. *Bmi1-CreER^{T2}*, *Sox9-CreER^{T2}*). An additional possibility for our *Hopx-CreER^{T2}* results may be the different sensitivities of CreER^{T2} activation in FSCs vs. CBC stem cell populations. The susceptibility of various crypt cell populations to CreER^{T2}-induced genotoxicity warrants further study.

The *Villin-CreER^{T2}* and *Lgr5-CreER^{T2}* mouse strains are commonly used, with hundreds of published studies employing these Cre drivers to manipulate genes for analysis of intestinal development, physiology and pathophysiology. In particular, these strains have been important to study ISC function. The genotoxicity and ISC defects uncovered in our study are a serious consideration for studies that employ these, or other Cre drivers, expressed in the intestinal crypt.

Mouse studies using Cre recombinase have become a mainstay for analysis of gene function *in vivo*. It is commonly assumed that Cre activation per se does not induce adverse events. However, Cre-mediated cellular toxicity resulting from illegitimate DNA cleavage at c*lox*P sites has been previously observed in cultured cells and mouse tissues.[6,7,30,31] Cre-mediated genotoxicity appears to be dosage dependent, and proliferating cells seemingly exhibit enhanced sensitivity,[7,8,10,30] which would predict that proliferating stem and progenitor cells would be particularly sensitive to Cre-mediated toxicity. However,

few studies have examined adult stem cell toxicity after CreER^{T2} activation *in vivo*. Our finding of CreER^{T2}-induced ISC toxicity would prompt stem cell biologists studying other adult stem cell populations to be cautious when activating CreER^{T2} alleles. Careful experimental design must include the proper controls to rule out Cre-mediated genotoxicity as a potential cause of stem cell phenotypes induced in studies using CreER mouse strains.

3.6 Author Contributions

NB and LCS designed the project. NB and EAC performed experiments. NB and LCS interpreted data and wrote the manuscript, and EAC provided critical feedback.

3.7 Acknowledgements

We thank Dr. Ivan Maillard, whose insightful questions led to the conception of the project, Yasmine Abushukur and Theresa Keeley for technical help, Erin Collin for maintaining the mouse colony, and the Nusrat/Parkos lab for the gift of the *Villin-Cre* mice and for supplementing our *Villin-CreER^{T2}* mouse stores. NB was supported by the Cellular and Molecular Biology program, a Rackham research grant and the Benard L. Maas Fellowship. The research was funded by NIH R01-DK096972 to LCS, and Core support from the Michigan Gastrointestinal Research Center Grant NIH P30-DK34933. The authors have no conflicts of interest.

3.8 Figures

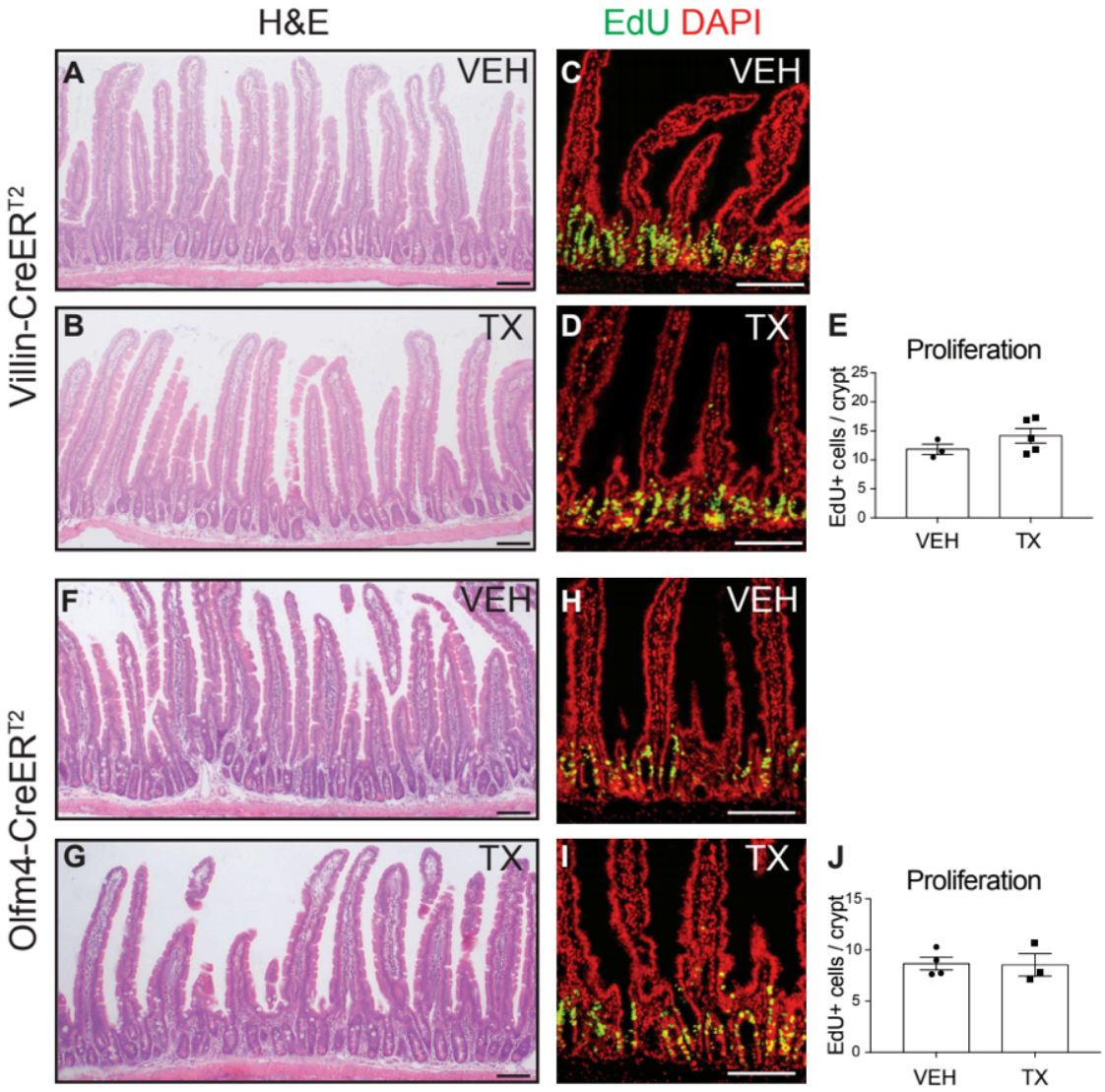

Figure 3.1 Normal intestinal histology in tamoxifen-treated *Villin-CreER^{T2}* and *Olfm4-CreER^{T2}* mice.

Villin-CreER^{T2} and *Olfm4-CreER^{T2}* mice were treated with tamoxifen (TX; 100 mg/kg) or vehicle (VEH) daily for 5 days, and intestinal tissue was collected 1 day following the final injection. Duodenal histology was assessed by (A-B, F-G) H&E staining. (C-E, H-J) Cellular proliferation was assessed by EdU incorporation. Proliferating cells are presented as the number of EdU-positive cells per crypt (mean +/- SEM, n=3-5 mice/group). Scale bars = 100μm.

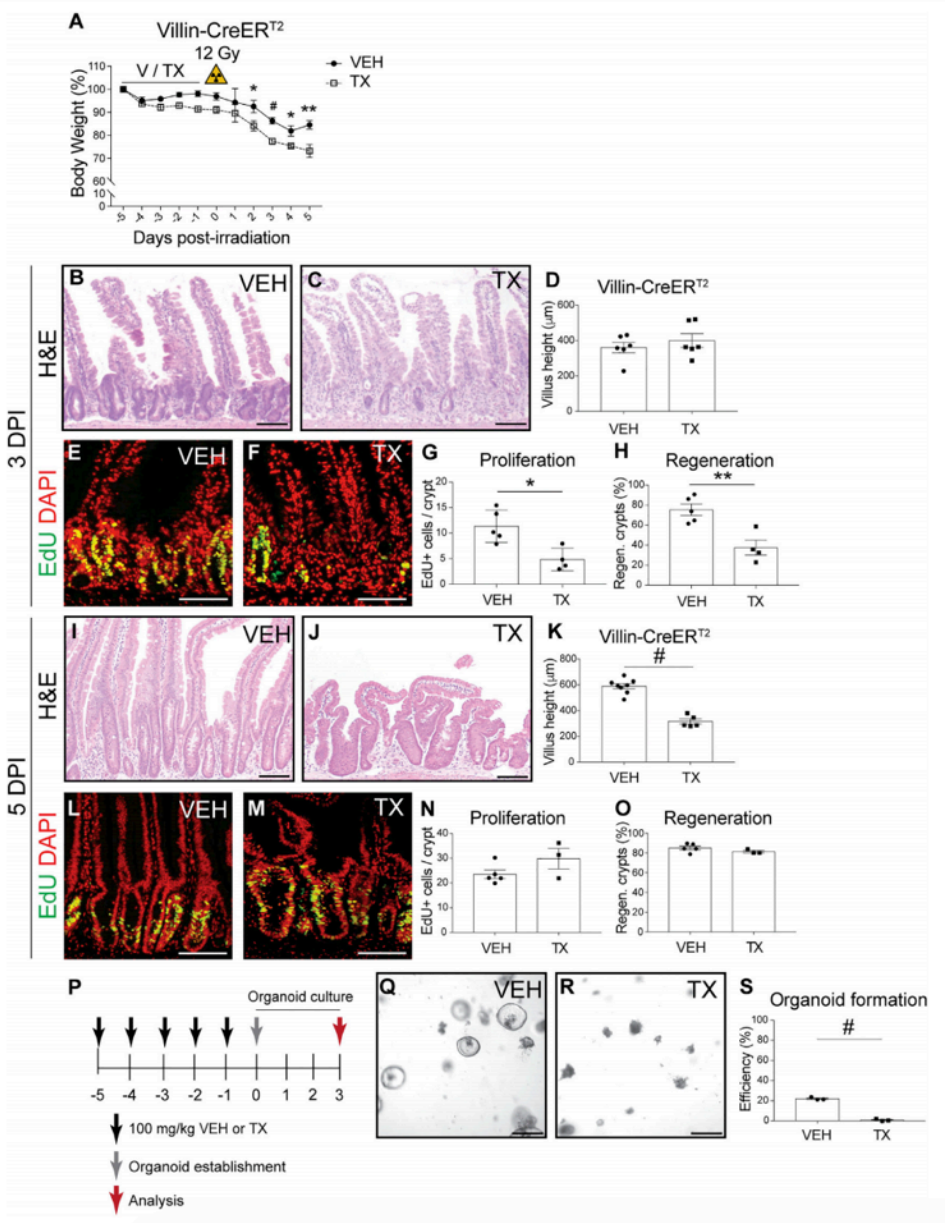

Figure 3.2 Impaired intestinal regeneration and organoid formation in tamoxifen-treated *Villin-CreER^{T2}* mice.

Villin-CreER^{T2} mice were treated with tamoxifen (TX; 100mg/kg) or vehicle (V; VEH) daily for 5 days, and 1 day later either (A-O) challenged with 12 Gy γ-irradiation or (P-S) tested for organoid forming efficiency. (A) Mouse body weight relative to weight at the initiation of treatment (*n*=7-15 mice/group). (B-O) Duodenal crypt regeneration was assessed at (B-H) 3 days post irradiation (DPI), and (I-O) 5 DPI by (B-C, I-J) H&E staining, and (E-F, L-M) EdU incorporation. (D, K) Villus height (*n*=5-8 mice/group), (G, N) cellular proliferation and (H, O) crypt regeneration were measured (*n*=4-5 mice/group). (P) Schematic of organoid formation assay to test stem cell activity in non-irradiated *Villin-CreER^{T2}* mice. Duodenal crypts were isolated from TX- or VEH-treated mice and plated in Matrigel to form organoids. (Q-R) Brightfield images of organoids 3 days post-establishment from crypts isolated from (Q) VEH-treated or (R) TX-treated *Villin-CreER^{T2}* mice. (S) Organoid forming efficiency was determined by counting organoid number and presented as percent of the number plated (*n*=3 mice/group with 3 technical replicates per mouse). Quantitative data are presented as mean +/- SEM (**P*<0.05, ***P*<0.01, $^{\#}$P<0.0001 TX vs. VEH by Student's *t*-test). Scale bars = 100μm (duodenum), 250μm (organoids).

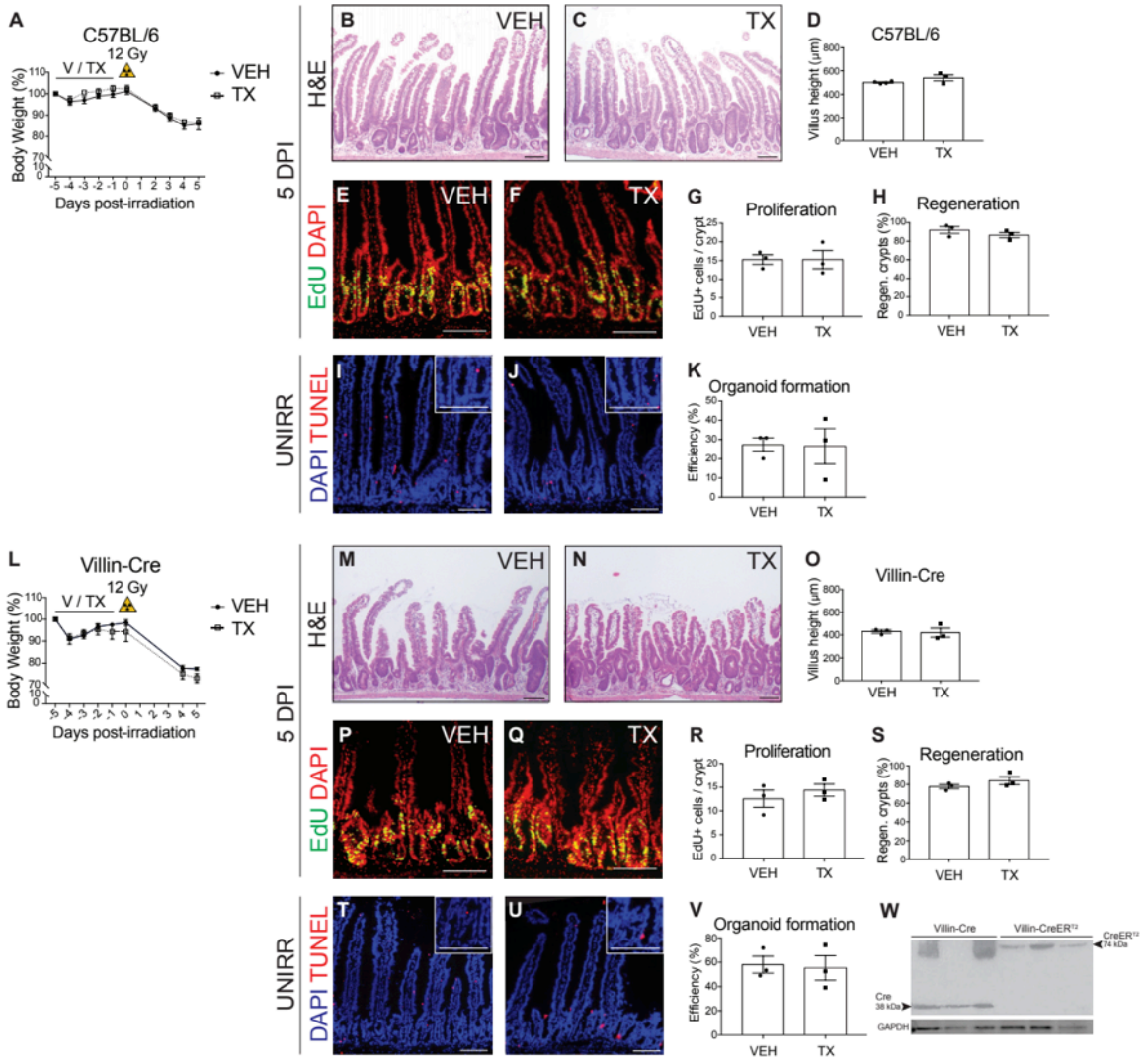

Figure 3.3 Normal intestinal regeneration and organoid formation in tamoxifen-treated C57BL/6 and *Villin-Cre* mice.

(A-H) C57BL/6 and (L-S) *Villin-Cre* mice were treated with TX or VEH daily for 5 days, irradiated (12Gy) 1 day later, and intestinal tissue was collected at 5 DPI. (A, L) Mouse body weight relative to weight at the initiation of treatment is presented as mean +/- SEM (n=3-6 mice/group). Duodenal crypt regeneration post-irradiation was assessed by (B-C, M-N) H&E staining and (E-F, P-Q) EdU incorporation. (D, O) Villus height measurements presented as mean +/- SEM (n=3-4 mice/group). (G, R) Proliferating cells are presented as the number of EdU-positive cells per crypt. (H, S) Regenerating crypts were defined as intact crypts with 4 or more EdU-positive cells and presented as percent of the total crypts. Quantitative data are presented as mean +/- SEM (n=3 mice/group). (I-J, T-U) TUNEL staining of unirradiated (UNIRR) TX- and VEH-treated C57BL/6 and *Villin-Cre* mice 24h following the last day of injection. (K, V) C57BL/6 and *Villin-Cre* duodenal crypts were isolated from UNIRR TX- or VEH-treated mice and plated (200 crypts/well) to form organoids. Organoid formation efficiency is presented as mean +/- SEM (n=3 mice/group with 3 technical replicates per mouse). (W) Western blot probing for Cre, and loading control GAPDH in duodenal crypt lysates of *Villin-Cre* and *Villin-CreER*^{T2} mice. Duodenum images scale bars = 100µm.

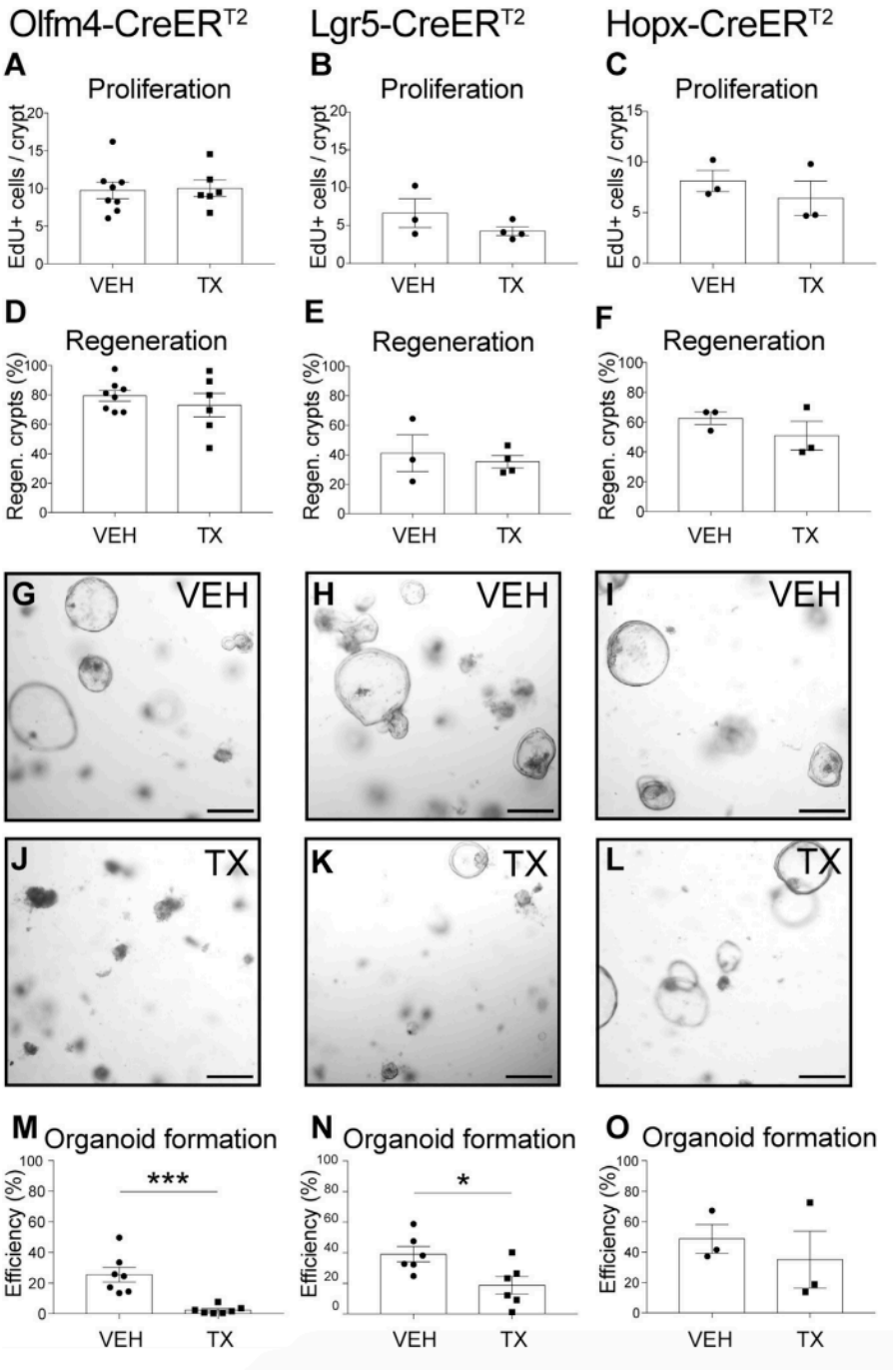

Figure 3.4 Reduced organoid forming efficiency after CreER^{T2} activation in intestinal stem cells.

Mouse strains with TX-inducible CreER^{T2} drivers specific for CBC (*Olfm4-CreER^{T2}* and *Lgr5-CreER^{T2}*) or facultative (*Hopx-CreER^{T2}*) ISCs were tested for (A-C) proliferation and (D-F) crypt regeneration after irradiation, or for (G-O) organoid forming efficiency in non-irradiated mice. (A-F) Mice were treated with TX or VEH daily for 5 days, irradiated a day later, and tissue was collected 3 DPI. (A-C) Cellular proliferation and (D-F) crypt regeneration were quantified (*n*=3-8 mice/group). (G-O) Organoids were established from duodenal crypts 1 day after TX- or VEH-treatment, imaged and counted at 3 days post establishment (*n*=3-7 mice/group with 3 technical replicates per mouse). Quantitative data are presented as mean +/- SEM (**P*<0.05, ****P*<0.001 TX vs. VEH by Student's *t*-test).

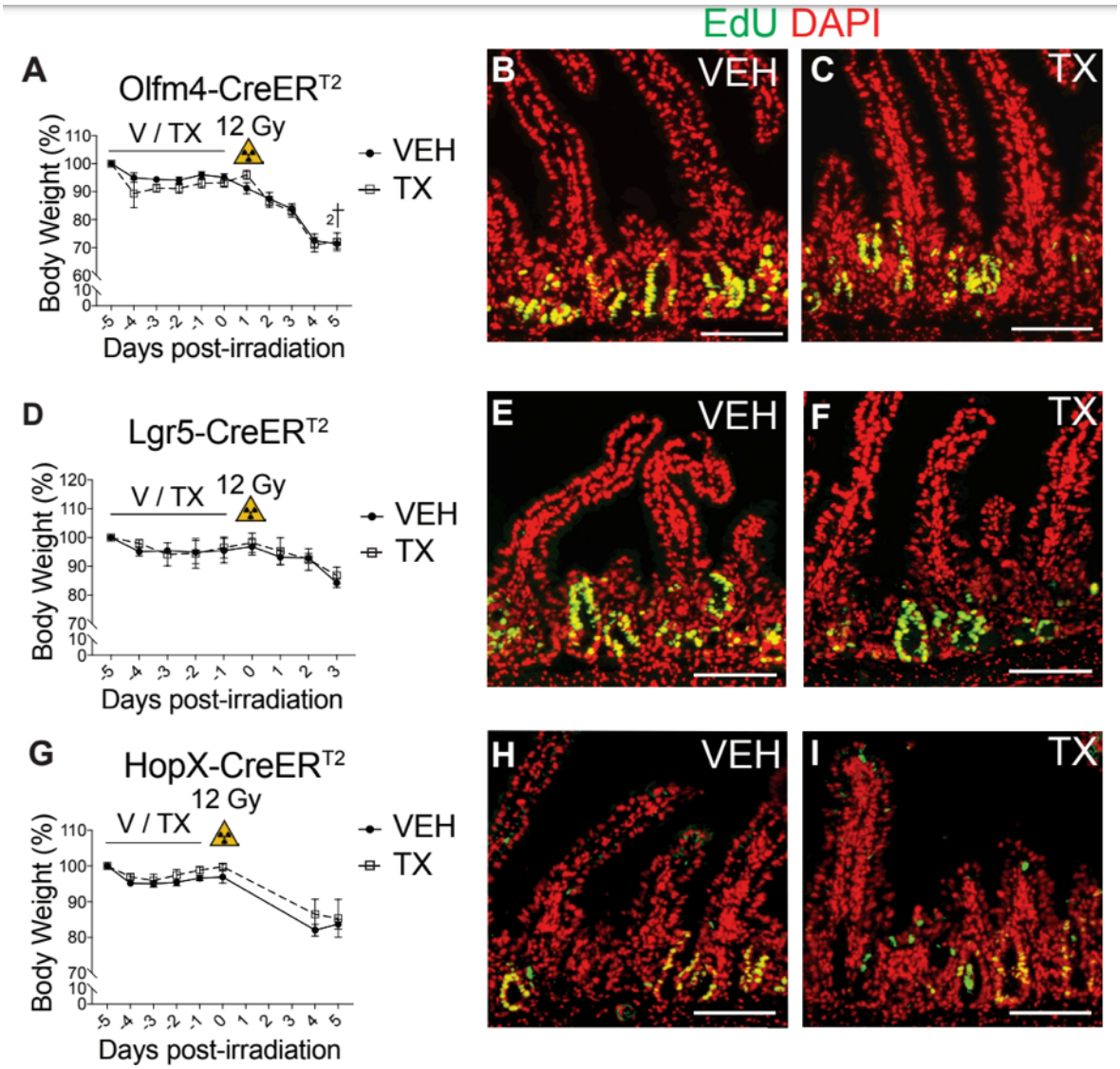

Figure 3.5 Normal post-irradiation regenerative responses after CreER^{T2} activation in intestinal stem cells.

Mouse strains with TX-inducible CreER^{T2} drivers specific for active (*Olfm4-CreER^{T2}* and *Lgr5-CreER^{T2}*) or facultative (*HopX-CreER^{T2}*) intestinal stem cells were treated with TX or VEH daily for 5 days, irradiated (12Gy) 1 day later and tissue was collected at 3DPI. (A, D, G) Mouse body weight relative to weight at the initiation of treatment is presented as mean +/- SEM (n=3-14 mice/group). (B-C, E-F, H-I) Cellular proliferation was assessed by EdU incorporation (n=3-8). Scale bars = 100μm.

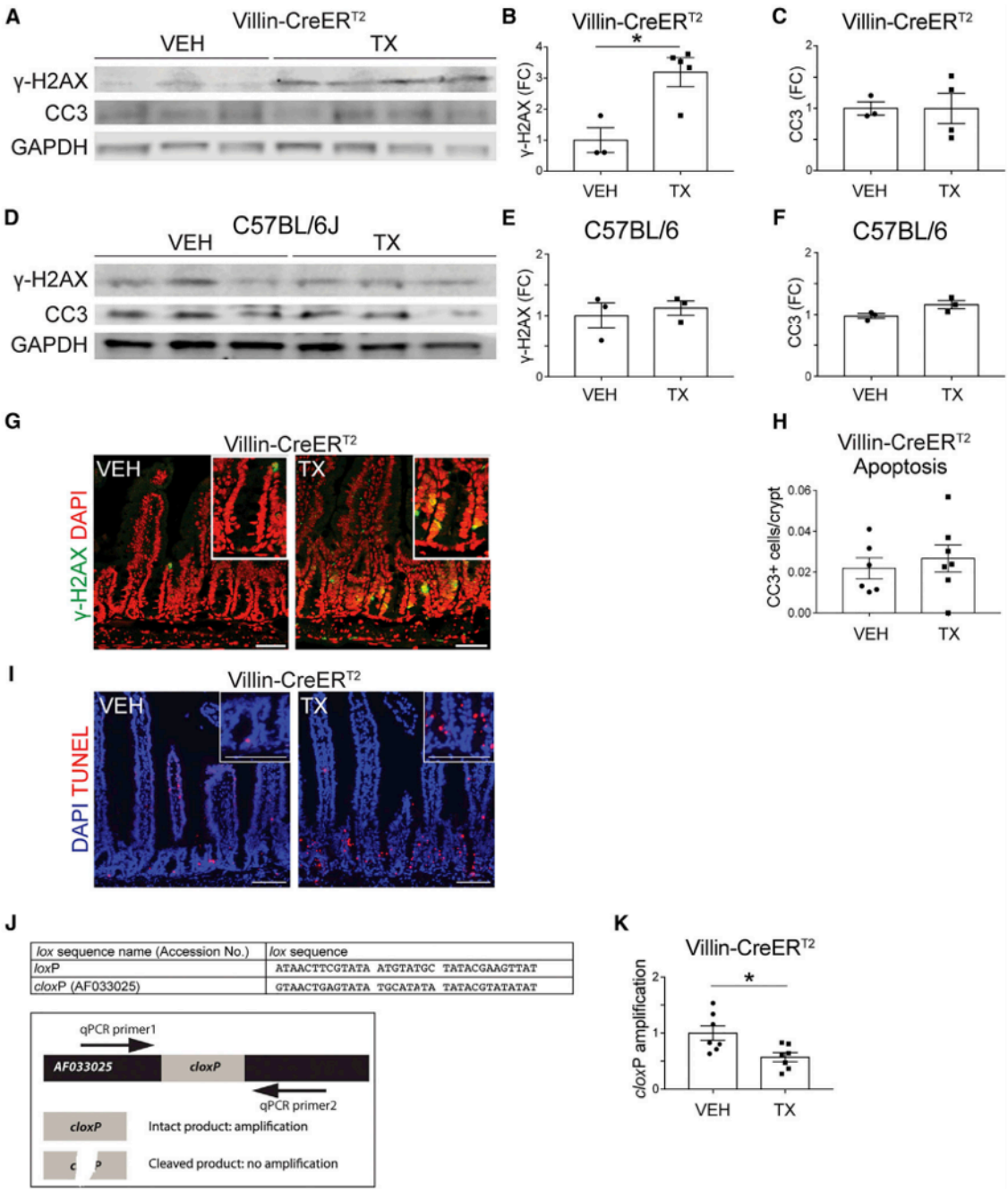

Figure 3.6 *Villin-CreER^{T2}* activation induces DNA cleavage at cryptic loxP sites.

Villin-CreER^{T2} or C57BL/6 mice were treated with VEH or TX daily for 5 days and intestinal crypts were collected 1 day following the last injection. (A, D) Western blots probing for γ-H2AX, cleaved caspase 3 (CC3), and loading control GAPDH were generated from duodenal crypt lysates prepared from (A) Villin-CreERT2 or (D) C57BL/6 mice treated with VEH or TX. (B-C, E-F) γ-H2AX and CC3 band signals were quantified and are displayed as means +/- SEM (*n*=3-4 mice/group; **P*<0.05 by Student's *t*-test). Immunofluorescent images of (G) γ-H2AX- and (I) TUNEL-stained VEH- or TX-treated *Villin-CreER^{T2}* duodenum at 1 day post-treatment. (H) Quantified CC3-positive cells per crypt from *Villin-CreER^{T2}* mice 1d post-treatment. (J) Known *lox*P sequence compared to the reported cryptic *lox*P (c*lox*P) AF033025 site (GenBank). Schematic of the qPCR assay designed to measure the amount of intact c*lox*P genomic DNA. (K) qPCR results from *clox*P assay normalized to *Gapdh* (*n*=3-6 mice/group; **P*<0.05, **P<0.01 by Student's *t*-test). Scale bars = 50 μm.

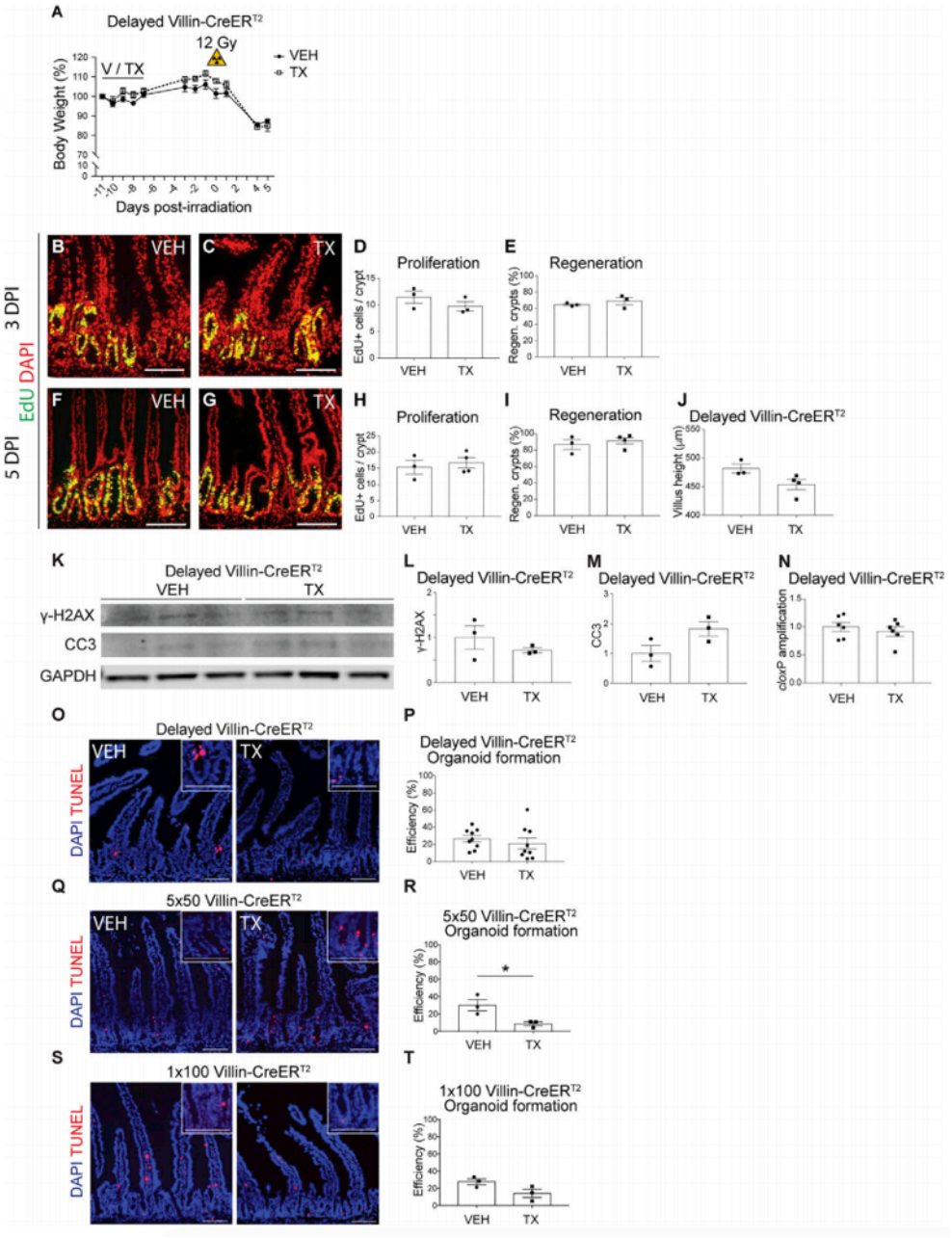

Figure 3.7 *Villin-CreER^{T2}* toxicity is mitigated by delay and reduced TX dose.

Body weight data from *Villin-CreER^{T2}* mice treated with VEH or TX daily for 5 days, followed by γ-irradiation after a 7-day delay (*n*=3-4 mice/group). (B-C, F-G) EdU-stained duodenal tissue sections at (B-C) 3DPI and (F-G) 5 DPI. (D, H) Proliferation, (E, I) regenerating crypts and (J) villus height were quantified. (K) Western blot analysis probing for γ-H2AX, CC3 and GAPDH, using duodenal crypt lysates from *Villin-CreER^{T2}* mice 7 days post-treatment. (L-M) γ-H2AX and CC3 band signal were quantified and displayed as mean +/- SEM (*n*=3 mice/group). (N) qPCR gene amplification of *clox*P normalized to *Gapdh* (*n*=6 mice/group). TUNEL staining of duodenum of non-irradiated (O) "delayed" VEH- or TX-treated *Villin-CreER^{T2}* mice, (Q) *Villin-CreER^{T2}* mice administered 5 daily doses of 50mg/kg TX and analyzed 1-day later (5x50), and (S) *Villin-CreER^{T2}* mice administered a single dose of 100mg/kg TX and analyzed 1-day later (1x100). Organoid forming efficiency was also determined for (P) delayed, (R) 5x50 and (T) 1x100 VEH- and TX-treated *Villin-CreER^{T2}* mice. (*n*=3-9 mice/group with 3 technical replicates per mouse; **P*<0.05 by Student's *t*-test). Scale bars = 100μm.

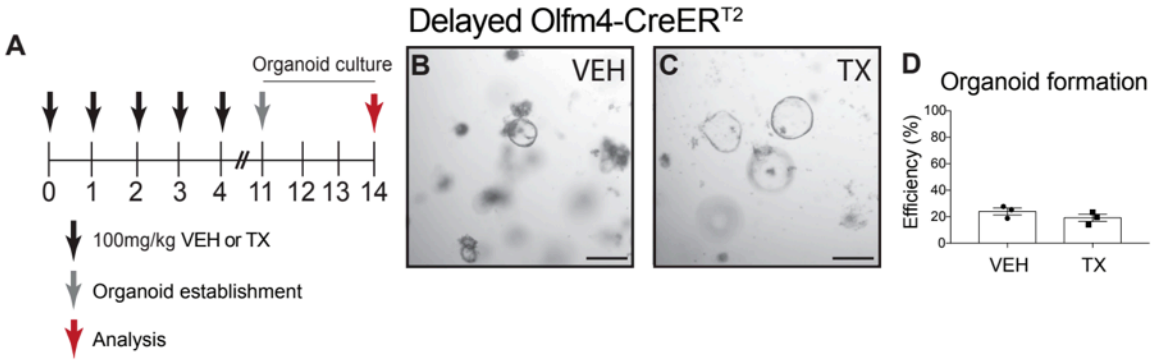

Figure 3.8 Tamoxifen-induced *Olfm4-CreER^{T2}* toxicity is abated by delay.

(A) Schematic of organoid formation efficiency assay. Organoids were established from duodenal crypts isolated from *Olfm4-CreER^{T2}* mice 7 days after treatment with VEH or TX. (B,C) Brightfield images of organoids 3 days post-establishment. (D) Organoid forming efficiency was determined by counting the number of organoids in each well at 3 days post-establishment (n=3 mice/group with 3 technical replicates per mouse). Scale bars = 250μm.

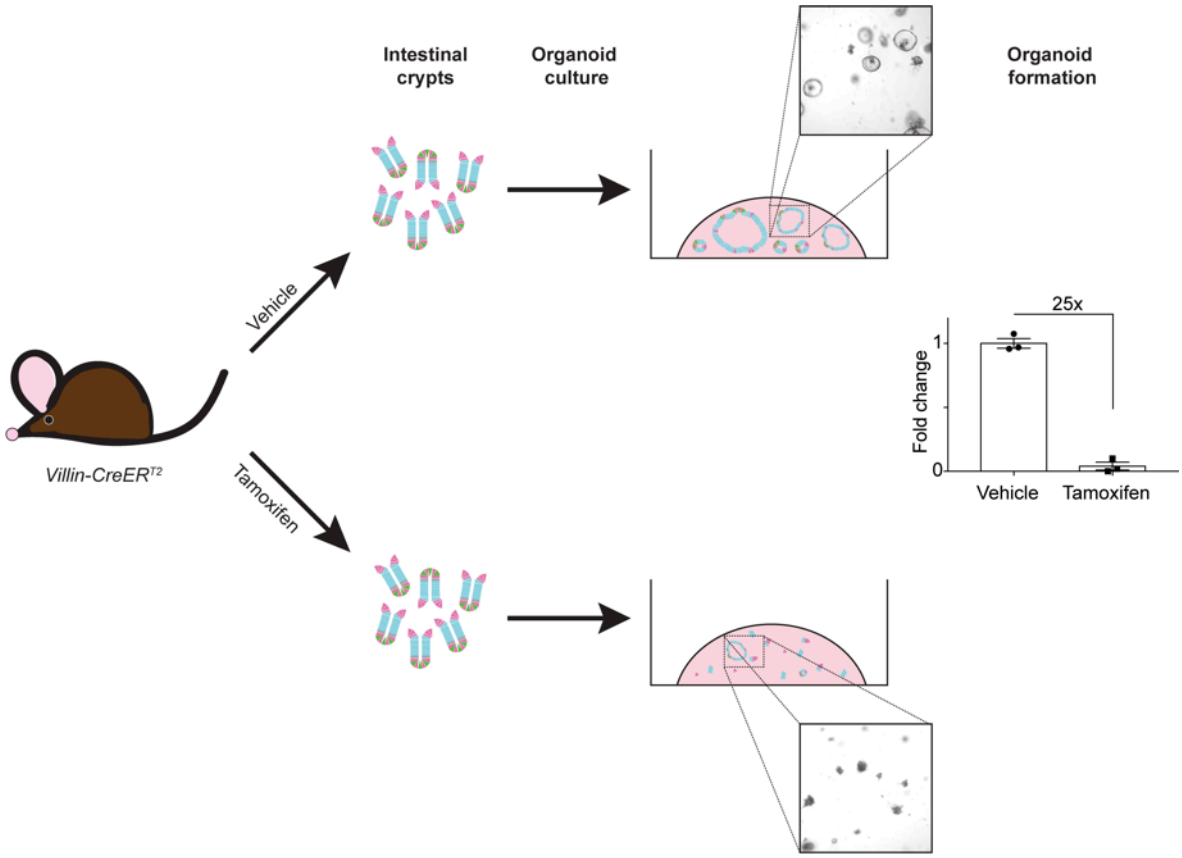

Figure 3.9 Tamoxifen-activated *Villin-CreER^{T2}* animals have impaired intestinal stem cell function.

Graphical model illustrating that isolated crypts from TX-activated *Villin-CreER^{T2}* mice have an impaired organoid forming capacity.

3.9 References

1. Bouabe, H. & Okkenhaug, K. Gene targeting in mice: a review. *Methods Mol. Biol.* **1064,** 315–36 (2013).

2. Metzger, D., Clifford, J., Chiba, H. & Chambon, P. Conditional site-specific recombination in mammalian cells using a ligand-dependent chimeric Cre recombinase. *Proc. Natl. Acad. Sci. U. S. A.* **92,** 6991–5 (1995).

3. el Marjou, F. *et al.* Tissue-specific and inducible Cre-mediated recombination in the gut epithelium. *Genesis* **39,** 186–93 (2004).

4. Schuijers, J., van der Flier, L. G., van Es, J. & Clevers, H. Robust cre-mediated recombination in small intestinal stem cells utilizing the olfm4 locus. *Stem cell reports* **3,** 234–41 (2014).

5. Barker, N. *et al.* Identification of stem cells in small intestine and colon by marker gene Lgr5. *Nature* **449,** 1003–7 (2007).

6. Thyagarajan, B., Guimarães, M. J., Groth, A. C. & Calos, M. P. Mammalian genomes contain active recombinase recognition sites. *Gene* **244,** 47–54 (2000).

7. Schmidt, E. E., Taylor, D. S., Prigge, J. R., Barnett, S. & Capecchi, M. R. Illegitimate Cre-dependent chromosome rearrangements in transgenic mouse spermatids. *Proc. Natl. Acad. Sci. U. S. A.* **97,** 13702–7 (2000).

8. Naiche, L. A. & Papaioannou, V. E. Cre activity causes widespread apoptosis and lethal anemia during embryonic development. *Genesis* **45,**

768–775 (2007).

9. Huh, W. J., Mysorekar, I. U. & Mills, J. C. Inducible activation of Cre recombinase in adult mice causes gastric epithelial atrophy, metaplasia, and regenerative changes in the absence of ‘floxed’ alleles. *Am. J. Physiol. Gastrointest. Liver Physiol.* **299,** G368-80 (2010).

10. Higashi, A. Y. *et al.* Direct hematological toxicity and illegitimate chromosomal recombination caused by the systemic activation of CreERT2. *J. Immunol.* **182,** 5633–40 (2009).

11. Madison, B. B. *et al.* Cis elements of the villin gene control expression in restricted domains of the vertical (crypt) and horizontal (duodenum, cecum) axes of the intestine. *J. Biol. Chem.* **277,** 33275–83 (2002).

12. Barker, N. *et al.* Identification of stem cells in small intestine and colon by marker gene Lgr5. *Nature* **449,** 1003–7 (2007).

13. Takeda, N. *et al.* Interconversion between intestinal stem cell populations in distinct niches. *Science* **334,** 1420–4 (2011).

14. VanDussen, K. L. *et al.* Notch signaling modulates proliferation and differentiation of intestinal crypt base columnar stem cells. *Development* **139,** 488–97 (2012).

15. Carulli, A. J. *et al.* Notch receptor regulation of intestinal stem cell homeostasis and crypt regeneration. *Dev. Biol.* **402,** 98–108 (2015).

16. Demitrack, E. S. *et al.* Notch signaling regulates gastric antral LGR5 stem

cell function. *EMBO J.* **34,** 2522–36 (2015).

17. Miyoshi, H. & Stappenbeck, T. S. In vitro expansion and genetic modification of gastrointestinal stem cells in spheroid culture. *Nat. Protoc.* **8,** 2471–82 (2013).

18. Lopez-Diaz, L. *et al.* Parietal cell hyperstimulation and autoimmune gastritis in cholera toxin transgenic mice. *Am. J. Physiol. Liver Physiol.* **290,** G970–G979 (2006).

19. Cohn, S. M., Schloemann, S., Tessner, T., Seibert, K. & Stenson, W. F. *Prostaglandins Mediate Intestinal Crypt Survival after Radiation Crypt Stem Cell Survival in the Mouse Intestinal Epithelium Is Regulated by Prostaglandins Synthesized through Cyclooxygenase-1*. *J. Clin. Invest* **99,** (1997).

20. Zhu, Y., Huang, Y.-F., Kek, C. & Bulavin, D. V. Apoptosis Differently Affects Lineage Tracing of Lgr5 and Bmi1 Intestinal Stem Cell Populations. *Cell Stem Cell* **12,** 298–303 (2013).

21. Huh, W. J. *et al.* Tamoxifen induces rapid, reversible atrophy, and metaplasia in mouse stomach. *Gastroenterology* **142,** 21–24.e7 (2012).

22. Li, N., Nakauka-Ddamba, A., Tobias, J., Jensen, S. T. & Lengner, C. J. Mouse Label-Retaining Cells Are Molecularly and Functionally Distinct From Reserve Intestinal Stem Cells. *Gastroenterology* **151,** 298–310.e7 (2016).

23. Kuo, L. J. & Yang, L.-X. Gamma-H2AX - a novel biomarker for DNA double-

strand breaks. *In Vivo* **22,** 305–9 (2008).

24. Kim, C.-K., Yang, V. W. & Bialkowska, A. B. The Role of Intestinal Stem Cells in Epithelial Regeneration Following Radiation-Induced Gut Injury. *Curr. Stem Cell Reports* **3,** 320–332 (2017).

25. Potten, C. S. Radiation, the ideal cytotoxic agent for studying the cell biology of tissues such as the small intestine. *Radiat. Res.* **161,** 123–36 (2004).

26. Wang, X. *et al.* Pharmacologically blocking p53-dependent apoptosis protects intestinal stem cells and mice from radiation. *Sci. Rep.* **5,** 8566 (2015).

27. Yan, K. S. *et al.* The intestinal stem cell markers Bmi1 and Lgr5 identify two functionally distinct populations. *Proc. Natl. Acad. Sci. U. S. A.* **109,** 466–71 (2012).

28. Tian, H. *et al.* A reserve stem cell population in small intestine renders Lgr5-positive cells dispensable. *Nature* **478,** 255–9 (2011).

29. Roche, K. C. *et al.* SOX9 Maintains Reserve Stem Cells and Preserves Radioresistance in Mouse Small Intestine. *Gastroenterology* **149,** 1553–1563.e10 (2015).

30. Loonstra, A. *et al.* Growth inhibition and DNA damage induced by Cre recombinase in mammalian cells. *Proc. Natl. Acad. Sci. U. S. A.* **98,** 9209–14 (2001).

31. Silver, D. P. & Livingston, D. M. Self-excising retroviral vectors encoding the

Cre recombinase overcome Cre-mediated cellular toxicity. *Mol. Cell* **8,** 233–43 (2001).

Chapter IV: Rapid Crypt Cell Remodeling Regenerates the Intestinal Stem Cell Niche After Notch Inhibition[4]

4.1 Summary

The Notch pathway has been established as a key niche factor important for intestinal stem cell (ISC) self-renewal. The current model posits that Notch inhibition causes ISC loss and secretory cell expansion, including Paneth cells. In this study, we observed rapid and dynamic crypt cell remodeling to restore homeostasis following disruption of the ISC Notch niche. Although ISCs were retained after Notch inhibition, we demonstrated reduced ISC function, and a surprising loss of Paneth cells by apoptosis. The rapid ISC-Paneth cell injury was followed by a proliferative surge and increased Notch signaling, with expansion of cells expressing Notch ligands *Dll1* and *Dll4*. Lineage tracing showed that *Dll1*-expressing cells were activated to proliferate and contribute to the replenishment of the vacant Paneth cell pool. Our study uncovered a dynamic, multi-cellular remodeling response to Notch inhibition in the intestinal crypt, with activation of

[4] Note this chapter is adapted from the following article in preparation:
Bohin, N.*, Keeley, T. M.*, Carulli, A. J., Carlson, E. A., Gao, J., Aifantis, I., Siebel C. W., Rajala, M. W., Myers, M. G., Jones, J. C., Brindley, C. D., Dempsey, P. J., Samuelson, L. C. Rapid Crypt Cell Remodeling Regenerates the Intestinal Stem Cell Niche after Notch Inhibition. *Cell Stem Cell*. [In Preparation]. * Equal contribution.

Notch signaling to re-establish the niche and restore homeostasis.

4.2 Introduction

As one of the most rapidly renewing tissues, the intestine has a great capacity for regeneration. Under homeostatic conditions, *Lgr5*-expressing crypt base columnar stem cells (CBCs) are responsible for replenishing the intestinal epithelium throughout lifespan.[1,2] This intestinal stem cell (ISC) population divides once a day to generate highly proliferative transit amplifying (TA) cells which differentiate into the various mature epithelial cell types. Most newly formed differentiated cells move out of the crypts and onto the villi, where they function in absorption or secretion before being extruded into the lumen. The exception is Paneth cells, which move to the crypt base to lie adjacent to CBCs, with a half-life of several weeks.[3,4]

When CBCs are injured, other crypt cell populations can replace their function, acting as facultative stem cells (FSCs; also called +4 cells, reserve stem cells and quiescent stem cells) by re-entering the cell cycle to generate progeny that can maintain the epithelium during the repair process, and to occupy vacant stem cell niche spaces to replace lost CBCs. FSC activation after intestinal injury has been demonstrated by lineage tracing from several different Cre-drivers that mark various lineage-committed (*Alpi*, *Dll1*) or slowly cycling (*Bmi1*, *HopX*, *Lrig1*, *mTert*) crypt cell populations.[5–13] In addition, recent studies have demonstrated that after radiation-induced crypt injury, even differentiated Paneth cells can reprogram into proliferative progenitors capable of forming various differentiated

intestinal cell types.[14] Thus, in response to injury, cells in the intestinal crypt exhibit remarkable cellular plasticity to reprogram their cell fate to regenerate the crypt and return to homeostasis.

Adult stem cells are regulated by their niche, the tissue-specific microenvironment of cells, secreted substances, and extracellular matrix that provide key signaling factors to orchestrate stem cell function. In the intestine, the stem cell niche includes both epithelial cell and stromal cell compartments. Wnt and Notch signaling have been identified as the primary niche pathways promoting ISC self-renewal.[15] Disruption of either Wnt or Notch signaling has been shown to induce CBC loss and crypt collapse.[16–19] While ISC Wnt signaling is regulated by ligands secreted from both epithelial and stromal cell sources,[20–23] Notch signaling is likely to be epithelial specific because it requires direct cell-to-cell contact.[15]

CBCs have been demonstrated to be Notch signaling cells,[24] with Notch1 identified as the primary receptor regulating CBC function.[25,26] Both pharmacologic Notch inhibition as well as genetic disruption of Notch signaling results in CBC loss, and in a gain in secretory cells, which includes increased expression of Paneth cell markers.[19,24,27,28] Paneth cells are the most likely source of Notch ligand due to their close association with CBCs at the crypt base.[29] Moreover, Paneth cells have been described to express both *Dll1* and *Dll4*,[30,31] the key Notch ligands regulating crypt cell homeostasis.[19] In spite of our understanding of niche regulation of ISCs during homeostasis, particularly with regards to Notch signaling, strikingly little is known about ISC niche responses following injury. Furthermore, earlier studies of pharmacologic or genetic Notch disruption were limited by the

reduced animal viability, which impeded analysis of the regeneration process.

Here, we introduce an intestinal crypt injury model based on short-term niche factor inhibition. We probe the setting of pharmacologic Notch inhibition to investigate the acute cellular response to niche disruption. We demonstrate that short-term Notch niche disruption leads to ISC dysfunction and dynamic cellular remodeling highlighted by rapid Paneth cell loss, a novel contrast to existing thinking as established by studies employing longer time points of Notch inhibition that demonstrated Paneth cell expansion. After short-term Notch disruption we observed expansion of cells expressing Notch ligand, and increased Notch signaling, with a regenerative response characterized by a proliferative surge and activation of FSCs. We show that *Dll1*-expressing secretory progenitors were activated to function as FSCs to regenerate the vacant Paneth cell population. Our study sheds light into how niche pathways and crypt cell plasticity orchestrate intestinal repair.

4.3 Experimental Procedures

4.3.1 Mice

Lgr5-GFP-IRES-CreER^{T2} (Jackson Lab, no. 008875),[1] *Olfm4-IRES-GFP-CreER^{T2}* (from Dr. Hans Clevers),[32] *Defensin-alpha4-Cre* (from Dr. Martin Myers),[33] *Dll1-mCherry* and *Dll4-mCherry* BAC transgenic mice (from Dr. Iannis Aifantis),[34] *Dll1-EGFP-ires-CreER^{T2}* (from Dr. Hans Clevers),[7] *Hopx-CreER* (Jackson Lab, no. 017606),[5] *ROSA26-LStopL-tdTomato* (*ROSA26-Tom*; Jackson Lab, no. 007909),[35] or *ROSA26-LStopL-mTmG* (*ROSA26-mTmG*; Jackson Lab,

no. 007576)[36] alleles were verified by PCR genotyping. All mice were maintained on a C57BL/6 strain background. Mice were housed in ventilated and automated watering cages with a 12-hour light cycle under specific pathogen-free conditions. Protocols for mouse usage were approved by the University of Michigan Committee on Use and Care of Animals. Adult mice of both sexes were used for analyses.

4.3.2 Animal treatment protocols and tissue collection

Mice were injected intraperitoneally with DBZ (30 μmol/kg) (SYNCOM, Netherlands) or Veh as described,[28] and intestinal tissue was collected at various time points. Some mice were injected with 5-ethynyl-2′-deoxyuridine (EdU, 25 mg/kg) (Life Technologies) 1.5 hours before tissue collection. Intestinal tissue was fixed in 4% paraformaldehyde overnight for paraffin sections as previously described,[24] as illustrated in **Figure 2.1**. Tissue prepared for frozen sections was fixed for 1 hour and incubated in 30% sucrose overnight before embedding in OCT (Tissue-Tek). Intestinal crypts were isolated for gene expression analysis or flow cytometry as described.[25] Some mice were treated with a single intraperitoneal injection of 100 mg/kg tamoxifen prior to DBZ or Veh treatment, as detailed in figure legends. *Defensin-alpha4-Cre*; *ROSA26-Tom* mice were treated with a mixture of humanized neutralizing monoclonal antibodies directed against DLL1 or DLL4, or an irrelevant isotype control antibody against herpes simplex virus gD protein (Gd).[37,38] Antibodies were injected intraperitoneally at 15 mg/kg for two daily doses and intestinal tissue was collected the next day.

4.3.3 Immunohistochemistry

Paraffin sections (4-5μm) were stained with periodic acid-Schiff and alcian blue (Newcomer Supply) to visualize mucin-containing goblet cells. Immunostaining with rabbit α-lysozyme (1:200, DAKO), rabbit α-GFP (1:200, Invitrogen), and rabbit α-cleaved-caspase 3 (1:50, Cell Signaling), rabbit α-muc2 (1:200, Santa Cruz), and rabbit α-CgA (1:200, Abcam) was performed as described (Lopez-Diaz, 2006). Co-immunostaining for cleaved caspase 3 and MMP7 was performed by co-incubating rabbit α-cleaved caspase 3 and rat α-MMP7 (1:400, Vanderbilt). Rabbit α-cleaved Notch 1 (NICD; 1:50, Cell Signaling) was used in conjunction with a TSA Superboost kit (Thermo #B40943). EdU-Click-iT kit (Life Technologies) was used to identify proliferating cells. Images were captured on a Nikon E800 microscope with Olympus DP controller software.

4.3.4 In situ hybridization

Olfm4 *in situ* hybridization was performed on paraffin sections as described.[25] Lgr5 *in* situ hybridization was performed on frozen sections as described.[39]

4.3.5 Quantitative morphometric analyses

The number of EdU–positive cells was counted on both sides of well-oriented crypts. At least 10 crypts were counted per animal for all analyses, and

counts were averaged per animal (N=3-4 animals/group). Nuclei per crypt were counted on both sides of well-oriented crypts on DAPI-stained fields. Lineage tracing was quantified by counting the number of lineage-marked cells and represented as the number of lineage-marked cells per crypt, or the number of lineage tracing events per crypt. Morphometric analyses were completed using ImageJ software (http://imagej.nih.gov/ij/). The number of cleaved caspase 3-positive cells was counted and divided by the total number of crypts. Approximately 150 crypts were counted per mouse.

4.3.6 Crypt isolation and gene expression analysis

Crypts were isolated from mouse duodenum as previously described.[25] RNA was isolated using RNeasy Mini kit (Qiagen) with DNase I treatment as per manufacturer instructions. cDNA was reverse transcribed with the iScript cDNA synthesis kit (BioRad) using 1 µg of total RNA. qPCR was performed as previously described.[40] *Olfm4*, *Lgr5*, *Notch1*, *Notch2*, *and Hes1* primers were previously described.[24,39,41] *Dll1* primers have sequences: CTG AGG TGT AAG ATG GAA GCG (forward) and CAA CTG TCC ATA GTG CAA TGG (reverse). *Dll4* primers have sequences: TCGTCGTCAGGGACAAGAATAGC (forward) and CTCGTCTGTTCGCCAAATCTTACC (reverse). *Jag1* primers have sequences: CAG AAT GAC GCT TCC TGT CG (forward) and TGC AGC TGT CAA TCA CTT CG (reverse). *Jag2* primers have sequences: TAT GAC AGC GGC GAC ACC TTC (forward) and CAA CAC AGA TGC CTC CGT TAT AGC (reverse). *Hprt* primers

have sequences: AGG ACC TCT CGA AGT GTT GGA TAC (forward) and AAC TTG CGC TCA TCT TAG GCT TTG (reverse).

4.3.7 Fluorescence-activated cell sorting (FACS) and mCherry-positive cell plating to form organoids

A previously described protocol for isolation, plating and culturing Lgr5-positive antral stem cells was adapted for the FACS isolation of single Dll1-mCherry-positive duodenal crypt cells from Veh and DBZ-treated mice, and their subsequent culture in Matrigel to form organoids.[39] The efficiency of organoid formation was determined by counting organoids 7 days following plating and normalizing to the number of plated Dll1-mCherry-positive cells.

4.3.8 Statistical analyses

All experiments were performed with 3-8 biological replicates per group. Quantitative data are presented as mean ± SEM. Comparisons between two groups were conducted with unpaired two-tailed Student *t* tests. Comparisons between 3 or more groups were analyzed by one-way ANOVA with Dunett's post-test. Significance is reported as *($P<0.05$), **($P<0.01$), ***($P<0.001$), and ****($P<0.0001$). Prism software (Graphpad) was used for statistical analyses.

4.4 Results

4.4.1 Acute pan-Notch inhibition leads to functional impairment of ISCs

We analyzed the immediate effect of Notch inhibition on ISC function and characterized the regenerative response after short-term Notch niche disruption by treating adult mice with a single dose of the gamma-secretase inhibitor dibenzazepine (DBZ). Intestinal tissue was isolated at various time points post-DBZ, which has a plasma half-life of less than 12 hours,[42] to characterize the dynamic crypt cell response to Notch inhibition (**Figure 4.1A**). We observed loss of expression of the CBC marker[43] and Notch target gene[24] *Olfm4* as early as 12 hours post-DBZ, with a return in expression by 3 days post-DBZ (**Figure 4.1B,C**). In contrast, *Lgr5* expression was not changed (**Figure 4.1B,C**), suggesting that the dynamic changes to *Olfm4* expression reflected loss of CBC Notch signaling rather than stem cell depletion.

To assess the effect of acute Notch inhibition on CBC function, we measured lineage tracing using two different CBC-specific Cre driver strains crossed to the *ROSA26-Tom* reporter: *Olfm4-GFP-CreER^{T2}* and *LGR5-GFP-CreER^{T2}*. The Tom lineage mark was activated by treatment with tamoxifen, followed by DBZ or vehicle treatment and analysis 1 day later (**Figure 4.1D**). We observed significantly fewer lineage-traced cells in DBZ-treated animals compared to vehicle-treated controls (**Figure 4.1E**). Quantification of the number of Tom-labeled cells per crypt showed that both *Olfm4* and *Lgr5* reporter mice had an

approximately 2-fold reduction in lineage tracing, indicating impaired CBC function (**Figure 4.1E**). Significantly reduced lineage tracing was observed in both proximal (**Figure 4.1E**) and distal small intestine (data not shown) after Notch inhibition.

4.4.2 Paneth cell apoptosis following Notch inhibition

Histological analysis of the crypt post-DBZ showed dynamic cellular remodeling. Remarkably, granule-filled Paneth cells at the crypt base were rapidly lost within 12 hours of DBZ-treatment, associated with the appearance of delaminated cells (**Figure 4.2A**). To further examine this effect, we immunostained tissue sections from vehicle and DBZ-treated mice for the Paneth cell marker lysozyme (**Figure 4.2B**). Lysozyme staining was virtually absent from DBZ-treated crypts as soon as 12 hours following DBZ administration (**Figure 4.2B**). To determine whether the loss of cells exhibiting these distinctive Paneth cell features was due to cellular remodeling or cell loss, we treated *Defensin 4-Cre;Tom* mice, which permanently label Paneth cells with a Tom lineage mark. We observed a marked loss of Tom-labeled cells 1 day post DBZ in these mice, demonstrating that Notch inhibition results in rapid Paneth cell loss (**Figure 4.2B** insets). Analysis of apoptosis by staining for cleaved caspase 3 showed a significant increase in apoptotic cells, which peaked at 1 day post DBZ treatment (**Figure 4.2C**). Co-staining for the Paneth cell marker MMP7 and cleaved caspase 3 showed that the apoptotic cells were Paneth cells (**Figure 4.2D**).

These data suggest that Notch signaling is required for Paneth cell maintenance, which is an unexpected finding as Paneth cells are not thought to be

Notch signaling cells. To confirm that the Paneth cell loss is a consequence of Notch inhibition and not to the inhibition of another gamma-secretase target, we analyzed *Defensin4-Cre;Tom* mice that were treated with a mixture of inhibitory antibodies to DLL1 and DLL4, the two Notch ligands required for crypt cell homeostasis.[38,44] Similar to our findings after inhibition of Notch signaling with DBZ, we observed reduced Paneth cell numbers after combined DLL1 and DLL4 Notch signaling blockade, showing that Paneth cell loss is due to Notch inhibition (**Figure 4.3**). The loss of Paneth cells may explain reduced CBC function shown by diminished lineage tracing post-DBZ (**Figure 4.1E**) as Paneth cells are known to express several ISC niche factors [29]. Notably, Paneth cells return by 3 days following acute Notch inhibition, with an apparent increase in numbers of granule-containing cells and Tom-marked cells by day 7 (**Figure 4.2A,B**). The rapid Paneth cell loss and return suggests dynamic crypt cell remodeling in response to Notch niche disruption to return to homeostasis.

4.4.3 Increased Notch activity and cell proliferation during the regenerative phase of crypt remodeling

We assessed proliferation at 1, 3 and 7 days following DBZ or vehicle treatment to determine if crypt remodeling included a regenerative response. Acute Notch inhibition resulted in a marked increase in proliferating cells at day 3, with 1.6-fold increased numbers of EdU-positive cells (**Figure 4.4A,B**). This proliferative surge was accompanied by dynamic changes in crypt cellularity. Decreased crypt cellularity was observed at 1 day post DBZ (**Figure 4.4C**), a time

point marked by loss of Paneth cells and diminished CBC stem cell function (**Figures 4.1** and **4.2**). However, at the time of the proliferative surge at day 3, crypts were expanded and there was increased cellularity, compared to vehicle-treated mice (**Figure 4.4A,C**).

Given the well-characterized role of Notch signaling in stimulating intestinal proliferation,[19,24,27,28,45,46] we investigated Notch signaling activity to determine if the hyperproliferative response coincided with the return of Notch signaling. Immunostaining for the Notch1 intracellular signaling domain (NICD) showed loss of Notch activity 12 hours post DBZ treatment (**Figure 4.5A,B**), which is consistent with the loss of expression of the Notch target gene *Olfm4* at that time point (**Figure 4.1**). While the number of NICD-positive cells remained significantly lower at 1 day post DBZ, Notch activity was returning, and NICD-positive cell numbers increased over time as we might expect given the aforementioned half-life of DBZ (**Figure 4.5B**). By day 3 the number of NICD expressing cells was increased in comparison to vehicle control, which corresponds to the time that we observed increases in proliferation and crypt cellularity (**Figure 4.4**). Notably, NICD-positive cells are preferentially observed in the mid-crypt region when they are returning, in contrast to the crypt base, which normally included NICD-positive cells.

The rebounding Notch activity following acute Notch inhibition is associated with increased mRNA abundance of Notch components, including the ligands *Dll1* and *Dll4*, and the *Notch1* receptor (**Figure 4.5C**). No significant changes in expression were observed for the other Notch components expressed in the intestinal epithelium, except for *Jag2* and *Notch2* receptor (**Figure 4.6**).

Surprisingly, expression of the Notch target Hes1 was not changed following acute Notch inhibition (**Figure 4.6**). In summary, acute Notch inhibition stimulates expression of the primary intestinal Notch ligands, concomitant with increased Notch activity.

4.4.4 Rapid expansion of Dll1- and Dll4-expressing cells during crypt regeneration

We made use of *Dll1-mCherry*[34] and *Dll4-mCherry* reporter mice to follow the cellular pattern of Notch ligand expressing cells during intestinal remodeling post DBZ treatment. Analysis of these reporter mice showed that *Dll1*- and *Dll4*-positive cells are normally present in both intestinal crypt and villus compartments in a scattered pattern consistent with secretory cell distribution (**Figure 4.7A**). We determined which cell types express *Dll1* and *Dll4* by co-imaging *mCherry* with markers of differentiated Paneth (lysozyme), goblet (Muc2) and endocrine (CgA) cells (**Figure 4.8**). Analysis of *Dll4-mCherry* mice showed that all three secretory cell types are marked with the mCherry reporter (**Figure 4.8**). However, analysis of *Dll1-mCherry* mice showed expression in goblet and Paneth cells, but not endocrine cells (**Figure 4.8**). This is likely a limitation of this BAC transgene as a *Dll1* knock-in allele has been shown to mark all three secretory cell types as well as secretory progenitor cells.[7]

Analysis of *Dll1-mCherry* and *Dll4-mCherry* cells after Notch inhibition showed increased numbers of marked cells (**Figure 4.7**). This finding suggests that increased mRNA abundance of Notch ligands (**Figure 4.5C**) is due to

increased numbers of *Dll1* and *Dll4* expressing cells. The expansion of *Dll1-mCherry* and *Dll4-mCherry* cells after Notch inhibition by DBZ corresponds to a surge in goblet cell numbers detected by PAS/Alcian blue staining (**Figure 4.9**). This finding is consistent with previous reports that showed secretory cell hyperplasia after several days of continuous Notch inhibition.[24,28]

Dll1- and *Dll4*-expressing cell expansion was profound, with expanded crypts at day 3 almost completely composed of Notch ligand-expressing cells (**Figure 4.7A**). This expansion was first detected 1 day post DBZ, with ligand expressing cells localized to the crypt base. Quantification of *Dll1-mCherry* cells by flow cytometry showed that cell number increased almost 3-fold at 1 day post DBZ (**Figure 4.7B**).

4.4.5 Acute Notch inhibition stimulates Paneth cell regeneration from Dll1-positive FSCs

Dll1-expressing secretory progenitors can be activated to function as FSCs to regenerate CBCs after crypt injury.[7] To determine whether Notch inhibition might activate *Dll1*-expressing cells, we measured the number of proliferating *Dll1-mCherry* cells, showing a 5-fold increase in EdU/mCherry double positive cells at 1 day post DBZ compared to vehicle-treated controls (**Figure 4.10A,B**). We next tested stem/progenitor function by measuring organoid-forming potential of sorted *Dll1-mCherry* crypt cells 1 day post DBZ. This analysis showed a 2-fold increase in organoid forming efficiency compared to *Dll1-mCherry* cells isolated from vehicle-treated mice (**Figure 4.10C**).

We tested whether Notch inhibition activated *Dll1*-expressing cells to function as FSCs to regenerate the Paneth cell pool using a lineage tracing approach. *Dll1-GFP-CreER^{T2}; ROSA26-Tom* mice were treated with tamoxifen to activate the lineage mark, followed by a single dose of vehicle or DBZ 24 hours later, and intestine was harvested 7 days later (**Figure 4.11A**). At this time point, the only Tom-marked cells in the Veh-treated control crypts were Paneth cells due to their longer half-life; all other *Dll1*-expressing cells had turned over (**Figure 4.11B**). In contrast, the DBZ-treated crypts contained numerous Tom-labeled crypt cells, including frequent lineage stripes (**Figure 4.11B** inset). Quantification of lineage traces showed that only the DBZ-treated mice exhibited lineage stripes (**Figure 4.11C**). Importantly, we found that Tom-positive cells generated from *Dll1*-positive FSCs post-DBZ included Paneth cells (**Figure 4.11D**). Quantification of lysozyme/Tom double positive cells showed increased numbers of labeled Paneth cells in DBZ-treated crypts compared to vehicle-treated crypts (**Figure 4.11D**). In light of the Paneth cell loss and regeneration after DBZ treatment, the observation of Tom-labeled Paneth cells in crypts from DBZ-treated mice demonstrates that Notch inhibition induced *Dll1*-expressing progenitors to function as FSCs and regenerate the Paneth cell pool.

We also carried out lineage tracing studies for another FSC marker using *HopX-CreER^{T2}*; *ROSA26-mTmG* mice, but did not observe enhanced lineage tracing events after DBZ treatment (**Figure 4.12**). Together these data indicate that Notch inhibition leads to activation of a subset of FSCs, *Dll1*-positive FSCs, facilitating their contribution to the recovery of the depleted Paneth cell pool.

However, *Dll1*-expressing progenitors did not contribute to the CBC pool, as lineage stripes were short lived, with no lineage traces detected at 2 months after treatment (**Figure 4.11B**). Thus *Dll1*-expressing progenitors were activated to contribute to crypt regeneration after injury induced by Notch inhibition, but did not displace the resident CBCs from the crypt base.

4.5 Discussion

Our study uncovered a rapid and dynamic crypt cell remodeling program stimulated by disruption of the ISC niche. We revealed that a pulse of Notch inhibition induces a multicellular crypt damage response, highlighted by a dramatic early Paneth loss by apoptotic cell death. Although CBC stem cells are retained, they exhibit impaired lineage-tracing activity and loss of Notch signaling, as shown by loss of expression of the Notch target gene *Olfm4*. A regenerative response follows the Paneth cell–CBC stem cell injury, with repair and return to homeostasis within a few days. The repair response involves expansion of Notch ligand-expressing cells, followed by a concurrent surge in both Notch signaling and crypt cell proliferation. The regenerative response involves cells expressing the Notch ligand *Dll1*, which are activated to proliferate and function as FSCs to transiently generate new epithelial cells, including Paneth cells, essentially adopting a CBC-like function to maintain the epithelium and replenish the Paneth cell pool. To our knowledge, this is the first report of acute Paneth cell loss resulting from inhibition of the ISC niche and the first report of a regenerative crypt response that is not associated with CBC stem cell loss.

Our findings differ in some respects from previous studies of Notch inhibition, which analyzed longer-lasting pharmacologic[24,28,47] or genetic[19,25,48] Notch depletion. In these studies, more long-lasting Notch inhibition led to *Lgr5* stem cell loss and a marked decrease in crypt cell proliferation. Thus, our observation of *Lgr5* stem cell retention and increased cell proliferation after a short Notch disruption was unexpected. Further, reduced lineage tracing from *Lgr5* and *Olfm4* reporter mice following our acute Notch inhibition studies could reflect a block in stem cells transitioning to TA cells, or defects in early daughter cell proliferation rather than, or in addition to CBC dysfunction. Nevertheless, there is general agreement among past studies that continuous Notch signaling is required to maintain the ISC compartment, with pathway interruption leading to rapid stem cell dysfunction and ultimately stem cell loss, depending on the timing of pathway inhibition.

Paneth cells have been proposed to be Notch niche cells due to their close physical association with CBCs at the crypt base and their expression of *Dll1* and *Dll4*, the two key Notch ligands regulating CBC function in the intestine.[19,29,31] Additionally, Paneth cells are thought to generate a number of other niche factors, including Wnt ligands and growth factors, as well as metabolic products, suggesting a more expanded niche role for Paneth cells to support their stem cell neighbors.[29,49] However, niche function for Paneth cells has been controversial, with some studies showing that Paneth cells can enhance stem cell function,[29,50] while others demonstrate apparently normal CBC function after Paneth cell depletion.[51–53] Our observation of reduced stem cell lineage tracing activity

associated with Paneth cell loss, and a return to normal stem cell activity with Paneth cell return (**Figure 4.13B-E**), would support a functional niche role for Paneth cells. Further, Notch signaling at the crypt base did not recover until Paneth cells were restored, suggesting that Paneth cells are the key Notch niche cells presenting Notch ligand to the CBC stem cell.

Our demonstration that CBCs restored their normal lineage tracing capacity several days after DBZ treatment, and are capable of contributing to Paneth cell restitution (**Figure 4.13B,D**), also supports a mutually supportive relationship between Paneth and CBC cells. This idea is in agreement with past literature, which provides evidence that ISCs have the capacity to reform their niche in an injury context.[54,55] This supports the higher level concept that, in addition to responding to niche signals, CBCs may also partner with the niche towards its re-formation when damaged.

Our observation of crypt hyperproliferation and FSC activation after short term Notch inhibition are hallmarks of the intestinal regenerative response to repair crypt damage. The damage induced by Notch interruption is different from previously described crypt injury methods, which target stem and proliferating progenitor cells by radiation or chemotherapeutic drug treatment, resulting in stem cell loss and crypt collapse. Short term Notch inhibition results in more modest crypt cell effects and CBC retention, which nevertheless stimulates a regenerative response. Interestingly, in accordance with our finding, another study observed a proliferative surge with increased crypt height after depletion of Paneth cells and other secretory cell types from the adult mouse intestine.[51] Thus, Paneth cell loss

might stimulate the regenerative response.

The second hallmark of intestinal regeneration is FSC activation to fuel epithelial cell restitution and CBC stem cell replacement.[56] In our study we observed activation of *Dll1*-expressing cells to function as FSCs to restore the Paneth cell pool. The rapid Paneth cell restoration by *Dll1*-expressing cells suggests that there is a concerted differentiation program to replenish this pool of cells and repair the Notch niche. Surprisingly, the activated *Dll1*-expressing cells did not contribute to the CBC pool, as lineage traces were short-lived. However, we showed that activated *Dll1*-expressing cells had increased organoid forming efficiency, suggesting that they have the potential to become stem cells if open niche spots occur because of CBC cell loss. Indeed, previous studies showed that *Dll1*-expressing progenitor cells have the capacity to regenerate lost CBCs after crypt damage caused by radiation.[7] Thus, FSC function is dependent on the specific cellular damage induced by the injury, underscoring the cellular plasticity and exquisite drive to regain homeostasis in the crypt. In contrast to *Dll1*-expressing cells, another FSC population that expresses *HopX* was not activated by Notch inhibition, showing that mobilization of distinct FSC populations also depends on the specific crypt cell damage.

To conclude, we propose a process whereby acute Notch inhibition stimulates a regenerative response stemming from rapid Paneth cell loss and impaired CBC activity, which is fueled by *Dll1*-expressing cell expansion and activation. This study introduces acute pan-Notch inhibition as a novel intestinal injury model targeting Paneth cells, to study selective activation of a subset of *Dll1*-

expressing secretory cell progenitors.

4.6 Author Contributions

AJC and LCS initially conceived the project, with subsequent conceptual contributions from NB and TMK. Methodology was developed by TMK, NB, AJC and LCS. The majority of the investigation and analysis was carried out by TMK and NB, with contributions from EAC, JCJ, CDB and PJD. Resources were provided by JG, IA, MWR and MGM. NB and LCS wrote the manuscript and all authors provided critical feedback. LCS provided supervision and obtained funding.

4.7 Acknowledgements

We thank Yasmine Abushukur for technical help and Erin Collin for maintaining the mouse colony. NB was supported by the Cellular and Molecular Biology program, a Rackham research grant and the Benard L. Maas Fellowship. The research was funded by NIH R01-DK096972 to LCS, and Core support from the University of Michigan Gastrointestinal Research Center Grant NIH P30-DK34933.

4.8 Figures

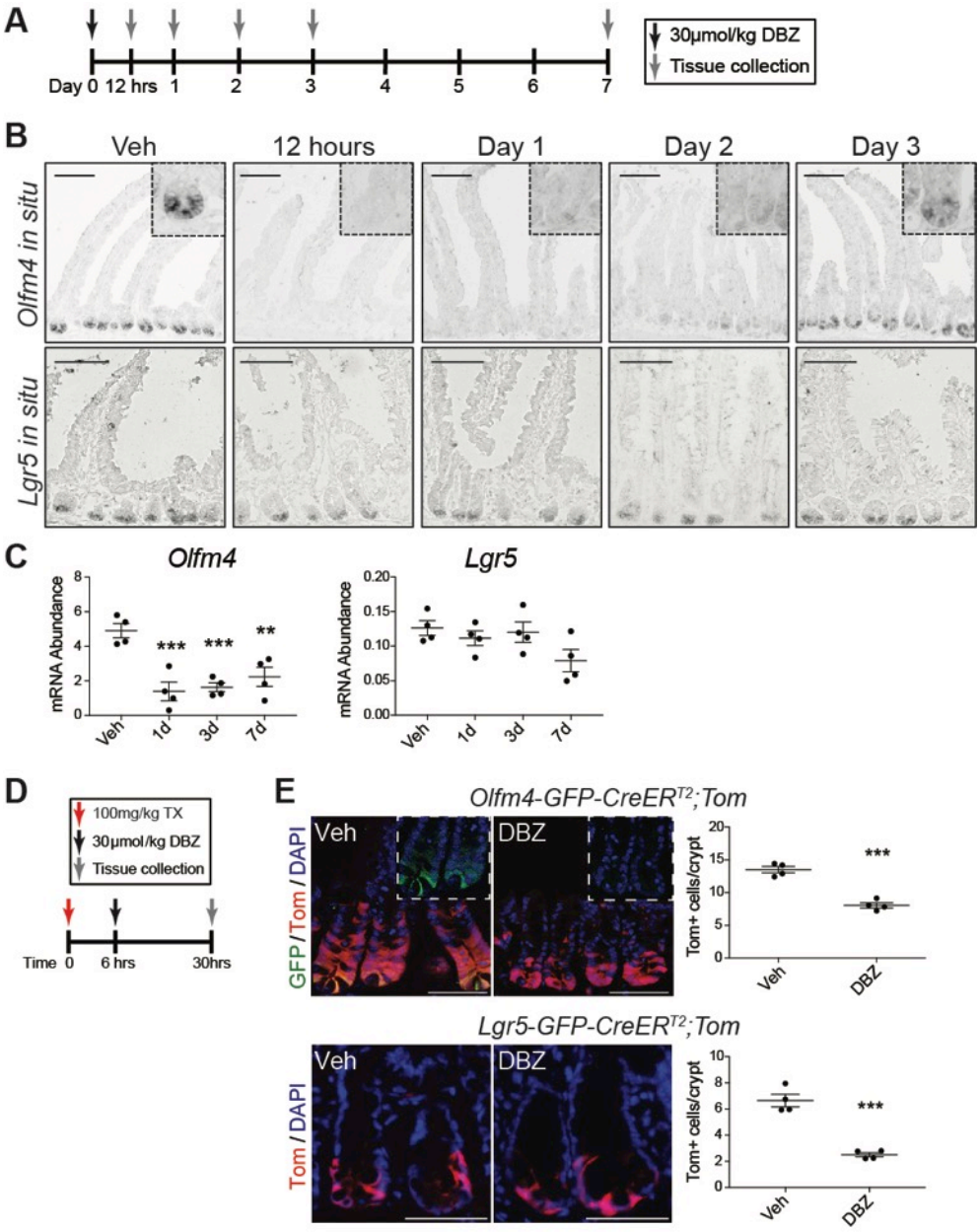

Figure 4.1 Impaired CBC function after Notch inhibition.

(A) Mice were treated with dibenzazepine (DBZ; 30 μmol/kg) or vehicle (Veh) and duodenal tissue was collected at various times. (B) *In situ* hybridization for crypt base columnar (CBC) stem cell markers *Olfm4* and *Lgr5*. Insets are 3x original magnification. Scale bars = 100μm. (C) qPCR analysis of stem cell marker mRNA abundance. (D) Stem cell function was measured by lineage tracing after tamoxifen activation and DBZ or Veh treatment, as depicted. (E) tdTomato (Tom) lineage stripes were measured in *Olfm4-GFP-CreER^{T2};ROSA26-Tom* (top) or *Lgr5-GFP-CreER^{T2};ROSA26*-Tom (bottom) duodenum. Insets show green channel to image CBCs. Quantification of the number of Tom+ cells per duodenal crypt in Veh- vs. DBZ-treated mice. Scale bars = 50μm. Quantitative data are presented as mean +/- SEM (***P<0.001, Veh vs. DBZ by Student *t*-test; n=3-4 mice per group, as shown).

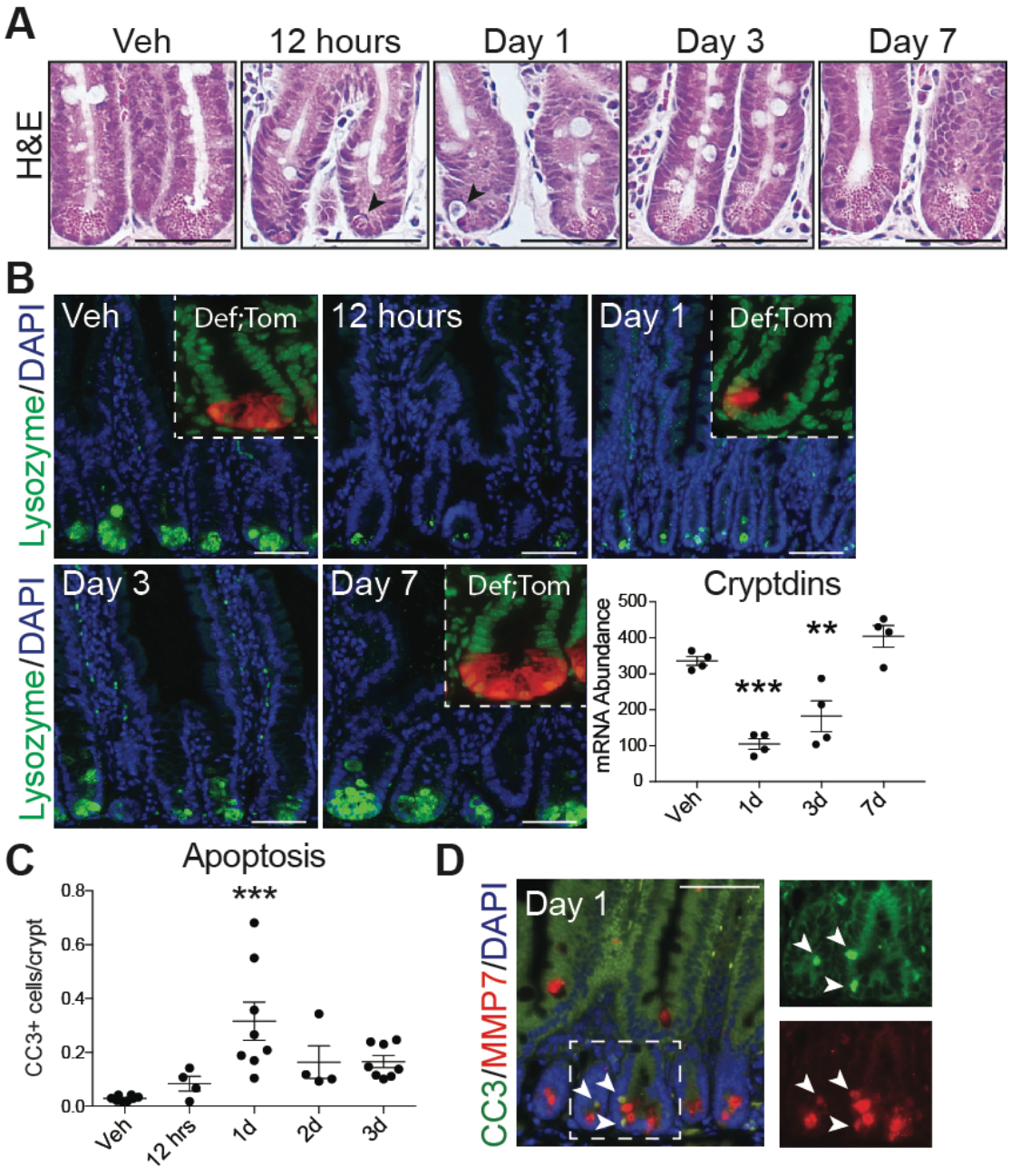

Figure 4.2 Paneth cell apoptosis after Notch inhibition.

Mice were treated with DZB or Veh and intestinal tissue was analyzed at various times. (A) H&E-stained duodenal crypts. Black arrowheads denote delaminated cells. (B) Duodenal tissue sections were immunostained for the Paneth cell marker lysozyme (green), with nuclear DAPI (blue). Insets depict ileal crypts from mice (*Defensin-alpha4-Cre;ROSA26-Tom*) with Paneth cells marked with Tom (red) and DAPI (green). (C, D) Apoptotic cells were detected by immunostaining for cleaved caspase 3 (CC3; green), (C) quantified in the duodenum at various time points following Veh or acute DBZ treatment, and (D) co-stained with the Paneth cell marker MMP7 (red) with DAPI (blue). Single green and red channel images are shown in the right. White arrowheads denote co-stained cells. Scale bars = 50μm. Quantitative data are presented as mean +/- SEM (***P<0.001 Veh vs. DBZ by one-way ANOVA and Dunnett's post-test; n=4-8 animals/group, as shown).

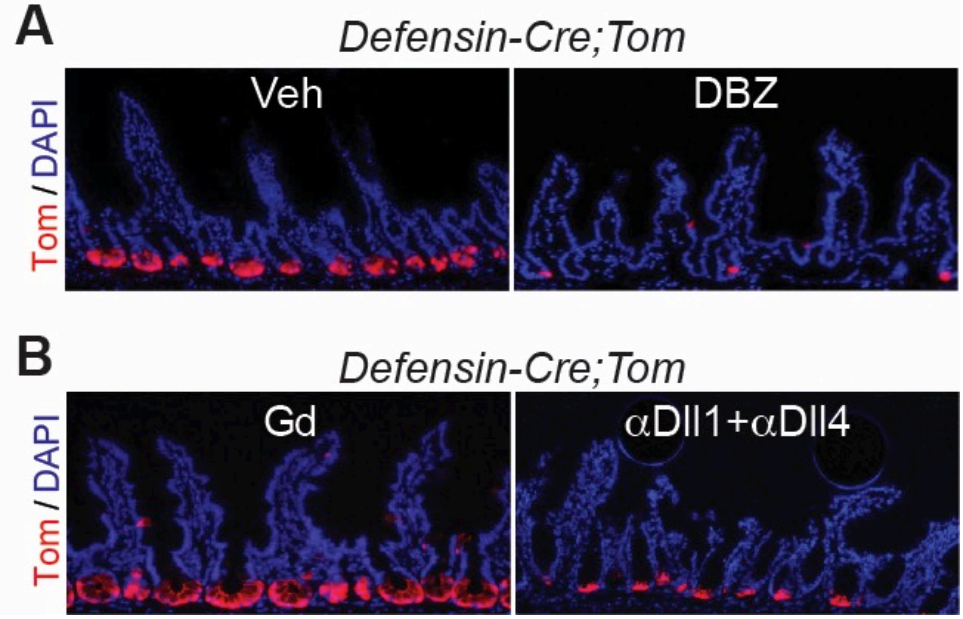

Figure 4.3 Loss of Paneth cells after Notch inhibition.

Paneth cells were visualized in *Defensin-alpha4-Cre; ROSA26-Tom* (*Defensin-Cre;Tom*) mice after Notch inhibition, as described in Methods. (A) These mice were treated with gamma-secretase inhibitor dibenzazepine (DBZ; 30 μmol/kg) or vehicle (Veh), and harvested 24 hours post-DBZ. (B) *Defensin-Cre;Tom* mice were treated with humanized monoclonal antibodies directed against control (Gd) or a mixture targeting DLL1 and DLL4 (15mg/kg) daily for 2 days, and analyzed the following day.

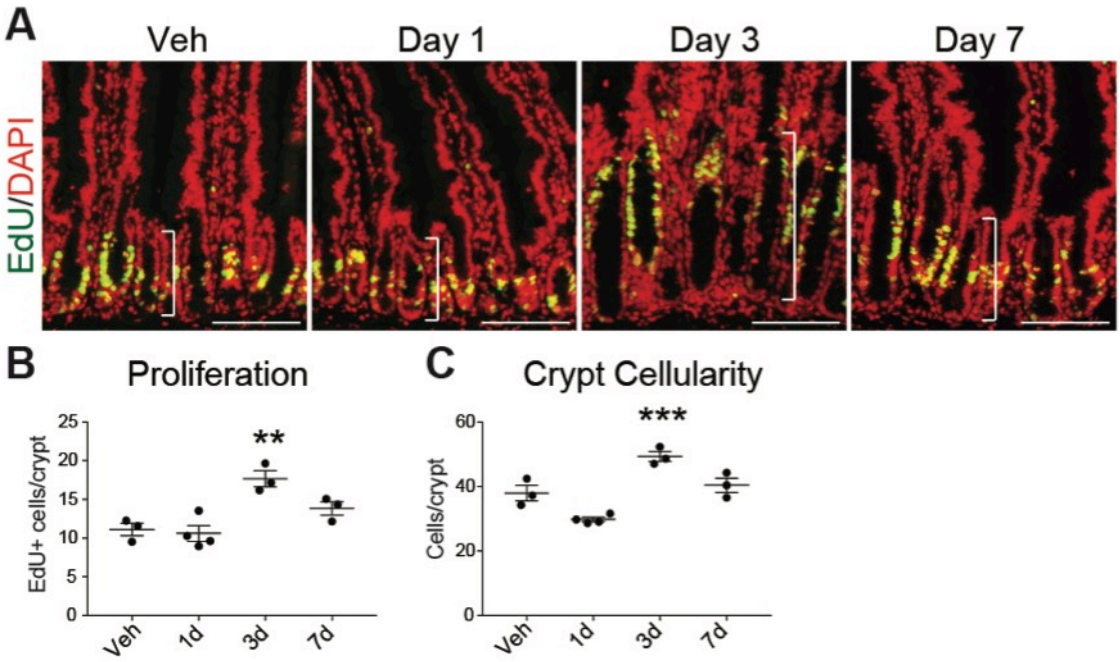

Figure 4.4 Proliferative surge and crypt expansion after Notch inhibition.

(A) Cellular proliferation was assessed in Veh- and DBZ-treated mouse duodenum at various time points by EdU incorporation (green) with DAPI (red). White brackets highlight crypt depth. (B) Quantification of the number of EdU-positive cells per crypt. (C) Crypt cellularity was determined by the number of DAPI-stained nuclei per crypt. Scale bars = 100μm. Quantitative data are presented as mean +/- SEM (*P<0.05, **P<0.01, ***P<0.001 Veh vs. DBZ by one-way ANOVA and Dunnett's post-test; n=3-4 animals/group, as shown).

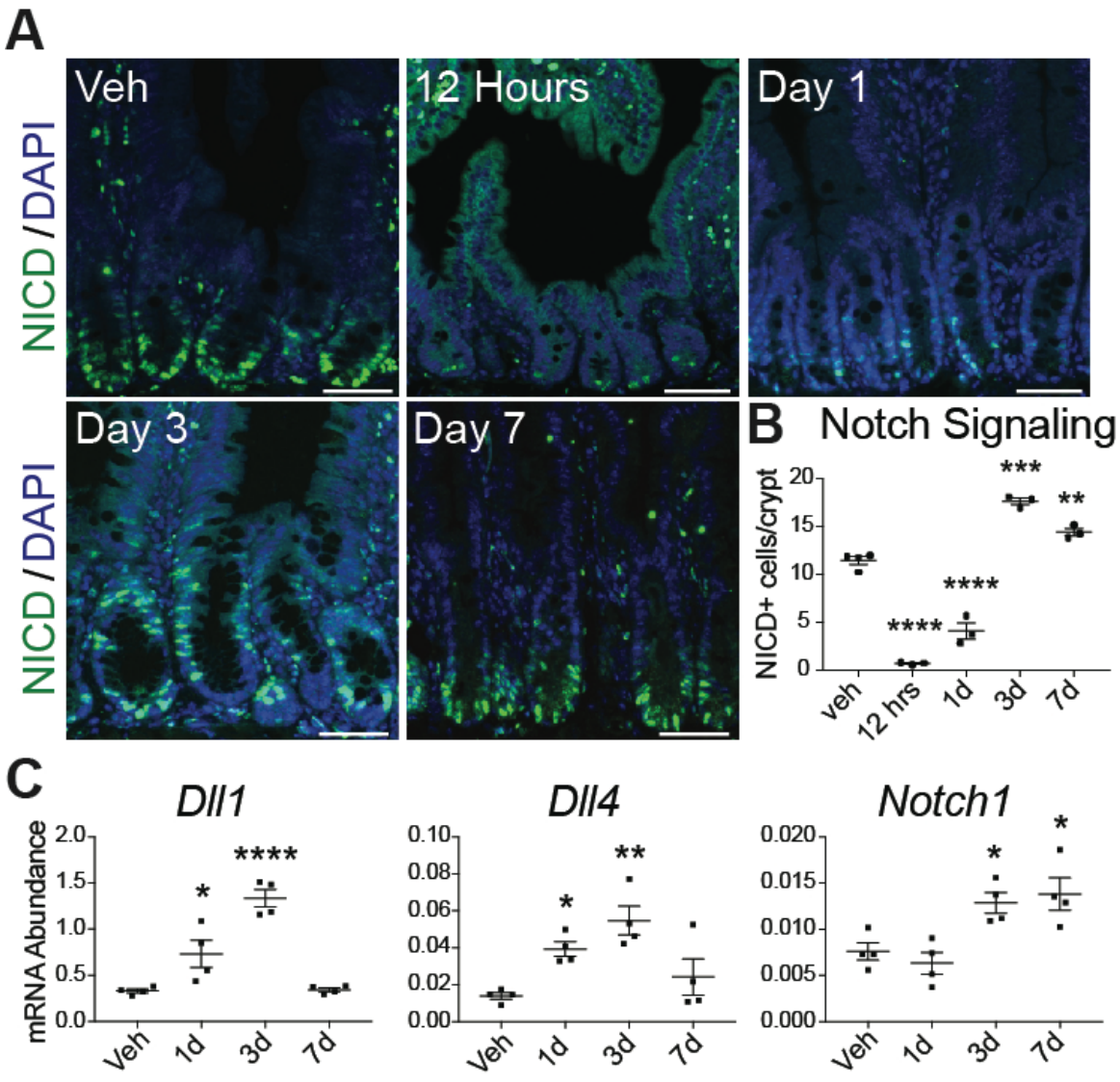

Figure 4.5 Notch activity surges during the regenerative phase.

(A) Notch activity at various times post DBZ treatment was determined by immunostaining for the Notch 1 intracellular domain NICD (green) with DAPI (blue). (B) Quantification of NICD-positive cells per duodenal crypt following Veh- or DBZ-administration. (C) qPCR analysis of mRNA abundance of key Notch components in Veh- and DBZ-treated mouse duodenal crypts. Scale bars = 50μm. Quantitative data are presented as mean +/- SEM (*P<0.05, **P<0.01, ***P<0.001, ****P<0.0001 Veh vs. DBZ by One-way ANOVA and Dunnett's post-test; n-3-4 animals/group as shown).

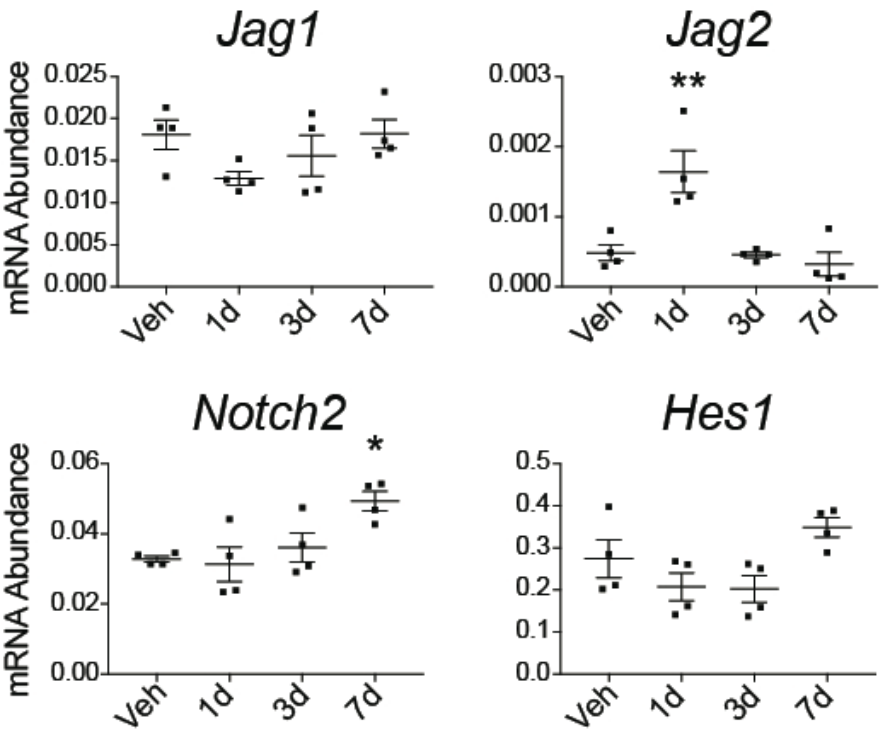

Figure 4.6 Analysis of Notch pathway component expression after Notch inhibition.

qPCR analysis of mRNA abundance of Notch components in duodenal crypt RNA isolated from Veh- or DBZ-treated mice at indicated time points (n=3-4 animals/group). Quantitative data are presented as mean +/- SEM.

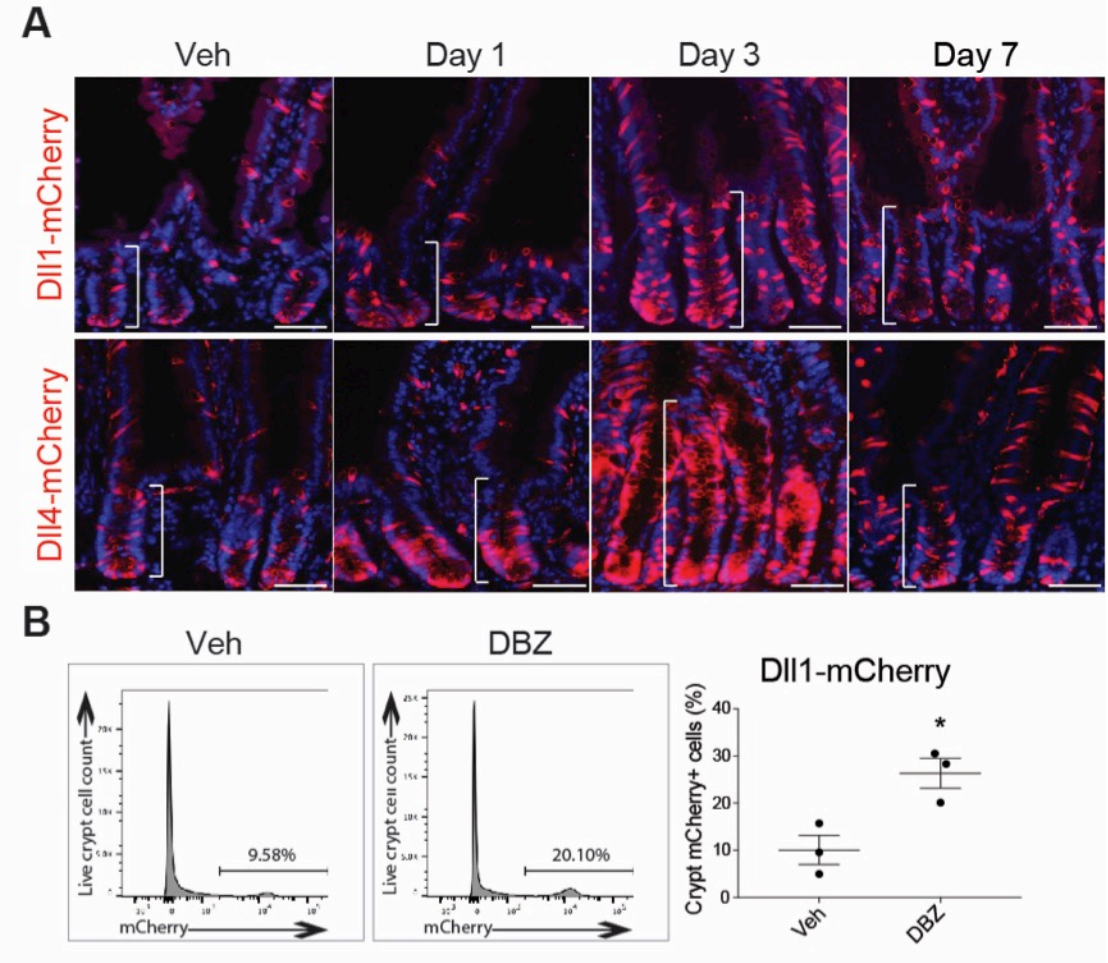

Figure 4.7 DLL1- and DLL4-positive cell expansion after Notch inhibition.

(A) *Dll1-mCherry* and *Dll4-mCherry* mice were treated with Veh or DBZ and mCherry marked cells (red) were imaged in duodenal sections with DAPI (blue). (B) FACS analysis of mCherry-positive cells in *Dll1-mCherry* duodenal crypts 1 day post Veh- or DBZ-treatment. Scale bars = 25 μ m. Quantitative data are presented as mean +/- SEM (***P<0.001 Veh vs. DBZ by Student's t-test; n=3-4 animals/group).

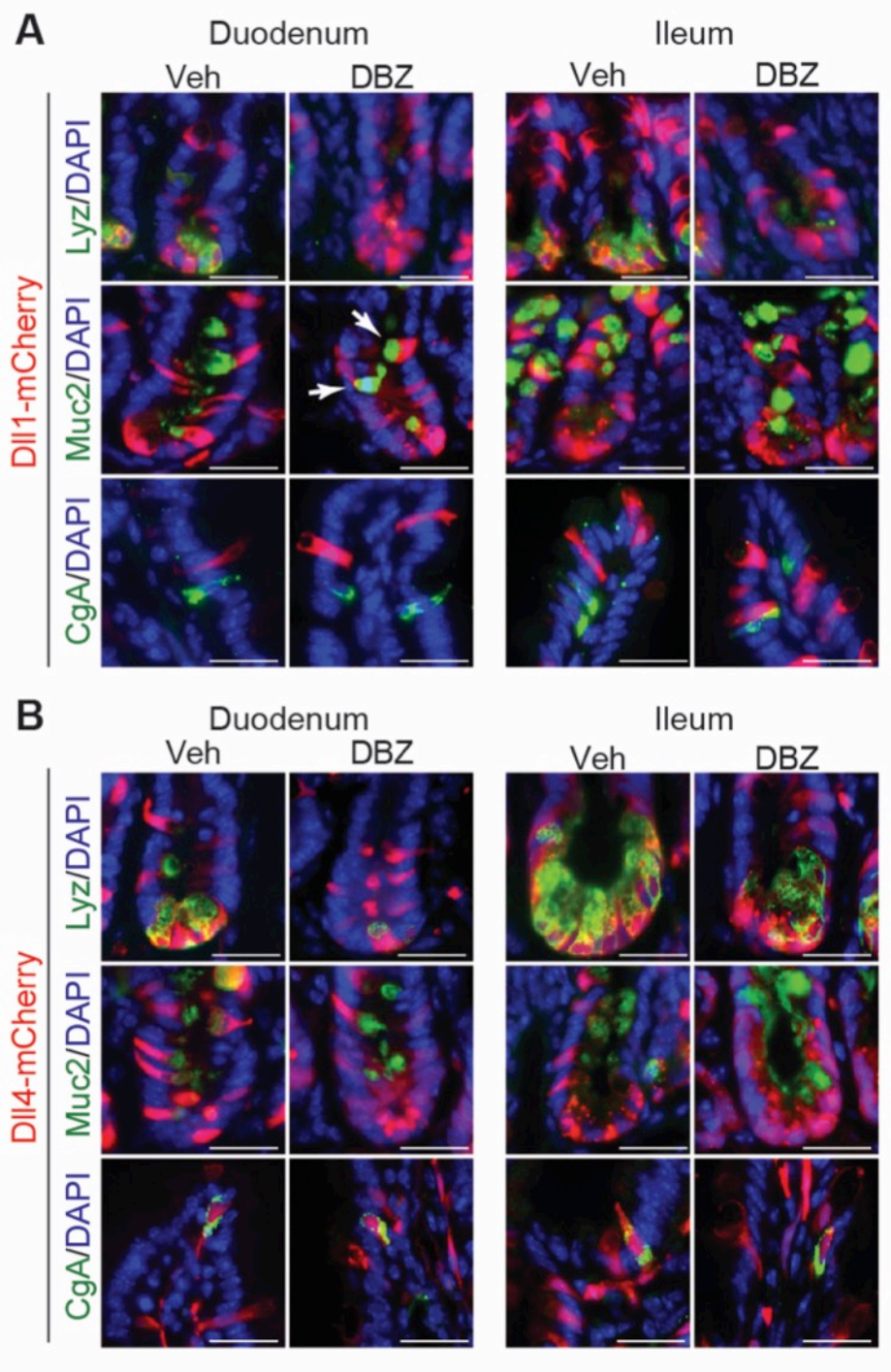

Figure 4.8 *Dll1-mCherry* and *Dll4-mCherry* transgenes are expressed in secretory cell types.

Analysis of Veh- and DBZ-treated (A) *Dll1-mCherry* and (B) *Dll4-mCherry* duodenum and ileum 1 day following treatment. Intestinal sections were imaged for mCherry and immunostained for various secretory cell markers (green), including the Paneth cell marker lysozyme (Lyz), the goblet cell marker mucin 2 (Muc2) and the enteroendocrine cell marker chromogranin A (CgA), with nuclear DAPI (blue). Scale bar = 25μm.

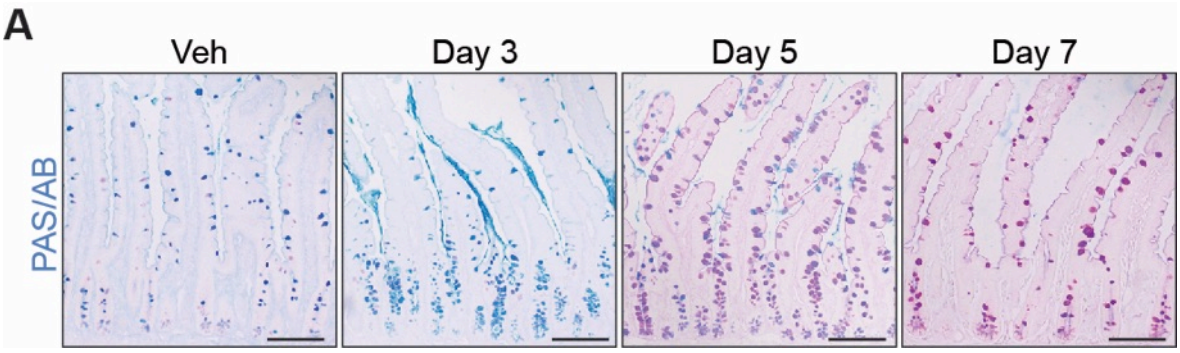

Figure 4.9 Notch inhibition results in secretory cell hyperplasia.

(A) Periodic acid-Schiff/ alcian blue (PAS/AB) stained duodenum at various times after acute DBZ treatment (n=3-5 animals/group). Scale bar = 100μm.

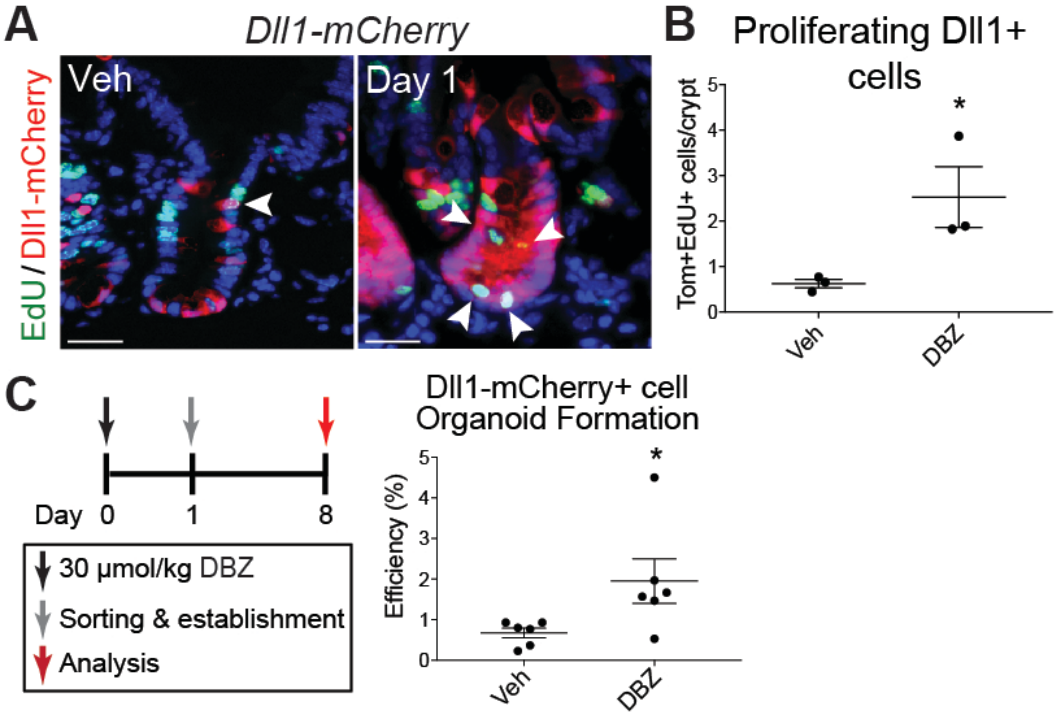

Figure 4.10 DLL1-positive cells form proliferating progenitors after Notch inhibition.

(A) *Dll1-mCherry* mice were treated with Veh or DBZ and proliferation was measured 1 day later by EdU incorporation. Arrowheads highlight mCherry (red) and EdU (green) co-stained cells, which represent proliferating *Dll1*-expressing progenitors. (B) The number of co-stained cells was quantified (n=3 mice/group). Scale bars = 25µm. (C) Schematic of organoid formation assay used to measure stem cell-like activity of mCherry-positive cells isolated from *Dll1-mCherry* mice 24 hours after Veh or DBZ. After FACS isolation, Dll1-mCherry positive cells were plated in Matrigel to form organoids. Organoid formation efficiency was determined by counting organoid number and presented as percent of the number of cells plated (n=6 mice/group with 3 technical replicates per mouse). Quantitative data are presented as mean +/- SEM (*P<0.05 Veh vs. DBZ by Student's t-test; n=3 animals/group).

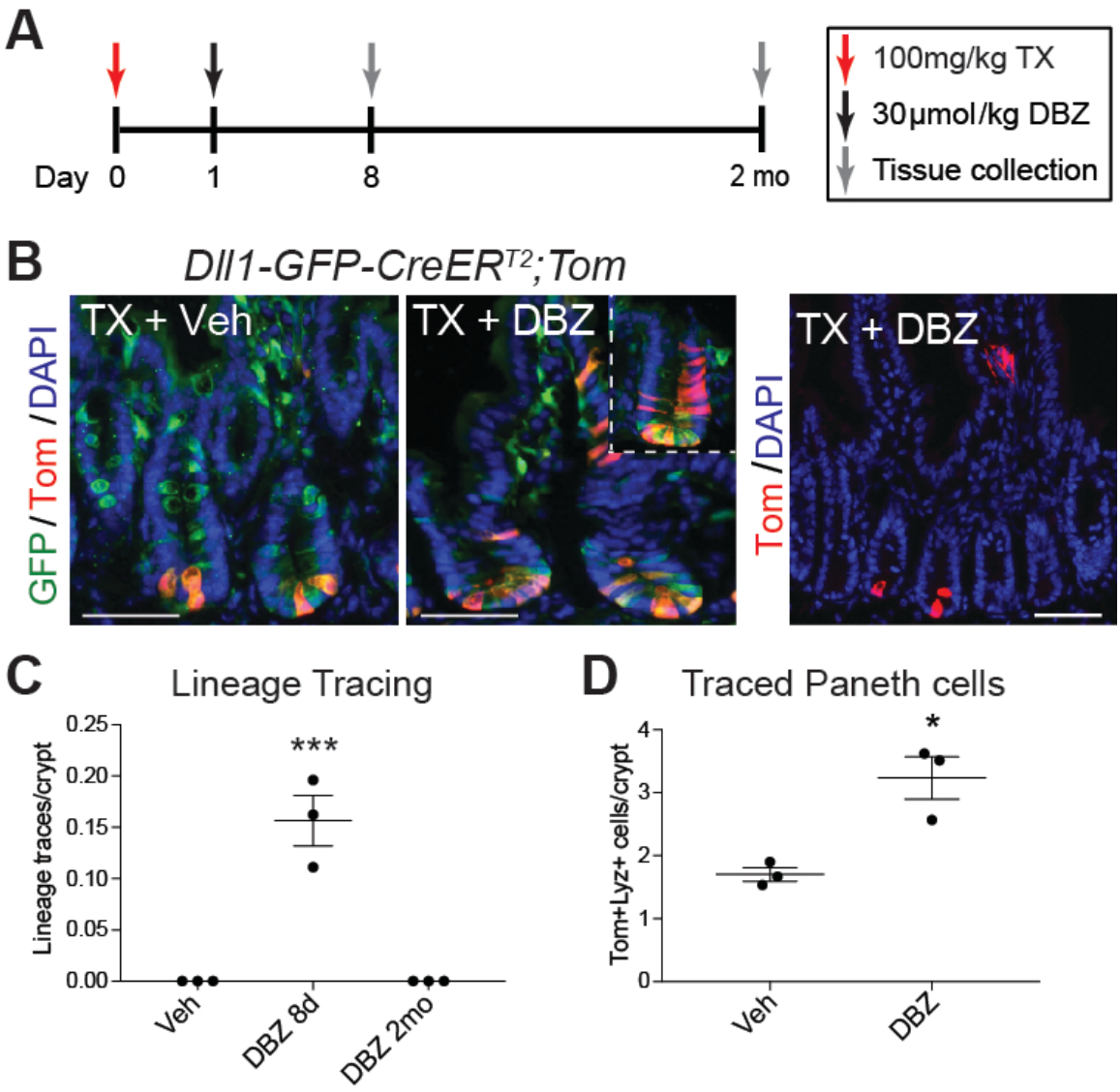

Figure 4.11 DLL1-positive progenitor cells regenerate Paneth cells.

(A) Schematic of the experimental design. *Dll1-GFP-CreER^{T2};ROSA26-Tom* mice were treated with TX followed by Veh or DBZ, with duodenal tissue harvested at 8 days or 2 months as indicated. (B-C) Analysis of duodenal lineage tracing. (B) Duodenal sections were stained for GFP (green) to visualize *Dll1*-expressing cells, and tdTomato (red) to visualize Tom lineage-marked cells at 8 days (left and middle) and 2 months (right) following TX treatment. The inset in the middle image shows an example of a lineage trace. Scale bars = 50 µm. (C) The number of lineage traces, defined as a ribbon of 4 or more Tom-positive cells, was quantified. (D) Paneth cells arising from *Dll1*-expressing progenitors were identified at 8 days by visualizing Tom and staining for lysozyme, and presented as the number of Tom/lysozyme double positive cells per duodenal crypt. Quantitative data are presented as mean +/- SEM (***P<0.001, *P<0.05 Veh vs. DBZ by One-way ANOVA and Dunnett's post-test , or Student's *t*-test).

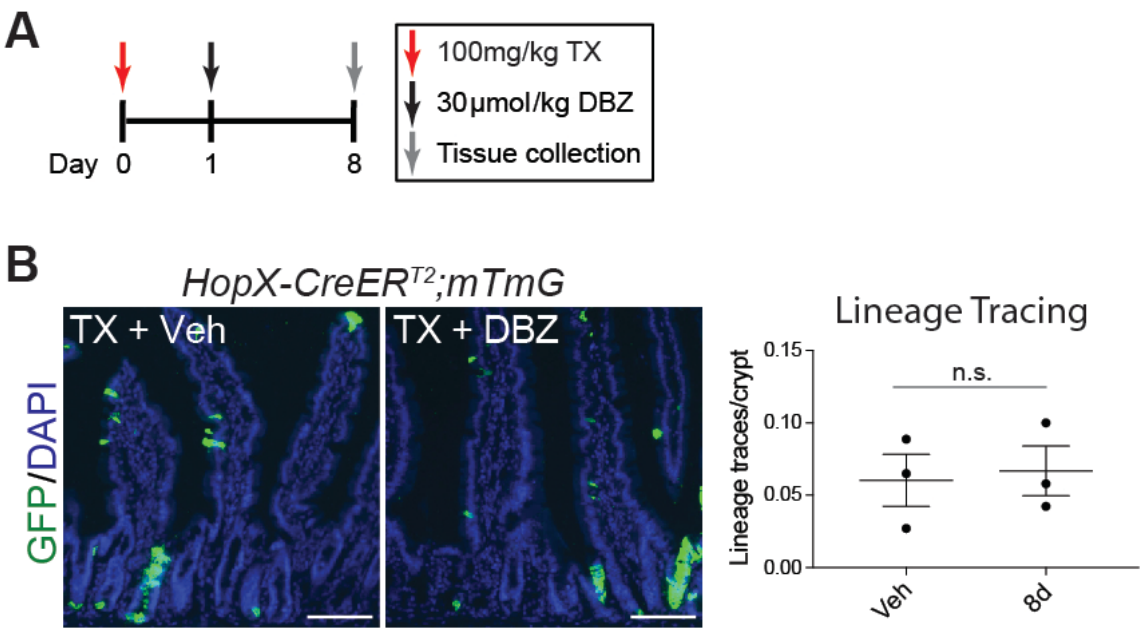

Figure 4.12 Notch inhibition does not activate HopX-positive cells to contribute to Paneth cell regeneration.

(A) Schematic of experimental design. *HopX-CreER^{T2};ROSA26-mTmG* animals were administered Veh or DBZ 24 hours following a single 100 mg/kg dose of TX, and tissue was harvested at 8 days. (B) *HopX-CreER^{T2};mTmG* animals displayed lineage traces (green) from HopX-marked facultative intestinal stem cells. The number of lineage traces, as defined by a ribbon of 4 or more GFP cells per crypt was quantified. (n=3 animals/group). Scale bar = 100µm. Quantitative data are presented as mean +/- SEM (Veh vs. DBZ by Student's *t*-test).

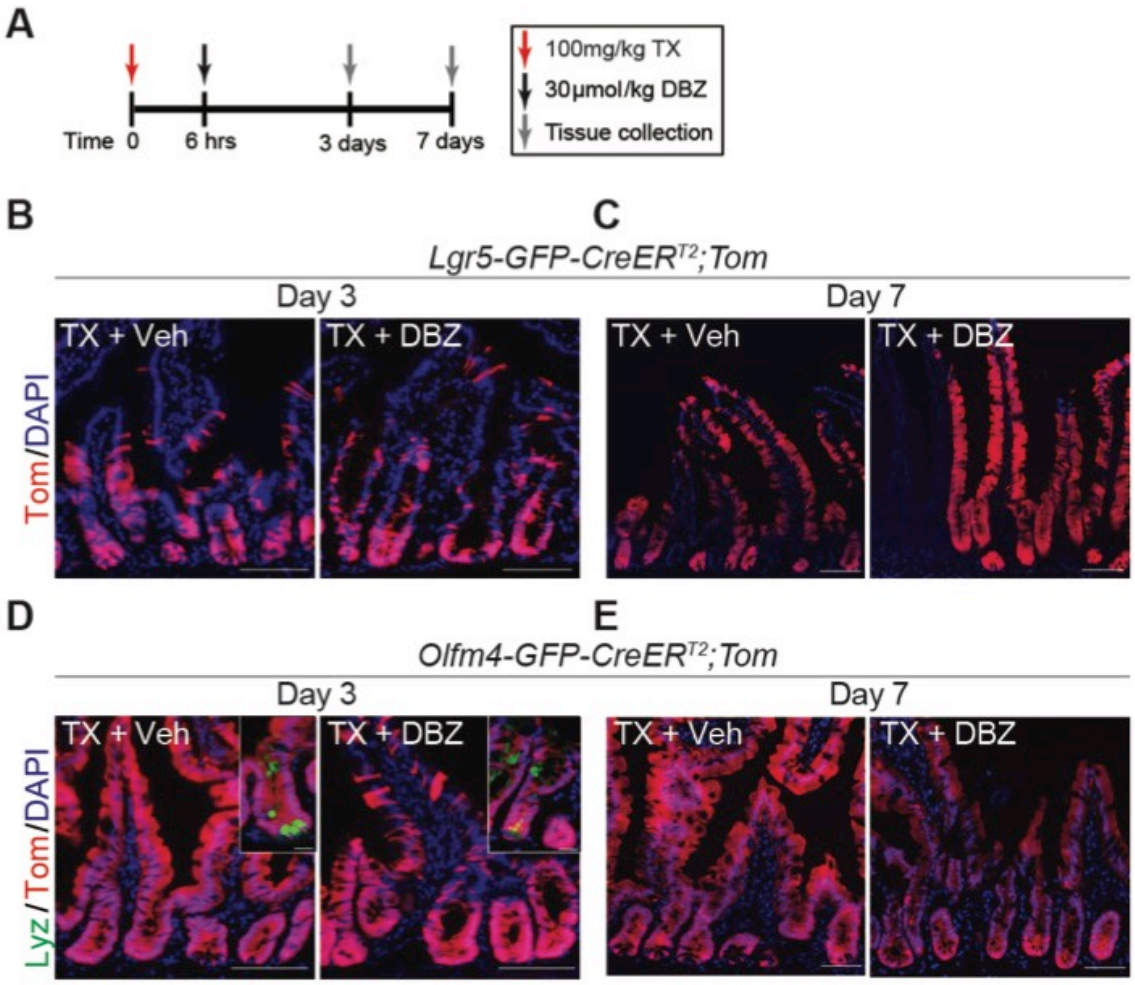

Figure 4.13 Impaired CBC function following acute Notch inhibition resolves concomitantly with Paneth cell return.

(A) Schematic of experimental design. *Lgr5-GFP-CreER^{T2};Tom* and *Olmf4-GFP-CreER^{T2};Tom* animals were administered Veh or DBZ 6 hours following a single 100 mg/kg dose of TX, and tissue was harvested (B,D) 3 or (C,E) 7 days after treatment. (B,C) *Lgr5-GFP-CreER^{T2};Tom* and (D,E) *Olmf4-GFP-CreER^{T2};Tom* mice displayed lineage tracing (red) from Lgr5- and Olfm4-marked CBCs, with (D) insets staining for Lyz-marked Paneth cells. (n=3 animals/group). Scale bar = 25µm.

4.9 References

1. Barker, N. *et al.* Identification of stem cells in small intestine and colon by marker gene Lgr5. *Nature* **449,** 1003–7 (2007).

2. Sato, T. *et al.* Single Lgr5 stem cells build crypt-villus structures in vitro without a mesenchymal niche. *Nature* **459,** 262–265 (2009).

3. Cheng, H., Merzel, J. & Leblond, C. P. Renewal of Paneth cells in the small intestine of the mouse. *Am. J. Anat.* **126,** 507–525 (1969).

4. Ireland, H., Houghton, C., Howard, L. & Winton, D. J. Cellular inheritance of a Cre-activated reporter gene to determine paneth cell longevity in the murine small intestine. *Dev. Dyn.* **233,** 1332–1336 (2005).

5. Takeda, N. *et al.* Interconversion between intestinal stem cell populations in distinct niches. *Science* **334,** 1420–4 (2011).

6. Tetteh, P. W. *et al.* Replacement of Lost Lgr5-Positive Stem Cells through Plasticity of Their Enterocyte-Lineage Daughters. *Cell Stem Cell* **18,** 203–213 (2016).

7. van Es, J. H. *et al.* Dll1+ secretory progenitor cells revert to stem cells upon crypt damage. *Nat. Cell Biol.* **14,** 1099–1104 (2012).

8. Sangiorgi, E. & Capecchi, M. R. Bmi1 is expressed in vivo in intestinal stem cells. *Nat. Genet.* **40,** 915–920 (2008).

9. Yan, K. S. *et al.* The intestinal stem cell markers Bmi1 and Lgr5 identify two functionally distinct populations. *Proc. Natl. Acad. Sci. U. S. A.* **109,** 466–71

(2012).

10. Montgomery, R. K. *et al.* Mouse telomerase reverse transcriptase (mTert) expression marks slowly cycling intestinal stem cells. *Proc. Natl. Acad. Sci. U. S. A.* **108,** 179–84 (2011).

11. Powell, A. E. *et al.* The pan-ErbB negative regulator Lrig1 is an intestinal stem cell marker that functions as a tumor suppressor. *Cell* **149,** 146–58 (2012).

12. Roth, S. *et al.* Paneth cells in intestinal homeostasis and tissue injury. *PLoS One* **7,** e38965 (2012).

13. Tian, H. *et al.* A reserve stem cell population in small intestine renders Lgr5-positive cells dispensable. *Nature* **478,** 255–9 (2011).

14. Yu, S. *et al.* Paneth Cell Multipotency Induced by Notch Activation following Injury. *Cell Stem Cell* **23,** 46–59.e5 (2018).

15. Dempsey, P. J., Bohin, N. & Samuelson, L. C. in *Physiology of the Gastrointestinal Tract* (eds. Said, H. M., Ghishan, F. K., Kaunitz, J. D., Merchant, J. L. & Wood, J. D.) 141–183 (Academic Press, 2018).

16. Korinek, V. *et al.* Depletion of epithelial stem-cell compartments in the small intestine of mice lacking Tcf-4. *Nat. Genet.* **19,** 379–383 (1998).

17. Ireland, H. *et al.* Inducible cre-mediated control of gene expression in the murine gastrointestinal tract: effect of loss of β-catenin. *Gastroenterology* **126,** 1236–1246 (2004).

18. Muncan, V. *et al.* Rapid loss of intestinal crypts upon conditional deletion of the Wnt/Tcf-4 target gene c-Myc. *Mol. Cell. Biol.* **26,** 8418–26 (2006).

19. Pellegrinet, L. *et al.* Dll1- and dll4-mediated notch signaling are required for homeostasis of intestinal stem cells. *Gastroenterology* **140,** 1230-1240.e1–7 (2011).

20. Gregorieff, A. *et al.* Expression Pattern of Wnt Signaling Components in the Adult Intestine. *Gastroenterology* **129,** 626–638 (2005).

21. Shtutman, M. *et al.* The cyclin D1 gene is a target of the beta-catenin/LEF-1 pathway. *Proc. Natl. Acad. Sci. U. S. A.* **96,** 5522–7 (1999).

22. Tetsu, O. & McCormick, F. β-Catenin regulates expression of cyclin D1 in colon carcinoma cells. *Nature* **398,** 422–426 (1999).

23. Vermeulen, L. *et al.* Wnt activity defines colon cancer stem cells and is regulated by the microenvironment. *Nat. Cell Biol.* **12,** 468–476 (2010).

24. VanDussen, K. L. *et al.* Notch signaling modulates proliferation and differentiation of intestinal crypt base columnar stem cells. *Development* **139,** 488–97 (2012).

25. Carulli, A. J. *et al.* Notch receptor regulation of intestinal stem cell homeostasis and crypt regeneration. *Dev. Biol.* **402,** 98–108 (2015).

26. Liu, Z. *et al.* The intracellular domains of Notch1 and Notch2 are functionally equivalent during development and carcinogenesis. *Development* **142,** 2452–63 (2015).

27. Riccio, O. *et al.* Loss of intestinal crypt progenitor cells owing to inactivation of both Notch1 and Notch2 is accompanied by derepression of CDK inhibitors p27Kip1 and p57Kip2. *EMBO Rep.* **9,** 377–83 (2008).

28. van Es, J. H. *et al.* Notch/gamma-secretase inhibition turns proliferative cells in intestinal crypts and adenomas into goblet cells. *Nature* **435,** 959–63 (2005).

29. Sato, T. *et al.* Paneth cells constitute the niche for Lgr5 stem cells in intestinal crypts. *Nature* **469,** 415–8 (2011).

30. Sato, T. *et al.* Long-term expansion of epithelial organoids from human colon, adenoma, adenocarcinoma, and Barrett's epithelium. *Gastroenterology* **141,** 1762–1772 (2011).

31. Sasaki, N. *et al.* Reg4+ deep crypt secretory cells function as epithelial niche for Lgr5+ stem cells in colon. *Proc. Natl. Acad. Sci. U. S. A.* **113,** E5399-407 (2016).

32. Schuijers, J., van der Flier, L. G., van Es, J. & Clevers, H. Robust cre-mediated recombination in small intestinal stem cells utilizing the olfm4 locus. *Stem cell reports* **3,** 234–41 (2014).

33. Burger, E. *et al.* Loss of Paneth Cell Autophagy Causes Acute Susceptibility to Toxoplasma gondii-Mediated Inflammation. *Cell Host Microbe* **23,** 177–190.e4 (2018).

34. Chakrabarti, R. *et al.* Notch ligand Dll1 mediates cross-talk between

mammary stem cells and the macrophageal niche. *Science* **360,** eaan4153 (2018).

35. Madisen, L. *et al.* A robust and high-throughput Cre reporting and characterization system for the whole mouse brain. *Nat. Neurosci.* **13,** 133–40 (2010).

36. Muzumdar, M. D., Tasic, B., Miyamichi, K., Li, L. & Luo, L. A global double-fluorescent Cre reporter mouse. *genesis* **45,** 593–605 (2007).

37. Wu, Y. *et al.* Therapeutic antibody targeting of individual Notch receptors. *Nature* **464,** 1052–1057 (2010).

38. Ridgway, J. *et al.* Inhibition of Dll4 signalling inhibits tumour growth by deregulating angiogenesis. *Nature* **444,** 1083–1087 (2006).

39. Demitrack, E. S. *et al.* Notch signaling regulates gastric antral LGR5 stem cell function. *EMBO J.* **34,** 2522–36 (2015).

40. Lopez-Diaz, L. *et al.* Parietal cell hyperstimulation and autoimmune gastritis in cholera toxin transgenic mice. *Am. J. Physiol. Liver Physiol.* **290,** G970–G979 (2006).

41. Gifford, G. B. *et al.* Notch1 and Notch2 receptors regulate mouse and human gastric antral epithelial cell homoeostasis. *Gut* **66,** 1001–1011 (2017).

42. Milano, J. *et al.* Modulation of notch processing by gamma-secretase inhibitors causes intestinal goblet cell metaplasia and induction of genes

known to specify gut secretory lineage differentiation. *Toxicol. Sci.* **82,** 341–58 (2004).

43. van der Flier, L. G. *et al.* Transcription Factor Achaete Scute-Like 2 Controls Intestinal Stem Cell Fate. *Cell* **136,** 903–912 (2009).

44. Tran, I. T. *et al.* Blockade of individual Notch ligands and receptors controls graft-versus-host disease. *J. Clin. Invest.* **123,** 1590–1604 (2013).

45. Stanger, B. Z., Datar, R., Murtaugh, L. C. & Melton, D. a. Direct regulation of intestinal fate by Notch. *Proc. Natl. Acad. Sci. U. S. A.* **102,** 12443–8 (2005).

46. Fre, S. *et al.* Notch signals control the fate of immature progenitor cells in the intestine. *Nature* **435,** 964–8 (2005).

47. Tian, H. *et al.* Opposing Activities of Notch and Wnt Signaling Regulate Intestinal Stem Cells and Gut Homeostasis. *Cell Rep.* **11,** 33–42 (2015).

48. Tsai, Y.-H. *et al.* ADAM10 regulates Notch function in intestinal stem cells of mice. *Gastroenterology* **147,** 822–834.e13 (2014).

49. Rodríguez-Colman, M. J. *et al.* Interplay between metabolic identities in the intestinal crypt supports stem cell function. *Nature* **543,** 424–427 (2017).

50. Farin, H. F., Van Es, J. H. & Clevers, H. Redundant sources of Wnt regulate intestinal stem cells and promote formation of Paneth cells. *Gastroenterology* **143,** 1518–1529.e7 (2012).

51. Kim, T.-H., Escudero, S. & Shivdasani, R. A. Intact function of Lgr5 receptor-expressing intestinal stem cells in the absence of Paneth cells. *Proc. Natl.*

Acad. Sci. U. S. A. **109,** 3932–7 (2012).

52. Durand, A. *et al.* Functional intestinal stem cells after Paneth cell ablation induced by the loss of transcription factor Math1 (Atoh1). *Proc. Natl. Acad. Sci. U. S. A.* **109,** 8965–70 (2012).

53. Garabedian, E. M., Roberts, L. J., McNevin, M. S. & Gordon, J. I. Examining the role of Paneth cells in the small intestine by lineage ablation in transgenic mice. *J. Biol. Chem.* **272,** 23729–40 (1997).

54. Mathur, D., Bost, A., Driver, I. & Ohlstein, B. A Transient Niche Regulates the Specification of Drosophila Intestinal Stem Cells. *Science (80-.).* **327,** 210–213 (2010).

55. Guo, Z. & Ohlstein, B. Bidirectional Notch signaling regulates Drosophila intestinal stem cell multipotency. *Science (80-.).* **350,** aab0988-aab0988 (2015).

56. Beumer, J. & Clevers, H. Regulation and plasticity of intestinal stem cells during homeostasis and regeneration. *Development* **143,** 3639–3649 (2016).

Chapter V: Summary and Perspectives

5.1 Molecular mechanism of FSC contribution to irradiation-induced intestinal regeneration

5.1.1 Summary

In Chapter II, I propose a mechanism of intestinal response to injury by which paracrine IGF1 signaling from the mesenchyme stimulates mTORC1 activity in FSCs, priming them for activation, leading to their subsequent contribution to the regenerative response (**Figure 2.10**). We show that the hallmark intestinal response to irradiation injury enhances expression of many different growth factors, pertinently IGF1, which we show to be expressed in pericryptal subepithelial cells (**Figure 2.2**). We find that inhibition of IGF1 signaling is prohibitive to proper intestinal regeneration (**Figure 2.3**), and that this effect is mimicked by inhibition of downstream mTORC1 signaling (**Figure 2.6 and 2.9**). We show that mTORC1 is critical to FSC contribution to the intestinal regenerative response 24-48 HPI (**Figure 2.8**). We also demonstrate that genetic intestinal epithelial cell-specific enhancement of mTORC1 activity has no discernable impact on intestinal regeneration (**Figure 2.9**). We also show that mTORC1-depleted mice display a significantly greater enhancement in IGF1 expression post-irradiation, compared to control animals (**Figure 2.9**), indicative of a feedback

mechanism potentially compensating for depleted mTORC1 activity. Thus, my data suggests that increased IGF1 expression post-injury leads to increased mTORC1 activity in crypt cells, promoting FSC contribution to intestinal regeneration.

5.1.2 Perspectives

We show that intestinal injury results in increased IGF1 expression from a pericryptal subepithelial cell (**Figure 2.2**). Identifying whether increased IGF1 expression results in increased secretion of IGF1 will be critical to show paracrine effects of IGF1 signaling. To this aim, determining the identify of these injury-responsive *Igf1*-expressing pericryptal subepithelial cells would be critical. A good place to start in identifying IGF1-expressing pericryptal subepithelial cells would be to test whether the Kaestner group's Foxl1-positive pericryptal telocytes or the Basler group's Wnt2b-secreting *Gli1* or *Acta2*-positive subepithelial myofibroblasts express IGF1 (e.g. using the Kaestner laboratories' published RNA sequencing data to see if *Igf1* is expressed in Foxl1-positive cells),[1–3] and if they respond to injury. Knowing the identity of IGF1-expressing cells would allow us to isolate them (via FACS sorting if a marker for which good FACS antibodies or a reporter mouse model exists, or laser capture microdissection) and test their function by co-culturing them with organoids. We could assess whether injury stimulates increased IGF1 secretion (e.g. testing cultured media from these cells in a baseline and injury context for IGF1) which we could test by Western Blotting analysis. We could also ablate *Igf1* in these cells (e.g. using the resulting cross

between the Kaestner laboratory's *Foxl1-CreER*^{T2} mice,[2] and floxed *Igf1* mice)[4] and assess whether we lose the injury-stimulated increased *Igf1* expression, and with it, whether intestinal regeneration is impaired. If we do see impaired intestinal regeneration with loss of *Igf1*-expressing pericryptal subepithelial cells, it would be requisite to check if IP administration of IGF1 rescues intestinal regeneration, given that we expect these cells to secrete other factors contributing to repair.[1,2] If that is the case, we could then conclude that injury stimulates IGF1 secretion from pericryptal subepithelial cells, and that this response is critical to effective intestinal regeneration.

The mechanism by which the injured intestine stimulates increased IGF1 levels has not yet been investigated. Perhaps specific signals coming from the damaged epithelium or inflammatory cells induce this response, and could be interrogated by cross-referencing factors shown to be secreted post-injury (e.g. inflammatory cytokines) with factors capable of stimulating increased *Igf1* expression (e.g. Interleukin-1)[5]. We could then test if these are the right signaling factors by looking to see if their injection can mimic the increased *Igf1* expression observed following injury. We could also assess if these same factors are responsible for enhancing the expression of the other growth factors that we identified in our qPCR array.

It would be interesting to test whether the other growth factors identified in our qPCR array as having their expression enhanced post-irradiation (e.g. *Ereg* coding for epiregulin, *Hgf*) are also secreted by the same pericryptal subepithelial cells that secrete IGF1. Interestingly, our *in situ* hybridization data maps *Ereg*

expression to the epithelium rather than the mesenchyme like *Igf1* (data not shown), suggesting that the growth factors that we identified to be associated with intestinal regeneration are coming from various intestinal cellular sources.

To conclusively determine that the pro-regenerative effect of IGF1 works through mTORC1, we would need to carry out an experiment to assess if mTORC1 can rescue regeneration in animals depleted of IGF1 signaling. This experiment could be carried out a number of ways, using a combination of pharmacological and genetic methods of modulating mTORC1 and IGF1. We might start by assessing whether activation of mTORC1 via leucine administration (as has been done previously)[6] rescues the impaired regenerative capacity observed by globally inhibiting IGF1 signaling pharmacologically (BMS administration). Another method we might employ would be to test the consequences of genetic depletion of IGF1 signaling (e.g. *Igf1* deletion) broadly throughout the intestinal mesenchyme (e.g. *PDGFRα-CreER^{T2}* mice), to more restricted intestinal mesenchymal populations (e.g. *Gli1-CreER^{T2}* mice) or in specific subepithelial cellular populations (e.g. *Foxl1-CreER^{T2}*), post-injury. We expect the results to mimic the regenerative impairment observed with pharmacologic inhibition of IGF1. We would then administer leucine to these animals[6] and assess regenerative capacity. We would expect leucine-mediated activation of mTORC1 to rescue the impaired regeneration of genetic depletion of IGF1 signaling.

An additional method by which we might determine that IGF1 works through mTORC1 to promote intestinal regeneration would be by assessing whether *Villin-*

CreER^{T2};Raptor$^{F/F}$ mice depleted of mTORC1 activity are spared from the pro-regenerative effect of IGF1 administration by IP injection. We would expect control (tamoxifen-treated *Villin-CreER^{T2}*) animals to have enhanced intestinal repair following IGF1 administration, as previously reported,[7] but that animals genetically depleted of mTORC1 would retain the impaired regenerative capacity that our studies report. This would indicate that the role of IGF1 in mediating effective intestinal repair occurs through the activity of mTORC1. Interestingly, our findings that genetically increased mTORC1 activity (albeit p-S6(S240/244)) is only slightly increased in this model; **Figure 2.9**) does not result in enhanced regeneration, while injection of IGF1 has been shown to lead to enhanced intestinal regeneration,[7] suggests there may be other mTORC1-independent mechanisms mediating the pro-regenerative effect of IGF1. Certainly, how different molecular mechanisms integrate their signals to regulate the intestinal regenerative response is an area that warrants further study.

My work proposed a mechanism by which injury-stimulated IGF1 signals to the crypts, and activates mTORC1 in FSCs, leading to their mobilization and contribution to the regenerative response. We show that mTORC1 activity is increased in the intestinal crypts post-injury (**Figure 2.5**), and that it is critical to FSC contribution to crypt re-population (**Figure 2.8**). However, to assess if the proposed model is valid, future work will first need to determine if mTORC1 activity is increased in FSCs in response to injury and IGF1 administration. This can be done in many different ways including: co-staining for p-S6(S240/244) and FSC markers for which immunostaining antibodies have been developed (e.g. HopX,

Bmi1), staining for p-S6(S240/244) on tissues from FSC reporter mouse models (e.g. *Bmi1-CreER^{T2};ROSA26-lacZ*), or looking for p-S6(S240/244) in sorted FSCs. The different FSC populations should be examined to determine if mTORC1 mobilizes a subset of FSCs over others (e.g. mitotically dormant Bmi1-positive FSCs). In addition to verifying if mTORC1 activity is induced in FSCs following damage, future work needs to determine if mTORC1 activity induces a change of FSC state from its homeostatic role to a stem cell pro-regenerative role. This has been proposed to occur in mitotically dormant satellite cells in skeletal muscle,[8] as described in Chapter I, with mTORC1 activity inducing their change to a mitotically active state able to repair injured muscle tissue. It has also been suggested in dormant FSCs by the Breault lab,[9,10] but has yet to be tested.

Further, significant work is also needed to determine whether non-quiescent FSC populations are differentially affected by mTORC1 status. One way to test this would be to isolate mRNA from *Bmi1*-expressing FSCs (whose contribution to repair we have shown to be regulated by mTORC1 in **Figure 2.8**), using reporter mice *Bmi1-CreER^{T2};ROSA26-Tom* to label FSCs, prior to and following mTORC1 activation (e.g. administer vehicle, leucine or IGF1, and FACS sort Tom-labeled cells). We would then assess whether mTORC1 activity leads to gene signature changes that might correspond to changes in functional states. Subsequently to testing *Bmi1*-expressing FSC populations, we could broaden our analysis to other FSC populations, such as fated progenitors (e.g. *Dll1*-expressing FSCs) or differentiated cells (e.g. Paneth cells) to assess if their mobilization post-injury might be differentially regulated by mTORC1 activity. We would propose that the

regenerative capacity of these cells would also be regulated by mTORC1 in a process recently described in other organs and coined “paligenosis.”[11] Paligenosis is a cellular process by which mature gastric chief cells and pancreatic acinar cells re-enter the cell cycle and fuel regeneration following injury in an mTORC1-dependent manner.[11] This process has yet to be investigated in the intestine.

Our findings reveal that understanding IGF1/mTORC1 signaling is critically important to understand mechanisms of crypt cell plasticity and cellular remodeling after stem cell injury. Further, our work studies the regulation of stem cell restitution by both epithelial and mesenchymal cell compartments, thus contributing to a fuller understanding of the various components of the stem cell niche. Understanding the pro-regenerative role of IGF1/mTORC1 signaling could lead to the conception of therapies aimed at treating intestinal disorders associated with mucosal injury.

5.2 Mechanism of intestinal stem cell sensitivity to CreER^{T2}-induced DNA damage

5.2.1 Summary

In Chapter III, we discovered that activation of CreER^{T2} throughout the intestinal epithelium is genotoxic, and that CBCs are particularly sensitive to CreER^{T2} activation. In *Villin-CreER^{T2}* mice, activation of Cre recombinase by tamoxifen treatment results in impaired regenerative capacity following irradiation (**Figure 3.2**). We also show that CreER^{T2} activation in Olfm4- and Lgr5-positive

CBCs, using *Olfm4-CreER^{T2}* and *Lgr5-CreER^{T2}* respectively, results in impaired organoid formation, indicative of reduced stem cell function (**Figure 3.4**). Investigations into the mechanism by which CreER^{T2} activation could lead to impaired cellular functions found increased incidence of DSBs in intestinal crypts, and c*loxP* site cleavage (**Figure 3.6**). No increase in apoptosis was associated with this observation (**Figure 3.6**), suggesting DNA repair mechanisms may be engaged to resolve the activated CreER^{T2}-inflicted cellular damage, which would explain the lack of observable intestinal phenotype in unchallenged CreER^{T2}-activated mice (**Figure 3.1**). We conclude our studies by showing that impaired CBC function and genotoxicity is repaired by 7 days after activation, and that no toxicity is observed when a single dose of tamoxifen is administered to activate CreER^{T2} (**Figure 3.7**). My findings suggest that investigators should delay organoid formation and inflicting intestinal damage following tamoxifen activation of CreER drivers.

5.2.2 Perspectives

An interesting question that arises from our studies is how Cre protein levels correlate to genotoxicity. We showed similar levels of Cre protein in our *Villin-CreER^{T2}* (which displayed toxicity) and *Villin-Cre* (which did not) mouse strains (**Figure 3.3W**), indicating the differences in toxicity are not related to differences in Cre protein levels. Rather, our data suggests that the genotoxicity has to do with the nuclear translocation properties of CreER^{T2}.

The long-term outcome of Cre action at c*loxP* sites would be an interesting avenue of research to the field. We show that impaired ISC function and genotoxicity is repaired a week after CreER^{T2} activation, however, we did not test for activated CreER^{T2}-induced mutations at c*loxP* sites resulting from inaccurate DNA repair. This could have significant implications to intestinal epithelial homeostasis and tumorigenesis. The literature reports that CreER^{T2} genome cleavage can lead to chromosomal abnormalities,[12–14] suggesting that CreER^{T2} may be capable of mutagenesis in the mouse intestine. Assessing the extent and occurrence of mutagenic events in response to CreER^{T2} induction would require importing new genetic models and developing new assays. One such method might be sequencing the c*loxP* region some time after CreER^{T2} activation and aligning with the c*loxP* sequence prior to activation to determine if mutagenesis has occurred. The mechanism of DNA repair might also be interrogated, as certain mechanisms are more likely to result in mutagenic events. Mouse models to detect intestinal mutagenesis could also be employed, testing enhanced tumor formation as a consequence of inaccurate DNA repair that would occur with c*loxP* cleavage. This remains an interesting area of future study that would certainly benefit the vast number of laboratories employing intestinal CreER^{T2} mouse models.

5.3 Mechanism of FSC repopulation following acute niche factor inhibition-mediated Paneth cell loss

5.3.1 Summary

In Chapter IV, I propose a novel method of intestinal damage targeting Paneth cells via acute inhibition of the niche Notch signaling pathway. We demonstrate that acute Notch inhibition results in a rapid loss of Paneth cells by apoptosis (**Figure 4.2**) concomitant with impaired CBC activity (**Figure 4.1**). This crypt damage stimulates a proliferative surge reminiscent of the post-irradiation regenerative response characterized in Chapter II (**Figure 4.4** compared to **Figure 2.1**). We see increased numbers of Notch signaling crypt cells (**Figure 4.5**), and an expansion of *Dll1*-expressing cells (**Figure 4.7**) that, our data confirms, includes *DLL1*-expressing FSCs being mobilized to contribute to Paneth cell repopulation (**Figure 4.10** and **4.11**). Interestingly, we demonstrate that *Dll1*-expressing, but not HopX-positive FSCs contribute to Paneth cell repopulation (**Figure 4.12**). Our data not only describe a novel method of ablating Paneth cells to further our understanding of the stem cell niche, and the critical role of Notch in its maintenance, but they demonstrate selective activation of a particular FSC population. We propose a model by which acute Notch inhibition results in Paneth cell loss, which contributes to impaired CBC activity and *Dll1*-expressing FSC contribution to repopulating the vacant Paneth cell population.

5.3.2 Perspectives

While our studies focused on characterizing the intestinal response to acute Notch inhibition, future work is needed to determine the mechanism by which acute Notch inhibition leads to Paneth cell apoptosis. Previous mouse studies of Notch inhibition for a longer time (via genetic or pharmacological means) has been reported to lead to secretory cell expansion (including Paneth cell) rather than Paneth cell loss.[15] However, the Paneth cell expansion observed under these conditions was based on a limited number of markers, and the morphology of the cells expressing Paneth cell markers was abnormal and could indicate immature secretory progenitors.[16] Accumulation of immature Paneth cells in response to damage via niche disruption could be a result of a process recently described by Klein and Jensen labs known as fetal reversion, describing cells' ability to revert to a fetal-like or immature generative state,[17,18] a plasticity that Paneth cells have been reported to possess.[19] Further work is required to determine if fetal reversion is induced following niche disruption, and to understand how the cellular changes observed after long-term (6 days) Notch inhibition relate to the acute cellular changes we observed with acute Notch inhibition.

Paneth cell differentiation and maintenance at the crypt base requires Wnt signaling.[15] Given a prior report showing that manipulation of Notch activity can impact Wnt signaling status in ISCs,[20] it could be posited that an interruption to Notch signaling could effect Wnt, thereby resulting in Paneth cell damage. However, the study employed chronic Notch inhibition methods, and showed an increase in Wnt signaling, and resulting secretory cell hyperplasia.[20] Nonetheless,

our studies of acute Notch inhibition demonstrate findings distinct from studies employing chronic Notch inhibition methods, it would thus be interesting to see what happens to Wnt signaling in response to acute Notch inhibition. To answer this question, Wnt signaling status could be evaluated in acutely Notch inhibited intestinal crypts via qPCR analysis of Wnt target genes, and assessment of nuclear β-catenin levels as a read-out of Wnt activity. Albeit preliminary, our assessment of some Wnt target genes following acute Notch inhibitor administration did not reveal changes in Wnt signaling (data not shown), suggesting that other mechanisms may be at play. Certainly, significant work is needed to delineate the integration of Notch signaling with other pathways in regulating the ISC niche.

We could also propose another hypothesis for the cause of Paneth cell loss following acute Notch inhibition. From our studies in Chapter IV and the intestinal Notch signaling literature, we understand that Notch is critical to regulating CBC survival and function.[15] As such, we might postulate that there exists a yet undiscovered Notch-dependent survival signal that CBCs deliver to Paneth cells, whose delivery is disrupted following acute Notch inhibition. Interruption of this survival-promoting signaling from CBCs to Paneth cells could fathomably cause Paneth cell apoptosis. We could test this hypothesis by performing gene expression profiling of CBCs (e.g. FACS sorting *Lgr5*-expressing CBCs using the *Lgr5-GFP-CreER*^{T2} mouse model) prior to and following acute administration of Notch inhibitor DBZ, to determine if they are undergoing genetic changes post-acute Notch inhibition that would indicate they have ceased signaling to Paneth

cells. Significant work would subsequently be needed to characterize this CBC-secreted Notch-dependent Paneth cell survival factor.

As we did not initially seek out to establish a new intestinal injury model, our discovery that niche disruption via acute Notch inhibition results in intestinal damage and stimulation of a regenerative response was of great surprise. The initial damage induced by Notch inhibition in Chapter IV differed from the effects of 12 Gy γ-irradiation first described in Chapter II in that acute Notch inhibition did not result in the CBC loss reported with many damage models aimed at stimulating a regenerative response (including irradiation),[21] but rather led to loss of CBC-supporting Paneth cells and impaired CBC activity. Both CBC loss post-irradiation and CBC damage post-DBZ, although the latter has not been as extensively characterized as the former, resulted in a regenerative response characterized by increased proliferation and crypt hyperplasia at 3 days post-injury (comparing **Figures 2.1** and **4.4**). In both models, regeneration was fueled by FSCs mobilized to repair the damage, we showed *Bmi1*-positive and *Dll1*-positive FSCs contributed to intestinal repair following irradiation and acute Notch inhibition respectively (comparing **Figures 2.9** and **4.11**). Further, in both injury models, the intestinal epithelium was being repaired towards a return to homeostasis by 7 days post-injury. However, while post-irradiation, FSCs repopulated the CBC compartment, in our Notch inhibition model FSCs contributed to repopulation of the vacant Paneth cell population. Further, in the latter model, we showed selective activation of *Dll1*-positive, and not *HopX*-positive FSCs (**Figure 4.12**). While we did not investigate epithelial reconstitution by different FSC populations

in our irradiation model ourselves, other labs have shown activation of *HopX*-positive and *Dll1*-positive FSCs post-irradiation,[22,23] indicating an inherent difference in the cellular remodeling incurred by our two injury models, which warrants further study.

As discussed, our finding that acute Notch inhibition results in Paneth cell loss with CBC retention, with stimulation of a regenerative response, was unexpected, as previously reported regenerative responses stem from CBC loss.[21] However, we do show that CBCs have impaired activity following acute Notch inhibition, which could indicate that even CBC damage can stimulate repair responses. We show that this impaired activity is transient, with CBC lineage tracing from Notch inhibited mice returning to control levels within a few days after Notch inhibitor administration, which also tracks with the return of Paneth cells. While these findings are indicative of Paneth cells serving a CBC-supporting function, our data showing CBCs contributing to the return of Paneth cells (**Figure 4.13**) puts into question whether the return of CBC activity is a result of Paneth cell re-emergence. Rather, we suggest that while Paneth cell return is driven in part by CBCs, the resolved CBC activity is a result of returning Notch signaling. Hence, we propose that the return in Notch signaling drives the return of baseline CBC activity, which, alongside DLL1-expressing FSCs, fuels Paneth cell repopulation.

An outstanding question from our study demonstrating that both CBCs and *Dll1*-expressing FSCs give rise to Paneth cells, is the question of how *Dll1*-expressing cells emerge. One theory is that CBCs give rise to these cells. However, concomitant with the expansion of *Dll1*-expressing cells as early as day

1 after administration of the Notch inhibitor, is the absence of Paneth cells and impaired CBC activity. It would seem unlikely from our data, that, with their impaired lineage tracing ability, acutely Notch inhibited CBCs are driving the dramatic expansion of *Dll1*-expressing cells. Rather, it would seem more likely that the crypt damage induced by acute Notch inhibition is resulting in remodeling of crypt cells to activate expression of Notch ligands DLL1 and DLL4 to enhance Notch activity. The mechanism for this could be such that the interruption in lateral inhibition resulting from loss of Notch signaling allows the de-repression of Notch ligand expression. One of our hypotheses posits that CBCs may be turning on *Dll1* expression, thereby changing their identity and function. This would be in line with a possible mechanism of Notch signaling support of CBCs in immature, post-natal intestine, via autocrine Notch signaling to support ISC function.

One method by which we might address the question of autocrine Notch signaling being induced following damage to support CBC function, is by crossing a CBC reporter mouse model, such as *Olfm4-GFP-CreER^{T2};ROSA26-LSL-YFP,* with *Dll1-mCherry* reporter mice to generate mice in which we can lineage trace from CBCs, and visualize *Dll1*-expressing cells. These mice would allow us to determine whether CBCs are giving rise to the expanded *Dll1*-expressing cell compartment that we observe following acute Notch inhibition, or whether acute Notch inhibition is inducing CBC cell reprogramming to a *Dll1*-expressing state.

5.4 Conclusions

Given the incredible plasticity of the intestinal crypt, cell reprogramming following the injury induced by acute Notch inhibition and Paneth cell loss is a likely scenario by which *Dll1*-expressing cells are arising. The emergence of a multitude of different markers to describe the FSC appears to describe cells with distinct cellular characteristics, and has given rise to many questions about how we characterize these cells prior to and following injury. The question of how damage might alter expression of putative FSC markers is an important question that is important to understanding the intestinal regenerative response,[24] and that our work in Chapter IV begins to address.

While our studies in Chapters II and IV begin to scratch the surface regarding understanding mechanisms of crypt cellular plasticity to return to homeostasis following injury, it is worth noting that very little is understood about the niche requirements of FSCs. While evidence is emerging to define cells serving a niche-supporting role to CBCs (e.g. Paneth cells,[25] Foxl1-positive telocytes)[2], little to no work has come to light about a niche cell serving a regulatory function to FSCs. Perhaps niche cells are common to both CBCs and FSCs. Our studies in Chapter II are in favor of this idea, suggesting that an IGF1-secreting pericryptal subepithelial cell, potentially the same CBC niche-supporting cell identified by other groups,[1–3] plays a critical role in the FSC niche. On the other hand, our studies in Chapter IV suggest that the epithelial niche Paneth cell, which we suggest is critical to maintaining proper CBC activity, is dispensable to the activity of *Dll1*-expressing FSCs, as we report these cells contribute to

regeneration in the absence of Paneth cells. Our studies suggest that the identity of the niche signals, rather the identity of the niche-supporting cells, are key to regulating FSC contribution to mucosal repair.

Nonetheless, myriad outstanding intestinal niche questions remain. Given the complexity of the intestinal niche, more work needs to be done to understand the intricate crosstalk between the various intestinal compartments, which will be critical to our understanding of intestinal remodeling following injury. Specifically, we have yet to understand how crypt plasticity is regulated by these different compartments. We and others have suggested that epithelial (e.g. Paneth cells)[25] and subepithelial cells (e.g. telocytes,[2] pericryptal myofibroblasts)[1] are involved in signaling to ISCs, potentially mediating remodeling of the crypts, although the specific mechanisms have not all yet been delineated. Additionally, infiltrating inflammatory cells responding to injury could also play a role in regulating these different compartments, likely through their secretion of specific cytokines.[26] It could be conceived that inflammatory signals stimulate cellular remodeling of the crypts directly, and/or that these signals regulate epithelial or subepithelial niche cell production of specific secreted factors (e.g. growth factors), which are themselves responsible for pro-regenerative crypt remodeling. Not to say that there couldn't also be feedback signaling from the epithelium to other cellular compartments stimulating or repressing secretion of pro-regenerative factors based on environmental cues (e.g. apoptosis, juxtacrine signaling). All in all, understanding the convoluted crosstalk of signaling between the various cellular

compartments in the intestinal niche would be a tremendous advance in our understanding of intestinal repair.

Our research contributes significantly to the field's understanding of the key niche pathways regulating ISC function during mucosal regeneration after stem cell damage. We have identified DLL1/DLL4/Notch and IGF1/mTORC1 signaling as critical niche signaling axes to regulating crypt cell plasticity and cellular remodeling post-injury. Our new acute Notch inhibition stem cell injury method will be a powerful research tool to understand cellular plasticity in the crypt, which is a poorly understood area of research. Our discoveries regarding the genotoxicity of widely employed CreER^{T2} mouse models caution the field about using the proper controls in order to promote dissemination of correctly interpreted findings, hence building on our work. We show that Notch and growth factor signaling play a major role in cellular remodeling. Overall these contributions have led to the characterization of some key players in intestinal regeneration, which will be vital to the eventual development of regenerative therapies for intestinal disorders, and the design of treatments for intestinal diseases associated with mucosal injury. Further, understanding mechanisms of cellular plasticity and pro-regenerative or protective mechanisms may also advance our understanding of how to block such processes in the context of oncogenic malignancies.

5.5 References

1. Valenta, T. *et al.* Wnt Ligands Secreted by Subepithelial Mesenchymal Cells Are Essential for the Survival of Intestinal Stem Cells and Gut Homeostasis. *Cell Rep.* **15,** 911–918 (2016).

2. Shoshkes-Carmel, M. *et al.* Subepithelial telocytes are an important source of Wnts that supports intestinal crypts. *Nature* **557,** 242–246 (2018).

3. Aoki, R. *et al.* Foxl1-expressing mesenchymal cells constitute the intestinal stem cell niche. *Cell. Mol. Gastroenterol. Hepatol.* **2,** 175–188 (2016).

4. Liu, J.-L. *et al.* Insulin-Like Growth Factor-I Affects Perinatal Lethality and Postnatal Development in a Gene Dosage-Dependent Manner: Manipulation Using the Cre/loxP System in Transgenic Mice. *Mol. Endocrinol.* **12,** 1452–1462 (1998).

5. Hahn, A. M., Myers, J. D., McFarland, E. K., Lee, S. & Jerde, T. J. Interleukin-driven insulin-like growth factor promotes prostatic inflammatory hyperplasia. *J. Pharmacol. Exp. Ther.* **351,** 605–15 (2014).

6. Yousefi, M. *et al.* Calorie Restriction Governs Intestinal Epithelial Regeneration through Cell-Autonomous Regulation of mTORC1 in Reserve Stem Cells. *Stem cell reports* **10,** 703–711 (2018).

7. Van Landeghem, L. *et al.* IGF1 stimulates crypt expansion via differential activation of 2 intestinal stem cell populations. *FASEB J.* **29,** 2828–42 (2015).

8. Rodgers, J. T. *et al.* mTORC1 controls the adaptive transition of quiescent stem cells from G0 to G(Alert). *Nature* **509,** 393–6 (2014).

9. Richmond, C. A. *et al.* Dormant Intestinal Stem Cells Are Regulated by PTEN and Nutritional Status. *Cell Rep.* **13,** 2403–11 (2015).

10. Richmond, C. A., Shah, M. S., Carlone, D. L. & Breault, D. T. An Enduring Role for Quiescent Stem Cells. *Dev. Dyn.* (2016). doi:10.1002/dvdy.24416

11. Willet, S. G. *et al.* Regenerative proliferation of differentiated cells by mTORC1-dependent paligenosis. *EMBO J.* **37,** e98311 (2018).

12. Loonstra, A. *et al.* Growth inhibition and DNA damage induced by Cre recombinase in mammalian cells. *Proc. Natl. Acad. Sci. U. S. A.* **98,** 9209–14 (2001).

13. Higashi, A. Y. *et al.* Direct hematological toxicity and illegitimate chromosomal recombination caused by the systemic activation of CreERT2. *J. Immunol.* **182,** 5633–40 (2009).

14. Schmidt, E. E., Taylor, D. S., Prigge, J. R., Barnett, S. & Capecchi, M. R. Illegitimate Cre-dependent chromosome rearrangements in transgenic mouse spermatids. *Proc. Natl. Acad. Sci. U. S. A.* **97,** 13702–7 (2000).

15. Dempsey, P. J., Bohin, N. & Samuelson, L. C. in *Physiology of the Gastrointestinal Tract* (eds. Said, H. M., Ghishan, F. K., Kaunitz, J. D., Merchant, J. L. & Wood, J. D.) 141–183 (Academic Press, 2018).

16. VanDussen, K. L. *et al.* Notch signaling modulates proliferation and

differentiation of intestinal crypt base columnar stem cells. *Development* **139,** 488–97 (2012).

17. Nusse, Y. M. *et al.* Parasitic helminths induce fetal-like reversion in the intestinal stem cell niche. *Nature* **559,** 109–113 (2018).

18. Yui, S. *et al.* YAP/TAZ-Dependent Reprogramming of Colonic Epithelium Links ECM Remodeling to Tissue Regeneration. *Cell Stem Cell* **22,** 35–49.e7 (2018).

19. Schmitt, M. *et al.* Paneth Cells Respond to Inflammation and Contribute to Tissue Regeneration by Acquiring Stem-like Features through SCF/c-Kit Signaling. *Cell Rep.* **24,** 2312–2328.e7 (2018).

20. Tian, H. *et al.* Opposing Activities of Notch and Wnt Signaling Regulate Intestinal Stem Cells and Gut Homeostasis. *Cell Rep.* **11,** 33–42 (2015).

21. Blanpain, C., Mohrin, M., Sotiropoulou, P. A. & Passegué, E. DNA-damage response in tissue-specific and cancer stem cells. *Cell Stem Cell* **8,** 16–29 (2011).

22. Takeda, N. *et al.* Interconversion between intestinal stem cell populations in distinct niches. *Science* **334,** 1420–4 (2011).

23. van Es, J. H. *et al.* Dll1+ secretory progenitor cells revert to stem cells upon crypt damage. *Nat. Cell Biol.* **14,** 1099–1104 (2012).

24. Bankaitis, E. D., Ha, A., Kuo, C. J. & Magness, S. T. Reserve Stem Cells in Intestinal Homeostasis and Injury. *Gastroenterology* (2018).

doi:10.1053/J.GASTRO.2018.08.016

25. Sato, T. *et al.* Paneth cells constitute the niche for Lgr5 stem cells in intestinal crypts. *Nature* **469,** 415–8 (2011).

26. Andrews, C., McLean, M. H. & Durum, S. K. Cytokine Tuning of Intestinal Epithelial Function. *Front. Immunol.* **9,** 1270 (2018).